2017

SURFACE CHEMISTY STUDY OF MONAZITE FLOTATION IN COAL REFUSE SYSTEMS

Wencai Zhang
University of Kentucky, wzh257@g.uky.edu
Digital Object Identifier: https://doi.org/10.13023/ETD.2017.167

STUDENT AGREEMENT:

I represent that my thesis or dissertation and abstract are my original work. Proper attribution has been given to all outside sources. I understand that I am solely responsible for obtaining any needed copyright permissions. I have obtained needed written permission statement(s) from the owner(s) of each third-party copyrighted matter to be included in my work, allowing electronic distribution (if such use is not permitted by the fair use doctrine) which will be submitted to UKnowledge as Additional File.

I hereby grant to The University of Kentucky and its agents the irrevocable, non-exclusive, and royalty-free license to archive and make accessible my work in whole or in part in all forms of media, now or hereafter known. I agree that the document mentioned above may be made available immediately for worldwide access unless an embargo applies.

I retain all other ownership rights to the copyright of my work. I also retain the right to use in future works (such as articles or books) all or part of my work. I understand that I am free to register the copyright to my work.

REVIEW, APPROVAL AND ACCEPTANCE

The document mentioned above has been reviewed and accepted by the student's advisor, on behalf of the advisory committee, and by the Director of Graduate Studies (DGS), on behalf of the program; we verify that this is the final, approved version of the student's thesis including all changes required by the advisory committee. The undersigned agree to abide by the statements above.

Wencai Zhang, Student

Dr. Rick Honaker, Major Professor

Dr. Zacharias Agioutantis, Director of Graduate Studies

SURFACE CHEMISTY STUDY OF MONAZITE FLOTATION IN COAL REFUSE SYSTEMS

DISSERTATION

A dissertation submitted in partial fulfillment of
the requirements for the degree of Doctor of
Philosophy in the College of Engineering at the
University of Kentucky

By

Wencai Zhang

Lexington, Kentucky

Director: Dr. Rick Honaker, Professor of Mining Engineering

Lexington, Kentucky

2017

ABSTRACT OF DISSERTATION

SURFACE CHEMISTY STUDY OF MONAZITE FLOTATION IN COAL REFUSE SYSTEMS

Rare earth mineral recovery from alternative resources such as coal and coal byproducts is increasingly important to provide an opportunity for economic recovery from U.S. sources. Currently, China produces the majority of the 149,000 tons of rare earth elements used annually worldwide of which the U.S. imports 11% or around 16,000 tons. There are no significant mining operations producing rare earth elements in the U.S. However, there are many U.S. sources containing rare earth minerals such as monazite including heavy mineral sand and phosphate operations. Monazite mineral particles of a few microns have also been detected in Fire Clay seam coal. Preliminary attempts to concentrate the rare earth mineral using flotation test results indicated that monazite was floated together with carbonate minerals. The flotation chemistry of a monazite-carbonate mineral system has received limited attention by researchers. As such, a systematic study of monazite flotation chemistry was conducted and the results reported in this dissertation.

The surface charging mechanisms of monazite in aqueous systems were studied using electrokinetic tests, solution equilibrium calculation, crystal structure analysis, and electrostatic model prediction. The surface charge of monazite was found to be developed by protonation/deprotonation reactions. In other words, the hydrogen and hydroxyl ions were potential determining ions instead of the lattice ions of monazite. Electrokinetic tests of natural monazite mineral showed that the isoelectric point (IEP) occurred at pH 6.0. Solution equilibrium calculation and electrostatic model predictions of cerium monazite ($CePO_4$) yielded an IEP of pH 7.2. The discrepancy between the two IEP values may be due to the different REE composition and/or the amount of carbon dioxide dissolved in solution.

A common collector used to produce a hydrophobic monazite surface is octanohydroxamic acid. Adsorption studies found multilayer formation of octanohydroxamic acid on monazite surfaces at pH values of 3.0, 6.0, and 9.0. A kinetic study showed that the maximum adsorption density and rate for below monolayer coverage occurred at a solution pH value of 9.0, which was attributed to the chemical reaction between octanohydroxamate species and surface active sites (e.g., $REE(OH)^{2+}$).

For beyond multilayer adsorption, maximum adsorption occurred at pH 11.0 due to the abundance of hydroxyl ions in solution. The contributing effect of hydroxyl ions was proven by titration tests and FTIR analyses.

When calcium ions existed in solution, specific adsorption of $Ca(OH)^+$ on monazite surfaces occurred in both neutral and basic environments as indicated by the electrokinetic results. At low concentrations, $Ca(OH)^+$ competed with octanohydroxamic acid for P-OH sites. However, higher dosages of $Ca(OH)^+$ served as active sites for octanohydroxamic acid. The monazite floatability was negatively affected by the hydration of the adsorbed calcium species. The calcium ion dissolved from calcite mineral surfaces, which exist in the coal sources, provided an explanation for the depression of monazite in the combined systems.

Single mineral flotation of monazite and calcite showed that sodium silicate and sodium hexametaphosphate efficiently depressed calcite while providing minimal effects on monazite recovery. However, in the monazite-calcite combined system, both monazite and calcite were depressed using the two regulators. Electrokinetic data and solution equilibrium calculations indicated that hydrolyzed species of calcium such as $Ca(OH)^+$ interacted with silicates and formed a compact hydrophilic layer on monazite surfaces by hydrogen bonding and surface reaction. The compact layer decreased collector adsorption due to steric hindrance. Using 6×10^{-5} M EDTA together with 2.5×10^{-4} M octanohydroxamic acid and 0.05 g/L sodium silicate, monazite recovery of more than 90% was achieved while only recovering 20% of calcite. Based on the fundamental study, rare earth concentrates with 4700 ppm of REEs were produced from the Fire Clay fine coal refuse using column flotation.

KEYWORDS: Flotation, Monazite, Calcite, Surface Charge, Octanohydroxamic Acid, Adsorption Mechanisms

Wencai Zhang

(Author's name)

04/28/2016

(Date)

SURFACE CHEMISTY STUDY OF MONAZITE FLOTATION IN COAL REFUSE SYSTEMS

By

Wencai Zhang

Dr. Rick Honaker

(Director of Dissertation)

Dr. Zacharias Agioutantis

(Director of Graduate Studies)

04/28/2017

(Date)

ACKNOWLEDGEMENTS

I would like to express my sincere thanks to my advisor, Dr. Rick Q. Honaker, for his guidance, motivation, and continual support throughout this work. Without his valuable expertise, participation and helpful subject-related suggestions, the achievement of this work would not be possible.

I would also like to express my deepest gratitude to Dr. John Groppo for his help during the last four years. The micro-flotation cell was designed and built by Dr. Groppo and sample characterization such as surface area measurement was also performed with the help of Dr. Groppo. I would like to further extend my gratitude to Dr. Barbara Knutson, Dr. Bhupendra K. Parekh, and Dr. James Hower for their efforts as my Ph.D. thesis committee members.

Special thanks to Dr. James Hower, Dr. Cortland Eble, and Dr. Dali Qian for their help regarding the mineralogy study part of rare earth in coal and coal byproducts. Mr. Jason S Backus trained me to run XRD and XRF of the pure minerals used for current study. The FTIR characterization was conducted in Dr. Zach Hilt's lab in the Chemical and Materials Engineering Department of the University of Kentucky. I sincerely appreciate all the help provided by the above professors.

I would like to express my sincere thanks to my friends and colleagues, Jinxiang Chen, Zifu Cui, Qingqing Huang, Jing Li, Lifeng Li, Yonggai Li, Xinbo Yang, Ao Zeng, Yumo Zhang, Tuopu Zhang, Cong Zhang, Lei Zhang, Yigong Zhang. I am very lucky to meet them during my Ph.D. study at Lexington.

I would have been nowhere close to writing this dissertation without the indispensable help of the department staff and meted out to me during my stay at the department of Mining Engineering. I would also take this opportunity to thank all my professors, friends and fellow graduate students who made my stay at the department truly memorable.

I was fortunate enough to be brought up by my wonderful parents, Chuanming Zhang

and Hengying Li, who have been extremely supportive of all my decisions throughout. My parents worked very hard to support me and my sister to receive higher levels of education. They gave me the chance to get more knowledge which can change my life. My grandfather, grandmother, and grandmother in-law passed away at the first half of 2014 and it is pity that I could not attend their funerals. I deeply appreciate the three elders' concern, love, education, and cultivation for me. My old sister, Wenmei Zhang, is my abecedarian in a sense and I still remember the time we two studied together. Fortunately, my sister is also going to obtain her doctor degree in medicine in this June. I would also acknowledge my fiancé, Xinxin Shao, for her support, encouragement, and concern during the last four years.

TABLE OF CONTENTS

LIST OF TABLES

LIST OF FIGURES

CHAPTER 1. INTRODUCTION

1.1 BACKGROUND

Rare earth elements (REEs) including the lanthanide elements plus yttrium and scandium have been widely used as raw materials for catalysts, alloys, ceramics, polishing, etc. The latest U.S. Geological Survey (USGS) data indicates that the U.S. has a total REE reserve of 1,400,000 metric tons which only accounts for 1.16% of global REE reserve (120,000,000 metric tons) (USGS, 2017). Only one rare earth mine, i.e., Mountain Pass, was operated intermittently during the last five years and domestic REE consumption of the U.S. relies heavily on imports. As such, exploration of alternative REE source materials is critically important. The U.S. Department of Energy (DOE) selected several projects to enhance the research into recovery of REEs from coal and coal byproducts.

The total REE content in world coal is about 61.33 Mt and the annually produced coal and coal byproducts contain enough REEs to meet current U.S. demand (Zhang *et al*., 2015; Honaker *et al.*, 2017). REEs in coal and coal byproducts mainly exist as minerals, ion-exchanged elements associated with clays, and chemically bonded elements with the organic matrix. Monazite particles have been detected in coal and fine refuse using Scanning Electron Microscopy – Energy Dispersive X-ray Spectrometer (SEM-EDX) (Honaker *et al.,* 2014; Zhang *et al*., 2017a).

Flotation is a fine-particle mineral processing technique and efficient separation is normally achieved using appropriate collectors and depressants to maximize the surface hydrophobicity differences between valuable and gangue minerals. Flotation has been widely used to separate fine monazite from heavy-sand minerals such as hematite, rutile, zircon, ilmenite, etc. Previous studies by Zhang *et al.* (2016, 2017 a, 2017 b) also proved that satisfactory concentration of monazite from coal and coal byproducts was achieved using octanohydroxamic acid as the collector. Calcite was found to be the floated together with monazite into the concentrate. However, the fundamental study of monazite-calcite flotation separation is limited.

The current study focused on the flotation chemistry involved in the monazite-calcite system when using octanohydroxamic acid as the collector. Surface charging mechanisms of monazite in aqueous systems were studied using electrokinetic tests, solution equilibrium calculation, and electrostatic model prediction. Adsorption mechanisms of octanohydroxamic acid on monazite surfaces were studied using adsorption kinetic, isotherm, thermodynamic, and titration tests. Surface chemical changes were characterized using zeta potential measurement and Fourier transform infrared spectroscopy (FTIR) analyses. Effects of calcium ions dissolved from calcite surfaces on octanohydroxamic acid and depressant adsorption on monazite surfaces were studied using adsorption and electrokinetic tests. Attempts to eliminate the calcium ion effects using chelating reagents such as citric acid and EDTA were conducted. An appropriate reagent scheme was proposed for rare earth recovery from coal and coal byproducts. Finally, conventional cell flotation and batch flotation tests were conducted to concentrate rare earth minerals from coal and coal byproducts.

1.2 OBJECTIVES

The overall objective of the current study was to understand the fundamental aspects involved in the monazite-calcite flotation system, which provides some guidelines for monazite recovery from coal and coal byproducts. The specific objectives included:

(1) Review the fundamentals regarding collector adsorption, monazite flotation, and solution species effects on flotation.
(2) Study the surface charging mechanisms of monazite in aqueous systems and determine the role of lattice ions, hydrogen, and hydroxyl ions.
(3) Study the adsorption mechanisms of octanohydroxamic acid on monazite surfaces at different solution pH values and collector dosages. Determine the difference between monazite-octanohydroxamic acid system and other systems such as bastnaesite-octanohydroxamic acid.
(4) Evaluate flotation behavior of pure and mixed minerals of monazite and calcite using micro-flotation apparatus and octanohydroxamic acid. Evaluate effects of

lattice ions dissolved from calcite surfaces on monazite flotation.

(5) Evaluate the effects of solution ions on the adsorption of octanohydroxamic acid on monazite surfaces and propose an appropriate mechanism to explain the effects.

(6) Select appropriate depressants and chelating reagents to depress calcite and eliminate dissolved ion effects on monazite flotation. Understand the fundamentals regarding the depressing and/or activation effects of these reagents.

(7) Concentrate rare earth minerals from coal and coal byproducts.

1.3 ORGANIZATION

The dissertation is organized into nine chapters. The first chapter is a brief introduction of the background and objectives of the current study. The second chapter gives a comprehensive review of collector adsorption mechanisms for various minerals, including monazite and bastnaesite. Effects of solution species on mineral flotation are also reviewed in this chapter for a better understanding of flotation chemistry.

The third chapter introduces experimental details including material, chemicals, micro-flotation apparatus and procedures, electrokinetic measurement, Fourier transform infrared spectroscopy (FTIR) characterization, adsorption apparatus, and procedures, etc. A case study of solution equilibrium calculation is also provided to explain how the calculation is conducted in the research dissertation. The corresponding test and calculation results as well as discussion are provided in the subsequent three chapters. Specifically, charging mechanisms of monazite, adsorption mechanisms of octanohydroxamic acid on monazite surfaces, and monazite-calcite separation studies are provided in the fourth, fifth, and sixth chapter, respectively. Concentration of rare earth minerals from coal and coal byproducts is also introduced in the seventh chapter.

The main conclusion of the dissertation are recapitulated in the eighth chapter. Suggestions for future study are attached to the last chapter, which is also the ninth chapter.

CHAPTER 2. LITERATURE REVIEW AND THEORETICAL PRINCIPLES

2.1 RARE EARTH IN COAL

Rare earth elements (REEs) are a group of 15 lanthanide elements (atomic numbers 57-71) and two transition metal elements (scandium and yttrium) (Binnemans *et al.*, 2013). There is a consistently high demand for REEs due to their applications in automotive catalytic converters, glass polishing and ceramics, metallurgical additives and alloys, petroleum refining catalysts, rare-earth phosphors for lighting, televisions, computer, radar, X-ray intensifying film, and permanent magnets, etc.

The world reserve of REEs was estimated to be 130 Mt. Most of the reserve is distributed in China (42.30%), Brazil (16.92%), Australia (2.46%), Malaysia (2.38%), and U.S.A. (1.38%) (Zhang *et al.*, 2015). More than 95% of all consumed REEs were supplied by China in 2014. However, the export/production ratio of REEs for China steadily decreased from 64% in 2000 to 19% in 2010 due to China's steadily growing domestic needs for REEs. The U.S. Department of Energy (DOE) identified neodymium (Nd), europium (Eu), terbium (Tb), dysprosium (Dy), and yttrium (Y) as the five most critical REEs (Binnemans *et al.*, 2013).

The average REE content of world coal is 69 ppm on whole coal basis, and Chinese and American coals contain 138 ppm and 62 ppm, respectively (Seredin and Dai, 2012). The total amount of REEs in coal was estimated to be 50 million tons which equate to nearly 50% of the REE reserve of traditional rare earth bearing minerals sources (Zhang *et al.*, 2015). Significant economic potential may be realized if the REEs in coal can be recovered or even partially recovered. Furthermore, there are many well-known coal beds with extremely high REE content such as those in the Far East coalfields in Russia (300-1000 ppm REEs), Fire Clay coal bed in eastern USA (500-4000 ppm REEs), and the Sydney Basin in Nova Scotia, Canada (72-483 ppm REEs) (Hower *et al.*, 1999; Seredin, 1996).

Significant work has been conducted at the University of Kentucky since 2014 to assess the feasibility of REE recovery from the Fire Clay coal bed (Honaker *et al.*, 2014).

Middling and fine refuse were collected from a preparation plant which uses the Fire Clay coal as feedstock. Mineralogical and preliminary separation tests were conducted. Size analyses of fine refuse, with carbon removed, show that nearly 70% of particles are smaller than 25 microns and contained 70% of total REEs. As shown in Figure 2.1, enrichment ratio of 2 could be achieved using appropriate collectors. Multi-stage flotation test including rougher, cleaner, and re-cleaner indicated that a gradual enrichment of REEs was achieved. X-ray diffraction results showed that clay minerals (mainly kaolinite, montmorillonite, and illite), carbonate minerals (mainly calcite and dolomite), and quartz were the main mineral phases. Meanwhile, carbonate minerals were enriched significantly together with REEs during the multi-stage flotation (Figure 2.2).

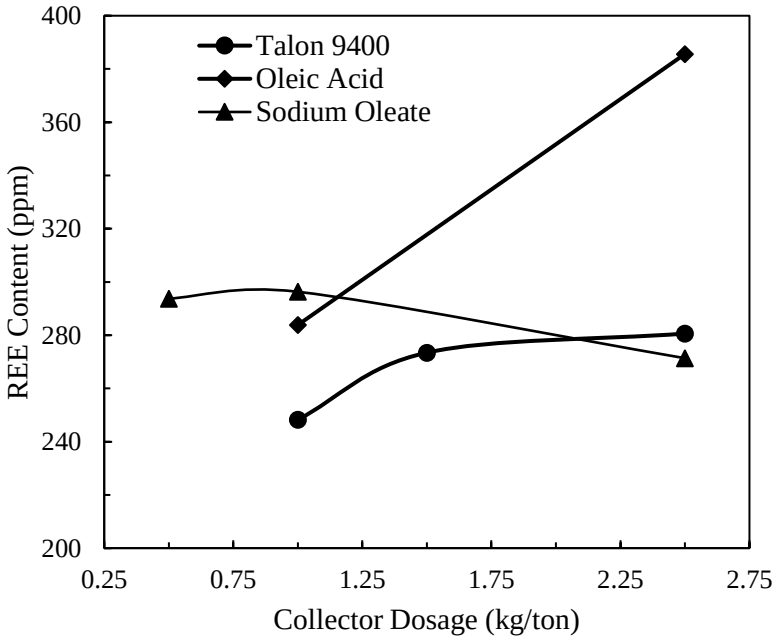

Figure 2. 1. Flotation performance of fine refuse with different collectors at neutral pH.

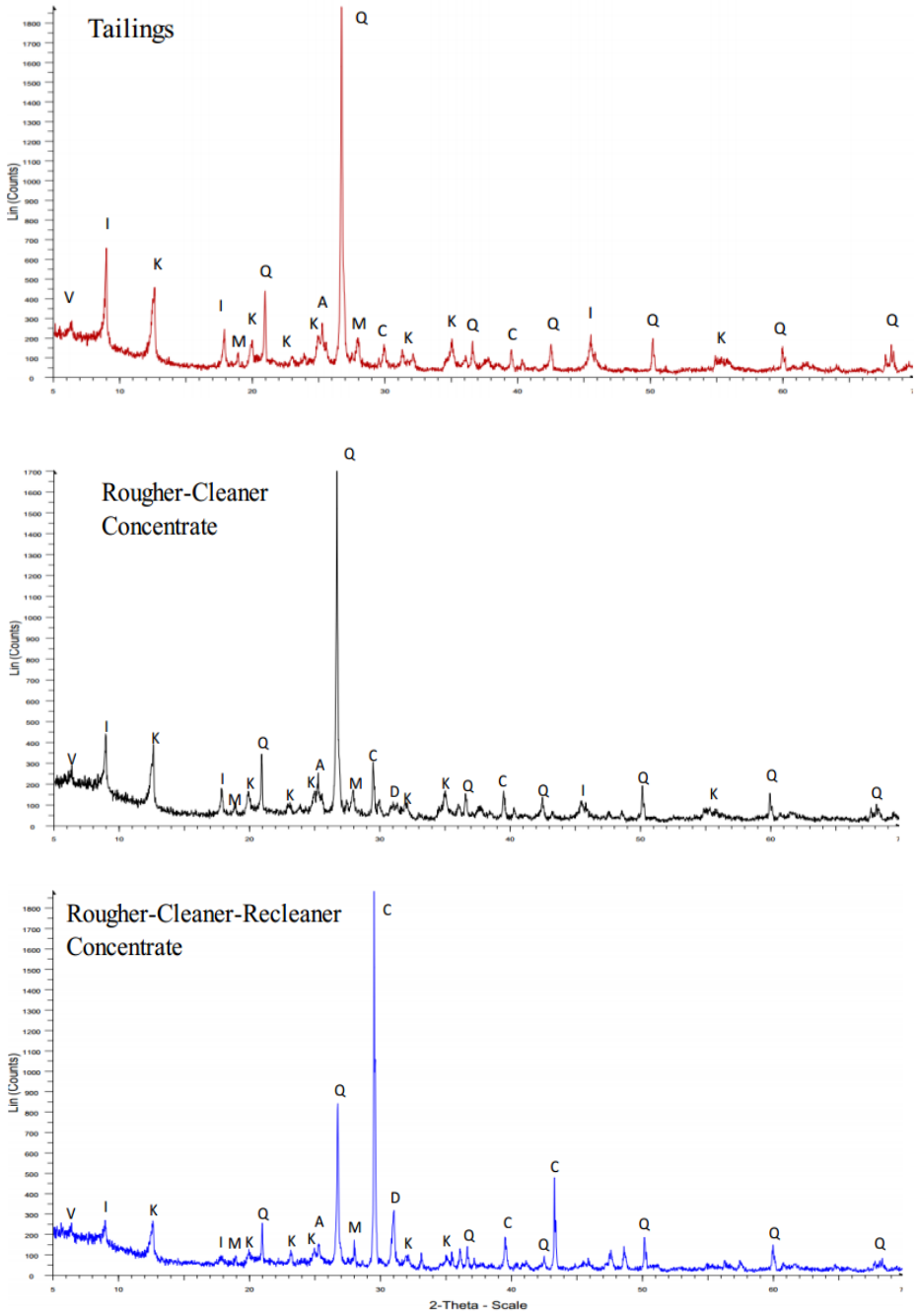

Figure 2. 2. XRD patterns of the products obtained from multi-stage flotation (A-Anatase, C- Calcite, D- Dolomite, I- Illite, K- Kaolinite, M-Montmorillonite, Q-Quartz, V-Vermiculite).

2.2 COLLECTOR ADSORPTION MECHANISMS

Since Sulman and Picard's first patent on the use of air bubbles for flotation in 1905, flotation had been widely used in mineral processing area, especially for minerals of small particle size (Fuerstenau et al., 2006). Significant work has been done in terms of

the fundamental aspects of flotation, such as flotation solution chemistry, electrochemistry, thermodynamics, flotation reagents (e.g., collectors and regulators), adsorption, *etc*. Collectors can selectively adsorb on mineral surfaces and induce hydrophobicity differences, which is the premise of flotation separation. Therefore, fundamental studies of collectors' adsorption are crucial. As proposed by Fuerstenau and Somasundaran (Ananthapadmanabhan and Somasundaran, 1985; Pradip and Fuerstenau, 1983), the interaction between collectors and mineral surfaces can be classified as follows:

Physisorption. Adsorption of reagent on mineral surface involving physical interactions, such as electrostatic force, Van der Waals force, etc.

Chemisorption. Adsorption of reagent on mineral surface involving chemical reactions with metal atoms (ions) located in the mineral lattice sites; adsorption is generally limited to a monolayer (Figure 2.3(a)).

Surface reaction. Interaction of reagent with mineral surface together with movement of metal atoms from their lattice sites; multilayers of reaction product may form (Figure 2.3(b)).

Surface precipitation. Adsorption of reagent on mineral surface involving the formation of precipitates at the interfacial region between mineral and liquid.

Bulk precipitation. Interaction of metal ions and reagent away from the surface out in the bulk solution. The precipitates produced in the bulk solution re-adsorb on mineral surface (Figure 2.3(c)).

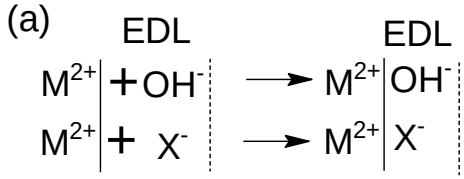

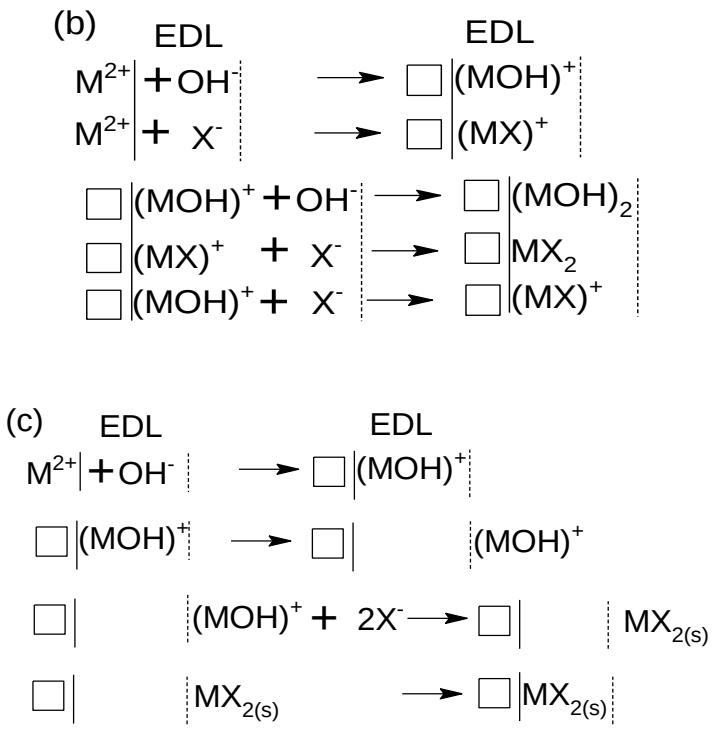

Figure 2. 3. Collector adsorption mechanisms, EDL means electrical double layer. (a) Chemisorption; (b) Surface reaction; (c) Bulk precipitation. (Fuerstenau *et al.*, 2007)

Generally the interaction between collector and mineral surface involves several of the mechanisms listed above. The adsorption mechanism also changes with respect to dosages, pH, temperature, etc.

2.2.1 Physical Adsorption

Collectors physically adsorb onto mineral surfaces via electrostatic force, van der Waals force, hydrophobic force, and hydrophilic bonding. Physical adsorption was observed mainly in the flotation of strong hydrophilic minerals such as silicates, alumina, and hematite by using ammonium or sulfonate collectors. The adsorption of ammonium and sulfonate collectors has been extensively studied by the electro-kinetic, surface force, contact angle, micro-flotation, spectroscopic characterization, etc.

Gaudin and Fuerstenau (1955) suggested that electrostatic and hydrophobic interactions contribute to the flotation of silica by using dodecylammonium (RNH_2) as collector. In dilute solution dedecyammonium ions are held to the silica surface by electrostatic attraction, while, at higher concentrations the adsorbed collector ions begin to associate

into patches of ions, called hemi-micelles (Figure 2.4, 2.5, 2.6 and 2.7). The hemi-micelles are actually two dimensional (2D) aggregates. Iwasaki *et al.* (1960) studied the flotation of hematite using several different collectors such as dodecylammonium chloride ($C_{12}H_{25}NH_3Cl$), octadecylammonium chloride ($C_{18}H_{37}NH_3Cl$), sodium dodecylsufate ($C_{12}H_{25}SO_4Na$), and sodium octadecylsulfate ($C_{18}H_{37}SO_4Na$). As shown in Figure 2.7, besides electrostatic interaction, carbon chain length also played significant role, which is related to the lateral interaction of hydrocarbon chains.

Somasundaran and Fuerstenau (1966) suggested a similar adsorption mechanism of alkyl sulfonate (RSO_4H) at the alumina-water interface, i.e., at a certain critical concentration or critical pH sulfonate ions are adsorbed individually as counter ions in the electrical double layer at low sulfonate concentrations due to the hindrance between the interacting hydrocarbon chains and electrostatic repulsion between the charged amino groups. The actual concentration of amine near the quartz surface becomes higher than the critical micelle concentration (CMC), adsorption increases rapidly through the formation of two-dimensional aggregates of the surfactant ions for hemi-micelles at the solid –solution interface.

The adsorption isotherm explained by hemi-micelle (HM) model can be divided into four distinct regions when plotted on a log-log scale, therefore, the HM model is also called the four-region model (Chandar *et al.*, 1987; Fan *et al.*, 1997; Somasundaran and Fuerstenau, 1966). The four-region model is as follows:

Region I – Surfactants adsorb electrostatically as individually ions;

Region II – The individual ions associate into hemi-micelles. In the hemi-micelles, the surfactants are oriented with their charged head groups toward the solid surface, while the hydrocarbon chains protrude into the aqueous phase, thus forming hydrophobic patches on the surface. Further adsorption results in an increasing number of surfactant aggregates, with molecules adsorbing in an opposite orientation once the surface is neutralized by the oppositely charged surfactant;

Region III – Adsorption occurs through the growth of aggregates already formed

in region II without an increase in the number of aggregates;

Region IV – Adsorbed layer exhibits the structure of a bilayer.

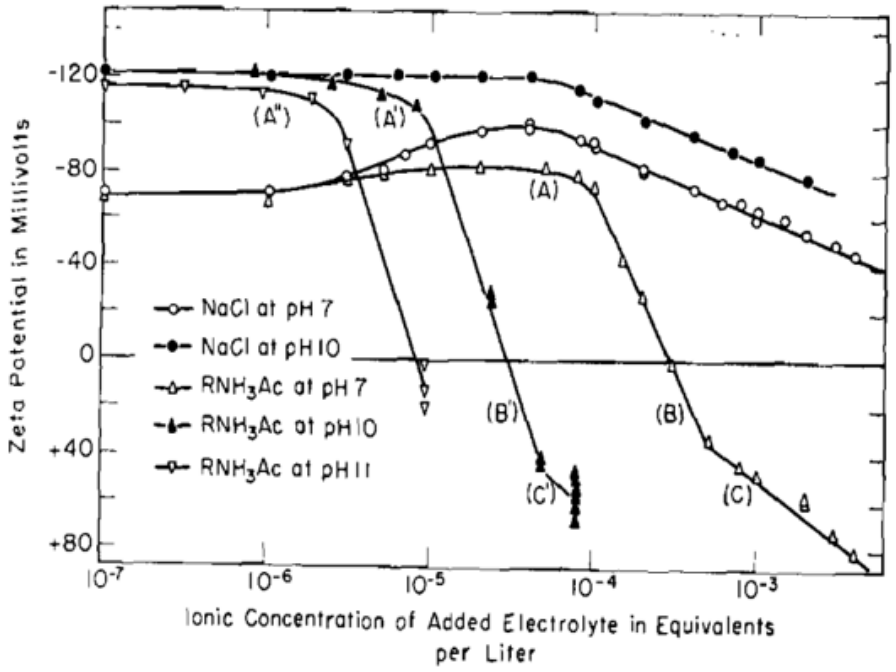

Figure 2. 4. Zeta potential of quartz in solutions of dodecylammonium acetate and sodium chloride at several different pH values. (Gaudin and Fuerstenau, 1955)

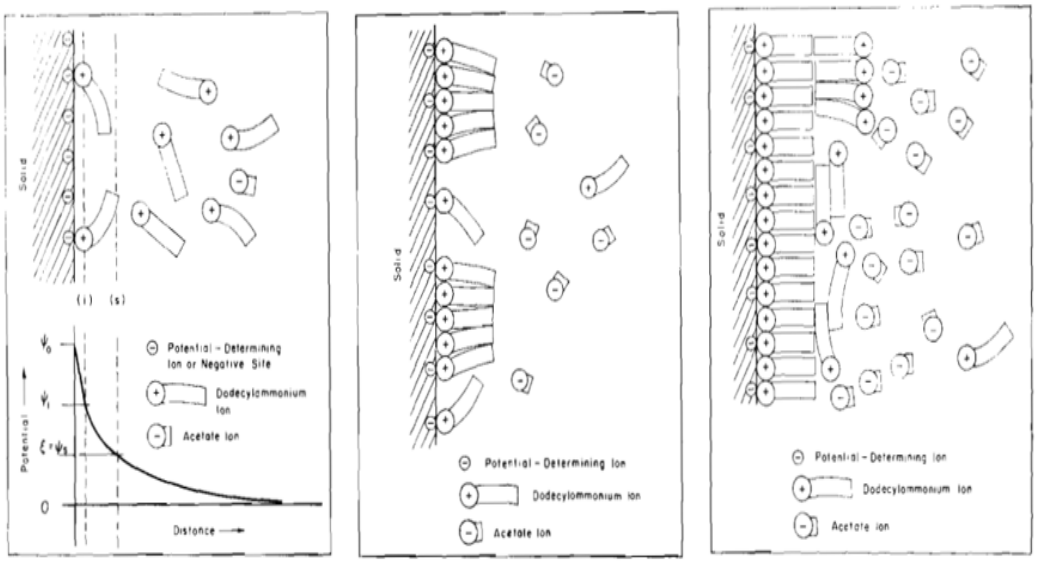

Figure 2. 5. Structure of the double layer and the distribution of potential in the double layer. (a) Conditions below those under which hemi-micelles form; (b) Conditions which give rise to hemi-micelle; (c) Multilayer adsorption. (Gaudin and Fuerstenau, 1955)

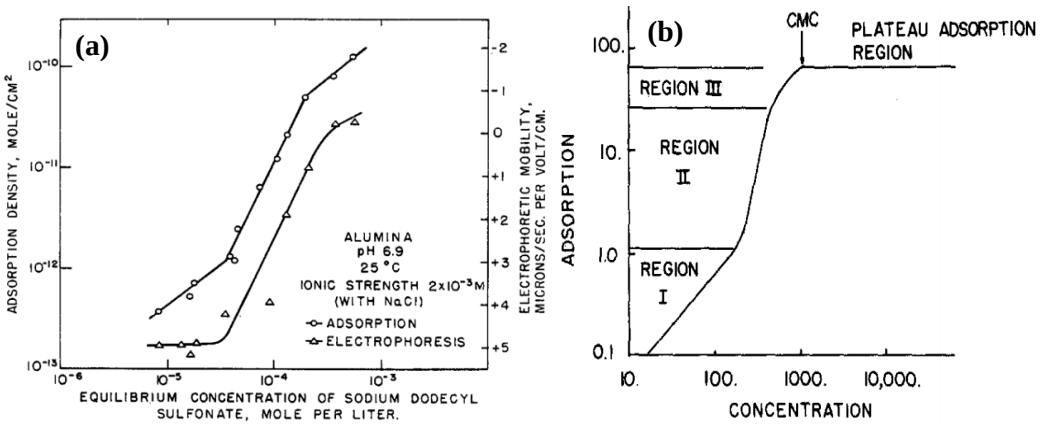

Figure 2. 6. (a) Adsorption of dodecyl sulfonate ions on alumina and the electrophoretic mobility of alumina as a function of the concentration at pH 6.9; (b) Illustration of adsorption of adsorption regions for surfactant adsorption on mineral oxide surfaces. (Somasundaran and Fuerstenau, 1966)

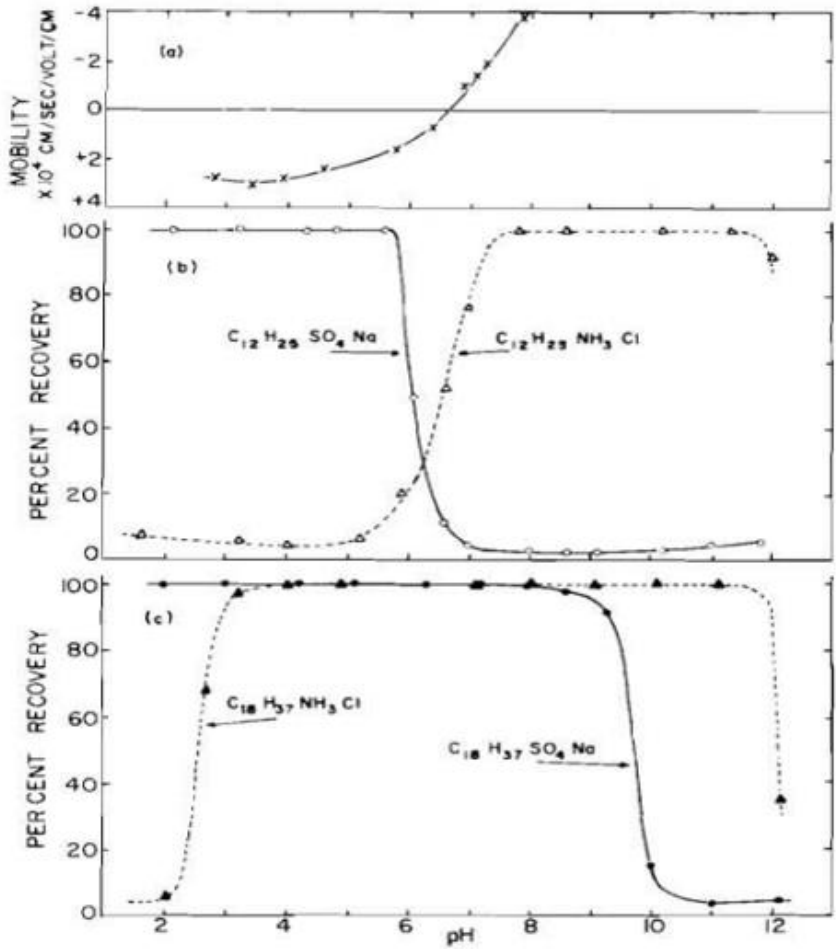

Figure 2. 7. (a) Electrophoretic mobility of hematite as a function of pH; (b) Flotation of hematite with 10^{-4} M dodecylammonium chloride and sodium dodecylsulfate; (c) Flotation of hematite with 10^{-4} M octadecylammonium chloride and sodium octadecylsulfate.(Iwasaki *et al.*, 1960)

Scamehorn *et al.* (1982) performed testing on the adsorption of alkylbenzene sulfonates on alumina and kaolinite and proposed a patchwise adosorption model, which incorporates bilayer adsorption, lateral interactions, and two-dimensional phase transitions (Figure 2.8 and 2.9). The patchwise adsorption model assumes that the surface is composed of patches with different adsorption energies, with the adsorption energy of each site within a given patch being uniform. The first layer and second layer of adsorption were assumed to be forming simultaneously, but for the region I, the second layer of adsorption is negligible. At region II, densely adsorbed phase is present on a patch at concentrations at or above that corresponding to the phase transition. After a phase transition occurred at most energetic patches at region II, the less energetic patches undergo phase transitions in region III. Above the CMC (region IV), the monomer concentration is constant and is the only adsorbed species (pseudo-phase separation model), therefore, increasing concentration has no influence on adsorption.

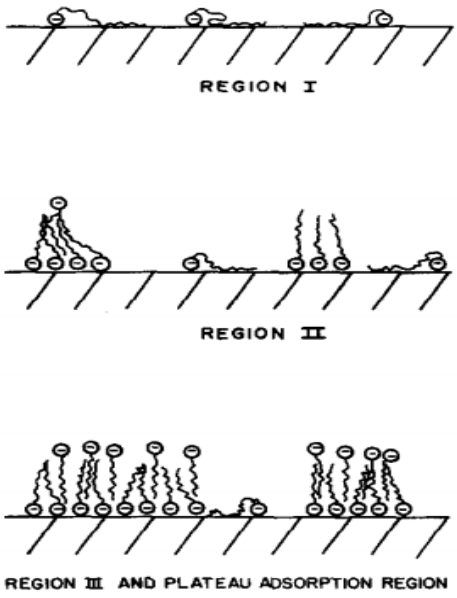

Figure 2. 8. Patchwise adsorption model. (Scamehorn *et al*., 1982)

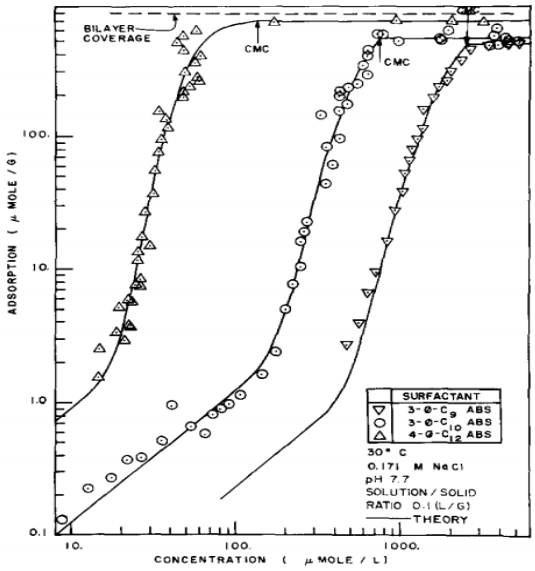

Figure 2. 9. Experimental and theoretical prediction results. (Scamehorn *et al.*, 1982)

Instead of the HM model, the more comprehensive patchwise adsorption model includes both the hydrophobic effect, surface aggregation, and surface heterogeneities. However, the nature of the surface and the counter ions was not taken into consideration. The pseudo phase separation model (PS) proposed by Harwell *et al.* (1984) took all of the above effects into consideration. The concept of admicelle was introduced in the PS model. The basic assumptions of the PS model are that surfactant aggregates forming at the solid/solution interface form locally on the surface because of surface heterogeneity and that these local aggregates, which are pictured as bilayered and are called admicelles, can be treated as pseudophase.

Chernyshova *et al.* (2000) proposed a mechanism of the successive 2D and 3D precipitation (2D-3DP) of alkyamines on quartz (see Figure 2.10). In the 2D-3DP model, the adsorption characteristics were split into three regions. At amine concentration $C_b < CHC$ (critical hemimicelle concentration), surface silanol groups interact with ammonium head groups through H-bonds (see Eq. 2.1), while the hydrocarbon chains have chaotical orientation. At $CHC \leq C_b < C_{pr}$ (precipitation concentration), the content of the adsorbed layer qualitatively changes: instead of species shown in Eq. 2.1, molecular amine H-bonded to surface silanol and protonated amine coordinated to deprotonated silanol oxygen (see Eq. 2.2) appear at the quartz surface. Adsorption

steeply increases and the hydrocarbon chains become highly organized. At $C_b \geq C_{pr}$ bulk amine precipitation takes place. Vidyadhar *et al.* (2002) used the 2D-3DP model to explain the promotion effect of alcohol to alkyl ammine adsorption on silica. In this case, the primary adsorption species are alkyl ammonium-water-alcohol complex, which is formed via hydrophobic interaction and H-bonding.

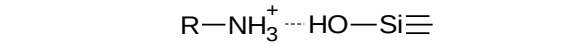

(Eq. 2.1)

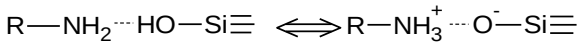

(Eq. 2.2)

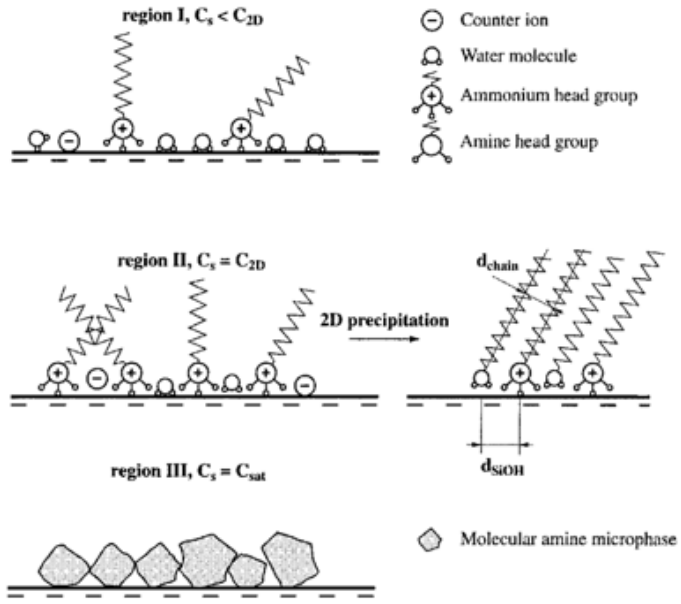

Figure 2. 10. Adsorption according to the 2D-3D precipitation mechanism. (Chernyshova *et al*., 2000)

2.2.2 Chemical Adsorption-Carboxylic Acids

Carboxylic collector and their salts such as oleic acid and sodium oleate have been widely used in the flotation of ilmenite ($FeTiO_3$), cassiterite (SnO_2), hematite (Fe_2O_3), spodumene ($LiAl(SiO_3)_2$), alunite ($KAl_3(SO_4)_2(OH)_6$), etc. Chemical reaction between surface active sites (cations) and oleic acid species is considered to be the main adsorption mechanism in spite that physical interaction also occurs.

Two types of active sites exist on ilmenite, i.e., titanium and iron. However, only one kind of active site contributes to the adsorption at certain pH vales, therefore, ilmenite

displays poor floatability (Fan *et al.*, 2009; Fan and Rowson, 2000; Mehdilo *et al.*, 2015). In strong acidic solutions (pH < 3), most of the ferrous ions were dissolved from the ilmenite surface and the remaining metallic ions were mainly titanium ions in the forms $Ti(OH)^{3+}$ and $Ti(OH)^{2+}$. In weakly acidic or weakly alkaline solutions (pH=5-8), titanium ions mainly existed in the form of $Ti(OH)_4$, while ferrous ions existed in the forms of Fe^{2+} and $FeOH^{+}$ function as active site (see Figure 2.11). Fe^{2+} can be converted to Fe^{3+} after microwave treatment, which more readily reacts with oleate (Fan *et al.*, 2009; Fan and Rowson, 2000). The solubility products for ferrous oleate and ferric oleate are $10^{-15.5}$ and $10^{-29.7}$ respectively.

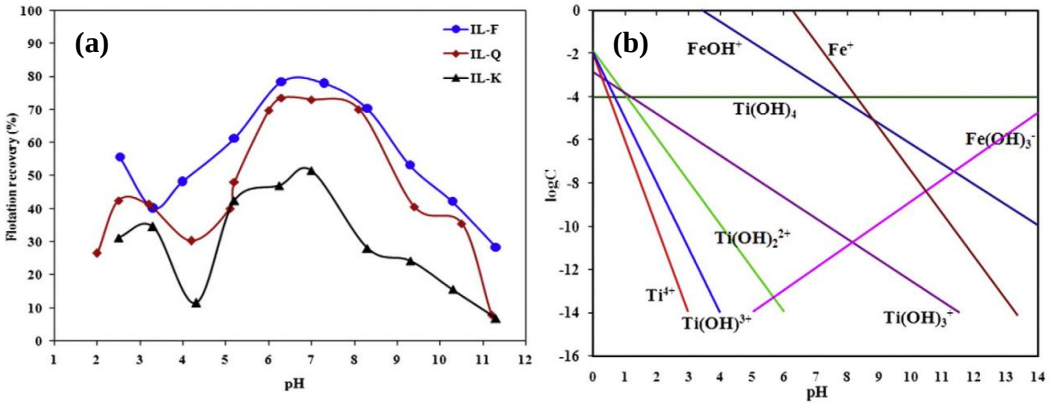

Figure 2. 11. (a) Flotation recovery of ilmenite samples as a function of pH (IL-F, IL-Q and IL-K indicate ilmenite samples of different sources) ; (b) Distribution diagram of surface species on ilmenite as a function of pH. (Fan *et al.*, 2009; Mehdilo et al., 2015)

The adsorption interaction of oleate collector on spodumene is chemisorption that involves the chemical reaction between the anionic carboxylate functional group in oleate collector and cationic Al surface sites on spodumene (Figure 2.12) (Moon and Fuerstenau, 2003). The surface Al on the {110} cleavage plane of spodumene was found to be the most favorable site for the selective chemisorption of oleate, while those in other aluminosilicates are buried deep inside the crystallographic unit cells of the minerals, making them unavailable for oleate adsorption (Figure 2.13) (Yu *et al.*, 2015).

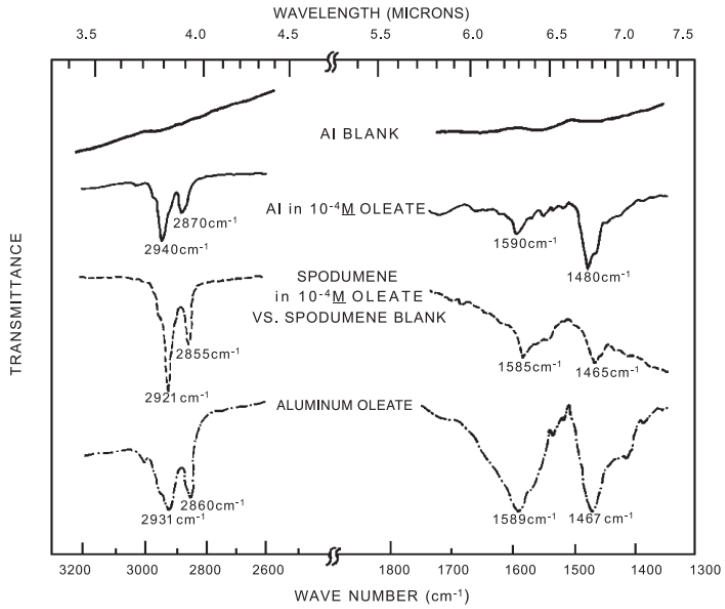

Figure 2. 12. Infrared spectra of surface oleate-aluminum foil treated in 10^{-4} M sodium oleate solution, for spodumene treated in 10^{-4} M sodium oleate solution and for bulk aluminum oleate. (Moon and Fuerstenau, 2003)

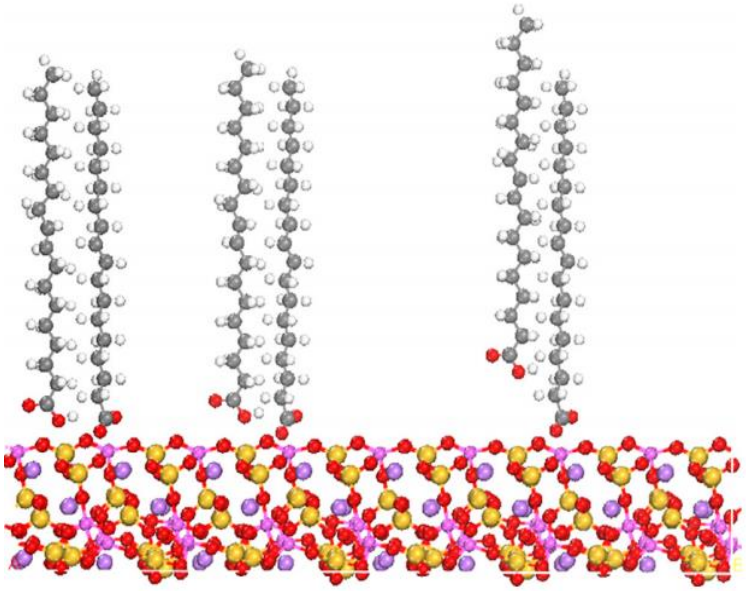

Figure 2. 13. Molecular model of ionic-molecular complexes of oleic acid adsorbing on spodumene surface (color: Pink-Al, Violet-Li, Red-O, and Yellow-Si). (Yu *et al*., 2015)

Previous studies of oleate adsorption on monazite involves some specific interactions. Several publications have reported that the maximum flotation recovery and adsorption of sodium oleate on monazite occurred at pH 8.0-9.0 (Abeidu, 1972; Cheng *et al*., 1993; Dixit and Biswas, 1969; Pavez and Peres, 1993). Monazite usually carries negative

charge in this pH range. Dixit and Biswas (1969) believed that oleate ion concentration (C_{OL^-}) and hydroxyl ion (C_{OH^-}) concentration contribute to this flotation and adsorption behaviors. Oleate ions is the activating species, while hydroxyl ions have depressing effect due to competitive adsorption. An equation of the type:

$$\Gamma = K_1 C_{OL^-}^{n1} K_2 C_{OH^-}^{n2} / C_{OL^-}^{n3} \qquad \text{(Eq. 2.3)}$$

was proposed to account for the experimental data.

Cheng *et al.* (1993) provided three reasons for the appearance of maximum recovery in pH 8.0-9.0, i.e., hydrolyzed rare earth ions such as $REE(OH)^{2+}$ and $REE(OH)_2^+$, acid-soap species ($(Ol)_2H^-$), and "bubble transfer hypothesis". Figure 2.14 shows monazite flotation results and species diagram of cerium phosphate ($CePO_4$) in water. Figure 2.15 shows the species diagram of sodium oleate. Accordingly, the maximum concentrations of hydrolyzed rare earth ions $Ce(OH)^{2+}$ and acid soap $(Ol)_2H^-$ occur in the neutral pH range.

However, the detailed information about the adsorption of sodium oleate on monazite surfaces such as adsorption mechanisms, adsorption isotherms, adsorption kinetics, adsorption thermodynamics, effects of temperature, and configuration of collector molecules on the monazite surface and in the interfacial region have not been studied.

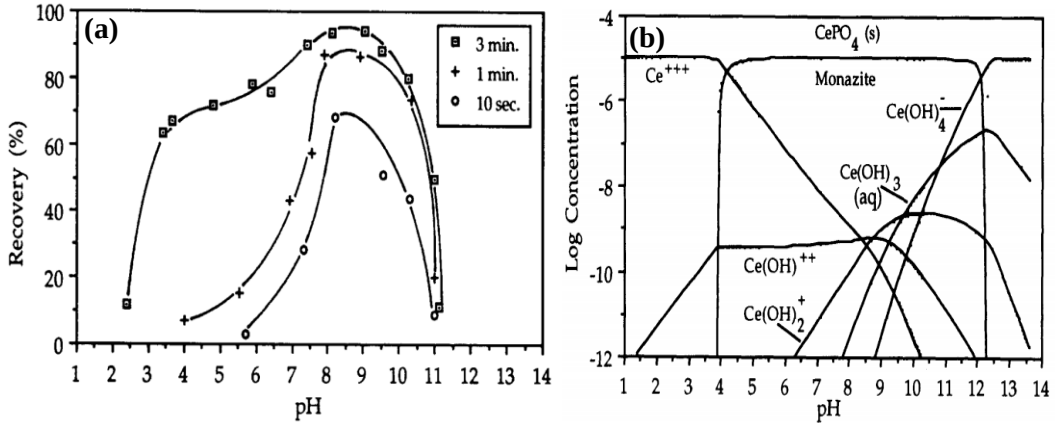

Figure 2. 14. Monazite flotation results and species diagram. (a) Flotation results; (b) Species diagram of monazite at 10^{-5} M total solution concentration. (Cheng *et al.*, 1993)

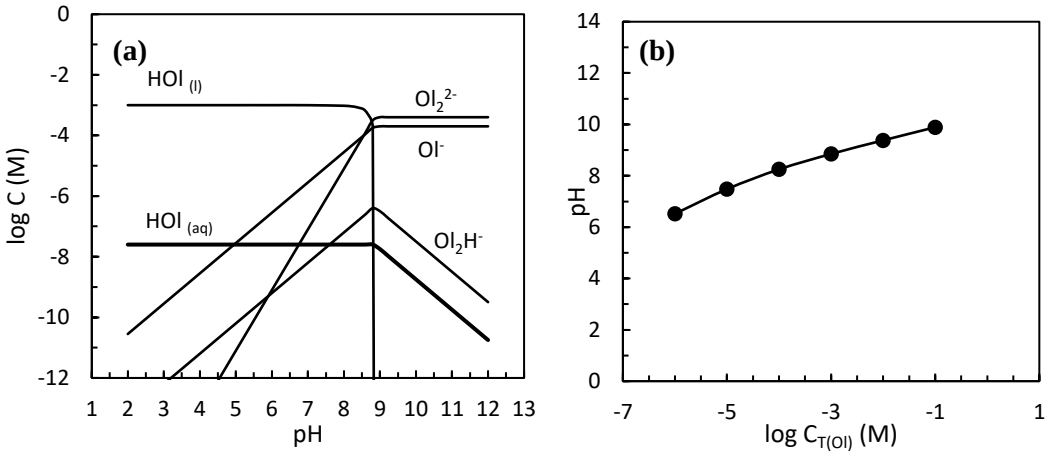

Figure 2. 15. Solution specie diagram of sodium oleate. (a) Changes with pH; (b) Changes of pH values corresponding to maximum acid-soap concentration with different total oleate concentration.

2.2.3 Chemical Adsorption-Hydroxamate Collectors

Chelates are metal complexes formed by a chelating agent and characterized by a ring structure with the metal as the central atom surrounded by the donor atoms of the chelating agent (Nagaraj, 1988). Donors, or donor atoms or ligand atoms, are those that bond directly to the central metal atom. Ligands are the functional groups containing the donor atom on the chelating agent that participate in bond formation with metals. Functional groups are a well-organized group of atoms on the chelating agent and contain the donor atoms. Acceptors are atoms or groups of atoms that accept electrons from donors. A metal is the acceptor in most instances (Nagaraj, 1988).

Chelating agents are a special class of metal complex-forming compounds (Nagaraj, 1988). They may be organic or inorganic molecules; the only requirement is that their complexes be characterized by a ring structure, such as the compound shown in Figure 2.16. For the complex shown in Figure 2.16, the metal platinum is coordinated with, or simply bonded to, two molecules of ethylene diamine. Platinum is actually bonded to four nitrogen atoms in such a way that two rings are formed. There are no restrictions on the nature of the bonds. Two of the bonds are ionic and the remaining two are coordinate covalent (Nagaraj, 1988).

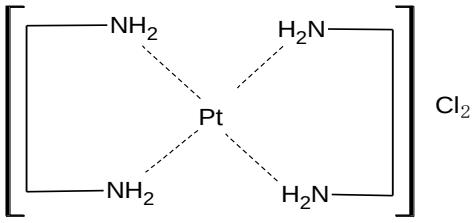

Figure 2. 16. Structure of a metal complex.

Literature, reviewed below, has reported the applications of chelating reagents in the flotation of chrysocolla ($(Cu,Al)_2H_2Si_2O_5(OH)_4 \cdot nH_2O$), goethite ($FeO(OH)$), hematite ($Fe_2O_3$), manganese dioxide ($MnO_2$), bastnaesite ($(Ce,La,Y)CO_3F$), malachite ($Cu_2CO_3(OH)_2$), cassiterite ($SnO_2$), phosphate minerals, oxidized copper, etc. The chelating reagents used include n-nitroso-n-phenylhydroxylamine salts, hydroxamate, dimethylglyoxime, benzoin oxime, benzohydroxamate, etc.

Peterson *et al.* (1965) found that with the addition of 3.3×10^{-4} M of potassium hydroxamate, complete flotation of 3 g of chrysocolla in 130 ml of deionized water was obatined at pH 6.0 and recovery was noted to decrease markedly above and below this pH. Peterson *et al.* (1965) proposed three possible reasons, i.e., hydrolysis of hydroxamate to hydroxamic acid, dissolution of chrysocolla, and lack of chemisorbed hydroxyl ions at the surface. The reaction mechanism proposed by Peterson et al. (1965) is shown in Figure 2.17.

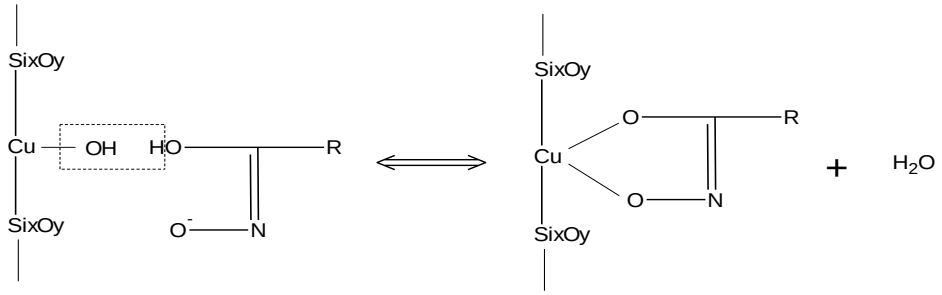

Figure 2. 17. Chemisorption of hydroxamate collector on chrysocolla surface. (Peterson *et al.*, 1965)

Fuerstenau *et al.* (1967) found similar flotation behavior for goethite with octanohydroxamate to that of chrysocolla, i.e., maximum flotation occurred at pH values corresponding to the maximum content of hydrolysis products of metal ions (see Figure 2.18). The reaction between goethite and hydroxamate is similar to that of

chrysocolla. The possible reasons for the lower recovery of goethite at acidic conditions are the hydrolysis of hydroxamate to hydroxamic acid or the lack of chemisorbed hydroxyl ions on the goethite surface.

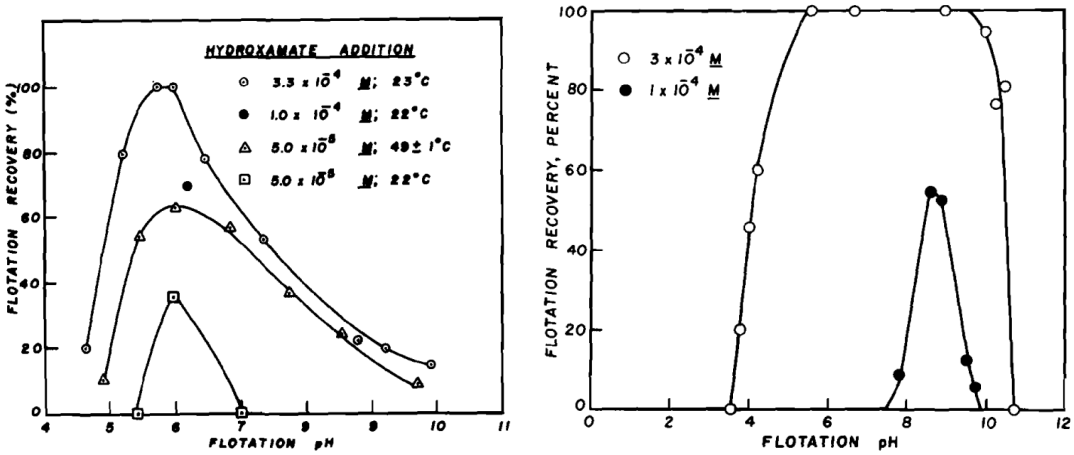

Figure 2. 18. Relationship between flotation recovery of goethite and pH. (a) Chrysocolla; (b) Goethite. (Fuerstenau *et al.*, 1967; Peterson *et al*., 1965)

Fuerstenau *et al.* (1970) used potassium octanohydroxamate to float hematite and found that the maximum recovery occurred at pH 8 to 8.5, which corresponds to the maximum concentration of hydrolysis products of iron (see Figure 2.19). Based on micro-flotation and FTIR tests, basic salts of metal collector are involved in the chemisorption process. Longer conditioning time enables more iron to dissolve from the mineral, therefore, flotation recovery is increased.

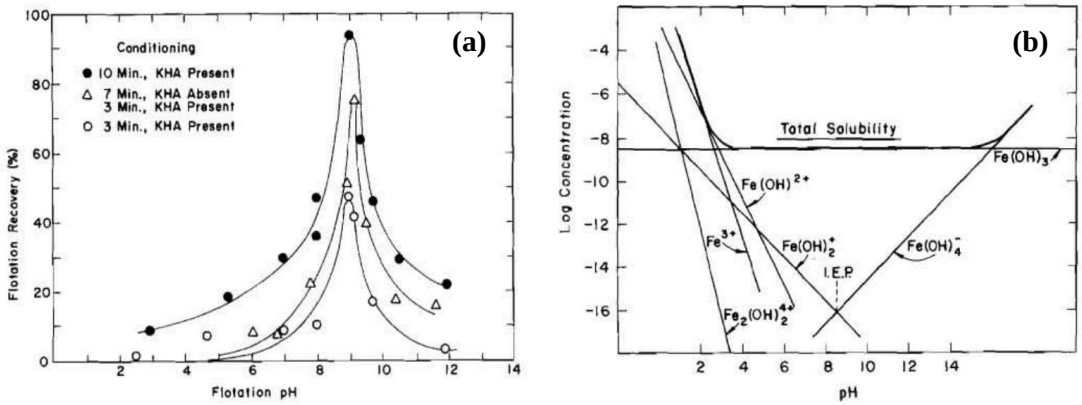

Figure 2. 19. Flotation of hematite with hydroxamate. (a) Relationship between pH and recovery; (b) Concentration of iron (III)-bearing species in equilibrium with solid hematite as a function of pH. (Fuerstenau *et al.*, 1970)

Raghavan and Fuerstenau (1975) studied the adsorption of octanohydroxamate on synthetic hematite. As shown in Figure 2.20, the results indicate that maximum adsorption occurs around pH 8.7, which corresponds to the PZC of the material, and increases in temperature significantly increased the adsorption. The *p*Ka of octyl hydroxamate is around 9; at pH 5.5 most of the hydroxamate should be in the form of hydroxamic acid. As such, the hydroxamic acid is considered to be the active species. A combination adsorption/surface reaction model is proposed (see Figure 2.21). Before monolayer adsorption, the reaction between surface –FeOH and hydroxamic acid occurs. After monolayer adsorption, the physical adsorption via hydrogen bonding or hydrophobic bonding between molecules occurs. When temperature is increased, the surface chelate formed has a greater tendency to displace iron from the surface sites and then interact with hydroxamic acid molecules in the vicinity of the surface to form 1:2 and 1:3 complexes. The increased adsorption at high temperature may also be due to the increased dissolution of the iron species, forming positively charged hydrolysis products which are likely to interact with hydroxamic acid and form basic ferric hydroxamates. Natarajan and Fuerstenau (1983) studied the adsorption of octanohydroxamate on manganese dioxide, and similar conclusions were proposed.

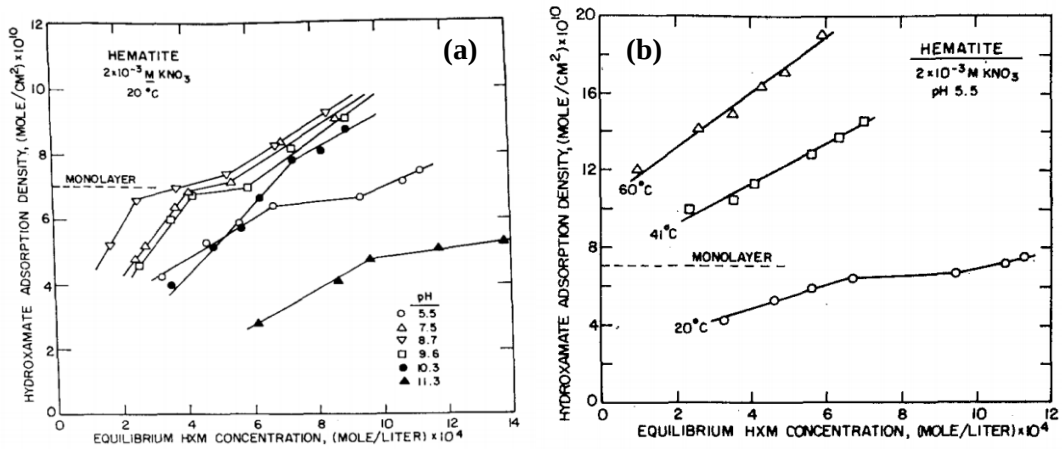

Figure 2. 20. (a) Adsorption isotherm at 20°C; (b) Adsorption isotherms at 60, 41, and 20°C. (Raghavan and Fuerstenau, 1975)

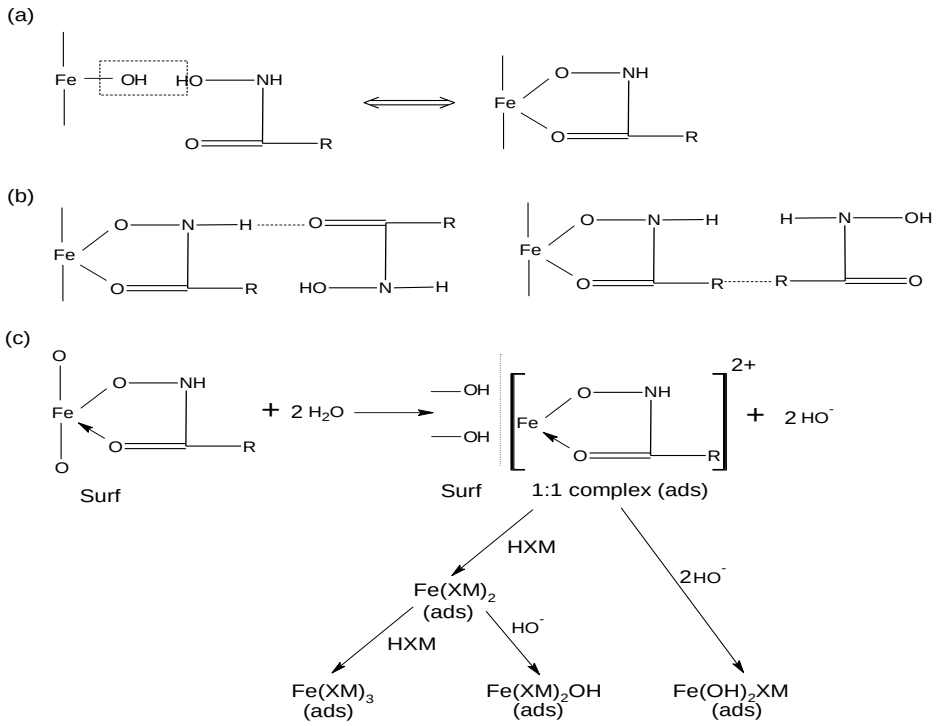

Figure 2. 21. Adsorption of hydroxamate on synthetic hematite surface. (a) Concentration below monolayer coverage; (b) Concentration over monolayer coverage; (c) At higher temperatures 60^{o}C.

Pradip and Fuerstenau (1983, 1985) systematically studied the adsorption of hydroxamate on semi-soluble minerals, including bastnaesite, calcite, and barite, and a surface reaction/chemisorption mechanism was proposed (Figure 2.22). Hydroxylation of the cations on the mineral surface assist surface reaction phenomena through first providing some surface atom movement. Re-adsorption of hydrolyzed species participate in surface reactions. Chemisorption occurs on the mineral surface through reaction between atoms coordinated in the surface crystal lattice and hydroxamate species. The reaction model is shown in Figure 2.23. Adsorption at elevated temperature exhibits increased uptake of potassium octanohydroxamate with temperature on barite, calcite, and bastnaesite.

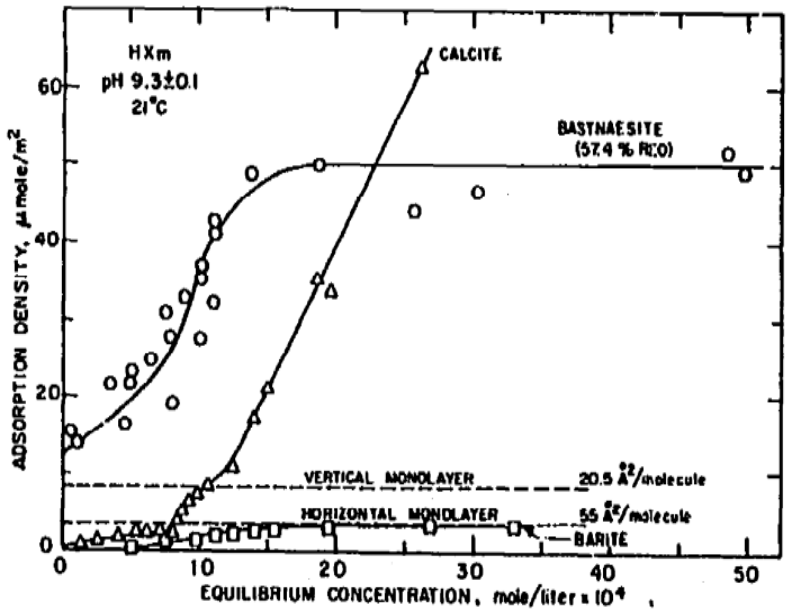

Figure 2. 22. Adsorption isotherm of hydroxamate on bastnaesite, calcite, and barite. (Pradip and Fuerstenau, 1983)

$$
\begin{array}{lll}
(Me^{2+}) & + OH^- & \rightarrow (MeOH^+) \\
(MeOH^+) & + OH^- & \rightarrow (Me(OH)_2) \\
(Me^{2+}) & + HCO_3^- & \rightarrow ((MeHCO3)^+) \\
(Me^{2+}) & + HXm & \rightarrow (MeXm^+) + H^+ \\
(MeOH^+) & + HXm & \rightarrow (MeXm^+) + H_2O \\
(Me^{2+}) & + Xm^{-1} & \rightarrow (MeXm^+) \\
(MeOH^+) & + Xm^{-1} & \rightarrow (MeXm^+) + OH^-
\end{array}
$$

Figure 2. 23. Surface reaction/chemisorption model. (Pradip and Fuerstenau, 1985)

Assis *et al.* (1996) studied the floatability of apatite, barite, quartz, gorceixite, micas, magnetite, limonite/goethite, calcite, and hematite using hydroxamate collector. The relative floatability of minerals was hematite < apatite, anatase < apatite, apatite < calcite, apatite < fluorite, siderite < calcite. The stability constants of metal/hydroxamate at 20 ^oC is Ca^{2+} 2.4, Fe^{3+} 11.4, Fe^{2+} 4.8; the solubility was hematite < apatite, anatase < apatite, apatite < siderite < fluorite < calcite. Therefore, the selectivity of minerals floated with hydroxamates depends on a balance between the

solubility of the mineral and the stability of the complex formed with the cations in the lattice.

Miller *et al*. (2001a, 2001b, 2011c) found that Cytec's collector Aero6493, a 30% alcoholic solution of hydroxamic acid, performs much better than traditional phosphate collectors (e.g., fatty acid/fuel oil). However, the reason for the improved efficiency has not been studied. A possible reason proposed is that the insoluble hydroxamic acid collectors selectively wet the mineral surface, while, specific chelation phenomena is not involved.

Hydroxamate collectors are also used together with xanthate to float mixed minerals of sulfide and oxide copper (Hanson and Fuerstenau, 1987; Fuerstenau *et al*., 2000; Lee *et al*., 2009; Hope *et al.*, 2012). Studies by Hanson and Fuerstenau (1987) indicated that octanohydroxamate, which strongly chelates copper ions in solution, will not adsorb on chalcocite (Cu_2S) unless the system is sufficiently oxidized to provide cupric ions at the mineral surface. Fuerstenau *et al.* (2000) assessed five different types of bidentate chelating reagents (N-O, O-O, S-N, S-S, and N-N) as collectors for both copper oxide and sulfide through contact angle measurements. The results indicated that potassium octanohydroxamate exhibits unusual potential for the flotation of copper oxide minerals. Lee *et al.* (2009) used n-octyl hydroxamate in conjunction with traditional sulfide collectors to float a blend of 70% sulphide ore and 30% oxide ore, the rougher scavenger copper recovery was as high as 95.5%.

Recently, studies pertaining to the adsorption of hydroxamate collectors on mineral surfaces via X-ray photoelectron spectroscopy, vibrational spectroscopy, Raman spectroscopy, and TOF-SIMS imaging have been reported (Cui *et al.*, 2012; Hope *et al.*, 2012; Ni and Liu, 2012; Buckley and Parker, 2013). Cui *et al.* (2012) found that hydroxamate treatment of Nd_2O_3 can form multilayers of Nd hydroxamate, but only after a conditioning time much longer than those used in flotation. Hope *et al.* (2012) studied the interaction of octanohydroxamate with chrysocolla and oxide copper surfaces by using vibrational spectroscopy and X-ray photoelectron spectroscopy, and

found that at low collector coverages, copper hydroxamate was formed at the mineral/collector interface. Multilayers were formed at higher concentrations, probably with minor (~15%) co-adsorption of hydroxamic acid. Ni and Liu (2012) found that octanohydroxamic acid adsorbs on calcite through weaker physical adsorption, while, strong chemisorption of the octanohydroxamic acid onto pyrochlore leads to a vertical head-on orientation. Buckley and Parker (2013) proposed that for hydroxamate adsorption onto iron oxide, the major chemisorbed species was bidentate hydroxamate, but at higher coverages, monodentate hydroxamate was also chemisorbed (see Figure 2.24).

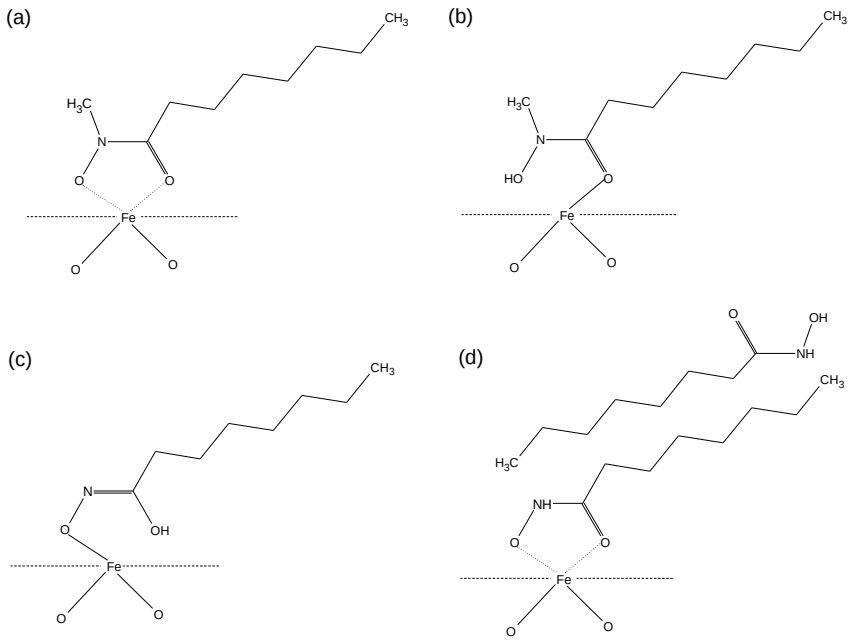

Figure 2. 24. Schematic structures of hydroxamate chemisorbed to Fe in oxide surface. (a) Bidentate; (b) Monodentate via O bonded to C; (c) Monodentate via O bonded to N; (d) Bidentate with co-adsorbed acid in keto form. (Buckley and Parker, 2013)

2.2.4 Surface and Bulk Precipitation

The precipitation reaction occurs when cations and anions in aqueous solution combine to form an insoluble ionic solid called a precipitate. For surface precipitation, the cations and anions involved in the reaction are in the interfacial region. The reaction is follows:

$$M_nA_m \leftrightarrow nM^{m+} + mA^{n-} \quad K_{sp} = [M^{m+}]^n[A^{n-}]^m \qquad \text{(Eq. 2.3)}$$

where M^{m+} and A^{n-} mean the cationic and anionic ions forming the precipitate M_nA_m; K_{sp} the solubility product of the precipitate.

The existence of an electrical potential at the solid-liquid interface will lead to preferential partitioning of oppositely charged counter-ions in the interfacial region. In such systems, under electrochemical equilibrium conditions, the activity in the interfacial region is related to that in the bulk by the equation (Ananthapadmanabhan and Somasundaran, 1985):

$$a_{i-s} = a_{i-b} exp \frac{\mu^0_{i-s} - \mu^0_{i-b}}{RT} \qquad \text{(Eq. 2.4)}$$

where a_{i-s} and a_{i-b} represent the activities of species *i* in the surface and bulk regions, respectively; and μ^0_{i-s} and μ^0_{i-b} represent the standard electrochemical potential of species *i* in the surface and bulk regions, respectively. The activity of a species can be higher in the interfacial region than in the bulk solution if favorable free energy changes accompany such a redistribution. Surface precipitation may predominate if the kinetics of release of metallic species are relatively slow.

It is difficult to distinguish bulk and surface precipitation. Generally, if active species accumulate in the interfacial region due to some favorable adsorption forces, surface precipitation will occur, otherwise, bulk precipitation will occur. In the absence of any favorable forces, both surface and bulk precipitation may occur simultaneously (Ananthapadmanabhan and Somasundaran, 1985; Pradip and Fuerstenau, 1983; Fuerstenau *et al*., 2000).

A classic example of bulk precipitation is the anionic collector flotation of semi-soluble minerals such as using oleic acid to float calcite ($CaCO_3$). Fuerstenau and Miller (1967) believed that the mechanism of fatty acid adsorption involves a specific chemical reaction between the collector and the surface, as follows:

$$CaCO_{3(s)} + 2\,RCOO^- \rightleftarrows Ca(RCOO)_{2(s)} + CO_3^{2-} \qquad \text{(Eq. 2.5)}$$

where $RCOO^-$ means the anions of fatty acid $RCOOH$.

Somasundaran (1969) proposed that below the PZC of calcite, oleate electrostatically adsorbed on calcite surfaces, while, above the PZC, oleate chemically adsorbed onto calcite surfaces. Bulk precipitation of calcium oleate was also be considered as a possibility, but only above about 4×10^{-5} M oleate (Figure 2.25).

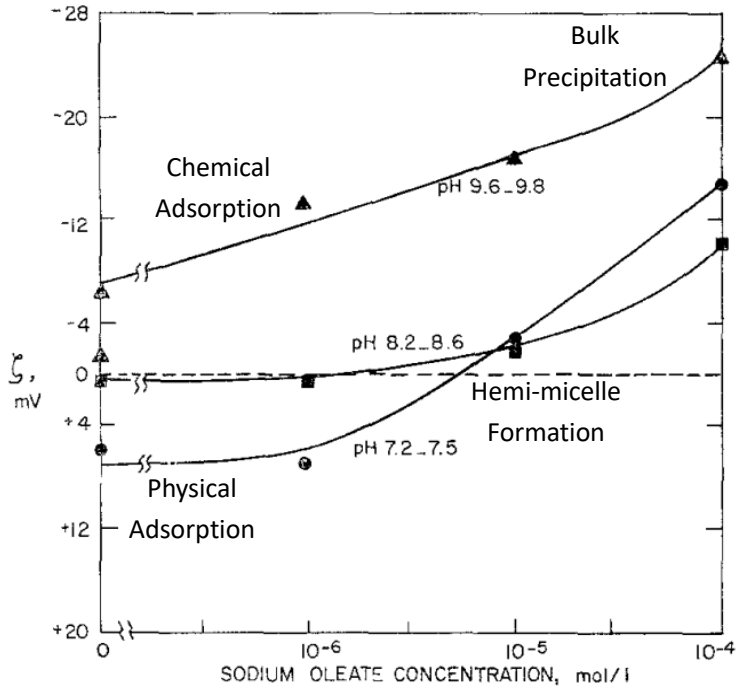

Figure 2. 25. Zeta potential of calcite as a function of sodium oleate concentration (initial) in solutions containing 10^{-3} M potassium nitrate as supporting electrolyte. (Somasundaran, 1969)

Antti and Forssberg (1989) used FTIR to study the adsorption of oleate onto calcite and found that at monolayer coverage a 1:1 calcium-oleate complex is formed via ion-exchange. Bulk precipitation of calcium oleate occurred after monolayer formation at pH 9, 10, and 11. Rao and Forssberg (1991) also obtained a similar conclusion. The ion-exchange reaction is as follows:

$$-\mathrm{CaOH} + \mathrm{RCOO^-} \rightleftarrows -\mathrm{Ca^+{}^-OOCR} + \mathrm{OH^-} \qquad \text{(Eq. 2.6)}$$

Young and Miller (2000) used in-situ Fourier infrared/internal reflection spectroscopy (FT-IR/IRS) with reactive internal elements (IREs) to study oleate adsorption at a calcite surface. Similar conclusions were obtained as in previous studies, i.e.,

chemisorption occurred at low oleate concentrations, while at higher oleate concentrations, surface precipitation of calcium dioleate predominated (Figure 2.26). In this case, the adsorption densities decreased with the increases in temperature due to surface passivation and increased solubility of calcium dioleate at 60 ^{o}C.

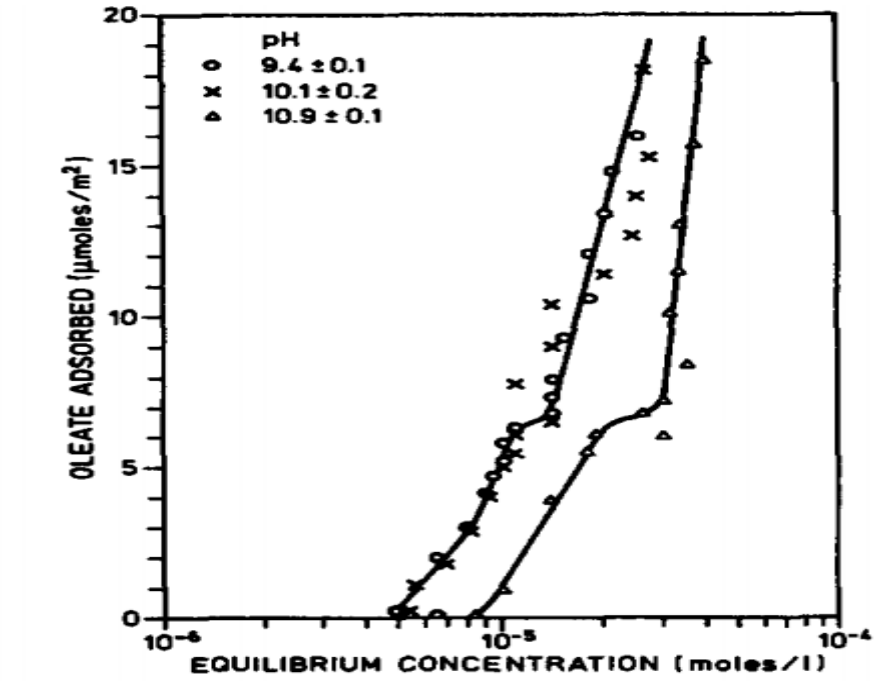

Figure 2. 26. Adsorption isotherms for oleate on calcite. (Young and Miller, 2000)

Overall, bulk precipitation occurred when the active metal atoms are pulled out of the crystal lattice via hydrolysis, and these hydrolysis species are readily released to the solution from the interfacial region.

The classical example of surface precipitation is the adsorption of multi-valent metal ions on silica. Figure 2.27 shows the adsorption of Co^{2+} at the silica surface as well as the species distribution of Co^{2+} in solution. Accordingly, in narrow pH ranges, Co^{2+} adsorption increases sharply, and near the pH ranges, the concentration of Co^{2+} reaches maximum. But these two ranges do not exactly coincide. Therefore, the adsorption cannot be simply explained with the “adsorption and hydrolysis” mechanism.

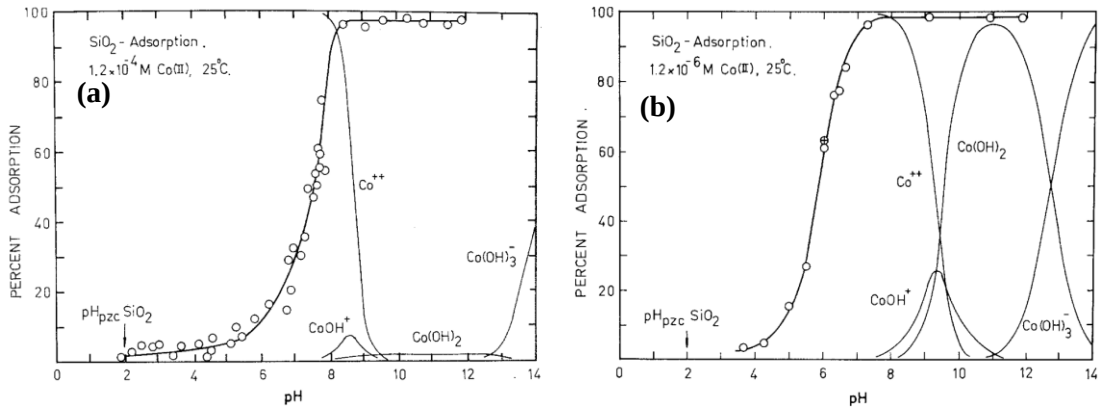

Figure 2. 27. Experimental adsorption isotherm for Co^{2+} adsorption at 1.2×10^{-4} M and 1.2×10^{-6} M on silica at 25ºC. Computed hydrolysis data for this concentration are also shown as the percentage of each aquo complex as a function of pH. (James and Healy, 1972)

Figure 2.28 shows a typical zeta potential dependence on pH and three charge reversals were observed. The first charge reversal pH (CR_1) corresponds to the point of zero charge of the mineral oxide. The second charge reversal occurs around the pH where the "adsorption" exhibits its sharp increase. The second charge-reversal point (CR_2) corresponds to the onset of surface precipitation of the adsorbate hydroxide on the original oxide surface. The third charge-reversal point (CR3) corresponds to the point of zero charge of the adsorbate hydroxide (Mackenzie and O'Brien, 1969; James and Healy, 1972a, 1972b, 1972c; Ananthapadmanabhan and Somasundaran, 1985). Before the onset of surface precipitation, electrostatic forces and hydrogen bonding induce the adsorption of metallic or hydrolyzed metallic ions (see Figure 2.29). James and Healy (1972c) reported that because of the quadratic dependence of solvation energy changes on the charge of the ion, this term decreases the adsorption of highly charges species. Due to the existence of electrical field in the interfacial region, the interfacial solubility product *Kc'* is smaller than the bulk solubility product K_c, therefore, surface precipitation occurs at lower pH values than bulk precipitation (James and Healy, 1972b). The equations describing the surface precipitation are as follows:

$$\log(K_c/K_c') = (G'_{Co^{2+}} + G'_{OH^-})/2.3RT \qquad \text{(Eq. 2.7)}$$

where G' represents the excess free energy of the ions in a medium where the electric field is not zero. The excess energy in joule/mole is:

$$G' = \frac{(ze)^2 N}{8\pi(r_{ion}+2r_w)\epsilon_0} \cdot \left(\frac{1}{\epsilon_i} - \frac{1}{\epsilon_b}\right) \cdot g(\theta) \qquad \text{(Eq. 2.8)}$$

where z is the charge on the ion; r_{ion} is the radius of ion; r_w is the radius of water; ϵ_i and ϵ_b are the dielectric constants of material in the interface and in bulk solution respectively; and $g(\theta)$ is the geometrical function.

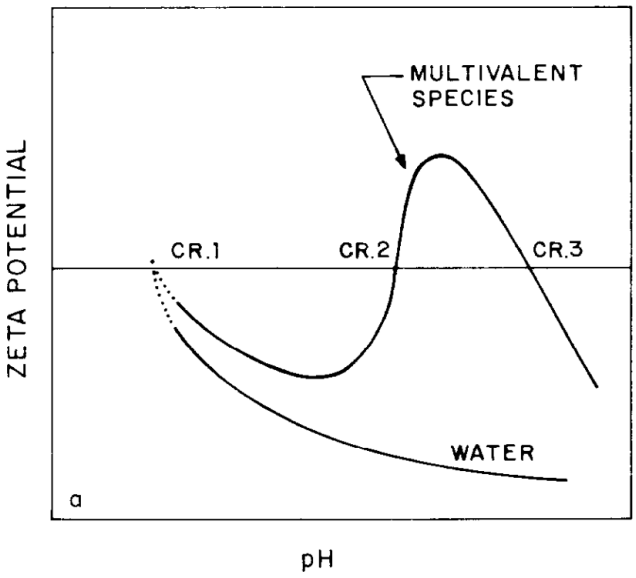

Figure 2. 28. Effects of multivalent species on zeta potential of silica.
(Ananthapadmanabhan and Somasundaran, 1985)

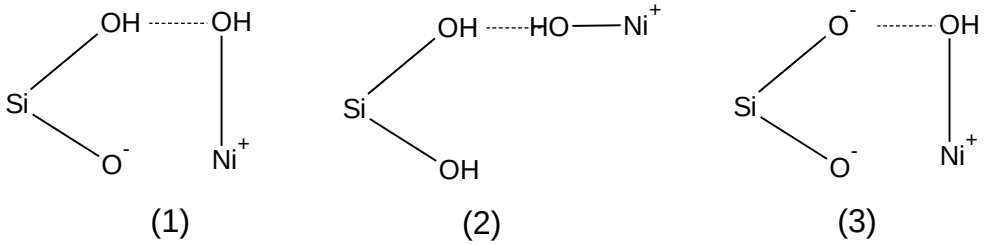

Figure 2. 29. Hydrogen bonding between hydrolyzed species of Ni and silica surfaces.
(Mackenzie and O'Brien, 1969)

2.3 EFFECTS OF SOLUTION SPECIES ON FLOTATION

Effects of solution species such as Ca^{2+} on flotation separation have been realized for many minerals such as silica, feldspar, pyrite, Cu-Zn sulfide, spodumene, etc. Both activation and depression effects of these solution species have been reported, which is dependent on the mineral characteristics, electrolyte concentration, pH, etc. The effects of solution species on monazite flotation have not been extensively studied. Ren *et al.*

(2000) observed significant depression of monazite in presence of 5×10^{-4} M potassium alum, which is attributed to the specific adsorption of hydrolyzed aluminum species.

Arnold and Aplan (1986) found that ions (e.g. Ca^{2+}, Mg^{2+}, Na^{+}, Cl^{-}, SO_4^{2-}) in the flotation pulp increase coal flotation recovery in the neutral pH range by thinning the hydrated layers around the surfaces of coal particles. Ca^{2+} and Mg^{2+} may also increase coal recovery by tying up the surface oxygen groups, rendering them less hydrophilic. However, Celik and Somasundaran (1986) found that Ca^{2+}, Fe^{3+}, and Al^{3+} depress coal flotation in the pH region corresponding to the formation of metal hydroxide precipitates (Figure 2.30). Surface precipitation and hydroxyl complex specific adsorption were considered as the adsorption mechanism. Li and Somasundaran (1993) reported that coal flotation was depressed at low NaCl concentrations (< 0.1 M), while, beyond that concentration, coal flotation was activated. Hydrophobicity of coal and attraction between coal and bubbles control coal flotation at low and high NaCl concentrations, respectively. Kurniawan *et al*. (2011) and Ozdemir *et al*. (2009) also found similar results at high salt concentrations and in addition to surface chemistry aspects, the increased recovery is also attributed to decreased bubble coalesce.

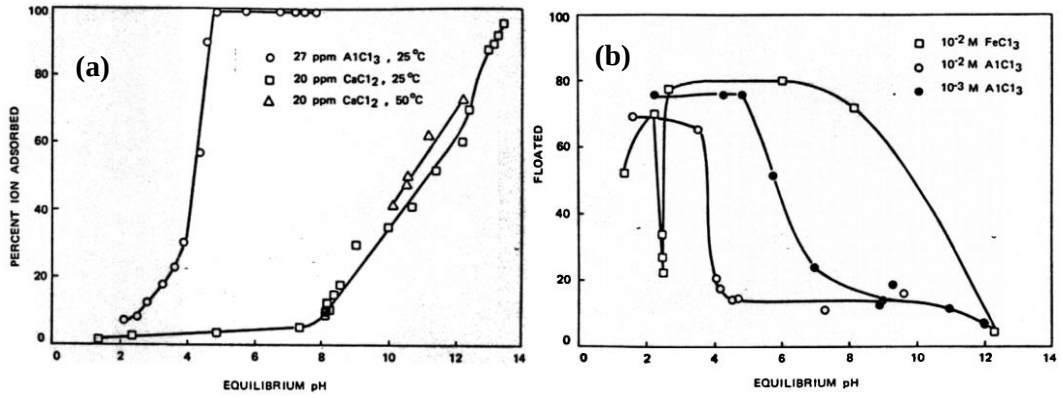

Figure 2. 30. (a) Abstraction of calcium and aluminum from coal; (b) Flotation of coal as a function of equilibrium pH in the presence of $FeCl_3$ and $AlCl_3$. (Celik and Somasundaran, 1986)

The activation effects of Ca^{2+}, Mg^{2+}, and Fe^{3+} on the flotation of spodumene ($LiAl(SiO_3)_2$) have been reported (Wang *et al*., 2007; Jie *et al*., 2014; Liu *et al*., 2015;). As shown in Figure 2.31, the spodumene recovery increased from around 20% to more

than 60% with the increases in Fe^{3+} concentration from 6×10^{-5} M to 1.6×10^{-4} M. The maximum flotation occurred at pH 7.1. X-ray electron spectrometer studies indicated that the Fe^{3+} could be adsorbed on the surface of spodumene in the form of iron oleate. Liu *et al.* (2015) proposed that chemisorption of oleate ions ($RCOO^-$ and $R(COO)_2^{2-}$) on the spodumene surface occurred via the formation of calcium and magnesium oleate with unsaturated Ca^{2+} and Mg^{2+} ions on the mineral surfaces.

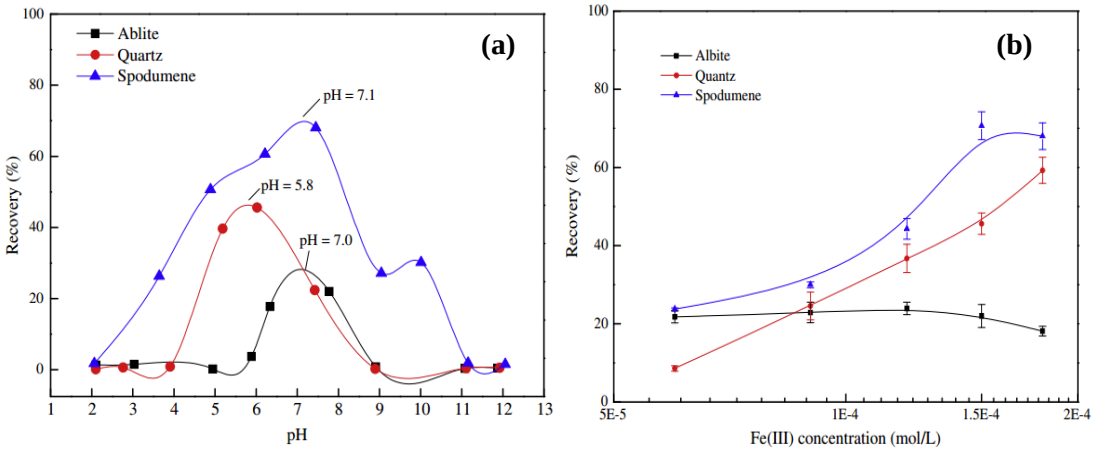

Figure 2. 31. (a) Flotation recovery of spodumene, albite, and quartz as a function of pH with 1.5×10^{-4} M Fe^{3+} and 2.0×10^{-4} M sodium oleate; (b) Flotation recovery as a function of Fe^{3+} concentration using 2.0×10^{-4} M sodium oleate at pH 6-7. (Jie *et al.*, 2014)

CHAPTER 3. MATERIAL AND METHODS

3.1 MATERIAL

3.1.1 Pure Minerals

Monazite pre-concentrate samples collected from a rare earth mine in China was purified using a shaking table and a high-gradient magnet. A monazite concentrate with high purity was obtained as determined by inductively coupled plasma mass spectrometry (ICP-MS) (Table 3.1). The X-ray diffraction Analyses indicated that monazite is the only major mineral in the sample (Figure 3.1). The 0.15x0.30 mm fraction of the concentrate was screened out and used for micro-flotation tests. A part of the concentrate was also ground into fine powder and used for electrokinetic and adsorption tests.

Table 3. 1 Elemental composition of the purified monazite sample.

Element	Ce	La	Nd	Th	Pr	Y	P
Content (%)	28.05	9.46	13.18	6.09	3.04	1.12	11.48

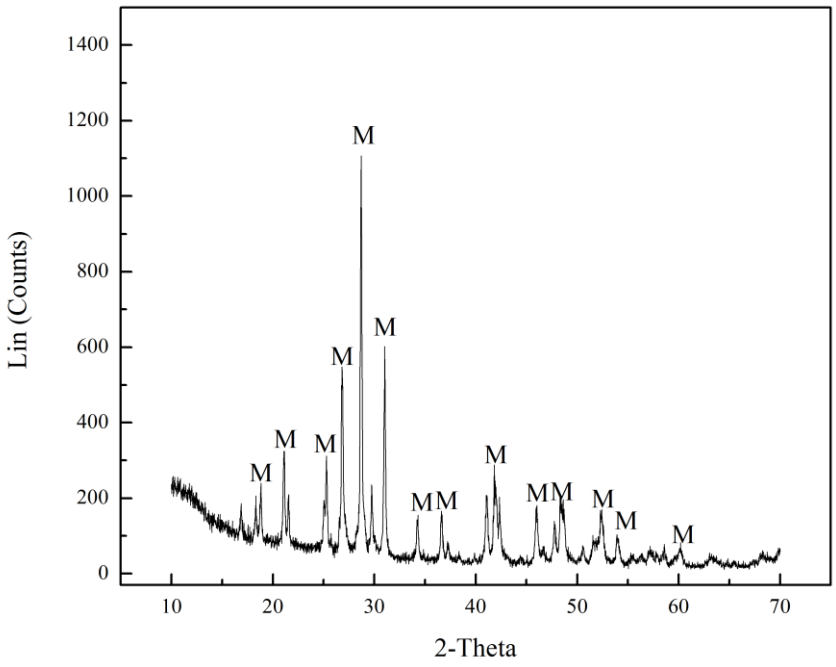

Figure 3. 1. XRD pattern of the purified monazite sample.

Chunk samples of calcite collected from a limestone mine located in Kentucky, USA, were crushed and ground to minus 300 μm. X-ray diffraction Analyses showed that calcite content in the sample was more than 95 % and, thus, it is directly used as a pure mineral. The pure minerals were used for micro-flotation, electrokinetic, adsorption and FTIR tests.

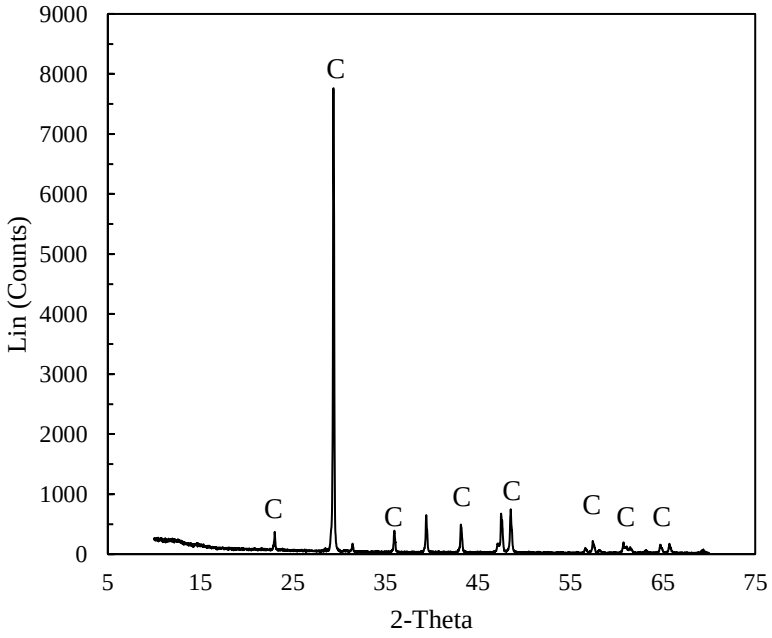

Figure 3. 2. XRD pattern of calcite (C) sample.

3.1.2 Chemicals

In the current study, octanohydroxamic acid was used as the monazite and calcite flotation collector. Hydroxamic acid is a typical kind of chelating reagent which can form stable chelates with metallic cations. Figure 3.3 shows the structure of an octanohydroxamic acid molecule. Methyl isobutyl carbinol (MIBC) was used as the flotation frother. Hydrochloric acid and sodium hydroxide solutions of appropriate concentrations were used as pH regulators. Potassium chloride solution of 1 mM was used as a supporting electrolyte for zeta potential measurement. Calcium chloride and sodium carbonate were used to study the effects of calcium and carbonate ions on octanohydroxamic acid D adsorption on monazite surfaces. Cerium chloride and phosphoric acid were used to study the role monazite lattice ions played in surface

charge development. Sodium silicate, sodium hexametaphosphate, citric acid, and ethylenediaminetetraacetic acid (EDTA) were used as regulators for monazite-calcite flotation separation. Details of the chemicals used in the present study are listed in Table 3.2.

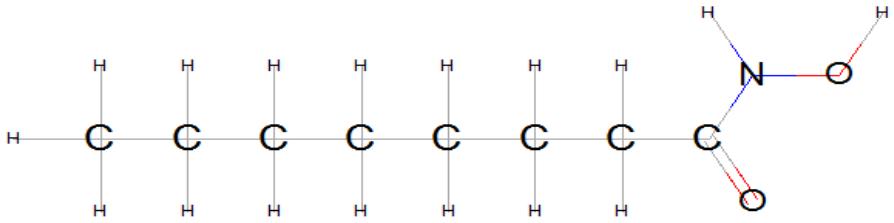

Figure 3. 3. Molecular structure of octanohydroxamic acid.

Table 3. 2 Details of the chemical used in the current study.

Chemical	Formula	Molecular Weight (g/mol)	Purity (%)	Source
Octanohydroxamic acid	$C_8H_{17}NO_2$	159.23	⩾95%	TCI America
Methyl Isobutyl Carbinol (MIBC)	$C_6H_{14}O$	102.17	⩾99%	Fisher
Hydrochloric acid	HCl	36.46	38.0% (w/w)	Fisher Scientific
Sodium hydroxide	NaOH	40.00	⩾97%	Fisher Scientific
Potassium chloride	KCl	39.10	⩾99%	Fisher Scientific
Calcium chloride dihydrate	$CaCl2 \cdot H_2O$	146.98	⩾99%	VWR
Sodium carbonate	Na_2CO_3	106.00	⩾99%	VWR
Iron (III) chloride hexahydrate	$FeCl_3 \cdot 6H_2O$	270.20	⩾98%	Sigma-Aldrich
Cerium chloride heptahydrate	$CeCl_3 \cdot 7H_2O$	372.48	⩾99%	VWR
Phosphoric acid	H_3PO_4	98.00	⩾85%	Fisher Scientific
Sodium silicate solution	$Na_2O \cdot nSiO_2$	NA	Technical	Fisher Scientific
Sodium hexametaphosphate	$(NaPO_3)_6$	611.77	Reagent	Fisher Scientific
Citric acid	$C_6H_8O_7$	192.12	⩾99%	VWR
EDTA	$C_{10}H_{16}N_2O_8$	292.24	⩾99%	VWR

3.2 EXPERIMENTAL DETAILS

3.2.1 Micro-flotation Tests

A 50 ml volume micro-flotation cell was used for the flotation tests (Fig. 3.4 and 3.5). Suspension of the particles was achieved using a magnetic stirrer. To reduce interference of carbon dioxide, air bubbles were produced by passing pure nitrogen through a porous frit. Conditioning was conducted in a glass beaker with one gram of pure minerals in a 50 ml solution. For combined mineral flotation tests, monazite was mixed with calcite with a mass ratio of 1:1. Solution pH values were initially adjusted followed by sequential addition of metallic cations, regulators, depressants, and collector with each conditioned for 5 min. Frother was added sequentially followed by 1 minute of conditioning. The solution pH values were measured and adjusted every 2.5 min during conditioning. Given that majority of the material was floated within the first 30 seconds, the initial pH values were considered to be more representative of the flotation conditions and reported in the present study. Difference in the pH values measured before and after each flotation test was typically 0.2 pH units.

During the flotation tests, the nitrogen flow rate was maintained at 55 ml/min while froth products were continuously removed over a period of 4 min. The concentrate and tailing samples were dried in an oven for 12 h and then cooled in a desiccator. Finally, flotation recovery values were calculated based on the product weights. For the mixed mineral flotation tests, monazite and calcite recovery values were calculated by using the assay values obtained from acid digestion. Three repeat tests were conducted under the same condition and the experiment error measured from the recovery data indicated a standard deviation value of 1.10 %.

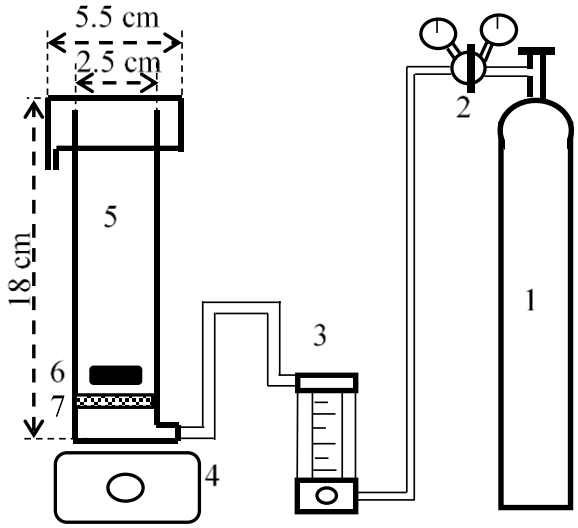

1-Nitrogen Tank; 2-Pressure Regulator; 3-Air Flowmeter; 4-Magnetic Stirrer; 5-Micro-flotation Cell; 6-Stirrer Bar; 7-Porous Material

Figure 3. 4. Schematic diagram of the micro-flotation apparatus.

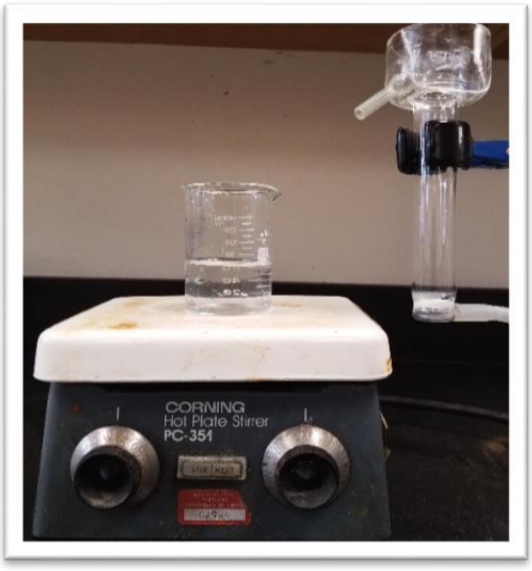

Figure 3. 5. Micro-flotation apparatus used for flotation tests.

3.2.2 Adsorption Tests

The purified monazite concentrate was ground to a mean diameter (d_{50}) of 3.50 μm (BET surface area 2.2513 m^2/g) using a mortar and pestle. The ground sample was used for the adsorption tests. The adsorption of octanohydroxamic acid on monazite under different conditions was evaluated by the abstraction from solution method, i.e.,

measuring the concentration difference of the collector in solution before and after adding the monazite powders. Adsorption tests were conducted in 50 ml homopolymer polypropylene bottles. For each test, monazite powder of 0.05 g was added into the bottle which contained 10 ml of collector solutions. pH value of the system was adjusted by adding hydrochloric acid and/or sodium hydroxide. After pH regulation, the slurry together with a magnetic stirring bar were sealed tightly in the bottle. Suspension of solid particles in the slurry was achieved by using magnetic stirrer with a constant rotating speed. After adsorption, the slurry was transferred into a centrifuge tube and centrifuged in an IEC Clinical centrifuge at 3175 rpm for 10 min. Octanohydroxamic acid concentration of the supernatant was determined using a Shimadzu 1280 UV-Vis spectrophotometer based on the ferric hydroxamate method and a calibration measurement of 503 nm (Natarajan and Fuerstenau, 1983; Raghavan and Fuerstenau, 1974). The overall adsorption test can be represented by Figure 3.6.

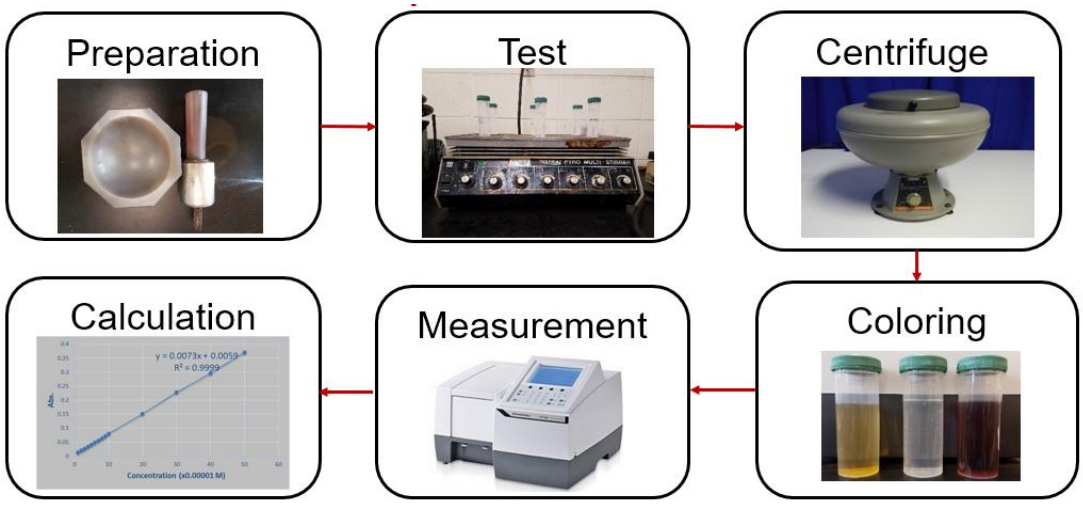

Figure 3. 6. Adsorption test procedures.

Feasibility of using the UV-Vis measurement to determine octanohydroxamic acid concentration in solution was also evaluated. Figure 3.7(a) shows that very good linearity existed between the absorbance and octanohydroxamic acid concentration in 0.1-1.0 mM range. To evaluate pH effects, absorbance of solutions with constant octanohydroxamic acid concentrations was measured at pH 3.0, 6.0, 9.0, and 11.0, respectively. As shown in Figure 3.7 (b), for a solution with less than 1 mM

octanohydroxamic acid, the effects of pH are minor, while the difference expands for higher concentrations. As such, when octanohydroxamic acid concentration is larger than 1 mM, dilution is needed to ensure the concentration is in 0.1-1.0 mM range.

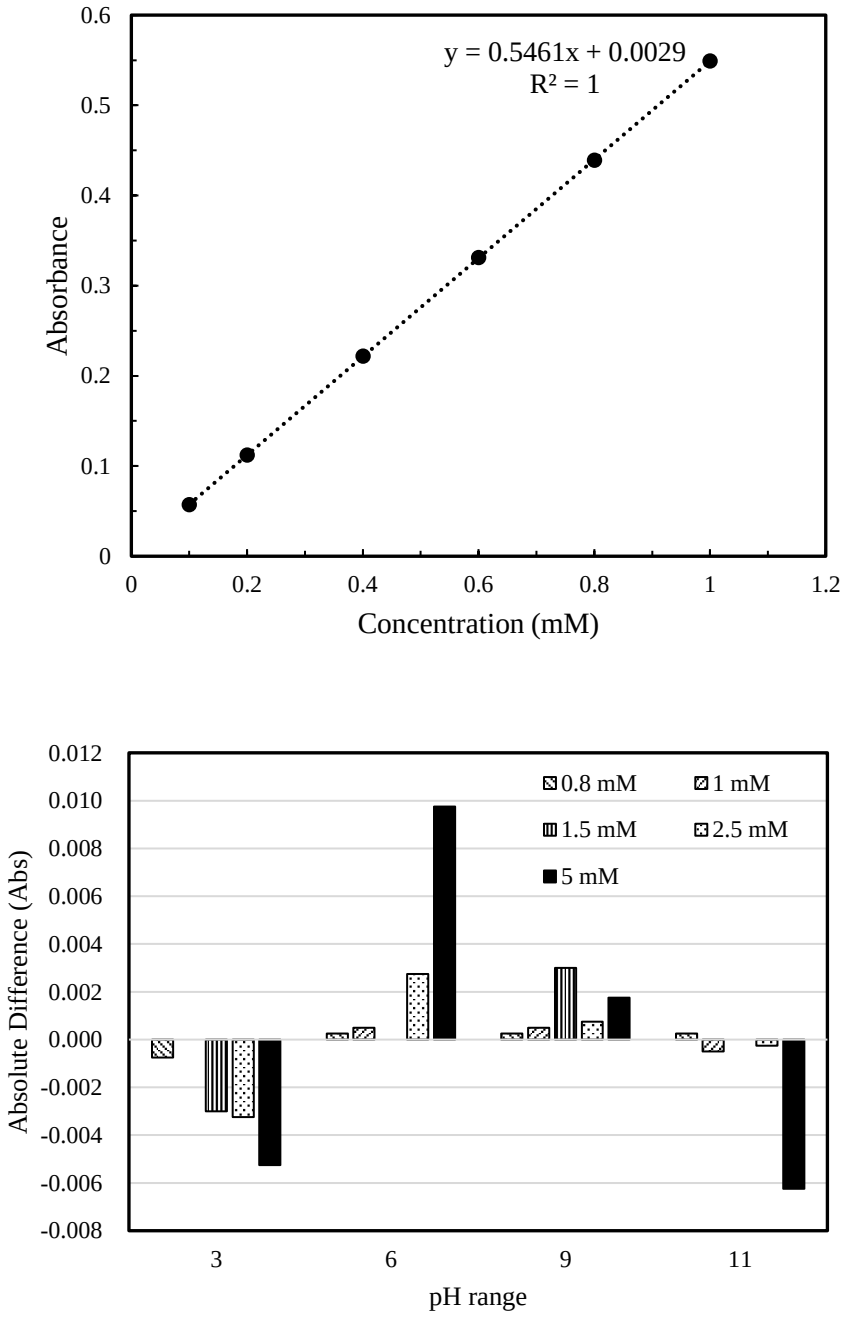

Figure 3. 7. Feasibility evaluation of using UV-Vis to determine octanohydroxamic acid concentration in solution: (a) linear regression of absorbance versus octanohydroxamic acid concentration; (b) absolute difference for the absorbance measured at different pH values and concentrations. (Absolute difference means the difference between absorbance measure at different pH values and the average value.)

The adsorption density (Γ, mg g^{-1}) of hydroxamic acid on monazite was calculated using the following equation:

$$\Gamma = \frac{(C_i - C_f) * V}{W}, \quad \text{(Eq. 3.1)}$$

where C_i and C_f represent the initial and final concentrations (mg L^{-1}) of octanohydroxamic acid in solution, respectively. V and W are the volume (L) of the solution and the weight (g) of monazite, with values of 0.01 L and 0.05 g, respectively. Three tests were conducted under the same condition and a standard deviation value of 0.11 mg g^{-1} was obtained.

3.2.3 Electrokinetic Tests

The mechanisms which give rise to the spontaneous separation of charge between two phases in contact are:

a. differences in the affinity of the two phases for electrons;
b. differences in the affinity of the two phases for ions of one charge or the other;
c. ionization of surface groups;
d. physical entrapment of non-mobile charge in one phase.

Mechanisms b and c are the main charging mechanisms of minerals in solution, which is classified in detail as follows:

a. preferential dissociation, such as silver iodide (AgI) in water, i.e., the dissociation of silver ion (Ag^+) to water is larger than that of iodide ion (I^-), and AgI surface carries negative charge;
b. preferential adsorption, such as scheelite in solution with an excessive amount of calcium (Ca^{2+}), i.e., scheelite surfaces will adsorb Ca^{2+} and carry a positive charge;
c. adsorption and ionization, such as silica in water;
d. crystal lattice ion displacement, such as clays, i.e., aluminum (Al^{3+}) displaced by Ca^{2+} and carries negative charge.

When mineral particles are put in water, the arrangement of charges on and near the

mineral surface is referred as the electrical double layer (EDL). The models used to depict the EDL include Holmholtz, Gouy-Chapman, Stern, etc. Figure 3.8 shows the Stern EDL model. As shown in the figure, the Stern layer is a compact region near the solid surface where adsorbed counter ions interact with the surface, while the diffuse layer, next to the Stern layer, is where remaining excess counter ions are distributed according to the Boltzmann distribution. The particles in the solution can be induced to move by applying an electric field across the system, which is called electrophoresis. The plane with which charges move together with the particle is called slipping plane. The potential at the slipping plane is referred to as zeta potential.

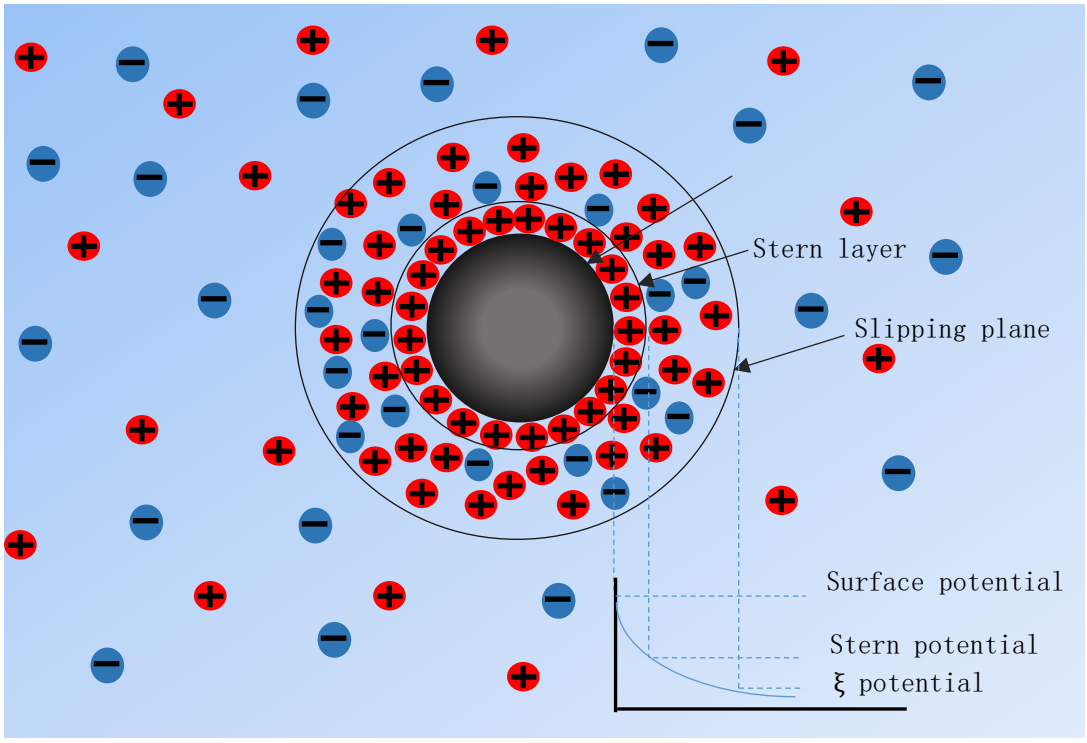

Figure 3. 8. Electrical double layer.

Within the EDL, indifferent ions electrically interact with particle surface. However, in addition to electrically interaction, specific interactions such as chemical adsorption and hydrocarbon chain association exist for some components. In this case, the potential distribution at the interface will change (see Figure 3.9). Therefore, electrokinetic studies are a good tool to investigate the interaction between chemicals and mineral surfaces.

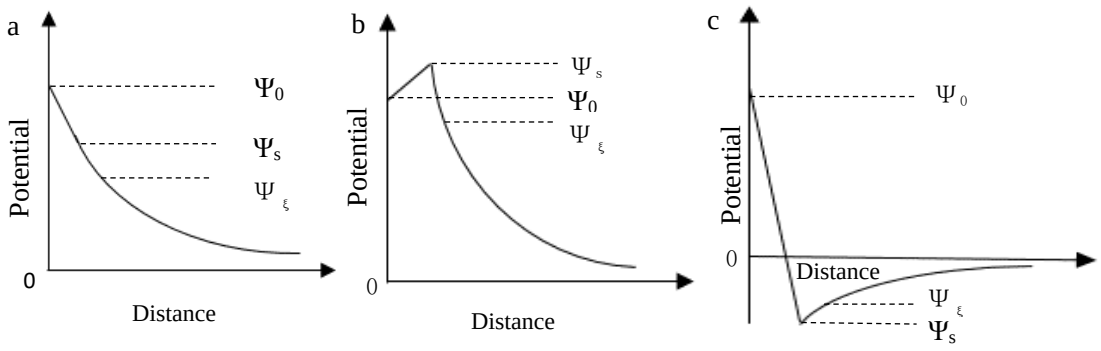

Figure 3. 9. Potential distribution within the EDL. (a) Particle surface without specific adsorption; (b) Specific adsorption of components carrying the same electrical sign; (c) Specific adsorption of components carrying the opposite electrical sign.

Samples used for the electrokinetic tests were the same as those used for the adsorption tests. For each experimental measurement, ground material in the amount of 0.02 g was mixed with 40 mL of supporting electrolyte solution (10^{-3} M KCl) in a 50 mL glass beaker. The suspension was placed into an ultrasonic bath for 1 min for particle dispersion. NaOH and HCl were used for regulating the solution pH to a predetermined value. After 5 min of conditioning, chemicals such as $CeCl_3 \cdot 7H_2O$ or phosphoric acid (H_3PO_4) of predetermined concentration were added based on the test purposes. The conditioning was conducted at 25 ^oC using a magnetic stirrer at constant rotating speed. Solution pH values were monitored during the process and the final pH values were reported in the current study. After conditioning, the suspension was collected and used for zeta potential measurement. Zeta potential was measured by using a ZetaPlus analyzer made by Brookhaven Instruments Corporation, which uses electrophoretic light scattering and the Laser Doppler Velocimetry method to determine particle electromobility (Figure 3.10). For the same condition, three times of measurement were conducted and the standard deviation was less than 1.5 mV.

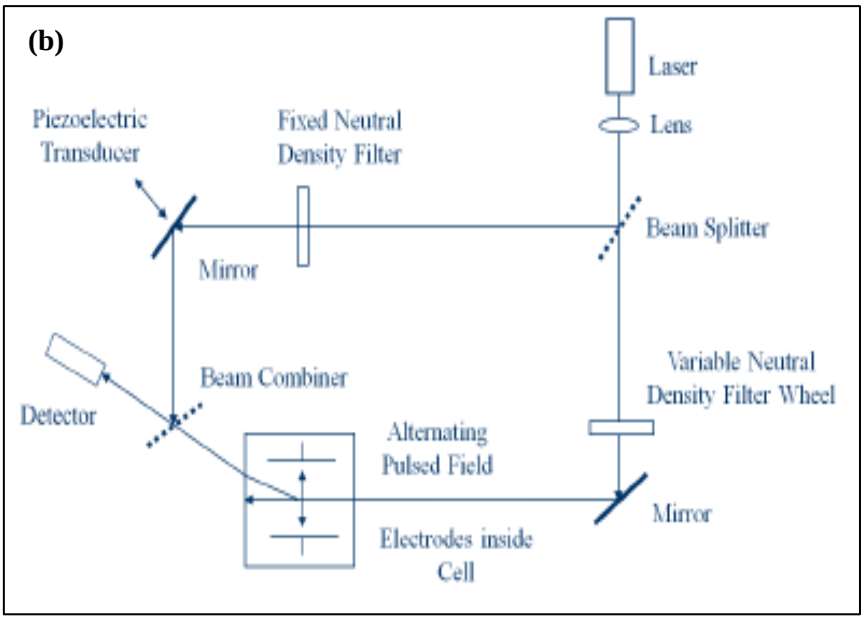

Figure 3. 10. Zetaplus zeta potential analyzer. (a) Equipment photo; (b) Schematic diagram.

3.2.4 Fourier Transform Infrared Spectroscopy (FTIR) Analyses

Fourier transform infrared spectroscopy (FTIR) is a technique used to obtain an infrared spectrum of adsorption, emission, photoconductivity, and Raman scattering of a solid, liquid, or gas. In infrared spectroscopy, infrared radiation is passed through a sample. Some of the infrared radiation is adsorbed by the sample and some of it is transmitted. The resulting spectrum represents the molecular adsorption and transmission. Each functional group has its unique adsorption peaks. For example, the characteristic peaks

of octyl hydroxamate are at 1650 cm^{-1} (amide I band), 3000 cm^{-1} (C-H stretching), 3250 cm^{-1} (N-H stretching), 1570 cm^{-1} (amide II band), 1000 cm^{-1} (C-H out of plane vibration), and 980 cm^{-1} (N-O stretching) (Fuerstenau *et al.*, 1970). Therefore, FTIR is useful to detect the mineral surface chemistry changes.

FTIR characterization was used for the following studies: i) adsorption mechanism of octanohydroxamic acid on monazite surfaces; ii) effects of calcium ions on octanohydroxamic acid adsorption on monazite surfaces. Pure monazite samples were ground to minus 2 μm using a mortar and pestle for FTIR tests to reduce light scattering. Conditioning procedures were similar to that used for adsorption tests. Based on the purposes of studies, corresponding chemicals were added during conditioning. After conditioning, the sample was centrifuged and supernatant was decanted followed by three stages of rinsing to remove any residual or physically-adsorbed collectors. Based on the fact that cerium is the main rare earth elements in monazite, cerium octanohydroxamate was synthesized by mixing cerium chloride with octanohydroxamic acid (1:3 molar ratio) in an acidic environment. Cerium oxide was synthesized by increasing the pH value of cerium chloride solution. FTIR analyses were conducted by using a Varian 7000e spectrometer which is based on the attenuated total reflection (ATR) method. The ATR crystal material used in the system is diamond. A few milligrams of mineral powders was placed directly on the optic window. The Analyses was conducted from 4000 to 700 cm^{-1} using 32 scans with a resolution of 4 cm^{-1}. The FTIR results were analyzed using the drawing and peak fitting tools of the Original software.

3.2.5 Titration Tests

The reaction between cerium and octanohydroxamic acid in solution was studied using titration tests which were conducted in a 100 mL beaker. Solutions of 50 mL and predetermined ingredients were first transferred into the beaker. The solution pH values were adjusted to 3.0 by using hydrochloric acid (25% v/w). Sodium hydroxide solution (10% w/w) was added into the solution to adjust the solution acidic/basic environment

and titration was stopped when solution pH value of 11.0 was reached. Mixing was achieved using a magnetic stirrer. The pH values corresponding to the amount of hydroxyl ions added were recorded continuously.

3.2.6 Batch Flotation Tests

Conventional flotation tests were conducted using a bench-top Denver flotation machine equipped with cells of different volumes. Slurry with 10% solid concentration was agitated for 1 min in the cell first to make it mixed thoroughly. Slurry pH values were adjusted using sodium hydroxide and hydrochloric acid. Octanohydroxamic acid (1.5 kg/ton) and MIBC (50 ppm) were added afterward followed by 5 min and 1 min of agitation, respectively. After conditioning, concentrate was floated for 20 min. The conditioning procedures for column flotation tests were same as that used for conventional flotation tests. The column flotation tests were conducted using a lab-scale column that was 2.5 m length and 5 cm diameter (Figure 3.11). Instead of running continuously, the tailings was reported back to the sump. Feed rate of 100 ml/min was used to get 60 min residence time for flotation. Froth zone depth of 15 cm was used to reduce the hydraulic entrainment. To produce concentrates with high REE content, multi-stages of flotation were tested using the flowsheet shown in Figure 3.12.

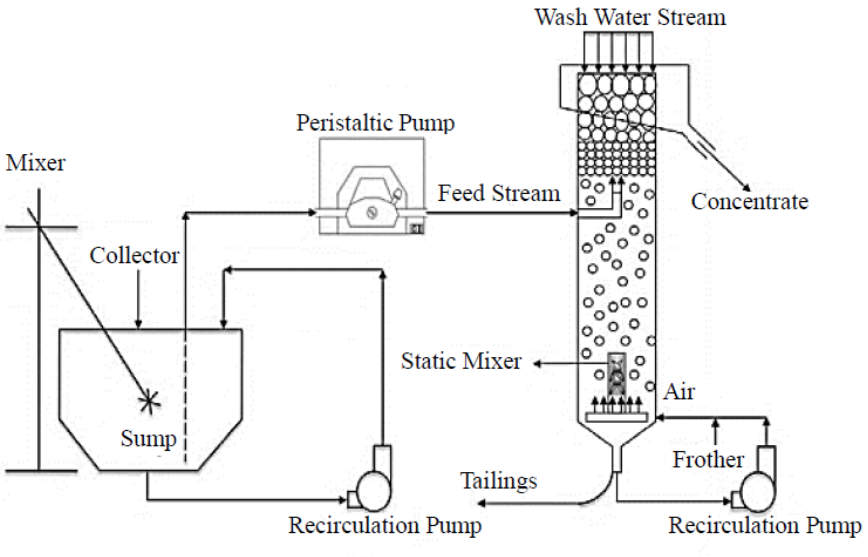

Figure 3. 11 Schematic diagram of the flotation column system used for REE recovery form Fire Clay fine refuse.

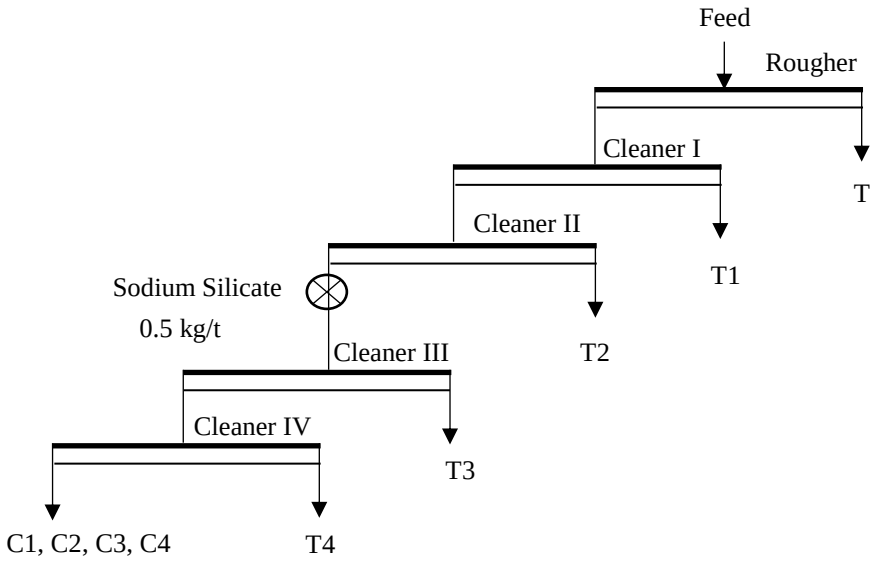

Figure 3. 12. Multi-stages column flotation test flowsheet for REE recovery from the Fire Clay fine refuse.

3.3 SOLUTION EQUILIBRIUM CALCULATION

A series of reactions including dissolution, precipitation, dissociation, association, and hydrolysis, etc., may occur when minerals and/or collectors are put in solution. In each reaction, distribution of the reactants and products can be described using the thermodynamic reaction constant. The overall system is also controlled by the mass conservation and the charge conservation laws. As such, activities and/or concentrations of all the species in a given system can be calculated.

In the current study, the solution equilibrium calculation is frequently used in different chapters for different purposes such as studying the surface charging mechanisms of monazite in aqueous solutions and the adsorption mechanism of octanohydroxamic acid on monazite surfaces. It is redundant to list all the details regarding those calculations. An example of solution equilibrium calculation is provided in this section. When Ce^{3+} is put in deionized water, a series of hydrolysis reactions will occur as described by the following equations:

$$Ce^{3+} + H_2O \leftrightarrows Ce(OH)^{2+} + H^+ \quad \text{(Eq. 3.2)}$$

$$Ce^{3+} + 2H_2O \leftrightarrows Ce(OH)_2^{+} + 2H^+ \quad \text{(Eq. 3.3)}$$

$$Ce^{3+} + 3H_2O \leftrightarrows Ce(OH)_{3(aq)} + 3H^+ \quad \text{(Eq. 3.4)}$$

$$Ce^{3+} + 4H_2O \leftrightarrows Ce(OH)_4^- + 4H^+ \quad \text{(Eq. 3.5)}$$

For each reaction, equilibrium was controlled by the reaction constant:

$$\beta_1 = \frac{[Ce(OH)^{2+}][H^+]}{[Ce^{3+}]} = 10^{-8.1} \quad \text{(Eq. 3.6)}$$

$$\beta_2 = \frac{[Ce(OH)_2^+][H^+]^2}{[Ce^{3+}]} = 10^{-16.3} \quad \text{(Eq. 3.7)}$$

$$\beta_3 = \frac{[Ce(OH)_{3(aq)}][H^+]^3}{[Ce^{3+}]} = 10^{-26.0} \quad \text{(Eq. 3.8)}$$

$$\beta_4 = \frac{[Ce(OH)_4^-][H^+]^4}{[Ce^{3+}]} = 10^{-38.0} \quad \text{(Eq. 3.9)}$$

As such, concentration of the hydrolyzed species can be expressed as:

$$[Ce(OH)^{2+}] = \frac{\beta_1[Ce^{3+}]}{[H^+]} \quad \text{(Eq. 3.10)}$$

$$[\mathrm{Ce(OH)_2^+}] = \frac{\beta_2[Ce^{3+}]}{[H^+]^2} \quad \text{(Eq. 3.11)}$$

$$\left[Ce(OH)_{3(aq)}\right] = \frac{\beta_3[Ce^{3+}]}{[H^+]^3} \quad \text{(Eq. 3.12)}$$

$$[Ce(OH)_4^-] = \frac{\beta_4[Ce^{3+}]}{[H^+]^4} \quad \text{(Eq. 3.13)}$$

The overall cerium concentration can be calculated using the following equation:

$$C_{total} = [Ce^{3+}] + [Ce(OH)^{2+}] + [\mathrm{Ce(OH)_2^+}] + \left[Ce(OH)_{3(aq)}\right] + [Ce(OH)_4^-]$$

$$= [Ce^{3+}] + \beta_1[Ce^{3+}]/[H^+] + \beta_2[Ce^{3+}]/[H^+]^2 + \beta_3[Ce^{3+}]/[H^+]^3 + \beta_4[Ce^{3+}]/[H^+]^4 \quad \text{(Eq. 3.14)}$$

As such, the concentration of Ce^{3+} can be calculated based on the total cerium concentration using the following equation:

$$[Ce^{3+}] = \frac{C_{total}}{1 + \beta_1/[H^+] + \beta_2/[H^+]^2 + \beta_3/[H^+]^3 + \beta_4/[H^+]^4} \quad \text{(Eq. 3.15)}$$

Cerium hydroxide precipitate may form based on

$$Ce(OH)_{3(s)} \leftrightarrows Ce^{3+} + 3OH^{-} \qquad \text{(Eq. 3.16)}$$

when the $[Ce^{3+}]$ reaches $10^{20.1}[H^{+}]^{3}$. In other words, the $[Ce^{3+}]$ is controlled by the solution pH values instead of total cerium concentration when precipitation occurs. Figure 3.13 shows the speciation diagram of Ce^{3+}-H2O system with 0.1 mM total cerium concentration. As shown in the figure, cerium hydroxide precipitate out at pH 8.23, causing decreases in the concentrations of hydrolyzed cerium species such as $Ce(OH)^{2+}$ and $Ce(OH)_2^{+}$.

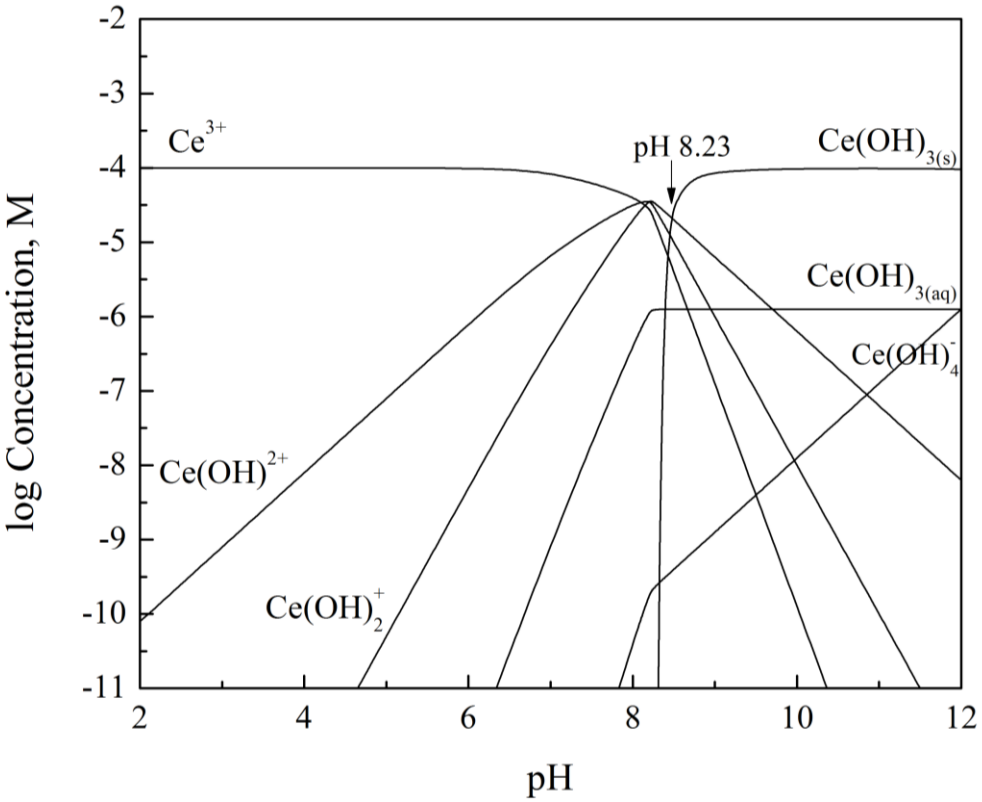

Figure 3. 13. Speciation diagram of 0.1 mM total cerium in H_2O.

CHAPTER 4. SURFACE CHARGES OF MONAZITE IN AQUEOUS SYSTEMS

4.1 ELECTROKINETIC TESTS

Hydroxyl and hydrogen ions can change surface charges by controlling surface group dissociation or surface hydrolysis (Parks, 1965; Quast *et al.*, 1987). Information about variations of surface charges with respect to pH values can be used to determine whether dissociation or hydrolysis occurs on the surface. The findings of the electrokinetic study revealed that the zeta potential of the monazite surface decreased by almost 60 mV when the solution pH value was increased from 3.0 to 9.5 (Figure 4.1), indicating that hydroxyl and hydrogen ions are potential determining ions for monazite surfaces. The IEP of monazite occurred at pH 6.0, which agreed with reported values in literature (Cheng, 1993).

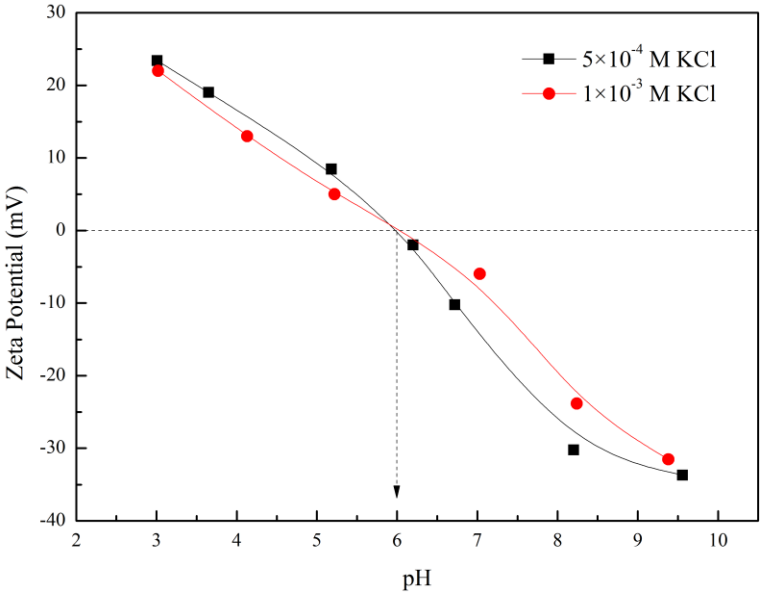

Figure 4. 1. Effects of pH on the electrokinetic properties of monazite using different concentrations of supporting electrolyte.

For some ionic minerals, especially those with high solubility, hydration of the surface ions may occur due to an ion-dipole interaction. When the total free energy changes for the lattice cations and anions are negative and different, preferential dissolution occurs and a surface charge is generated (Somasundaran, 1967; Bowden et al., 1977;

Veeramasuneni *et al.*, 1997). In this case, the surface charge can be regulated by adding lattice ions into solution.

Figure 4.2 shows the effects of adding Ce^{3+} and PO_4^{3-} on the zeta potential of monazite. At pH 6.0 and 9.0, the surface charge were increased significantly by 40 mV with an increase in the Ce^{3+} concentration from 0 M to 10^{-4} M. However, zeta potential remained relatively unchanged in a solution having a pH value of 3.0 for Ce^{3+} concentrations up to 10^{-4} M. Under a solution pH of 9.0, concentrations exceeding 10^{-4} M resulted in the formation of precipitates which varied the changing pattern of the zeta potential. At pH 6.0 and pH 3.0, decreases in the zeta potential at high concentration (10^{-2} M) were due to the increased electrolyte strength and the double layer compression. Relative to Ce^{3+}, the effects of the phosphoric species were minor (Figure 4.2(b)). Under the solution pH values studied, the changes in zeta potential were generally a slight reduction by an amount between 10 to 20 mV and the polarity remains unchanged.

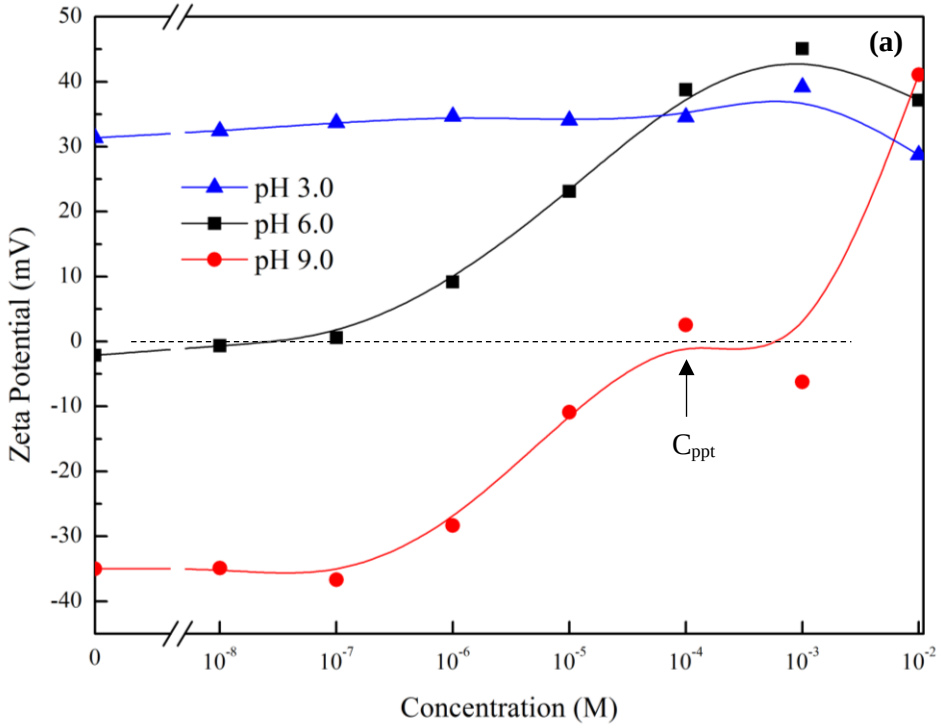

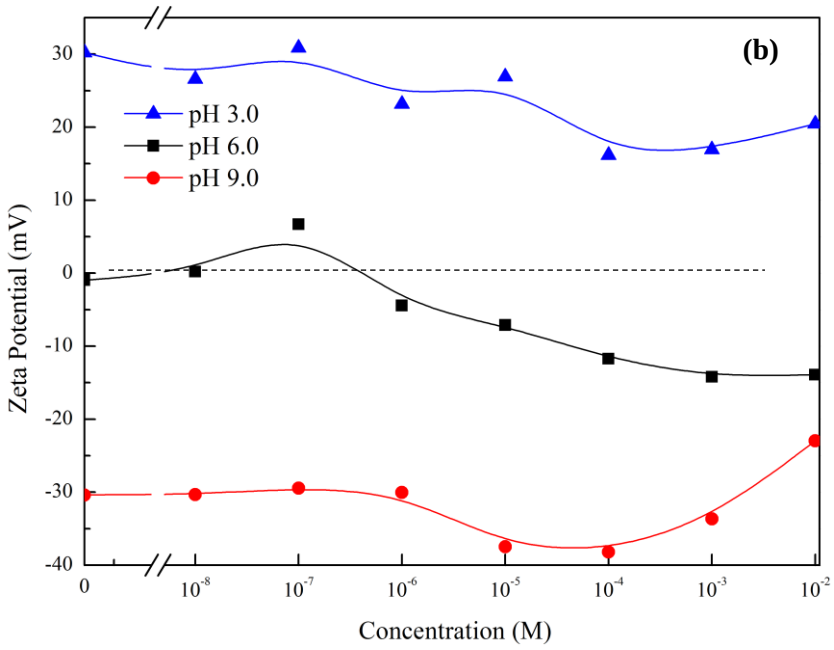

Figure 4. 2. Effect of Ce^{3+} and PO_4^{3-} concentration on the zeta potential of monazite at different pH values: (a) Ce^{3+} effects; (b) PO_4^{3-} effects.

The Ce^{3+} and PO_4^{3-} ions hydrolyze in solution and the different hydrolyzed species have different affinities for monazite surfaces. Figures 4.3(a) and 4.3(b) show the speciation diagrams of cerium and phosphate, respectively, at a concentration of 1×10^{-4} M in water. In basic and acidic environments, $Ce(OH)_{3(s)}$ and Ce^{3+} were dominant species, respectively. The concentrations of $Ce(OH)^{2+}$ and $Ce(OH)_2^+$ increased with pH and reached a maximum at around pH 8.0 before decreasing due to the precipitation of cerium ions. Based on the fact that significant charge changes were observed at higher pH values (e.g., 6.0 and 9.0), the possibility that Ce^{3+} regulated monazite surface charges through selective adsorption was excluded since more Ce^{3+} existed in solution at low pH values (Figure 4.3(a)).

Figure 4.2 (a) shows that when the cerium concentration increased from 0 M to 10^{-4} M, same zeta potential changes (about 40 mV) occurred for pH 6.0 and pH 9.0. As such, total charges carried by cerium species adsorbed onto monazite surfaces should be the same for the two pH values. The adsorption density (Γ) of chemicals on particle surfaces is positively correlated to the chemical concentration (C) in bulk solution, which can be represented using the following equation [Paria and Khilar, 2004]:

$$\Gamma = rCexp(\frac{-\Delta G^0_{ads}}{RT}) \quad \text{(Eq. 4.1)}$$

where r is the radius of the adsorbed ion. The charges (Γ_σ) achieved by monazite via adsorption can be calculated using the following equation:

$$\Gamma_\sigma = r \sum_i C_i z_i \, exp(\frac{-\Delta G^0_{ads}}{RT}) \quad \text{(Eq. 4.2)}$$

where C_i and z_i represent the concentration and charge of species *i* in bulk solution. Speciation diagram shows that $Ce(OH)^{2+}$ has the same concentration at pH 6.0 and 9.0 (Figure 4.3(a)). As such, it can be concluded that the effects of Ce^{3+} on the electrokinetic properties of monazite were due to its hydrolyzed species $Ce(OH)^{2+}$. Hydrolyzed products of the multi-valent cations were more likely to be adsorbed on the mineral surfaces due to smaller secondary solvation energies (Fuerstenau et al., 1965; James and Healy, 1972a, 1972b, 1972c). For the phosphate group, the dominant species over the solution pH values studied are mainly HPO_4 and $H_2PO_4^-$. Given that the hydrolyzed species are dominant, the possibility that cerium and phosphate ions are adsorbed onto the monazite surface and embedded in their lattice sites can be eliminated.

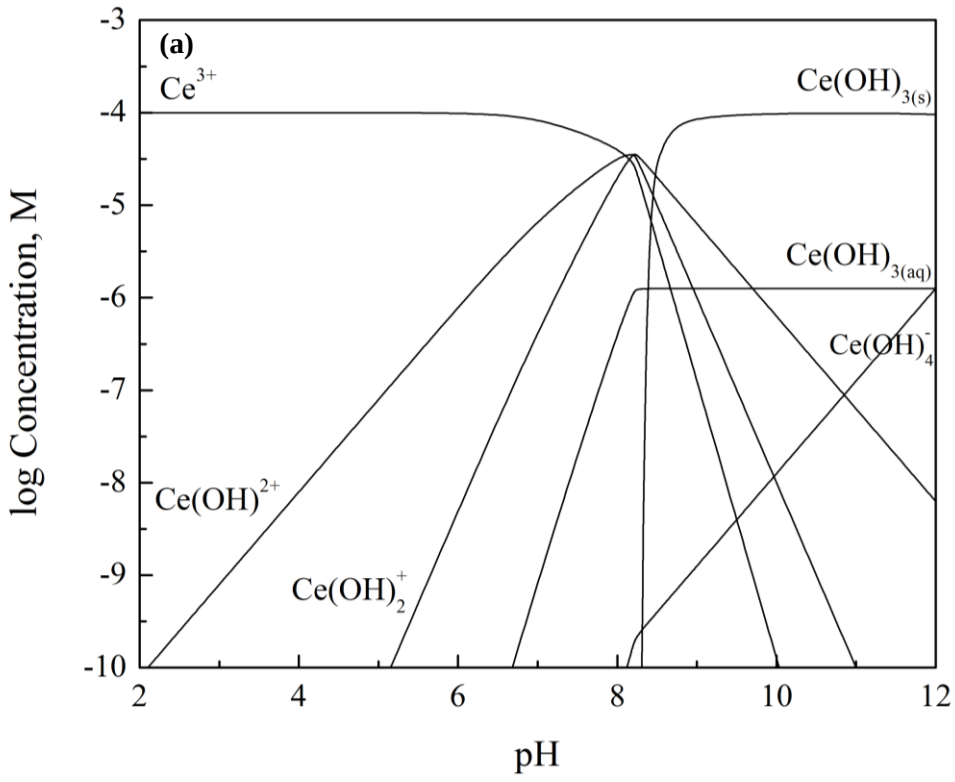

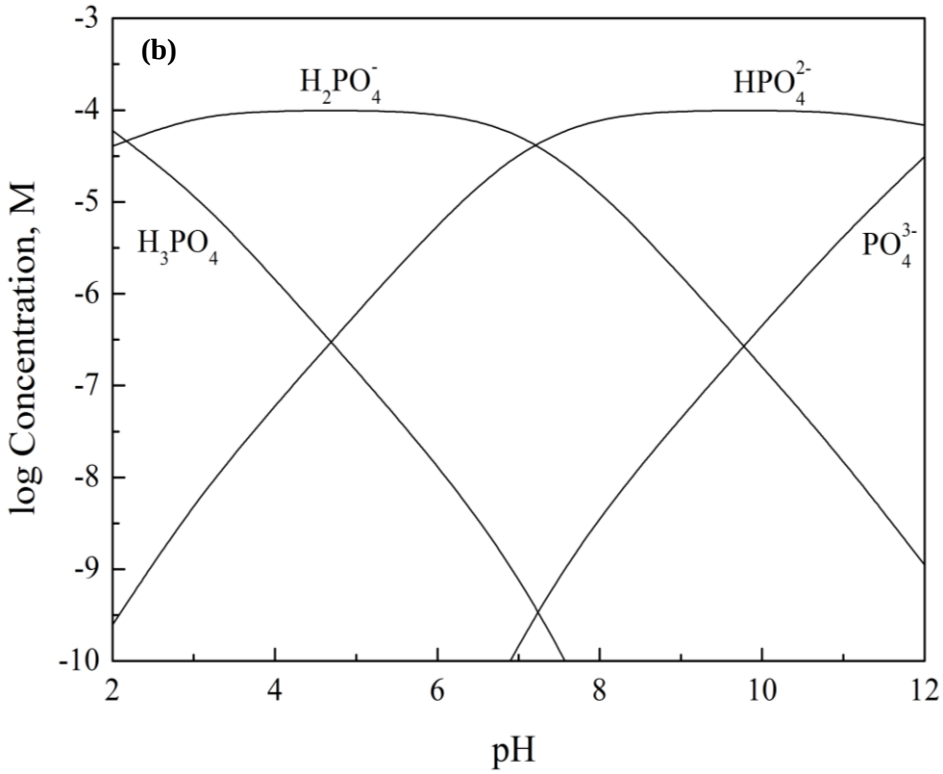

Figure 4. 3. Speciation diagrams of 0.1 mM (a) Ce^{3+} and (b) PO_4^{3-} in water.

4.2 SOLUTION EQUILIBRIUM CALCULATION

A solution equilibrium calculation was conducted for cerium monazite ($CePO_4$) -water in both closed (under vacuum) and open (under atmospheric pressure) systems. In the open system, the partial pressure used for carbon dioxide (CO_2) was $10^{-3.5}$ atm. In the closed system, the effect of carbon dioxide was not considered. Reaction constants used for the solution equilibrium calculation are shown in Table 4.1. The concentrations of solution species were calculated based on the solubility of monazite and mass conservation principle.

Table 4. 1 Reactions and reaction constants used for solution equilibrium calculation.

Reactions	Reaction Constants
$CePO_4 \leftrightarrows Ce^{3+} + PO_4^{3-}$	$10^{-24.3}$
$Ce^{3+} + H_2O \leftrightarrows Ce(OH)^{2+} + H^+$	$10^{-8.1}$
$Ce^{3+} + 2H_2O \leftrightarrows Ce(OH)_2^+ + 2H^+$	$10^{-16.3}$
$Ce^{3+} + 3H_2O \leftrightarrows Ce(OH)_{3(aq)} + 3H^+$	$10^{-26.0}$
$Ce^{3+} + 4H_2O \leftrightarrows Ce(OH)_4^- + 4H^+$	$10^{-38.0}$
$Ce(OH)_{3(s)} \leftrightarrows Ce^{3+} + 3OH^-$	$10^{-21.9}$
$Ce^{3+} + PO_4^{3-} \leftrightarrows CePO_{4(aq)}$	$10^{11.35}$
$Ce^{3+} + 2PO_4^{3-} \leftrightarrows Ce(PO_4)_2^{3-}$	$10^{18.48}$
$Ce^{3+} + HPO_4^{2-} \leftrightarrows Ce(HPO_4)^+$	$10^{4.32}$
$Ce^{3+} + 2HPO_4^{2-} \leftrightarrows Ce(HPO_4)_2^-$	$10^{7.25}$
$Ce^{3+} + H_2PO_4^- \leftrightarrows Ce(H_2PO_4)^{2+}$	$10^{1.92}$
$Ce^{3+} + CO_3^{2-} \leftrightarrows Ce(CO_3)^+$	$10^{7.56}$
$Ce^{3+} + 2CO_3^{2-} \leftrightarrows Ce(CO_3)_2^-$	$10^{12.19}$
$Ce^{3+} + HCO_3^- \leftrightarrows Ce(HCO_3)^{2+}$	$10^{2.44}$
$CO_{2(g)} + H_2O \leftrightarrows H_2CO_3$	$10^{-1.47}$
$H_2CO_3 \leftrightarrows HCO_3^- + H^+$	$10^{-6.35}$
$HCO_3^- \leftrightarrows CO_3^{2-} + H^+$	$10^{-10.33}$
$H_3PO_{4(aq)} \leftrightarrows PO_4^{3-} + 3H^+$	$10^{-21.72}$
$H_3PO_{4(aq)} \leftrightarrows HPO_4^{2-} + 2H^+$	$10^{-9.38}$
$H_3PO_{4(aq)} \leftrightarrows H_2PO_4^- + H^+$	$10^{-2.17}$
$HOl_{(l)} \leftrightarrows HOl_{(aq)}$	$10^{-7.6}$
$HOl_{(aq)} \leftrightarrows H^+ + Ol^-$	$10^{-4.95}$

Data sources: Kragten *et al.*1978, 1987; Lee *et al.* 1992; Cetiner *et al*. 2005.

The isoelectric point (IEP) calculation using solubility methods has been reported in literature (Parks and Bruyn, 1962; Somasundaran, 1967; Somasundaran *et al.*, 1985; Cheng, 2000). Based on the Poisson-Boltzmann equation, the electrostatic potential changes monotonously with respect to the distance from a plane near the particle surface to locations in the bulk solution when specific adsorption does not occurred (Hunter, 2013). Therefore, when the electrostatic potential at the slip plane equals zero, it is zero at any location in the region from the slipping plane to the bulk solution. The volume charge densities in all of these locations are zero, which means the total

concentrations of negative and positive charges are equal. The IEP value determined using this method usually corresponds to pH values under which the solubility of the solid was minimum (Beck, 1954; Parks and Bruyn, 1962; Somasundaran, 1967; Somasundaran *et al.*, 1985).

Figure 4.4 shows changes of positive and negative charge concentrations with respect to pH values in both closed (under vacuum) and open (under atmospheric pressure) systems. The pH value corresponding to an equal amount of positive and negative charges occurred at 7.2 and 4.5 in the closed and open system, respectively. Therefore, when measured under atmospheric pressure at 25 ^{o}C, the IEP of monazite is between pH 4.5 and pH 7.2. The lower IEP value obtained in the open system is mainly due to the appearance of HCO_3^- and CO_3^{2-} species. The dissolution of carbon dioxide depends on conditioning time, temperature, and pressure, etc. Therefore, the IEP value measured in the lab can vary in the range between pH 4.5 and pH 7.2 and, thus, partially explains the inconsistency of the data reported in literature and the discrepancy between the solution equilibrium calculation and the electrokinetc tests (pH 7.2 versus pH 6.0)

Minimum solubility of monazite was calculated to be between pH 7.0 and 9.0 in both closed and open systems (Figure 4.5). In the closed system, pH values corresponding to minimum solubility were close to the IEP of the bulk solution. However, in the open system, this agreement did not exist due to the effects of carbon dioxide dissolved in water. Oelkers and Poitrasson (2002) reported that the dissolution rate of natural monazite is around 10^{-18} ~ 10^{-17} mol/cm^2/s at 70 ^{o}C. Therefore, nearly 10^{-10} M of total cerium species is expected in solution when conditioning monazite in deionized water for 5 min in a closed system. The electrokinetic results indicated that the zeta potential of monazite was nearly constant at this concentration (see Figure 4.2(a)). Therefore, specific adsorption does not occur in this system and the point of zero charge (PZC) of monazite surface is pH 7.2.

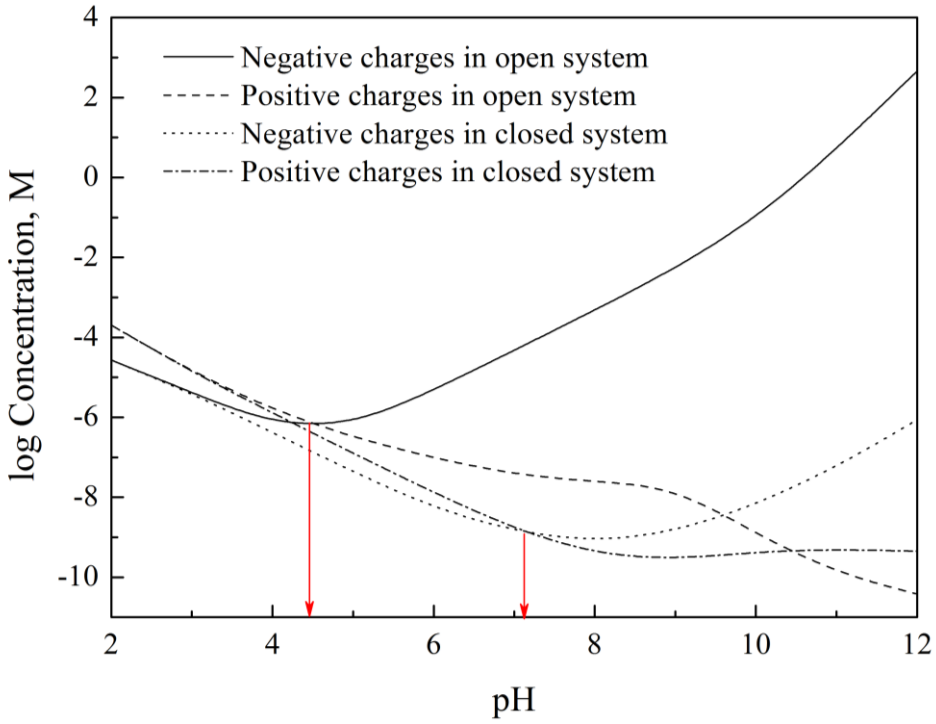

Figure 4. 4. Total concentration of positive and negative charges in bulk solution in closed and open systems at 25 ^{o}C.

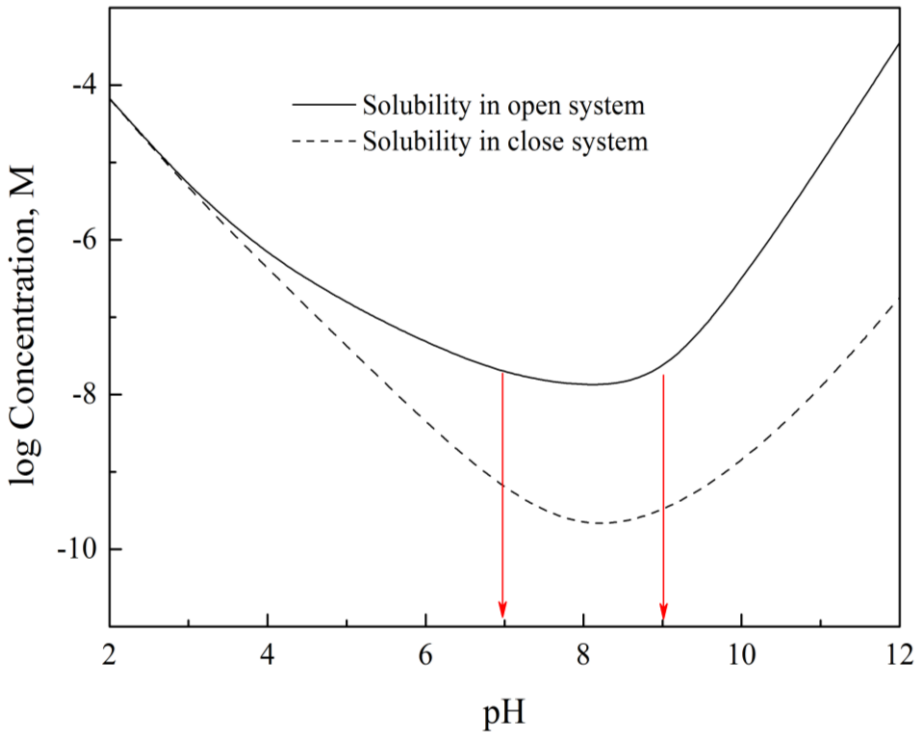

Figure 4. 5. The solubility of monazite at different pH values in both open and close systems at 25 ^{o}C.

The establishment of the surface charges of some minerals such as hematite and calcite

can be explained by the adsorption of the hydrolyzed species from solution (Parks and Bruyn, 1962; Somasundaran, 1967; Degen and Kosec, 2000). For example, the IEP of calcite is around pH 8.2, as determined using the speciation diagram of calcite in water. At pH 8.2, the concentration of the dominant species Ca^{2+} is close to that of HCO_3^-. Somasundaran and Agar (1967) concluded that Ca^{2+} and HCO_3^- are potential determining ions for calcite together with H^+ and OH^-. The surface charge of calcite is developed through preferential hydrolysis of surface ions or the adsorption at the interface of the complexes formed in solution.

Figure 4.6 showed the speciation diagram of monazite-water in a closed system. At pH 7.2 corresponding to the IEP, Ce^{3+}, HPO_4^{2-} and $H_2PO_4^-$ are the dominant species which seem to behave like potential determining ions. However, based on the fact that the electrokinetic properties remained constant after the addition of 10^{-8} M of cerium or phosphate, the role of the Ce3+, HPO_4^{2-}, and $H_2PO_4^-$ in determining surface charges onto the surface is barely detectable.

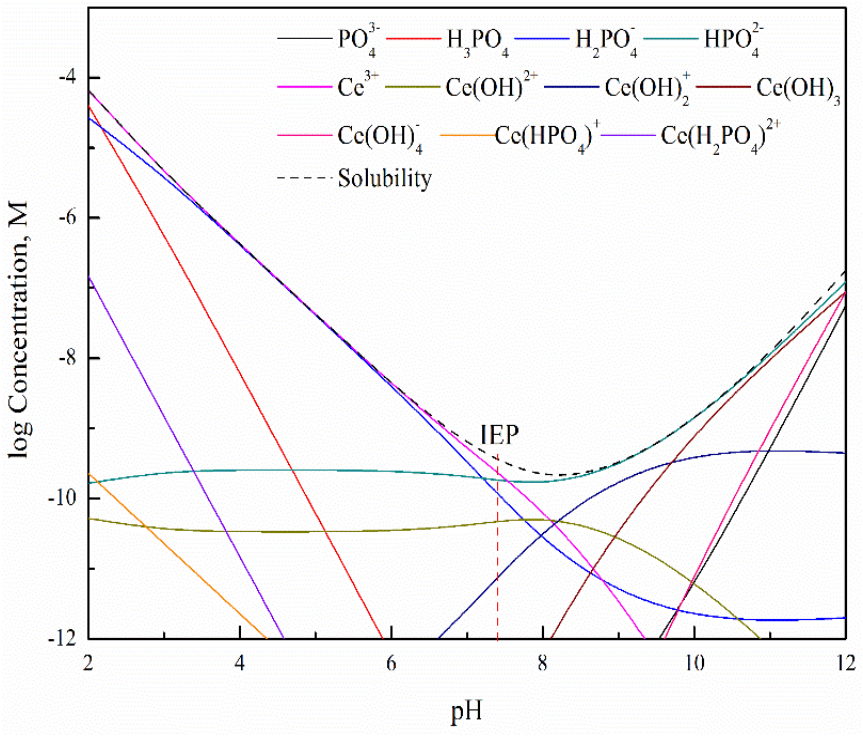

Figure 4. 6. The speciation diagram of monazite-water in the closed systems.

4.3 CRYSTAL STRUCTURE OF MONAZITE

An analysis of the crystal structure of monazite was conducted to identify the plane of weakness that will be exposed at the surface upon particle breakage. The monazite crystal occurs in the monoclinic space group with $P2_1/n$ settings. The rare earth atoms in monazite are surrounded by nine-coordinated oxygen atoms forming a polyhedral structure. The phosphate atoms are coordinated with four oxygen atoms forming a distorted tetrahedral structure. The polyhedral structures are connected by phosphate tetrahedrons forming polyhedron-tetrahedron chains. The chains are connected laterally by sharing polyhedral edges as shown in Figure 4.7 (Beall *et al.*, 1981; Mullica *et al.*, 1984; Ni *et al.*, 1995).

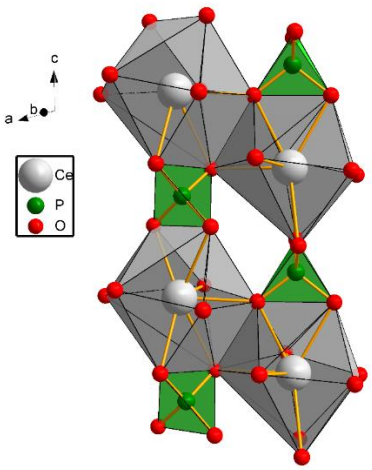

Figure 4. 7. Ball and stick structure of two conjoint polyhedral – tetrahedron chains.

All of the RE-O bonds are ionic dominated while the covalent fractions of P-O bonds are very high, namely, 29%-43% [Li *et al.*, 2007, 2009]. The lattice energies of the P-O bonds are nearly an order of magnitude larger than those of RE-O bonds. For example, in the $CePO_4$ crystal, the lattice energy of the P-O bond is around 6105 kJ/mole, while the Ce-O bond is only 591 kJ/mole. Therefore, when the crystal is crushed under pressure, minimum deformation of the P-O bond will occur while preferential breakage is likely along the Ce-O bond (Li *et al.*, 2007, 2009).

According to the crystal structure data, the cleavage planes occur either parallel to the

polyhedron-tetrahedron chains or across the polyhedrons. The tetrahedron plane is difficult to damage due to the strength of the P-O bond. Parker *et al.* (1937) statistically analyzed the persistence of the forms on monazite. Their findings indicate that the (100) plane has an unusually high persistence number of 97, indicating that cleavages are more likely to occur at the (100) plane. The (100) plane in the monazite crystal is parallel to the polyhedron-tetrehedron chain, which agrees with the crystalline data reported by (Li *et al.*, 2007, 2009).

Figure 4.8 shows the ball-stick and space fill model of the cleavage surface occurring at the (100) plane. Two types of Ce-O-P arrangements exist on the surface, which were labelled as Type-A and Type-B in Figure 4.8. For the Type-A, two Ce-O bonds of Ce atoms that are broken along with two O atoms connected with P are oriented outside each with one O-Ce broken bond. Type-B involves a Ce-O bond where the Ce is broken and one of the O atoms is connected with P oriented outside with one broken O-Ce bond. The schematic diagrams of the two arrangements were shown in Figure 4.9.

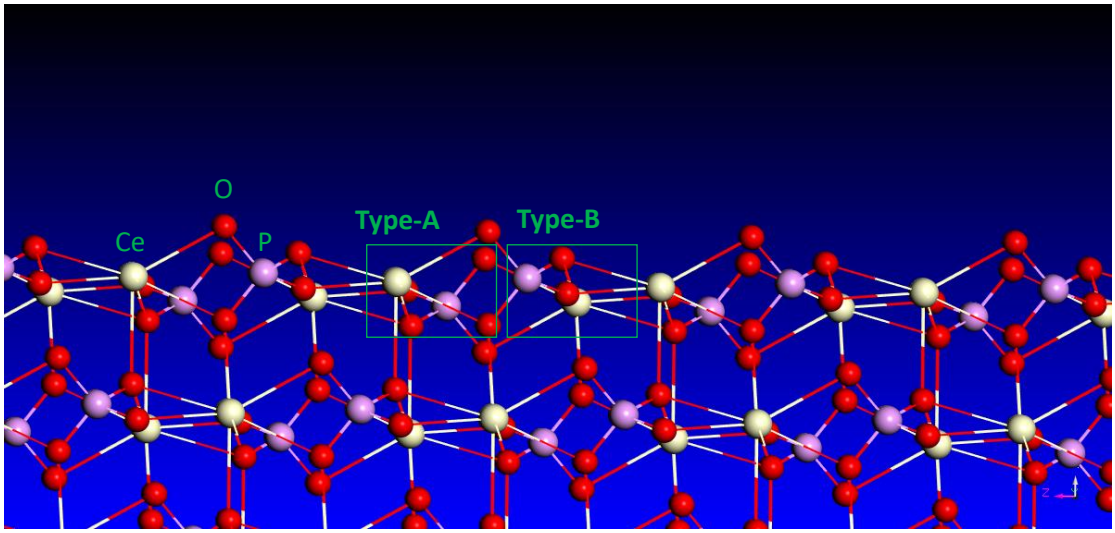

Figure 4. 8. The cleavage surface of monazite along the (100) plane.

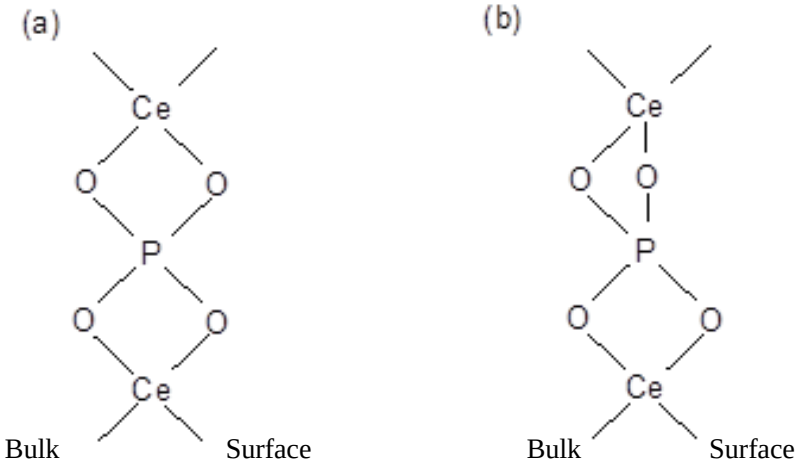

Figure 4. 9. The arrangement of surface atoms on the cleavage occurring on (100) plane (left sides represent bulk minerals).

4.4 ELECTROSTATIC MODEL PREDICTION OF (100) PLANE PZC

Surface hydration - amphoteric dissociation model has been used widely to explain the origin of the surface charge for oxides and hydroxides, including some complex oxides such as kaolinite and zircon (Parks and Bruyn, 1962; Yopps and Fuerstenau, 1964; Parks, 1965; Yoon *et al.*, 1979; Sverjensky, 1994). When oxide or hydroxide minerals are dispersed in water, surface hydroxides will form due to the unsaturated electronic charge of atoms with broken bonds. When the activity of the hydrogen ions (H^+) near the surface changes, either protonation or deprotonation can occur, i.e.,

$$\equiv \mathrm{SOH} + \mathrm{H}^+ \rightleftarrows \equiv \mathrm{SOH}_2^+ \qquad \text{(Eq. 4.3)}$$

$$\equiv \mathrm{SOH} \rightleftarrows \equiv \mathrm{SO}^- + \mathrm{H}^+ \qquad \text{(Eq. 4.4)}$$

where $\equiv \mathrm{SOH}$, $\equiv \mathrm{SOH}_2^+$, and $\equiv \mathrm{SO}^-$ represent species. The combined form of the above equation is

$$\equiv \mathrm{SO}^- + 2\mathrm{H}^+ \rightleftarrows \equiv \mathrm{SOH}_2^+ \qquad \text{(Eq. 4.5)}$$

and the surface charge of oxides and hydroxides is controlled by the degree of protonation of surface species $\equiv \mathrm{SO}^-$. The intrinsic constant of the above reaction is

$$K_{int.,H^+,k} = \frac{[\mathrm{SOH}_2^+]}{[\mathrm{SO}^-][\mathrm{H}^+]^2} \qquad \text{(Eq. 4.6)}$$

The $[SOH_2^+]$ equals $[SO^-]$ when the surface charge equals zero and the above equation could be rearranged as

$$K_{int.,H^+,k} = [H^+]^{-2} \quad \text{(Eq. 4.7)}$$

The relationship between PZC and intrinsic constant can be written as

$$PZC = 0.5 \log K_{int.,H^+,k} \quad \text{(Eq. 4.8)}$$

When the cleavage (100) plane is placed into water, both the cerium oxygen and phosphate oxygen sites will be hydrated. The number of hydroxyl groups connected to cerium is determined by the number of broken bonds. The information about the hydrated species and site densities on the surface are listed in Table 2. Electrical charges of cerium cations with broken bonds were calculated using Paulings' bond valence theory. Because 40% of the P-O bonds are covalent, the charges of the oxygen anions connected to phosphate and cerium are difficult to determine.

Table 4. 2 The hydrolyzed surface species and site densities on the cleavage occurring on (100) plane.

Hydrolyzed surface species	Site density (sites/nm^2)
$\equiv Ce^{\frac{2}{3}+}O^{2-}H$	4.41
$\equiv Ce^{\frac{1}{3}+}O^{2-}H$	2.20
$\equiv Ce^{\frac{2}{3}+}PO^{x-}H$	2.20
$\equiv Ce^{\frac{2}{3}+}Ce^{\frac{1}{3}+}PO^{x-}H$	2.20
$\equiv Ce^{\frac{1}{3}+}PO^{x-}H$	2.20

For the cerium oxygen sites, the point of zero charge, which is corresponds to the solution pH value providing an equal number of positive and negative surface sites, can be calculated via the electrostatic-based approach. Kossiakoff and Harker (1938) suggested that, in the ionization process of inorganic acids, the free energy changes (ΔG) associated with the removal of H^+ ions from acid molecules to a water molecule can be divided into several steps, i.e., 1) broken O-H bond in the acid molecule (ΔG_1), 2) formation of the O-H bond in H_3O^+ (ΔG_2), 3) removal of the proton from the

electrostatic field of the anion (ΔG_3), 4) reorientation of the water molecules (ΔG_4) and 5) compression of the water molecules (ΔG_5). Based on the fact that ΔG_1, ΔG_2, and ΔG_5 are constant, and ΔG_3 and ΔG_4 are included in the potential change accompanying the proton transfer, the ΔG is given as

$$\Delta G = \Delta G_{potential} + \Delta G_{constant,} \quad \text{(Eq. 4.9)}$$

The protonation of the surface species $\equiv SO^-$ can be regarded as the reverse process of ionization, i.e., two H^+ ions are removed from a H_3O^+ to the surface. For simple oxides, Parks and Bruyn (1962) developed the following expression:

$$PZC = A - B\left(\frac{Z_S}{R}\right) \quad \text{(Eq. 4.10)}$$

$$A = \frac{2e^2}{2.3kT\epsilon r_2} - \frac{\Delta G_{constant}}{4.6kT} \quad \text{(Eq. 4.11)}$$

$$B = \frac{e^2}{2.3kT\epsilon} \quad \text{(Eq. 4.12)}$$

Yoon *et al.* (1979) replaced the formal charge of cation in the equation by Pauling' bond valence and obtained another form of the equation:

$$PZC = A - B\left(\frac{s}{R}\right) - 0.5log\frac{2-s}{s} \quad \text{(Eq. 4.13)}$$

where s and R mean the bond valence of metallic cation and the distance between metallic cation and hydrogen ion. The bonds in the Al_2O_3 and MgO crystals are considered to be completely ionic bonding. Both of them obtained constant values of A and B using the information of these two crystals. Therefore, these equations are limited to the crystal involving covalent bonding such as silica, which requires crystal field corrections. However, for monazite crystals, cerium oxygen sites are completely ionic bonds, and the free energy changes of their amphoteric dissociation are similar to that of Al_2O_3 and MgO. Therefore, the following equation applies:

$$PZC_{Ce^{\frac{2}{3}+}O^{2-}H} = 18.43 - 53.12\left(\frac{2}{3}\times\frac{1}{3.55}\right) - 0.5\,log\frac{2-2/3}{2/3} = 8.30 \quad \text{(Eq. 4.14)}$$

$$PZC_{Ce^{\frac{1}{3}+}O^{2-}H} = 18.43 - 53.12\left(\frac{1}{3}\times\frac{1}{3.55}\right) - 0.5\,log\frac{2-1/3}{1/3} = 13.09 \quad \text{(Eq. 4.15)}$$

The combined PZC of cerium oxygen sites can be calculated based on the atomic fraction on the surface,

$$\mathrm{PZC_{CeOH}} = \frac{2}{3} \times 8.30 + \frac{1}{3} \times 13.09 = 9.90 \qquad \text{(Eq. 4.16)}$$

It's difficult to apply this approach to the phosphate oxygen sites due to their covalent bond characteristics. Regil *et al.* (2003) measured the intrinsic constant ($\log K_{int.,H^+,k}$) of phosphate oxygen sites hydration using potentiometric titrations and the value was found to be equal to 9.0. Therefore, the PZC of the phosphate oxygen sites equals 4.5. The amount of phosphate oxygen sites equals the cerium oxygen sites based on the structure of the (100) plane. Therefore, the overall PZC of the cleavage along (100) plane equals 7.20 (= [4.5 + 9.9]/2), which agrees with the electrokinetic tests and solubility calculations.

4.5. CONCLUSIONS

This chapter provided a systematic and fundamental study of monazite charging mechanisms in aqueous systems. Electrokinetic tests, solution equilibrium calculations, crystal structure analyses, and electrostatic model predictions were used. The results indicated that charges on monazite in water were developed by protonation/deprotonation reactions. Hydrogen and hydroxyl ions were potential determining ions for monazite. The specific findings of this chapter included:

(1) Electrokinetic measurements of the natural monazite showed that its isoelectric point (IEP) occurred at pH 6.0.

(2) When cerium chloride was added into solution, significant changes of monazite zeta potential were observed in both neutral and basic environments, which was ascribed to the specific adsorption of $Ce(OH)^{2+}$ on monazite surfaces via hydrogen bonding.

(3) When phosphoric acid was added into solution, monazite zeta potential changed slightly and no charge reversal was observed. The possibility that Ce^{3+} and PO_4^{3-} regulated monazite surface charges through preferential liberation and/or adsorption was excluded.

(4) Solution equilibrium calculation indicated that the IEP of cerium monazite ($CePO_4$) occurred at pH 7.2 and pH 4.5 in closed and open systems, respectively. The dissolution of carbon dioxide in solution increased total negative charges, which required more acidic condition to neutral the charges.

(5) Crystal structure analyses and electrostatic model predictions showed that IEP of monazite (100) plane occurred at pH 7.2, which agreed with the solution equilibrium calculation results.

CHAPTER 5. ADSORPTION OF OCTANOHYDROXAMIC ACID ON MONAZITE SURFACES

5.1 ADSORPTION KINETIC, ISOTHERM AND THERMODYNAMIC MODELS

5.1.1 Kinetic Models

Kinetic tests were used to measure the rate (k) at which collector adsorption takes place in the solid/solution system. Kinetic studies provided critical information such as the time (t) required for reaching equilibrium and the equilibrium collector concentration (Q_e) on the solid surface. Kinetic studies of octanohydroxamate adsorption on minerals such as ferric oxide, manganese dioxide, barite, calcite, and bastnaesite have been reported in literature (Raghavan and Fuerstenau, 1975; Natarajan and Fuerstenau, 1983; Pradip and Fuerstenau, 1983). However, few of these studies attempted to fit the results with kinetic models. In the current study, the pseudo-first-order and pseudo-second-order models were used to analyze the kinetic results. These models have been successfully applied to other systems such as fatty acid-fluorite, fatty acid-hematite, xanthate-zinc sulfide, xanthate-lead sulfide, etc. (Free and Miller, 1997; Fredriksson and Holmgren, 2008, 2007, 2006). The pseudo-first-order model is generally represented in the form:

$$\ln(Q_e - Q_t) = -k_1 t + \ln Q_e \qquad \text{(Eq. 5.1)}$$

where Q_e (mg g^{-1}) and Q_t (mg g^{-1}) are the amount of collector adsorbed at equilibrium and at time t (h), respectively, and k_1 (h^{-1}) the rate constant of pseudo-first-order equation.

The pseudo-second-order equation is expressed as:

$$\frac{t}{Q_t} = \frac{1}{h} + \frac{t}{Q_e} \qquad \text{(Eq. 5.2)}$$

where h equals $k_2 Q_e^2$ and represents the initial sorption rate while k_2 (g mg^{-1}h^{-1}) is the rate constant of pseudo-second-order equation (Jazi *et al*., 2014; Peng *et al*., 2014).

5.1.2 Isotherm Models

Systematic adsorption isotherm studies provided critical information, such as the amount of surfactant adsorbed per unit area or mass of solid, surfactant concentration in the solution, the extent of the adsorption (monolayer or multilayer), and the orientation of the adsorbed molecules relative to the surface and solution (Raghavan and Fuerstenau, 1975; Natarajan and Fuerstenau, 1983; Pradip and Fuerstenau, 1983; Ni and Liu, 2012). Batch adsorption results were analyzed using appropriate models such as the Langmuir, Freundlich, and Fowler-Guggenheim models. These models have been used to describe the adsorption of surfactants on mineral surfaces and the Langmuir and Freundlich models were the most often applied (Yehia *et al.*, 1993; Aktas and Woodburn, 1994; Rath, 1997; Ofor and Anusiem, 1999; Beattie *et al.*, 2006; Tekin and Ates, 2012; Qu *et al.*, 2016). The Langmuir, Freundlich, and Fowler-Guggenheim models were used to fit the adsorption data in this study.

5.1.2.1 Langmuir model

The Langmuir equation is based on a kinetic approach and assumes a homogeneous surface, a single layer of adsorbed material, constant temperature, and no lateral interaction among adsorbed molecules (Langmuir, 1918; Ng *et al.*, 2002; Oguz, 2005; Hamdaoui and Naffrechoux, 2007; Memon, 2009; Peng *et al.*, 2014; Idris, 2015). The Langmuir equation is expressed as:

$$Q_e = \frac{Q_m k_L C_e}{1+k_L C_e} \qquad \text{(Eq. 5.3)}$$

where Q_e is the amount of collector adsorbed at equilibrium (mg g^{-1}), and C_e the equilibrium concentration of the collector in the bulk solution (mg L^{-1}), Q_m the maximum adsorption capacity (mg g^{-1}), and k_L the constant related to free energy of adsorption (L mg^{-1}). When monolayer coverage is achieved, the maximum adsorption capacity is calculated using the molecular size and surface area. The surface coverage can be described by:

$$\theta = Q_e/Q_m \qquad \text{(Eq. 5.4)}$$

and, thus, the Langmuir equation can be written as:

$$\frac{\theta}{1-\theta} = k_L C_e \quad \text{(Eq. 5.5)}$$

The k_L value was calculated from the intercept and slope of the linear plot of Q_e^{-1} versus C_e^{-1}. However, when the maximum surface coverage is not known, Q_m and k_L values can be calculated using the following equation:

$$\frac{1}{Q_e} = \frac{1}{k_L Q_m}\frac{1}{C_e} + \frac{1}{Q_m} \quad \text{(Eq. 5.6)}$$

5.1.2.2 Freundlich model

The Freundlich model is an empirical equation which assumes 1) adsorption of the molecules on a heterogeneous surface, 2) interactions between adsorbed molecules, and 3) multilayer adsorption (Freundlich, 1907; Rath and Subramanian, 1997; Ng *et al.*, 2002; Hamdaouiand and Naffrechoux, 2007; Jazi, 2014; Mobasherpour *et al.*, 2014;). The Freundlich model can be written as:

$$Q_e = k_F C_e^{1/n} \quad \text{(Eq. 5.7)}$$

where k_F ($mg^{1-(1/n)}$ $L^{1/n}$ g^{-1}) and *n* are constants indicating the relative adsorption capacity of the adsorbent and the intensity of the adsorption, respectively. A higher value for 1/*n* means a larger change in effectiveness over different equilibrium concentrations. The linear form of Freundlich model is:

$$\ln Q_e = \ln k_F + \frac{1}{n}\ln C_e \quad \text{(Eq. 5.8)}$$

The values for k_F and *n* are calculated from the intercept and slope of the linear plot of $\ln Q_e$ versus $\ln C_e$.

5.1.2.3 Fowler-Guggenheim model

The Fowler-Guggenheim isotherm takes into account the localized adsorption with lateral interaction and can be written as (Fowler and Guggenheim, 1939; Khelifa *et al.*, 2004; Hamdaoui and Naffrechoux, 2007):

$$k_{FG}C_e = \frac{\theta}{1-\theta}\exp\left(\frac{2\theta W}{RT}\right) \quad \text{(Eq. 5.9)}$$

where k_{FG} is the equilibrium constant (L mg^{-1}), θ the fractional coverage, R the gas constant (8.314×10^{-3} kJ mol^{-1} K^{-1}), T the temperature (K), and W the interaction energy between adsorbed molecules. Positive and negative values of W represent attractive and repulsive interactions among adsorbed molecules, respectively. Eq. 5.9 can be linearized to the following equation:

$$\ln\left[\frac{C_e(1-\theta)}{\theta}\right] = -\ln k_{FG} + \frac{2W\theta}{RT} \quad \text{(Eq. 5.10)}$$

5.1.3 Thermodynamic Models

The Gibbs free energy (ΔG^0_{ads}), enthalpy (ΔH^0_{ads}) as well as entropy (ΔS^0_{ads}) were calculated using the isotherm data at different temperatures based on the following equations:

$$\frac{\theta}{1-\theta} = \frac{C_e}{55.5}\exp\left(\frac{-\Delta G^0_{ads}}{RT}\right) \quad \text{(Eq. 5.11)}$$

$$\Delta H^0_{ads} = \frac{\Delta G^0_{ads,1}/T_1 - \Delta G^0_{ads,2}/T_2}{(1/T_1 - 1/T_2)} \quad \text{(Eq. 5.12)}$$

$$\Delta S^0_{ads} = \frac{\Delta G^0_{ads,1} - \Delta G^0_{ads,2}}{(T_2 - T_1)} \quad \text{(Eq. 5.13)}$$

where $\Delta G^0_{ads,1}$ and $\Delta G^0_{ads,2}$ are the standard free energies of adsorption at two different temperatures T_1 and T_2, respectively. Eq. 5.11 is the Stern-Langmuir equation where θ is surface coverage, C_e equilibrium concentration of collectors in solution (M), ΔG^0_{ads} standard free energy of adsorption (kJ mol^{-1}) at temperature *T* (K), and the constant 55.55 is the molarity of water. This equation has been used in several hydroxamate adsorption studies (Pradip and Fuerstenau, 1985, 1983; Raghavan and Fuerstenau, 1975). The free energy of adsorption can be divided into different contributions, i.e., chemical interaction, electrostatic interaction, hydrophobic bonding, solvation effects, etc.

5.2 ADSORPTION KINETICS

Adsorption kinetics were used to evaluate the efficiency of octanohydroxamic acid adsorption on monazite at different pH values. The adsorption of octanohydroxamic acid on monazite as a function of time for different pH values is shown in Figure 5.1. Adsorption reached equilibrium after 48 h of interaction for all of the studied pH values. Therefore, an adsorption time of 48 h was used for the isotherm and thermodynamic studies.

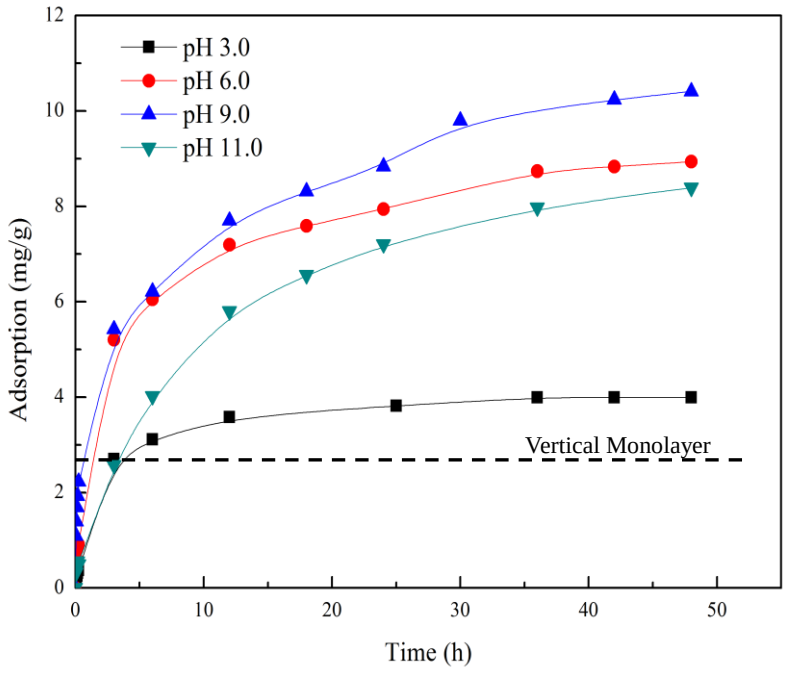

Figure 5. 1 Adsorption kinetics of octanohydroxamic acid on monazite at different pH values using 160 mg L^{-1} initial octanohydroxamic acid concentration.

The vertically and horizontally oriented monolayer adsorption densities of the octanohydroxamic acid was estimated to be 2.90 mg g^{-1} and 1.08 mg g^{-1} assuming the cross sectional area of the octanohydroxamic acid to be 20.5 $Å^2$ and 55 $Å^2$, respectively. Therefore, monolayer adsorption was achieved for all of the studied pH values. Furthermore, the collector adsorption rates associated with partial monolayer coverage were larger than the rates observed under conditions that resulted in adsorption above monolayer coverage. As such, the kinetic data were divided into two parts, i.e., partial coverage and multilayer coverage, and simulated using kinetic models separately. The

modelling results of below and above monolayer adsorptions are shown in Figure 5.2 and Table 5.1, Figure 5.3, and Table 5.2, respectively.

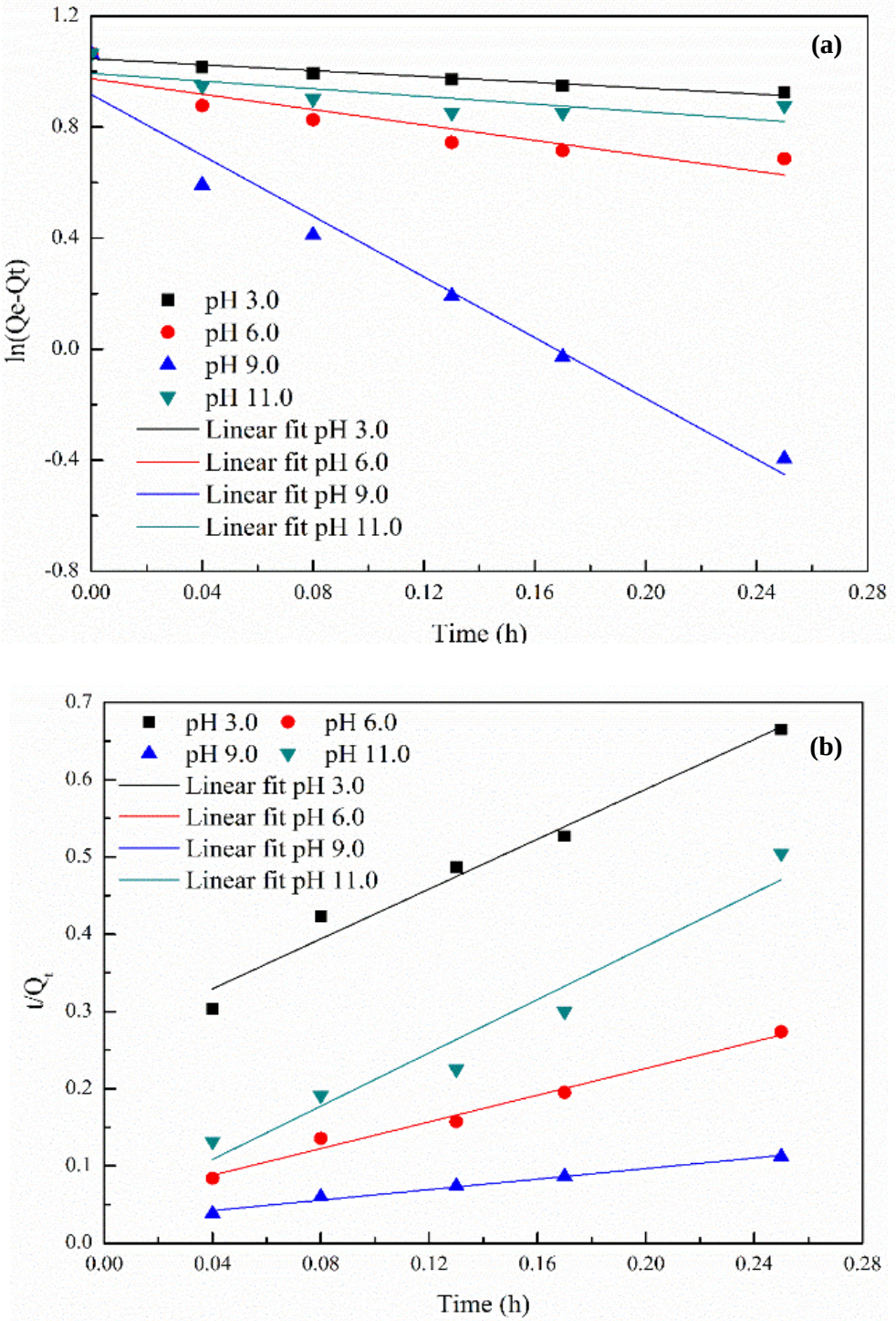

Figure 5. 2. Modelling of adsorption data below monolayer coverage using (a) pseudo-first-order and (b) pseudo-second-order equations.

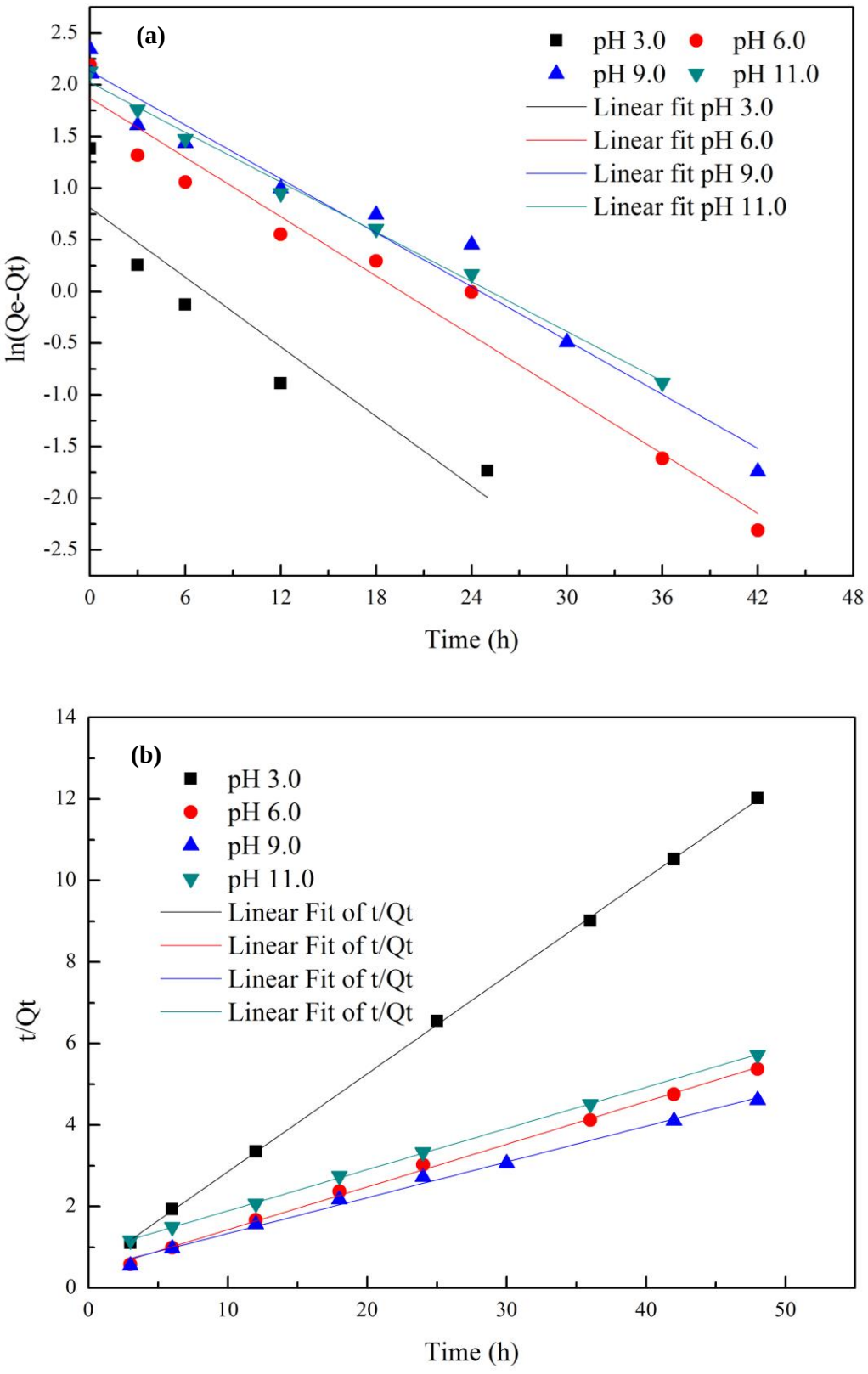

Figure 5. 3. Modelling of adsorption data for greater than monolayer coverage using (a) pseudo-first-order and (b) pseudo-second-order equations.

Table 5. 1. Kinetic parameters for the adsorption of octanohydroxamic acid on monazite under conditions provided less than a monolayer coverage.

	Pseudo-first-order			Pseudo-second order			
pH	k_1	$Q_{e,cal}$	R^2_{adj}	k_2	$Q_{e,cal}$	h	R^2_{adj}
	h^{-1}	mg g^{-1}		g $mg^{-1}h^{-1}$	mg g^{-1}	mg g^{-1} h^{-1}	
3.0	0.53	2.85	0.9256	9.84	0.62	3.78	0.9656
6.0	1.39	2.65	0.7737	14.01	1.16	18.74	0.9803
9.0	5.48	2.50	0.9599	4.05	2.94	34.99	0.9843
11.0	0.69	2.70	0.5049	75.29	0.58	25.32	0.9293

Table 5. 2. Kinetic parameters for the adsorption of octanohydroxamic acid on monazite under conditions provided more than a monolayer coverage.

	Pseudo-first-order			Pseudo-second order		
pH	k_1	$Q_{e,cal}$	R^2_{adj}	k_2	$Q_{e,cal}$	R^2_{adj}
	h^{-1}	mg g^{-1}		g mg^{-1} h^{-1}	mg g^{-1}	
3.0	0.11	2.25	0.8471	0.13	4.16	0.9997
6.0	0.10	6.50	0.9641	0.03	9.54	0.9976
9.0	0.09	8.43	0.9658	0.02	11.39	0.9936
11.0	7.55	7.55	0.9937	0.01	9.89	0.9997

For both the below and beyond monolayer adsorption stages, adsorption can be accurately modelled by the pseudo-second order model with R^2_{adj} larger than 0.92, which indicates the rate of surface reaction (i.e., direct adsorption/desorption process) controls the overall sorption kinetics (Ho and McKay, 1999; Plazinski *et al.*, 2009; Yan *et al.*, 2015). For the below monolayer stage, both the maximum initial adsorption rate (h) and equilibrium adsorption ($Q_{e,cal}$) occurred at pH 9.0 indicating a higher affinity of octanohydroxamate species for the monazite surfaces. The higher affinity may be due to the presence of more active sites on the monazite surfaces at pH 9.0. A speciation diagram of both cerium and lanthanum indicated that maximum concentrations of hydrolyzed species, i.e., $Ce(OH)^{2+}$, $Ce(OH)_2^+$, $La(OH)^{2+}$, and $La(OH)_2^+$, occurred around pH 9.0 and the hydrolyzed species are surface active sites (Figure 5.4). The

speciation of octanohydroxamic acid may have minor contribution to the maximum h and $Q_{e,cal}$ values based on the fact that a nearly equal amount of octanohydroxamic acid molecules (RCONHOH) and octanohydroxamate anions ($RCONHO^-$) existed in solution at pH 9.0 (Figure 5.4(c)).

For the beyond monolayer adsorption stage, both the k_1 and k_2 values indicate that the adsorption rate of octanohydroxamic acid on monazite decreased with an increase in solution pH values from 3.0 to 11.0. Based on the fact that the R^2_{adj} values for all pH conditions are larger than 0.99 when modelled by pseudo-second-order equation, it is reasonable to exclude the possibilities that processes such as transport of solute in the bulk solution and diffusion of solute across the liquid film control the adsorption kinetics. Furthermore, the concentration of surface active sites are symmetrically distributed around pH 9.0. Therefore, the decreases of adsorption rate with increases in pH values were not relevant to the concentrations of active species.

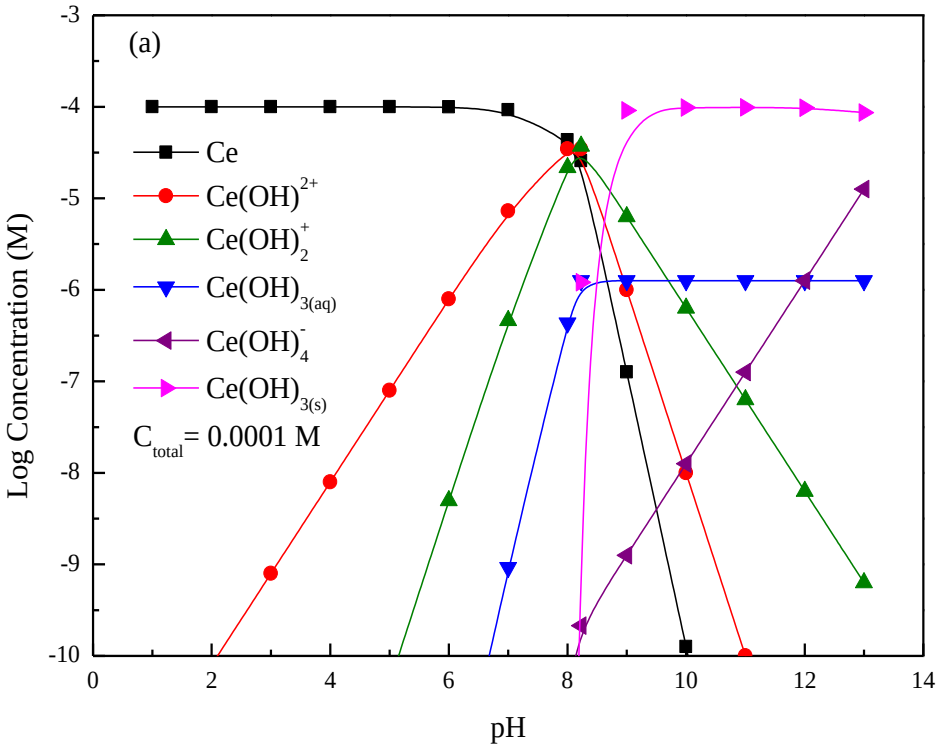

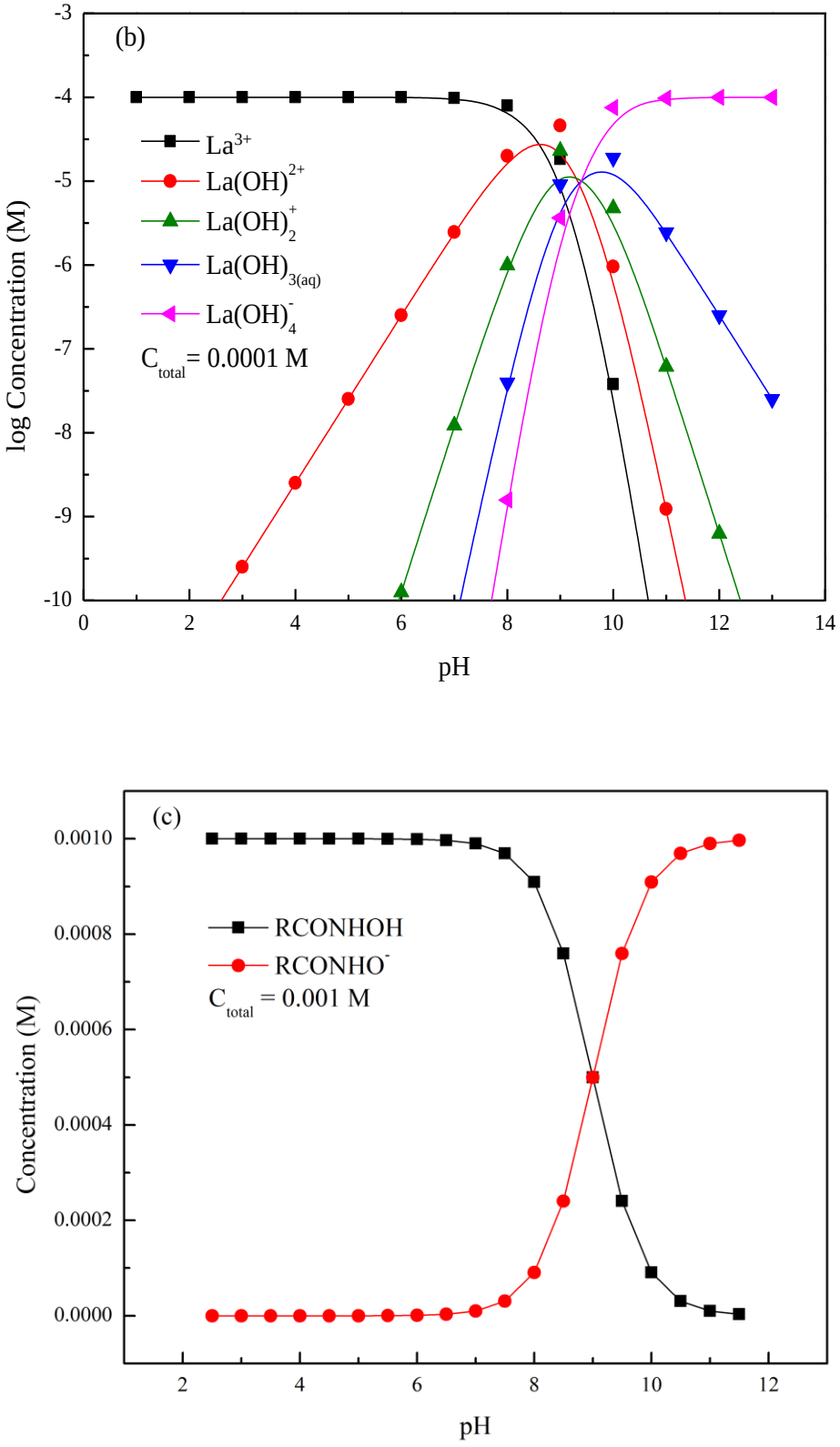

Figure 5. 4. Speciation diagrams of (a) cerium, (b) lanthanum, and (c) octanohydroxamic acid in solution. (Thermodynamic constants used for speciation calculation were referred from Kragten and Decnop-Weever, 1987, 1978).

5.3 ADSORPTION ISOTHERMS

The adsorption isotherm reveals the distribution of the adsorption molecules in liquid phase and solid phase when the adsorption reaches an equilibrium. Figure 5.5 shows the adsorption isotherm of octanohydroxamic acid on monazite at 20 ^{o}C and different pH values. Multilayer adsorption was achieved with higher collector dosages for each of the pH values studied. The isotherms were divided into two parts when fitting test results with three adsorption models, i.e., 1) concentrations below monalayer coverage and 2) concentrations above monalayer coverage. The division of the isotherms into two components was validated by the kinetic results.

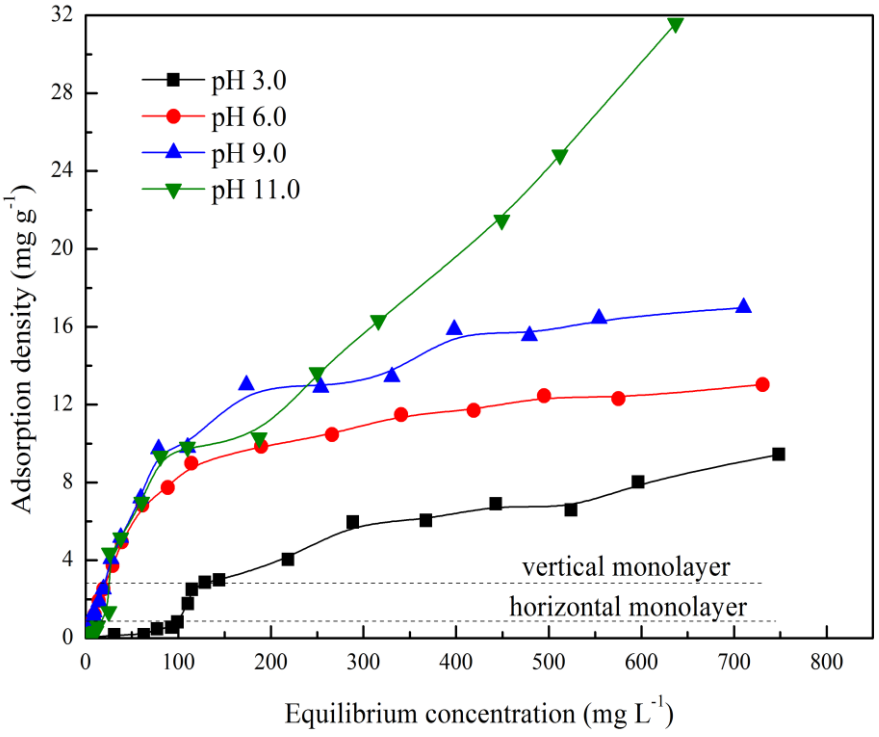

Figure 5. 5. Adsorption isotherms at 20 ^{o}C for different solution pH values.

The Langmuir, Freundlich, and Fowler-Guggenheim models were used to model adsorption data for conditions providing less than a monolayer coverage. The values of the three isotherm model parameters and associated adjusted coefficient of determination (R^2_{adj}) values are listed in Tables 5.3 and 5.4. Octanohydroxamic acid adsorption on monazite was not well described by the Langmuir model using either theoretical maximum adsorption density or the value calculated directly from the model.

Both Fowler-Guggenheim and Freundlich sufficiently describe the adsorption experimental data. The interaction energies between adsorbed molecules (W) were negative for all of the studied pH values indicating the existence of lateral interaction, which explained the ineffectiveness of Langmuir model. The free energies of adsorption with respect to different equilibrium octanohydroxamic acid concentrations were calculated using Eq. (5.11) and shown in Figure 5.6. Sharp increases of negative ΔG^0_{ads} values were observed for all pH values studied at specific collector dosages corresponding to a surface coverage of around 0.2, at which lateral interaction between adsorbed molecules starts playing a role.

Table 5. 3. Langmuir and Fowler-Guggenheim parameters for octanohydroxamic acid adsorption on monazite surfaces in case of below monolayer.

	Langmuir 1			Langmuir 2			Fowler-Guggenheim		
pH	k_L	Q_m	R^2_{adj}	k_L	Q_m	R^2_{adj}	k_{FG}	W	R^2_{adj}
	L mg^{-1}	mg g^{-1}		L mg^{-1}	mg g^{-1}		L mg^{-1}	kJ mol^{-1}	
3.0	0.22	2.90	0.1459	-0.01	-0.19	0.8912	0.00	-7.50	0.9048
6.0	0.19	2.90	0.6237	-0.02	-3.73	0.9217	0.02	-4.34	0.9582
9.0	0.20	2.90	0.6418	-0.03	-3.28	0.9738	0.02	-3.62	0.9727
11.0	0.03	2.90	0.8765	-0.02	-1.74	0.9575	0.01	-3.31	0.9195

Table 5. 4. Freundlich parameters for octanohydroxamic acid adsorption on monazite in the cases of surface coverage below and above monolayer formation.

	Below monolayer			Above monolayer		
pH	k_F	$1/n$	R^2_{adj}	k_F	$1/n$	R^2_{adj}
	mg$^{1-(1/n)}$ L$^{1/n}$ g^{-1}			mg$^{1-(1/n)}$ L$^{1/n}$ g^{-1}		
3.0	9.72×10^{-9}	4.02	0.9383	0.12	0.66	0.9371
6.0	0.056	1.32	0.9579	1.94	0.30	0.9119
9.0	0.07	1.22	0.9714	1.02	0.45	0.9287
11.0	0.02	1.33	0.9493	0.63	0.58	0.9610

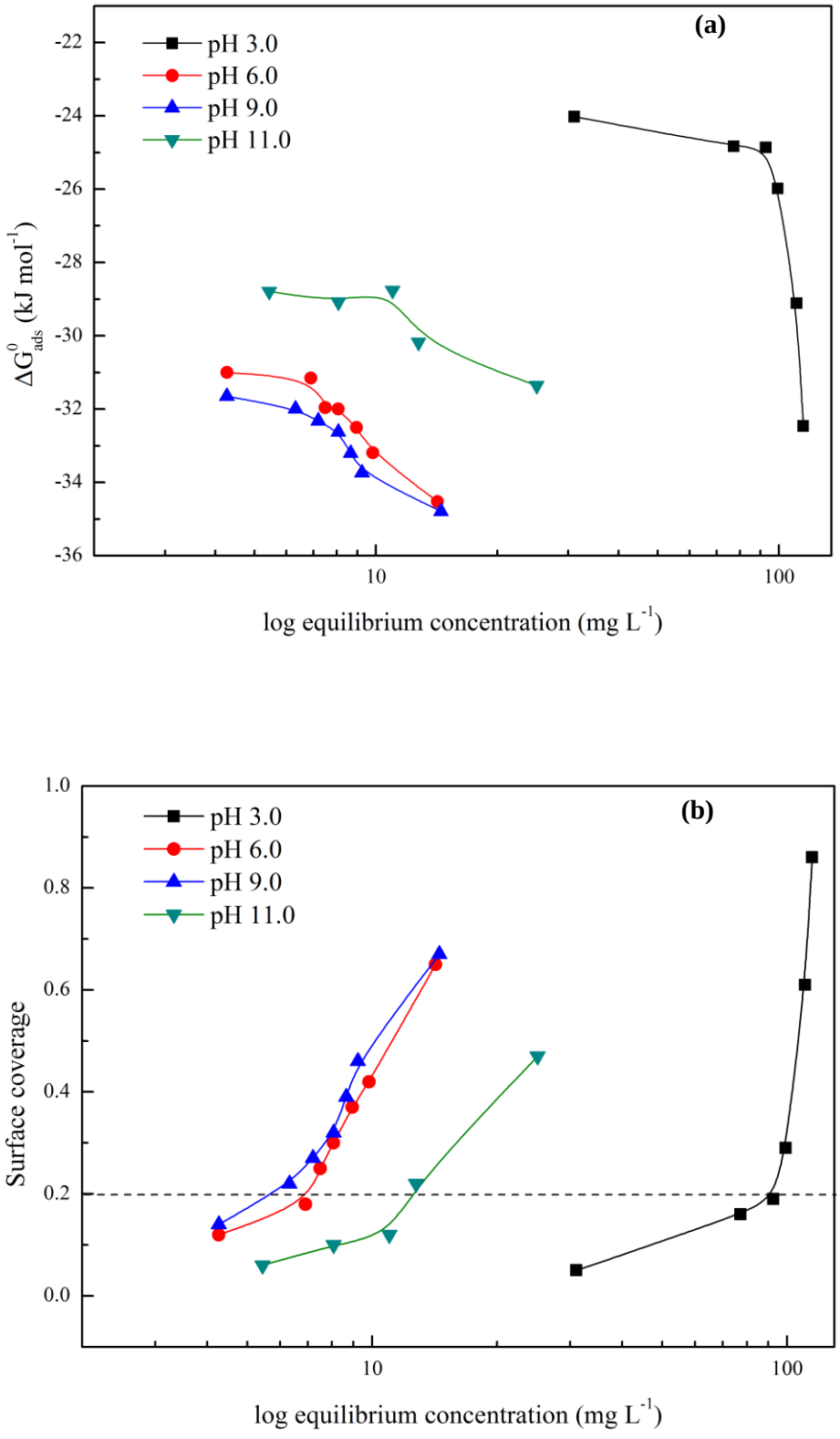

Figure 5. 6. Standard free energy and surface coverage for adsorption below monolayer coverage as a function of equilibrium concentration. (a) Standard free energy; (b) surface coverage.

The free energies of adsorption at 10% of surface coverage (Δ=0.1) at pH 3.0, 6.0, 9.0, and 12.0 are -24.14, -31.02, -31.48, and -29.08 kJ mol^{-1}, respectively, which is close to the number reported by Free and Miller (1997) where chemisorption was suggested to occur between oleate and fluorite surfaces. As such, chemisorption occurred for all the studied pH values when partial coverage was achieved, while octanohydroxamic acid has a stronger affinity for monazite surfaces at high pH values. After about three layers of adsorption (100 mg L^{-1} equilibrium concentration), the adsorption density gradually leveled off for solution pH values of 6.0 and 9.0 as shown in Figure 5.5, which indicates that the rates of adsorption and desorption became equal and adsorption equilibrium was achieved. However, for a pH value of 11.0, adsorption densities continued to increase after a plateau at 200 mg L^{-1} and, thus, equilibrium was not achieved within the studied dosage range. This finding indicated the occurrence of surface precipitation (Pradip and Fuerstenau, 1985; Rao *et al.*, 1989; Kellar *et al.*, 1991, 1992). At higher concentrations, the adsorption advantage of pH 9.0 due to more surface active sites (see Figure 5.5) disappeared as adsorption continued with an increase in the pH value, i.e., hydroxyl ion concentrations.

5.4 ADSORPTION THERMODYNAMICS

The effect of temperature on octanohydroxamate adsorption has been investigated in several mineral systems and higher selectivity could be achieved in industrial minerals flotation via increasing temperature (Raghavan and Fuerstenau, 1975; Natarajan and Fuerstenau, 1983; Pradip and Fuerstenau, 1985; Kellar *et al.*, 1991, 1992; Sreenivas and Padmanabhan, 2002). In this study, the adsorption of octanohydroxamic acid on monazite for pH 9.0 was examinated at 20 ^{o}C, 40 ^{o}C, and 60 ^{o}C. Test results are shown in Figure 5.7. The isotherms were divided into two regions I and II which correspond to partial coverage and multilayer coverage, respectively.

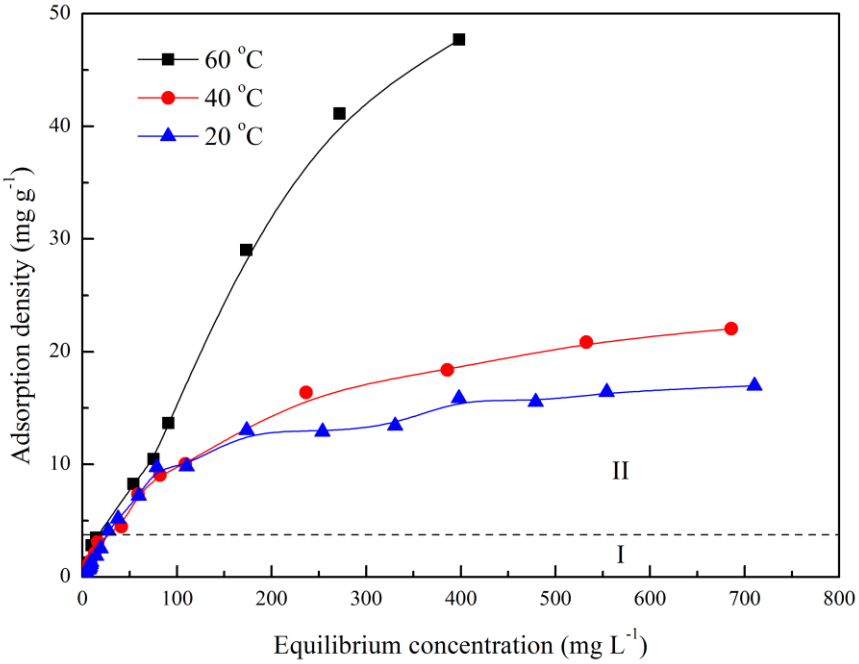

Figure 5. 7. Isotherms at pH 9.0 for the adsorption obtained at different conditioning temperatures.

The free energies of adsorption corresponding to 50% surface coverage calculated using Eq. (5.11) are listed in Table 5.5 along with enthalpy and entropy changes. A free energy difference of only -0.88 kJ mol^{-1} occurred as the temperature was increased from 20 °C to 60 °C. The adsorption process below monolayer coverage is entropically driven since the enthalpy change is negative and adsorpiton increased with increase in temperatures. Negative changes of enthalpy indicate the adsorption process was exothermic which is contrary to the findings of studies performed on other systems, such as iron oxide, calcite, barite, and bastnaesite in which it was found that hydroxamate adsorption was endothermic (Raghavan and Fuerstenau, 1975; Pradip and Fuerstenau, 1985, 1983). The postive entropy change is caused by the disordering of water molecules bonded with the mineral surfaces. Furthermore, water molecules around carbon chains of collector molecules in solution are also ordered and collector adsorption may break the orderly structure, thus, increasing the entropy.

Table 5. 5. Thermodynamic parameters for octanohydroxamate adsorption on monazite.

Temperature (°C)	ΔG^0_{ads} (kJ mol^{-1})	ΔH_{ads} (kJ mol^{-1})	ΔS_{ads} (kJ mol^{-1} K^{-1})
20	-33.76		
40	-34.23	-27.31	0.022
60	-34.64		

Table 5.6 shows the solubilies of different minerals and the enthalpy changes of octanohydroxamic acid adsorption on these minerals. Minerals with higher solubilities usually expect postive ΔH^0_{ads} values, while for insoluble minerals such as monazite and cassiterite ΔH^0_{ads} values are negative. Raghavan and Fuerstenau (1975) proposed that hydroxamate-metal cations precipitation reaction is an endothermic process which is also true for surface precipitation. As such, for adsorption below monolayer coverage, octanohydroxamic acid adsorbs on semisoluble minerals through endothermic surface precipitation, while on minerals with low solubilities the adosrption occurs through exothermic chemisorption. Changes of region I to region II with increases in concentrations in octanohydroxamic acid-monazite system correspond to the transformation from chemisorption to surface precipitation. The similar kind of transformation was also observed in fluorite-oleate system by Kellar *et al.* (1991, 1992) using insitu-FTIR.

Table 5. 6. Mineral solubility and enthalpy changes of octanohydroxamic acid adsorption onto these minerals.

Mineral	Dissolution Reaction	log K_{sp}	ΔH_{ads} (kJ mol^{-1})	ΔS_{ads} (kJ mol^{-1} K^{-1})	Surface Coverage
Calcite	$CaCO_{3(s)} = Ca^{2+} + CO_3^{2-}$	-8.48	45	0.250	0.5
Barite	$BaSO_{4(s)} = Ba^{2+} + SO_4^{2-}$	-10.05	20	0.157	0.5
Bastnaesite	$REEFCO_{3(s)} = REE^{3+} + F^- + CO_3^{2-}$	-16.00	187	0.830	0.5
Monazite	$CePO_{4(s)} = Ce^{3+} + PO_4^{3-}$	-26.27	-27.31	0.022	0.5
Monazite	$CePO_{4(s)} = Ce^{3+} + PO_4^{3-}$	-26.27	-7.74	0.101	0.9
Cassiterite	$SnO_{2(s)} + 2H_2O = Sn^{4+} + 4OH^-$	-63.39	-36.8	NA	0.1
Xenotime	$YPO_{4(s)} = Y^{3+} + PO_4^{3-}$	-25.00	14.25	0.114	NA

(Data sources: Plummer and Busenberg, 1982; Monnin and Galinier, 1988; Cetiner *et al.*, 2005; Rai *et al.*, 2011; Zhang, 2016)

Values of ΔH^0_{ads} for octanohydroxamic acid adsorpiton on monazite changed from -

27.31 kJ mol^{-1} to -7.74 kJ mol^{-1} with increases in surface coverage from 0.5 to 0.9 (see Table 5.6). Sreenivas and Padmanabhan (2002) also reported similar findings for octanohydroxamic acid adsrption on cassiterite, i.e., ΔH^0_{ads} values varied between -36.8 kJ mol^{-1} obtianed at octanohydroxamic acid concentration of 1×10^{-3} M and 5.2 kJ mol^{-1} obtained at a surfactant concentration of 1×10^{-3} M. The changes of ΔH^0_{ads} values from negative to positive prove the transformation from chemisorption to surface precipitation. This transforamtion explains the relationships between minerals' flotation recoveries and solubilities when using hydroxamic acids as collectors as reported by Assis *et al.* (1996).

5.5 REACTION BETWEEN CERIUM AND OCTANOHYDROXAMIC ACID IN AQUEOUS SOLUTION

Adsorption is a process that occurrs at the liquid-mineral interface which could lead to complete monolayer or multi-layer coverage of the collector. Similarites exist between the reactions that occur at the liquid-mineral interfaces and bulk solution. Titration tests are widely used to study reactions in solutions that involve hydroxyl ions. In the current study, the reactions between cerium and octanohydroxamic acid in an aqueous system were studied using titration tests.

For the solutions containing 1) cerium only, 2) octanohydroxamic acid only, and 3) a cerium and octanohydroxamic acid mixture, more hydroxyl ions were needed to obtain the same pH values compared to a solution of deionized water, which indicated the occurrence of reactions resulting in the consumption of hydroxyl ions (Fig. 5.8). For a 1×10^{-3} M cerium solution, pH values were decreased gradually from 7.2 to 6.2 with an increase in OH^- concentration from 3×10^{-5} mole to 1.6×10^{-4} mole after which the pH value increased rapidly resulting in the precipitation of cerium hydroxide. For the solution containing both 1×10^{-3} M cerium and 3×10^{-3} M octanohydroxamic acid, pH values increased slowly from 4.0 to 5.0 with an increase in OH^- concentration between 5×10^{-5} and 1.4×10^{-4} mole, after which the solution pH value increased rapidly and precipitation of cerium octanohydroxamate occurred as shown by the brown color

solids in Fig. 5.9. With the increase in pH values, precipitates of brown color were gradually fomed, which indicates that hydroxyl ions contribute to the reaction between cerium and octanohydroxamic acid. The effects of hydroxyl ions are due to the formation of basic cerium octanohydroxamates, which can be described by the following equations (Raghavan and Fuerstenau, 1975):

$$(RCONHO)Ce^{2+} + OH^- \rightarrow (RCONHO)Ce(OH)^+ \quad \text{(Eq. 5.14)}$$

$$(RCONHO)Ce(OH)^+ + OH^- \rightarrow (RCONHO)Ce(OH)_2 \quad \text{(Eq. 5.15)}$$

$$(RCONHO)_2Ce^+ + OH^- \rightarrow (RCONHO)_2Ce(OH) \quad \text{(Eq. 5.16)}$$

The basic cerium octanohydroxamates exhit a tendency to polymerize and form precipitates. The same reaction mechanism was suggested to occur on a monazite surface at pH 11.0 with high collector concentrations.

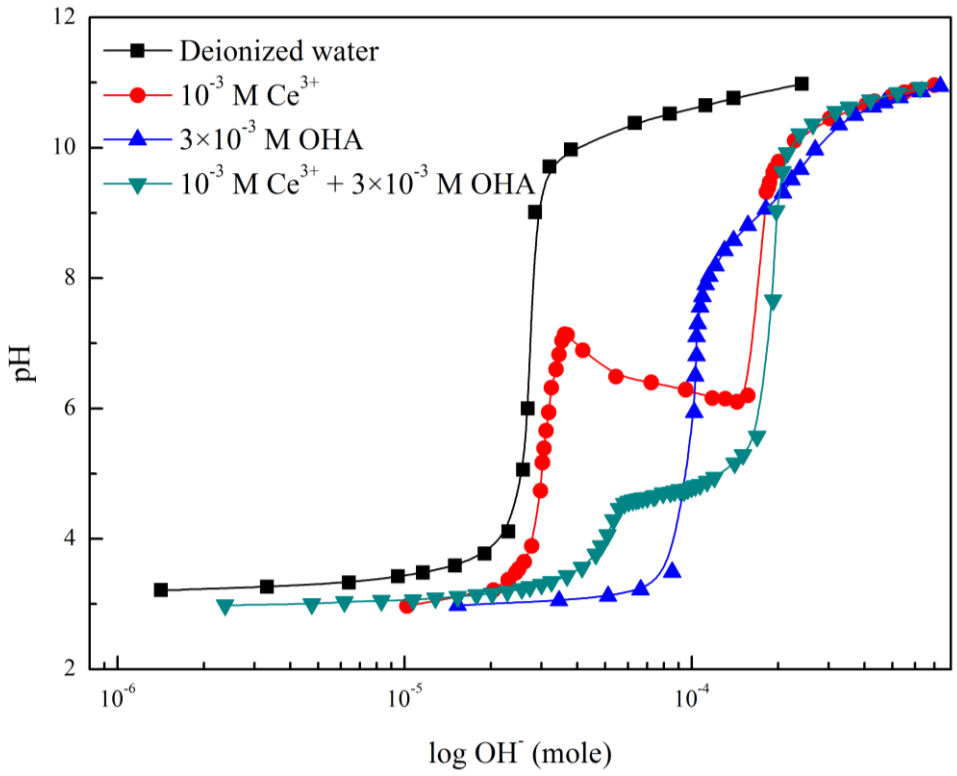

Figure 5. 8. Solution pH values as a function of hydroxyl ion addition in solutions of i) Type I deionized water, ii) cerium only, iii) octanohydroxamic acid only, and iv) cerium and octanohydroxamic acid mixture.

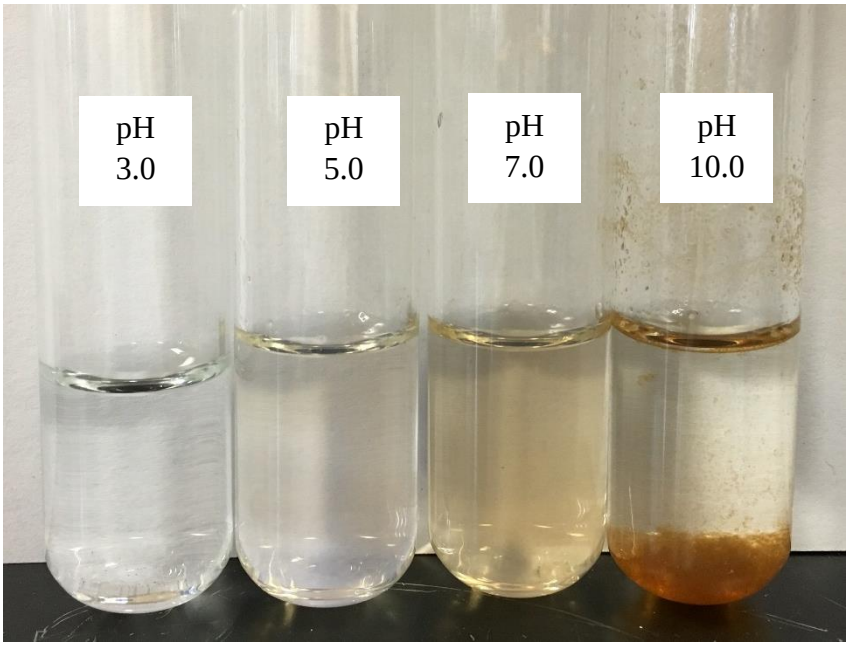

Figure 5. 9. The appearance of solution containing 1×10^{-3} M Ce^{3+} and 3×10^{-3} M hydroxamic acid at different pH values.

5.6 FTIR CHARACTERIZATION

FTIR analyses were used to detect the surface chemistry changes with respect to pH values and temperature. The IR spectrums of monazite, octanohydroxamic acid, cerium oxide, and cerium octanohydroxamate are shown in Figure 5.10. Peaks at 964 cm^{-1} and 988 cm^{-1} were assigned to cerium oxygen and phosphate oxygen bonds. Based on octanohydroxamic acid structure the carbonyl oxygen will serve as a donor center in the metal chelates. As a consequence, there will be electron withdrawal from the carbonyl group which, in turn, will increase the electron density in the C-N bond. The electron withdrawal will cause decreases in C=O bond frequency and increases in C-N bond frequency (Chatterjee, 1978). As shown in Figure 5.10, the C=O bond frequency at 1659 cm^{-1} and C-N bond frequency at 1330 cm^{-1} were shifted to 1604 cm^{-1} and 1378 cm^{-1}, respectively. As such, cerium chelates with a ring structure were suggested to form.

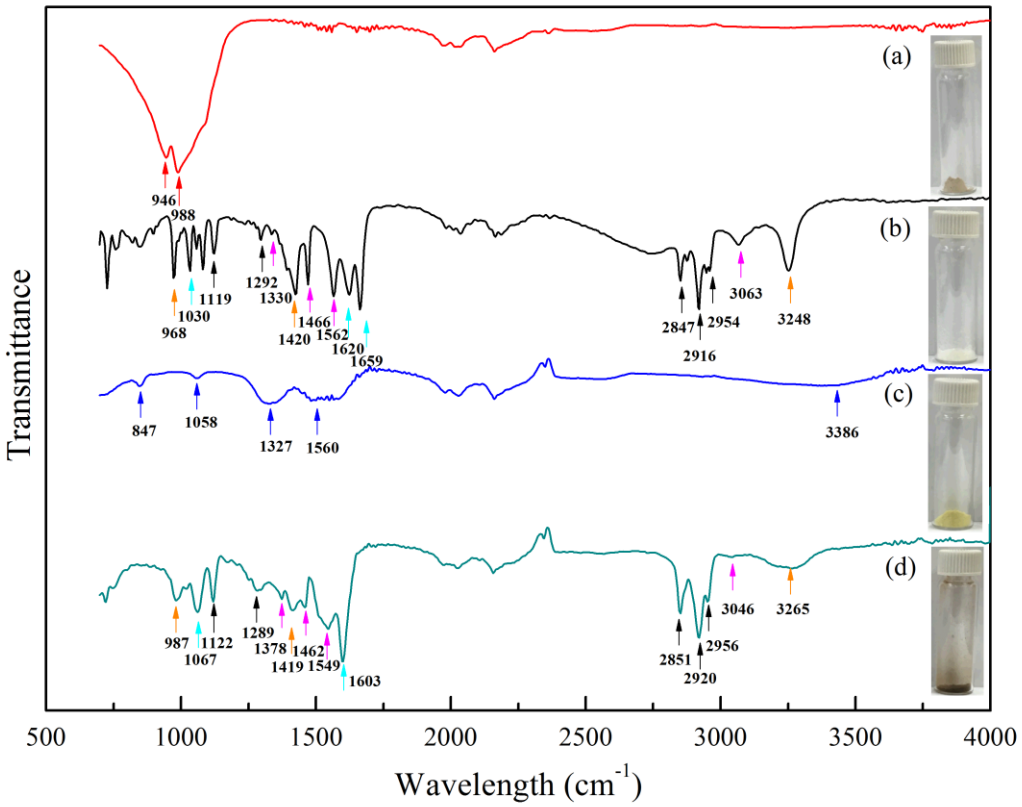

Figure 5. 10. FTIR Spectrum of (a) monazite, (b) octanohydroxamic acid, (c) cerium oxide, and (d) cerium octanohydroxamate.Notes: for spectrum (b) and (d), ↑ means C-H or C-C-C stretch, ↑ means N-O stretch, N-O-H in place bend, or N-H stretch, ↑ means C-O or C=O stretch, ↑ means C-N stretch or N-H bend.

FTIR analyses were conducted for monazite conditioned in 800 mg L^{-1} octanohydroxamic acid for 48 hours. As shown in Figure 5.11, octanohydroxamate functional groups were detected on monazite surfaces with rinsing after conditioning for all the studied pH values. As such, chemical interaction occurred for all the studied pH values. Furthermore, the peak at 1604 cm^{-1} (the C=O stretch) became more significant with an increase in pH value from 3.0 to 11.0, which indicates a stronger interaction in the basic environment which agreed with the adsorption data (Fig. 5.5). An elevation in temperature from 20 ^{o}C to 60 ^{o}C increased the strength of the peaks at 1604 cm^{-1}, indicating a rise in collector adsorption with temperature. The same C=O peak position (1604 cm^{-1}) for all the studied pH values indicates rare earth-octanohydroxamate chelates were formed for all of these conditions.

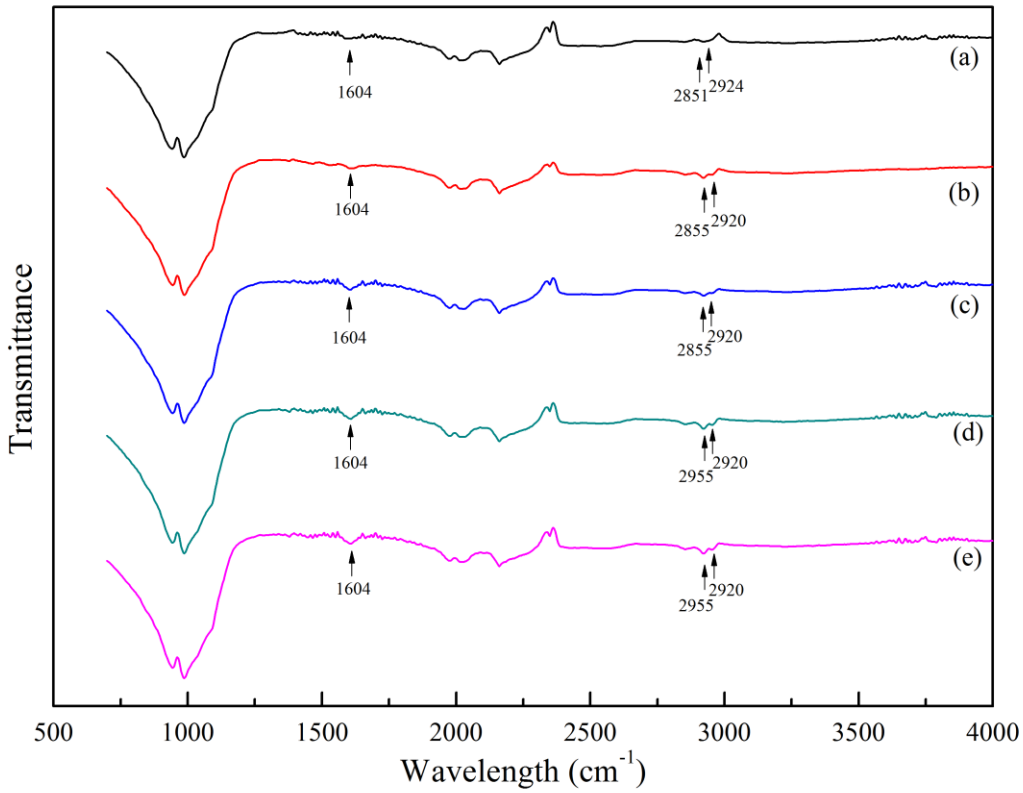

Figure 5. 11. FTIR spectrum of monazite conditioned in 800 mg L^{-1} octanohydroxamic acid for 48 hours: (a) pH 3.0 at 20 ^{o}C; (b) pH 6.0 at 20 ^{o}C; (c) pH 9.0 at 20 ^{o}C; (d) pH 11.0 at 20 ^{o}C; (e) pH 9.0 at 60 ^{o}C.

Band position of the asymmetric -CH_2 bond occurred at 2924 cm^{-1} for pH 3.0, while for the other pH values the band shifted to 2920 cm^{-1}. Similar shift was also observed by Kellar *et al.* (1991, 1992) in the fluorite-oleate system where frequencies of -CH_2 gradually decreased with increases in adsorption density. Kellar *et al.* (1991, 1992) suggested that the oleate adsorbed onto fluorite surfaces changes from a gauche state to a more rigid trans state. For the monazite-octanohydroxamte system, similar reactions were suggested to occur. Despite the fact that rare earth-octanohydroxamate chelates were formed for all of the studied pH values, the alky chains were in a more mobile and disordered form at pH 3.0 while for the other studied pH values, the alky chains were in a rigid state. Namely, chemisorption and surface precipitation occurred at lower and higher pH values, respectively. Furthermore, the band positon of -CH_2 of cerium octanohydroxamate also occurred at 2920 cm^{-1}, which also proves the occurrence of surface precipitation. Adsorption isotherm study indicates that multilayer adsorption

was achieved for all the studied pH values when using 800 mg L^{-1} octanohydroxamic acid and conditioning for 48 h. As such, physisorption via hydrophobic bonding following chemisorption was likely occur at pH 3.0.

5.7 MICRO-FLOTATION TESTS

Collector adsorption on mineral surfaces improves the degree of surface hydrophobicity and allows the material to be recovered by a froth flotation process at a rate that is economically viable. As shown in Figure 5.12, the maximum recovery of monazite occurred around pH 9.0 for all collector concentrations evaluated while nearly 100% flotation was achieved using a collector dosage of 40 mg L^{-1} and 5 min of conditioning as opposed to the 48 hours used to establish equilibrium. More surface active sites existed at pH 9.0 as indicated by the adsorption kinetic data (Table 5.1). As a result, adsorption rates and capacity were high which resulted in the higher flotation recovery values. As shown in Fig. 5.12(b), an increase in the conditioning temperature elevated monazite recovery which was due to improved adsorption densities as indicated by the thermodynamic and FTIR studies.

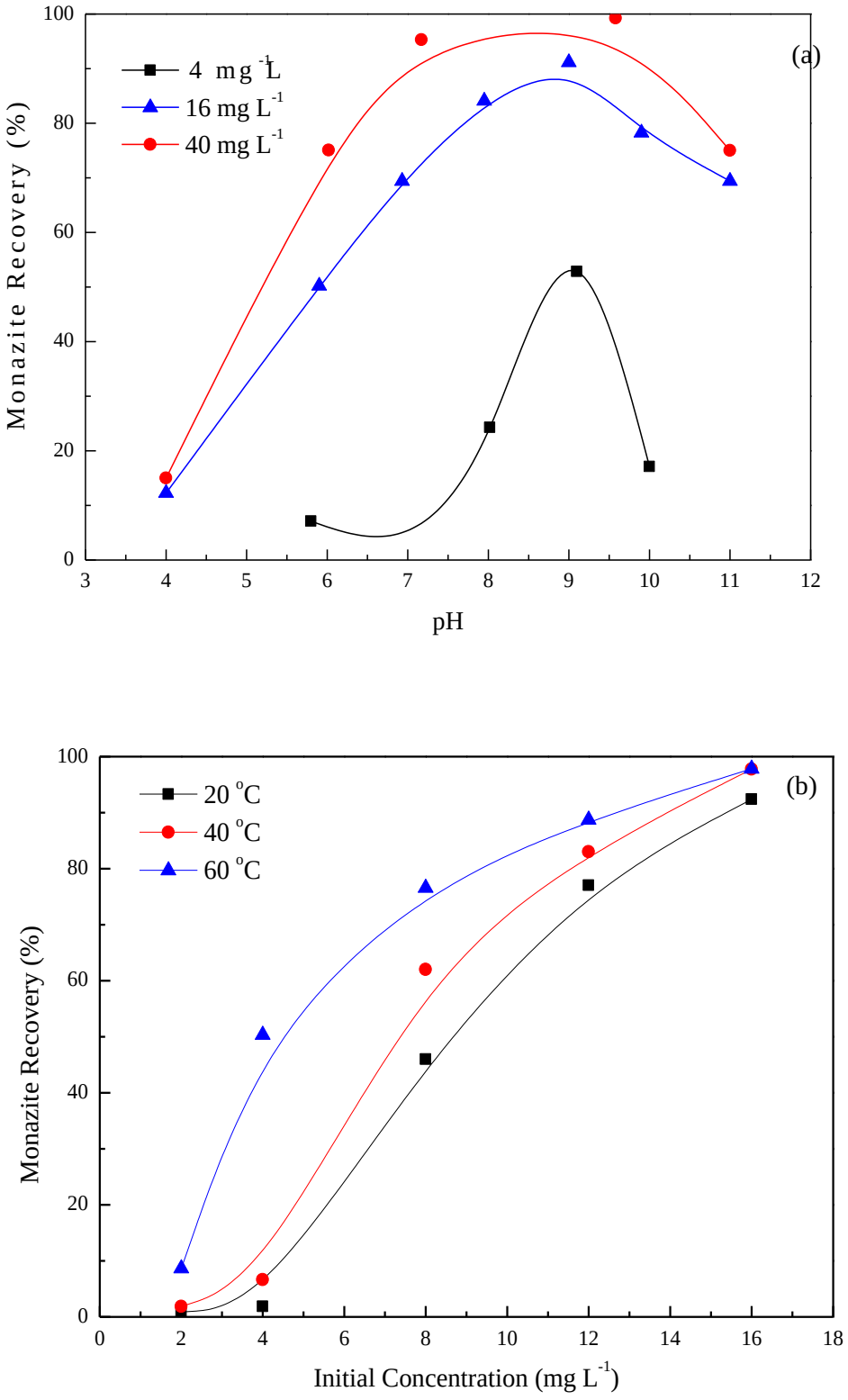

Figure 5. 12. Micro-flotation results of monazite using octanohydroxamic acid. (a) Effect of pH at 20 °C for three octanohydroxamic acid concentrations; (b) effect of conditioning temperature at pH 9.0 over a range of octanohydroxamic acid concentrations.

5.8 CONCLUSIONS

This chapter systematically studied the adsorption mechanisms of octanohydroxamic acid on monazite surfaces by adsorption kinetic, isotherm and thermodynamic tests, FTIR analyses, titration tests, and micro-flotation tests. Chemical adsorption of the collector on monazite surfaces was proven, while at different adsorption stages and pH values, the adsorption mechanisms were different. The specific findings were as follows:

(1) Adsorption equilibrium was achieved after 48 hours of interaction between 1×10^{-3} M octanohydroxamic acid and monazite surfaces. Adsorption kinetic data could be effectively described by the pseudo-second-order kinetic model with R_{adj}^2 values larger than 0.92;

(2) Multilayer adsorption of the collector on monazite surfaces occurred at pH values of 3.0, 6.0, 9.0, and 11.0. Adsorption free energies for below monolayer coverages were less than -20 kJ mol^{-1} at all the pH values, indicating the occurrence of chemical adsorption;

(3) For below monolayer adsorption, maximum adsorption rate and density occurred at pH 9.0, which was due to the chemical reaction between the collector and surface active sites such as $REE(OH)^{2+}$. For beyond monolayer adsorption, maximum adsorption density occurred at pH 11.0 due to the abundance of hydroxyl ions in solution, which was proven by titration tests;

(4) Adsorption density increased with the increases in temperature. The enthalpy (ΔH) and entropy (ΔS) changes were -27.31 kJ mol^{-1} and 0.022 J mol^{-1} K^{-1}, respectively, which indicated that the adsorption was an exothermic and entropy increase process;

(5) Based on the thermodynamic parameters of different mineral systems, transformation from chemisorption to surface precipitation and/or reaction with the increases in the collector dosages and/or solution pH values was suggested. The changes of the asymmetric $-CH_2$ bonds from 2920 cm^{-1} to 2924 cm^{-1} with the increases in pH values proved the transformation.

CHAPTER 6. MONAZITE-CALCITE FLOTATION SEPARATION

6.1 MICRO-FLOTATION TESTS

Mineral floatability is closely related to solution pH values, which influences the solution species of collectors and ions present in solution. Figure 6.1 shows the flotation recovery results obtained when monazite and calcite were floated separately in single-mineral flotation tests using a collector dosage of 1×10^{-4} M. A maximum recovery of around 90 % was obtained for monazite at pH 9.0 while calcite recovery at the same pH value was only around 22 %. Maximum calcite recovery was realized at pH 10.0. The results imply that an effective separation could be realized using octanohydroxamic acid at a solution pH of 9.0. However, test results obtained when mixing the two minerals at a 1:1 ratio provided a different outcome.

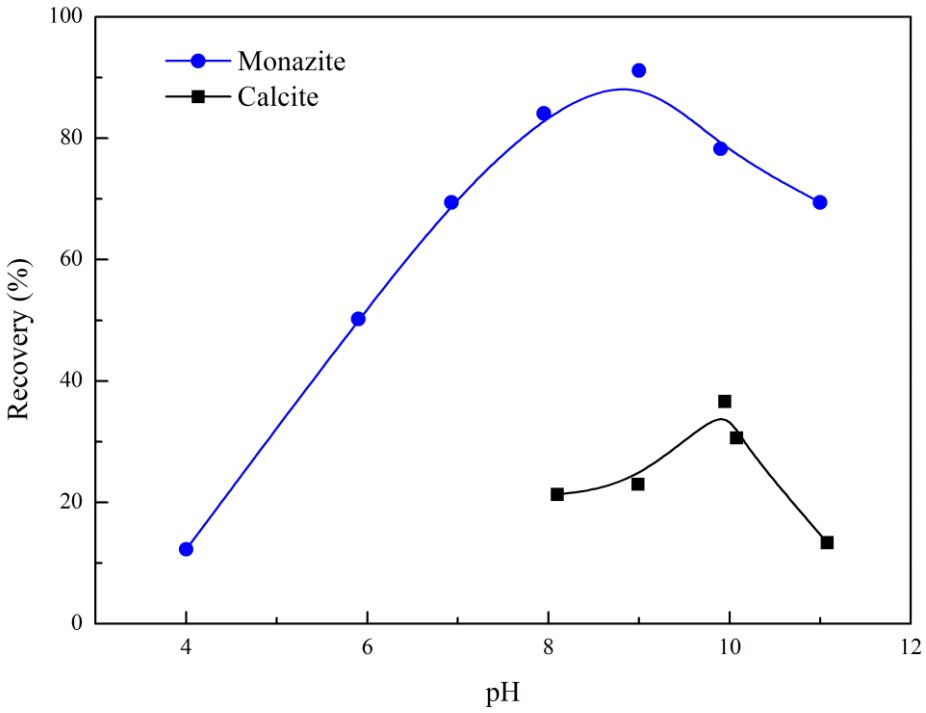

Figure 6. 1. Effects of pH values on monazite and calcite flotation when using 1×10^{-4} M octanohydroxamic acid.

While maintaining the solution pH at a value of 9.0, octanohydroxamic acid dosage was varied in tests involving both single-mineral and mixed-mineral flotation systems. As shown in Figure 6.2, the presence of calcite suppresses the flotation of monazite when

using octanohydroxamic acid dosages less than 2.5×10^{-4} M. Furthermore, the recovery of calcite reached values approaching 100 % at high collector dosage levels. As such, selectivity was significantly lower in the mixed-mineral system and declined substantially with an increase in octanohydroxamic acid concentration. At the dosage of 1×10^{-4} M as used in the pH experiments (Figure 6.1), the monazite recovery in the mixed-mineral system was only around 40 % compared to the 90 % value obtained from the single-mineral tests while the calcite recovery remained relatively unchanged.

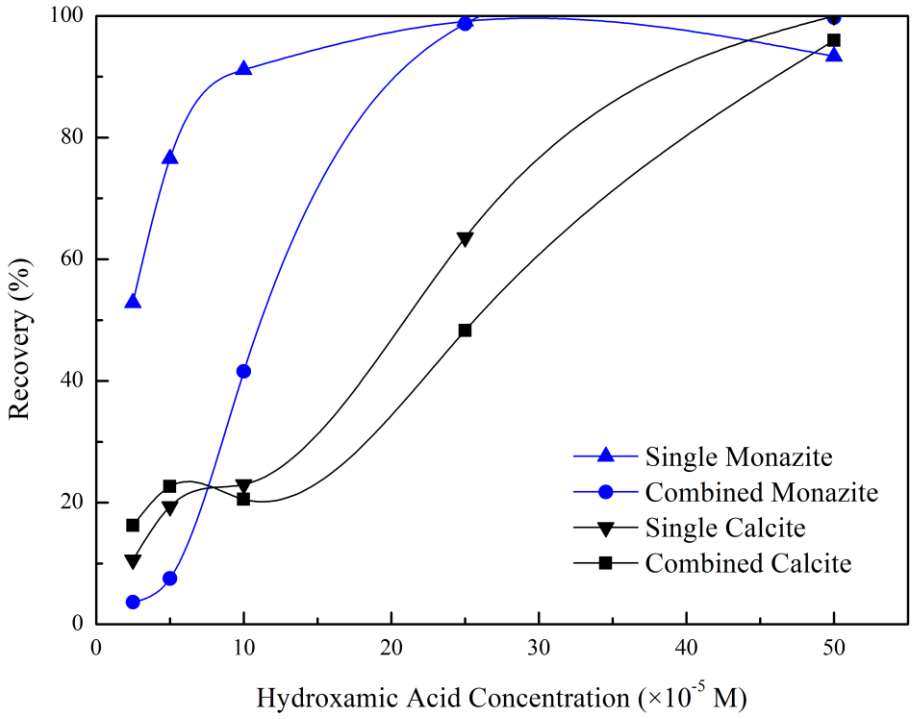

Figure 6. 2. Effects of octanohydroxamic acid concentration on monazite and calcite flotation at pH 9.0.

Calcite is a sparingly soluble mineral and crystal ions will dissolve from its surfaces in water. As previously discussed, the influence of calcium and carbonate ions on flotation have been reported in literature. Figure 6.3 shows the effects of calcium and carbonate ions on monazite flotation. Monazite recovery values decreased exponentially with the increases in calcium ions concentration while carbonate ions showed negligible effects. Therefore, depression in monazite recovery in the presence of calcite shown in Figure 6.2 may be attributed to the dissolution of calcium ions from the calcite surfaces.

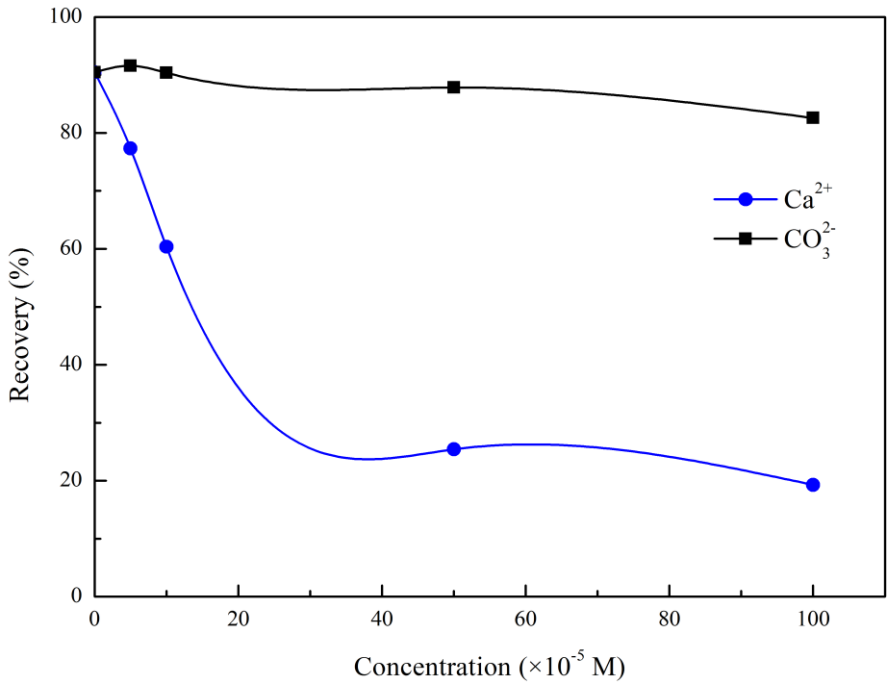

Figure 6. 3. Effects of calcium and carbonate ions on the flotation of monazite using 1×10^{-4} M octanohydroxamic acid.

6.2 ADSORPTION TESTS

In an effort to develop a fundamental understanding of flotation results, adsorption density was measured over a range of solution pH values and calcium ion concentrations. As shown in Fig. 6.4, maximum adsorption density values for the monazite and calcite were obtained at pH 9.0 and 10.0, respectively, which agreed well with the optimum recovery values obtained from the micro-flotation tests (Figure 6.1). The vertically-oriented monolayer adsorption density of the octanohydroxamic acid was estimated to be 8.1 μM/m^2 assuming the cross sectional area of the octanohydroxamic acid molecule to be 20.5 Å^2 (the number of adsorbed monolayers = molecular size (m^2) × adsorption density (M/m^2) × Avogadro number (6.02×10^{23})) (Ni and Liu, 2012). As such, 75 % of the monazite surface was covered by octanohydroxamic acid at pH 9.0 when the bulk concentration was 1×10^{-3} M.

Micro-flotation tests indicated that calcium ions decreased monazite recovery, most likely due to a negative effect on the surface hydrophobicity. To better understand the effect, the adsorption of calcium ions onto the monazite surfaces and the corresponding

impact on octanohydroxamic acid adsorption were also evaluated. The adsorption density of octanohydroxamic acid decreased initially with an increase in calcium concentration before reaching a minimum at a concentration of 5×10^{-6} M (Figure 6.5). The adsorption density of the calcium ions increased slightly from 1.5 to 2.1 μM/m^2 with an elevation in the calcium concentrations from 5×10^{-5} to 5×10^{-3} M (2 to 200 ppm). For concentrations below 5×10^{-5} M, adsorption tests were not conducted due to the lower limits of the ICP-OES analyzer. However, it is reasonable to assume that the adsorption density was below 1.5 μM/m^2 for the lower calcium ion concentrations. Monolayer coverage of bare dehydrated Ca^{2+} ions corresponds to an adsorption density of 52.9 μM/m^2. However, James and Healy (1972a) found that inner hydration sheaths of metallic cations remain adsorbed on a silica surface. The radius used for monolayer coverage calculations was the radius of bare cations plus the diameter of a water molecule. In this case, the monolayer coverage of calcium corresponds to 3.76 μM/m^2. Using this value, only half of the monazite surface was covered by calcium ions at pH 9.0 within the studied calcium concentrations.

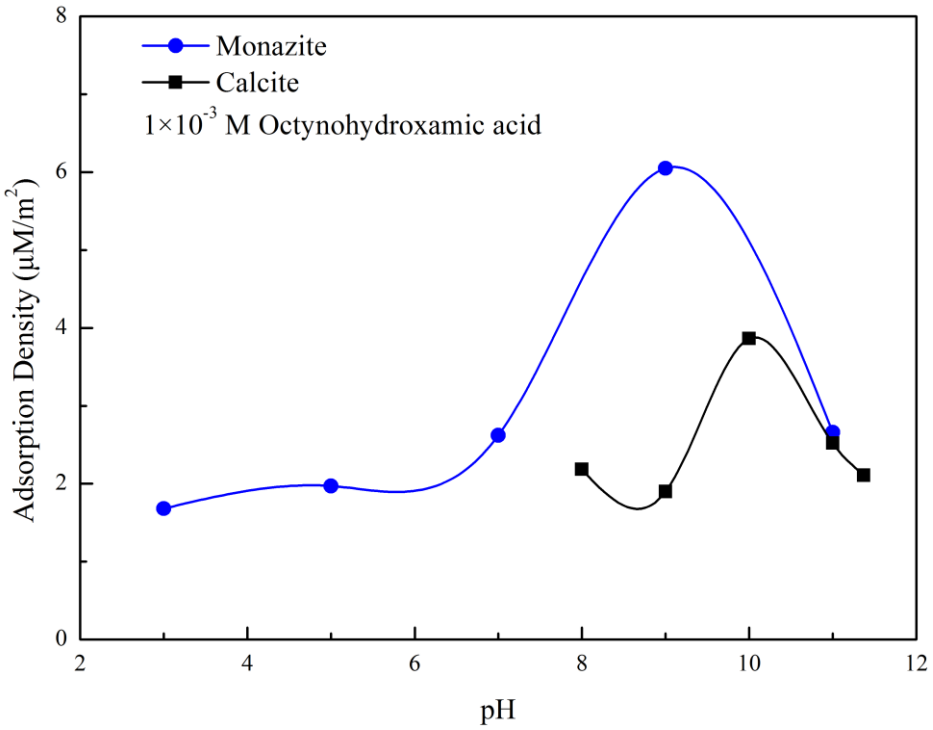

Figure 6. 4. Effect of pH on the adsorption of octanohydroxamic acid on monazite and calcite.

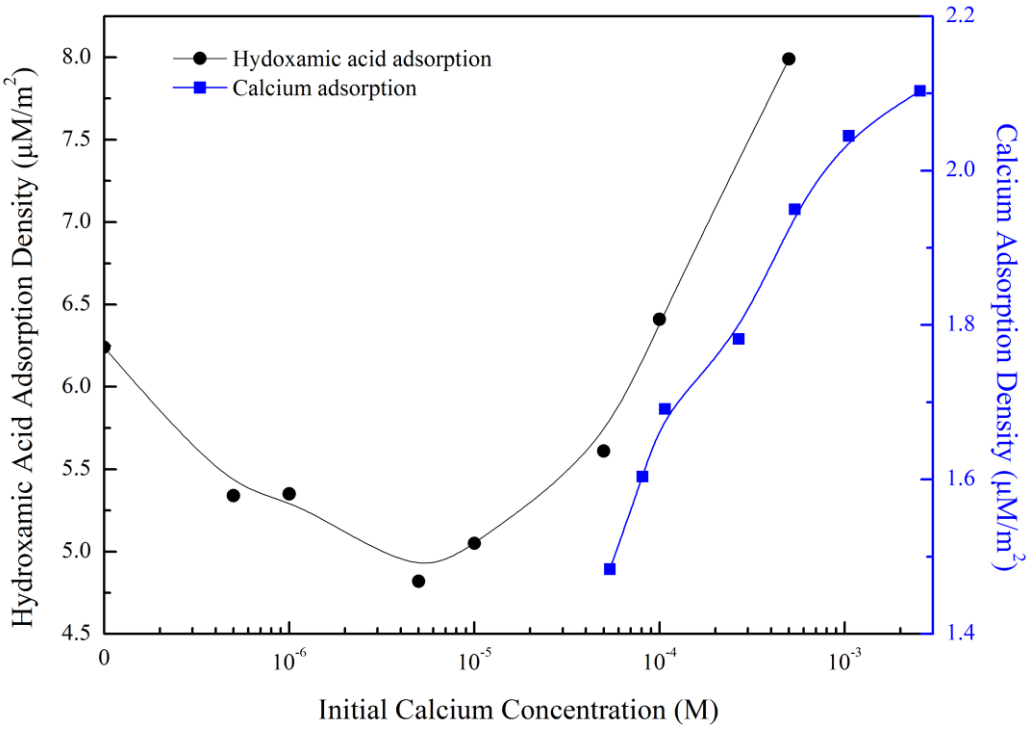

Figure 6. 5. Effects of initial concentration of calcium ions on the adsorption of 1×10^{-3} M octanohydroxamic acid and calcium ions on monazite surface at pH 9.0.

6.3 ELECTROKINETIC TESTS

The adsorption mechanism was investigated using electro-kinetic tests based on the fact that the isoelectric point (IEP) of mineral particles typically shift when specific adsorption occurs in the Stern layer. As shown in Figure 6.6, the IEP of pure monazite was located at a solution pH value of 6.5 which agreed with values reported in literature (Cheng *et al*., 1993; Cheng, 2000). The zeta potential of monazite is pH sensitive which indicates that hydrogen and hydroxyl ions are potential determining ions for monazite. The influence of calcium ions on the electro-kinetic properties of monazite was more evident in basic solutions. For a calcium concentration of 1×10^{-6} M, the effect was negligible. However, with the addition of 1×10^{-5} M and 1×10^{-4} M calcium ions, the absolute charges of monazite decreased when pH values were larger than 8.2 and 7.0, respectively. Since the concentrations of calcium ions were much smaller than that of the supporting electrolyte (1 mM KCl), compression of electrical double layer was minor and specific adsorption of the calcium ions on monazite was expected to occur. When the calcium ion concentration was increased to 1×10^{-3} M and 5×10^{-3} M, the

IEP of the monazite was significantly shifted to the right side, providing evidence of strong specific adsorption.

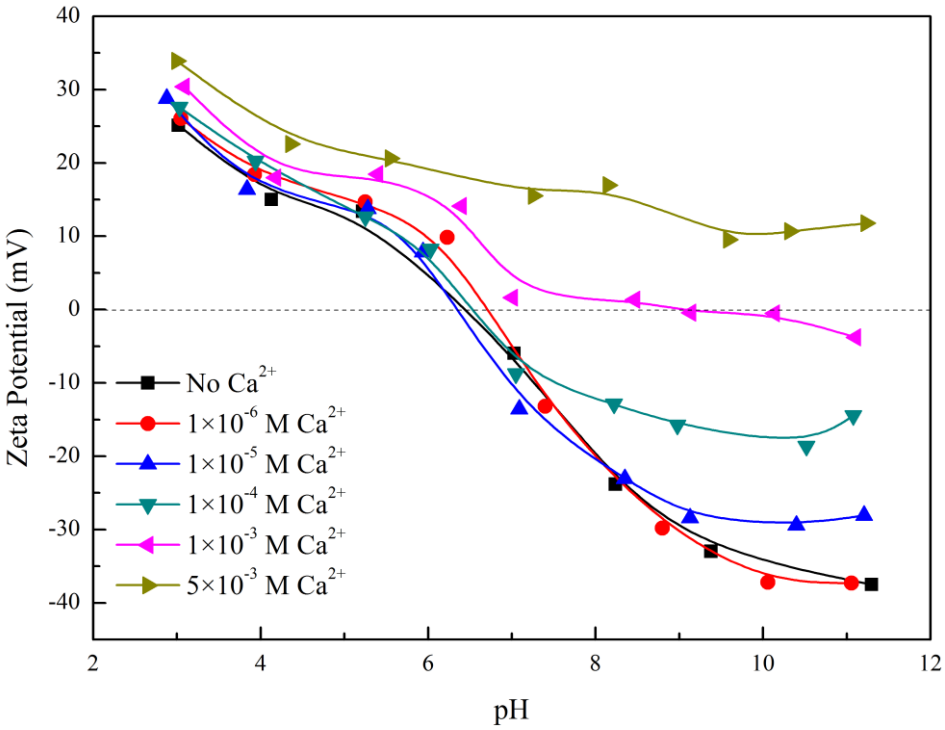

Figure 6. 6. Effects of calcium ions on the electro-kinetic properties of monazite at different pH values.

6.4 FTIR ANALYSES

FTIR analyses were conducted to evaluate the surface chemical changes of monazite after the adsorption of octanohydroxamic acid. Fig. 6.7 shows the spectrum of octanohydroxamic acid, monazite, and monazite conditioned in octanohydroxamic acid. Assignments of selected FTIR bands of solid octanohydroxamic acid are shown in Table 6.1. The bands of monazite at 945 cm^{-1} and 982 cm^{-1} were assigned to rare earth oxygen and phosphate oxygen bonds. After adsorption of octanohydroxamic acid, new bands at 1604 cm^{-1} appeared, indicating the occurrence of chemical adsorption. Octanohydroxamic acid showed two peaks around 1609 cm^{-1}, i.e., 1562 cm^{-1} and 1620 cm^{-1}, representing the C-N stretch/N-H bend and C=O stretch, respectively. Therefore, it is reasonable to suggest that the chemical reaction which occurred between octanohydroxamic acid and monazite involved the C-N, N-H, and C=O groups.

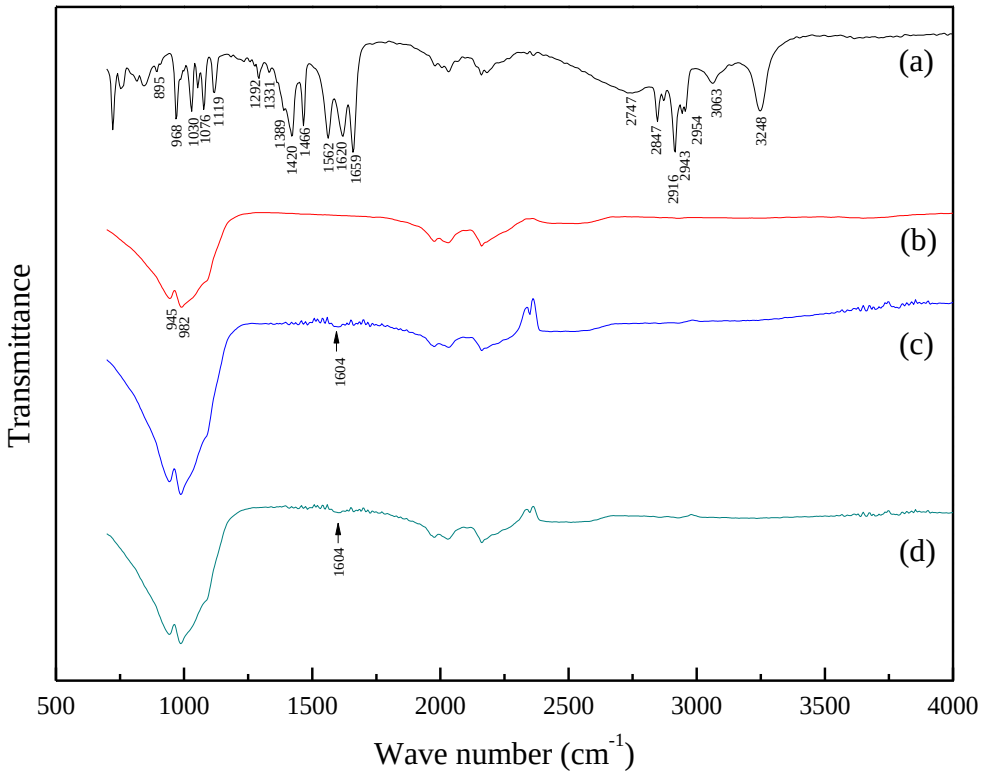

Figure 6. 7. FTIR spectrum of monazite and octanohydroxamic acid. (a) octanohydroxamic acid; (b) monazite conditioned in water at pH 9.0; (c) monazite conditioned in 1×10^{-3} M octanohydroxamic acid at pH 9.0; (d) monazite conditioned in 3×10^{-3} M octanohydroxamic acid at pH 9.0.

Table 6. 1. Assignments of selected FTIR bands from solid octanohydroxamic acid.

FTIR cm^{-1}	Assignment	FTIR cm^{-1}	Assignment
895	C-C-C skeletal stretch	1562	C-N stretch, N-H bend
968	N-O stretch	1620	C=O stretch
1030	C-O stretch	1659	C=O stretch
1076	C-C-C stretch	2747	O-H stretch
1119	C-H symmetric deformation	2847	C-H symmetric stretch for CH2/CH3
1292	$(CH_2)_n$ wag	2916	C-H symmetric stretch for CH2/CH3
1331	CH3 deformation	2943	C-H antisymmetric stretch for CH2/CH3
1389	-OH bend of N-O-H	2954	C-H antisymmetric stretch for CH2/CH3
1420	N-O-H in place bend	3063	Fermi resonance of C-N stretch and N-H bend
1466	C-N stretch	3248	N-H stretch

For the calcite system, no new peaks appeared after conditioning with 1×10^{-3} M octanohydroxamic acid as shown in Figure 6.8, which indicates weak adsorption at the lower collector dosage level. When the dosage was increased to 5×10^{-3} M octanohydroxamic acid, adsorption peaks occurred at 1608, 2855, 2924, and 2954 cm^{-1} which existed even after rinsing. As such, evidence indicates the existence of strong chemical adsorption of the collector onto the calcite surfaces at the higher collector concentration. The similar peaks (1604 cm^{-1} for monazite and 1608 cm^{-1} for calcite) indicate a nearly identical chemical adsorption mechanism given that the 4 cm^{-1} shift may be due to the difference in active sites.

As shown in Figure 6.2 and 6.3, the presence of calcium ions has a negative effect on monazite flotation recovery which is likely due to the impact on collector adsorption. When Ca^{2+} was added to the monazite system, the FTIR adsorption peak for monazite conditioned in octanohydroxamic acid solution shifted from 1604 cm^{-1} to 1607 cm^{-1}, and to 1608 cm^{-1} (Figure 6.9). Therefore, in terms of octanohydroxamic acid adsorption, the surface characteristics of monazite gradually transformed to that of calcite when calcium concentration was increased in solution. Monazite conditioned in 5×10^{-3} M

Ca^{2+} and 3×10^{-3} M and octanohydroxamic acid showed very strong adsorption peaks at 1608, 2855, 2924, and 2954 cm^{-1}, which did not occur for monazite and calcite conditioned in the same dosage of collector without the addition of Ca^{2+}. It is reasonable to suggest that precipitation occurred in the monazite-calcium-octanohydroxamic acid system. A titration test of a solution containing 5×10^{-3} M Ca^{2+} and 3×10^{-3} M octanohydroxamic acid showed that precipitates of white color started forming at pH 8.1.

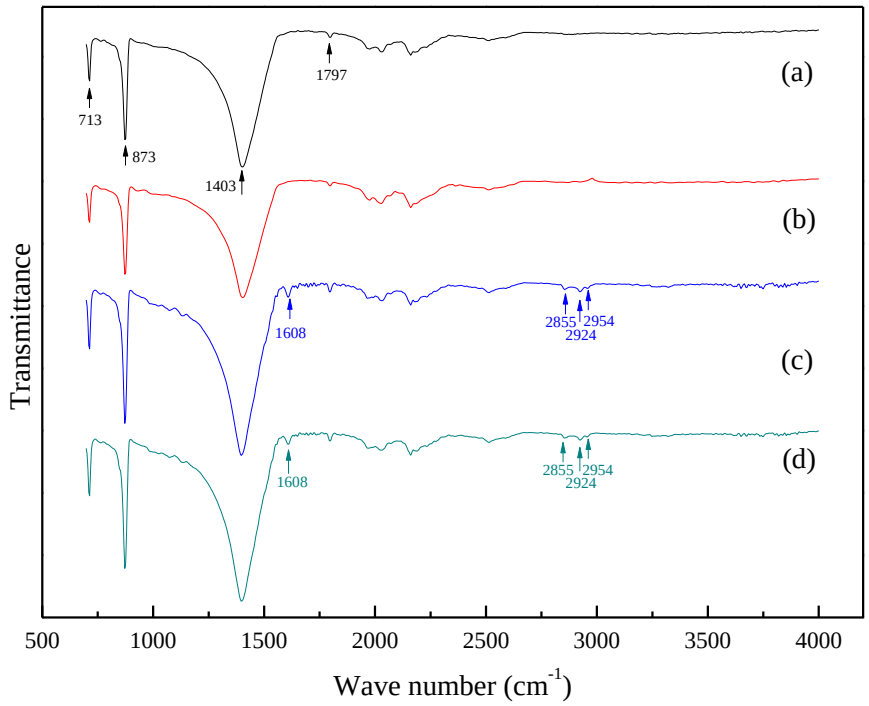

Figure 6. 8. FTIR spectrum of calcite (a) conditioned in water at pH 9.0; (b) conditioned in 1×10^{-3} M hydroxamic acid at pH 9.0; (c) conditioned in 5×10^{-3} M hydroxamic acid at pH 9.0 without rinsing; (d) conditioned in 5×10^{-3} M hydroxamic acid at pH 9.0 with rinsing.

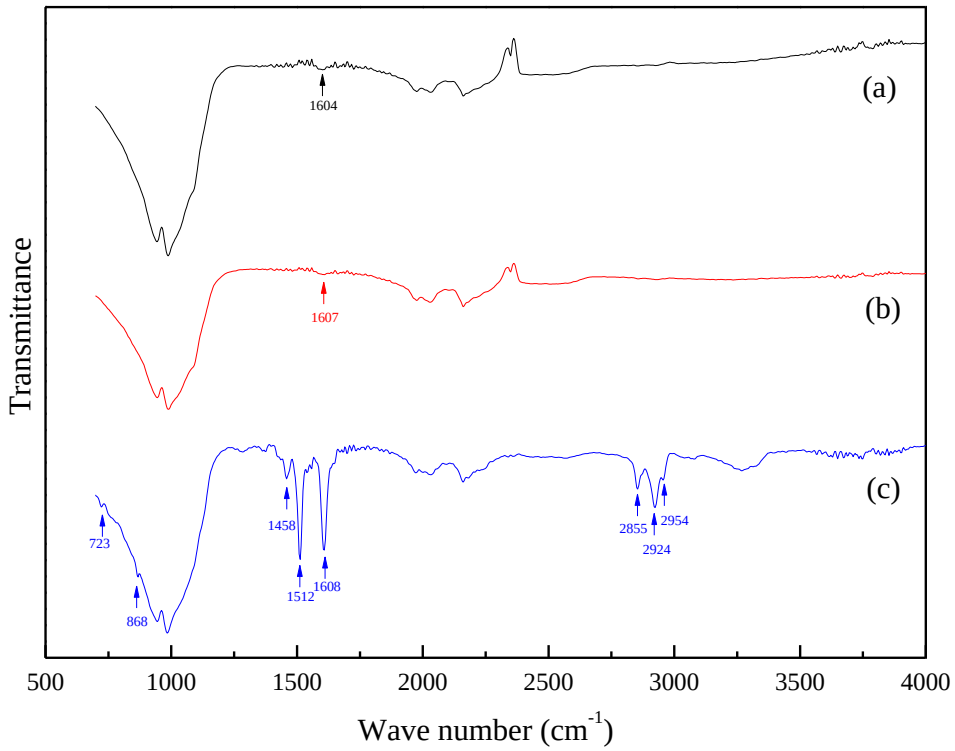

Fig. 6. 9. Effect of Ca^{2+} on the adsorption of octanohydroxamic acid on monazite: (a) monazite conditioned in 1×10^{-3} M hydroxamic acid at pH 9.0; (b) monazite conditioned in 1×10^{-3} M Ca^{2+} and 1×10^{-3} M hydroxamic acid; (c) monazite conditioned in 5×10^{-3} M Ca^{2+} and 3×10^{-3} M hydroxamic acid.

6.5 DEPRESSION MECHANISM OF Ca^{2+} FOR MONAZITE FLOTATION

6.5.1 Crystal Characteristics of Monazite

Monazite crystal occurs in monoclinic space group with P21/n settings. Cleavages usually occur along (100) planes (Figure 6.10). The rare earth and oxygen atoms exposed on the fresh surface are unsaturated. When placed in water, hydrolysis occurs due to electrical compensation leaving the surface sites divided into two different types, i.e., rare earth oxygen (REE-OH) and phosphate oxygen (P-OH) sites.

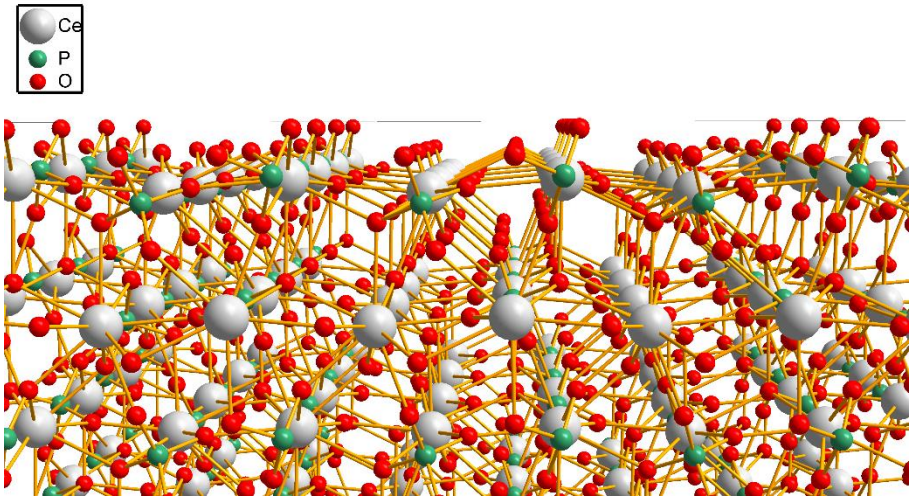

Figure 6. 10. Ball and stick model of the cleavage of monazite ($CePO_4$) occurring on (100) plane.

The dissolution rate of monazite at 25 °C and pH 9.0 is less than 10^{-17} mol/cm^2/s (Oelkers and Poitrasson, 2002). Therefore, the dissolution of rare earth and phosphate atoms is minimal thereby eliminating the possibility of specific adsorption for the pure mineral-water systems used in this study. As such, the isoelectric point (IEP) and the point-of-zero charge (PZC) are equal with a value of about 6.5 as shown in Figure 6.6.

The surface charge of monazite can be represented by the single site surface protonation reactions, i.e.,

$$\equiv SO^- + \equiv H^+ \rightleftharpoons \equiv SOH \qquad \text{(Eq. 6.1)}$$

$$\equiv SOH + \equiv H^+ \rightleftharpoons \equiv SOH_2^+ \qquad \text{(Eq. 6.2)}$$

where $\equiv SO^-$, $\equiv SOH$, and $\equiv SOH_2^+$ represent surface species, i.e., rare earth – oxygen and phosphate – oxygen sites, and $\equiv H^+$ represents the hydrogen ion near the charged surface (Parks, 1965; Somasundaran and Agar, 1967; Yoon *et al.*, 1979). The surface charge was controlled by the equilibrium of the above equations. At the pH > 6.5, more surface sites were deprotonated and $\equiv SO^-$ was dominant.

6.5.2 Adsorption of Calcium Ions on Monazite

Concentrations of different calcium species in solution are controlled by the following reversible reactions (Somasundaran and Agar, 1967):

$$Ca^{2+} + OH^- \rightleftharpoons CaOH^+, K_1 = 10^{1.40}, \quad \text{(Eq. 6.3)}$$

$$Ca(OH)^+ + OH^- \rightleftharpoons Ca(OH)_{2(aq)}, K_2 = 10^{1.37}, \quad \text{(Eq. 6.4)}$$

$$Ca(OH)_{2(aq)} \rightleftharpoons Ca(OH)_{2(s)}, K_2 = 10^{2.45}. \quad \text{(Eq. 6.5)}$$

The equilibrium concentrations of Ca^{2+}, $CaOH^+$, and $Ca(OH)_{2(aq)}$ in a solution containing 5×10^{-3} M of total calcium ions were calculated and are shown in Figure 6.11. Ca^{2+} ion is the dominant species in the pH range of 3-12 while concentrations of hydrolyzed species of calcium, i.e., $CaOH^+$, increase with a rise in the solution pH value. Electro-kinetic tests (Figure 6.6) indicate that adsorption of calcium onto the monazite surface occurred more readily in the basic pH environment, which coincided with the pH range where hydrolysis of calcium ions occurred. Based on these findings, the solution species resulting in the specific adsorption was mainly $Ca(OH)^+$.

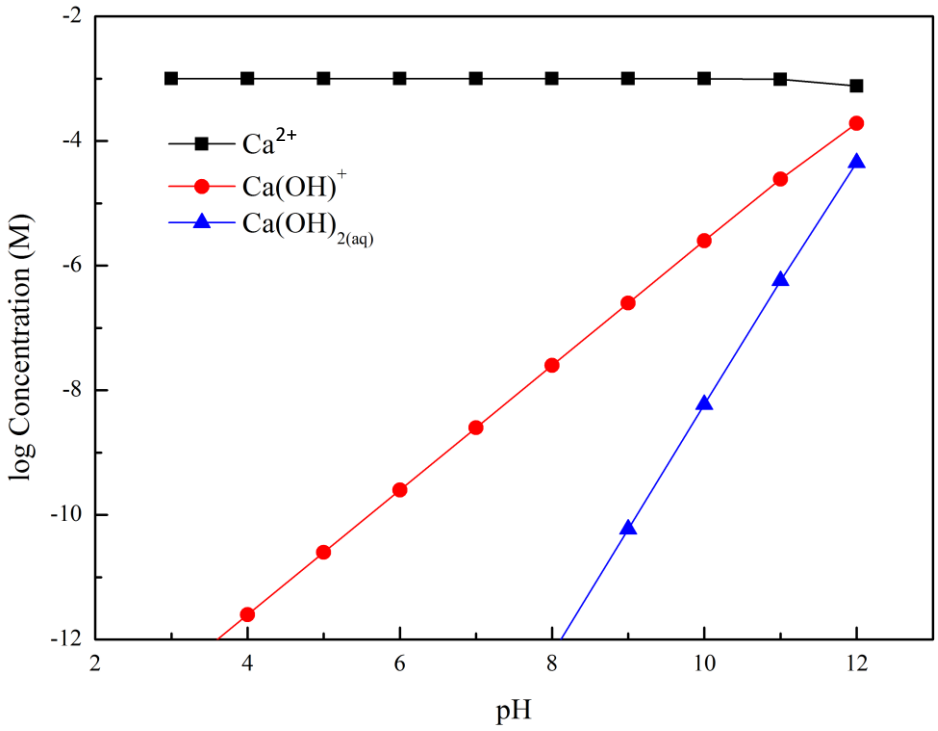

Figure 6. 9. Specification diagram of calcium ions in solution.

The precipitation of calcium hydroxide occurs at pH > 13.1. As such, at pH 9.0, the adsorption of octanohydroxamic acid by calcium hydroxide forms in solution does not need to be considered. As previously presented in this dissertation (section 5.3), the adsorption study indicated that calcium adsorption on monazite was less than a

monolayer. The adsorption occurred within the Stern layer and thickness of the adsorbed layer was the radius of calcium ions plus the diameter of a hydroxyl group, i.e., 1.00 Å plus 2.66 Å. With the addition of 1×10^{-4} M Ca^{2+}, the adsorption density of the calcium ions onto monazite surfaces is around 1.5 μM/m^2. Based on the adsorption layer thickness, adsorption density, and dissociation reactions of calcium in solution, the $Ca(OH)^+$ concentration and pH value corresponding to calcium precipitation near monazite surface were calculated to be 1.5 M and 11.30, respectively. Hydroxyl ions were likely repelled from the surface due to electrostatic repulsion, which means pH > 11.30 in bulk solution is required for the occurrence of surface precipitation. Therefore, at pH 9.0, calcium ions were adsorbed as hydrolyzed species ($CaOH^+$) on the monazite surfaces, which is also true for the higher concentrations investigated in the current study.

The adsorption of $CaOH^+$ on monazite is more likely to occur on the neutralized and deprotonated rare earth oxygen and phosphate oxygen sites via hydrogen bonding and electrostatic interactions, respectively, which could be represented by the following equations:

$$\equiv \mathrm{REEOH} + \mathrm{CaOH^+} \rightleftharpoons \equiv \mathrm{REEOH \cdots OHCa^+} \quad \text{(Eq. 6.6)}$$

$$\equiv \mathrm{REEO^-} + \mathrm{CaOH^+} \rightleftarrows \equiv \mathrm{REEOCaOH} \quad \text{(Eq. 6.7)}$$

$$\equiv \mathrm{POH} + \mathrm{CaOH^+} \rightleftarrows \equiv \mathrm{POH \cdots OHCa^+} \quad \text{(Eq. 6.8)}$$

$$\equiv \mathrm{PO^-} + \mathrm{CaOH^+} \rightleftarrows \equiv \mathrm{POCaOH} \quad \text{(Eq. 6.9)}$$

6.5.3 Effects of Calcium on the Adsorption of Octanohydroxamic Acid on Monazite

Surface hydrolysis has been proven necessary for octanohydroxamic acid adsorption on minerals (Peterson *et al.*, 1965; Fuerstenau *et al.*, 1967, 1970; Nararajan and Fuerstenau, 1983; Pradip and Fuerstenau, 1983, 1985; Nagaraj, 1988). In the current study, the importance of surface hydrolysis was also observed, i.e., optimum flotation and adsorption occurred at pH 9.0 where concentrations of rare earth hydrolyzed species reached maximum.

Based on the fact that octanohydroxamic acid is strongly complexed with the rare earth

atoms, the effects of $CaOH^+$ on the adsorption of octanohydroxamic acid on rare earth oxygen sites may be ignored. However, for the phosphate oxygen sites, both $CaOH^+$ and octanohydroxamic acid adsorbed via hydrogen bonding and competitive adsorption was expected to occur, which explains the decreases of hydroxamate adsorption when a small dosage of calcium ions was added.

Adsorption density of octanohydroxamic acid was increased with the addition of a higher dosage of calcium ions (see Figure 6.5). It was reasonable to suggest that the phosphate oxygen sites were covered with a layer of $Ca(OH)^+$ attached via hydrogen bonding or electrostatic attraction. The electrostatically adsorbed $CaOH^+$ with the hydroxyl group oriented away from the solid surface provides alternative active sites for octanohydroxamic acid adsorption, which agrees with the fact that the hydrolysis of metal atoms on minerals is required for formation of chelates with octanohydroxamic acid (Fuerstenau *et al.*, 1970, 1967; Nararajan and Fuerstenau, 1983; Peterson *et al*., 1965; Pradip and Fuerstenau, 1983, 1985). The shifts of the adsorption peaks (1604, 1607, 1608 cm^{-1}) of monazite which interacted with both calcium and octanohydroxamic acid also suggested the formation of calcium-hydroxamate chelates on monazite surfaces.

The primary hydration sheath of $CaOH^+$ adsorbed via hydrogen bonding increased the surface hydrophilicity. The combined effects were that stronger surface hydrophobicity was not observed with the addition of calcium ions despite the adsorption of additional octanohydroxamic acid. The interaction model between monazite, octanohydroxamic acid, and calcium ions was shown in Figure 6.11. However, surface and bulk precipitation of calcium hydroxamate occurred with the addition of higher dosages of calcium and octanohydroxamic acid, i.e., 5×10^{-3} M of Ca^{2+} and 3×10^{-3} M octanohydroxamic acid in the current study.

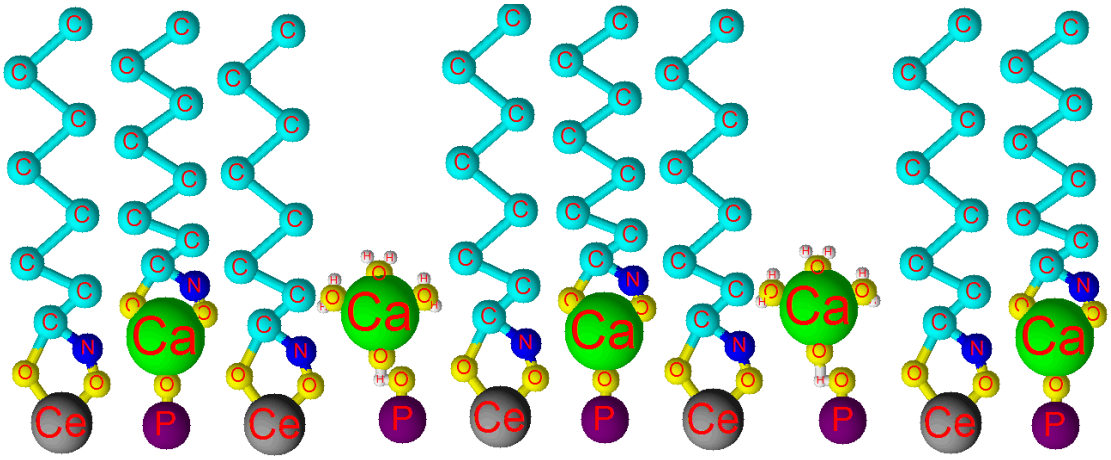

Figure 6. 10. Model of interaction among monazite, calcium ions, and octanohydroxamic acid.

6.6 Effects of Depressants on Flotation Selectivity

6.6.1 Micro-flotation Tests

Selective flotation is normally obtained by selecting appropriate depressant types and dosages. In the current study, sodium silicate and sodium hexametaphosphate (SHMP) were used as depressants. Effects of depressant dosages on monazite and calcite flotation in both single and combined systems were investigated. Zhang et al. (2017b) showed that maximum flotation recovery of monazite using 1×10^{-4} M octanohydroxamic acid occurred at pH 9.0. As such, all the micro-flotation tests were conducted at pH 9.0. As shown in Figure 6.12 and 6.13, both sodium silicate and SHMP provided minor effects on the floatability of monazite in single mineral tests. However, calcite recovery values were decreased significantly with the increases in depressant dosages, i.e., complete depression occurred using either 5×10^{-6} M SHMP or 0.025 g/L sodium silicate. As such, both SHMP and sodium silicate seem to be promising depressants for monazite-calcite flotation separation.

However, when flotation tests were conducted in monazite-calcite combined systems, depression of monazite occurred for both SHMP and sodium silicate (Figure 6.12 and 6.13). Efficient separation of monazite and calcite at pH 9.0 when using SHMP and 2.5×10^{-4} M octanohydroxamic acid was impossible based on the fact that monazite was depressed simultaneously with calcite. However, with a small dosage (i.e., 0.01 g/L) of

sodium silicate, monazite recovery of nearly 90% was obtained while only recovered 30% of calcite. The reason might be that SHMP can form stable chelates with calcium ions on monazite surfaces and prevent the collector adsorption (Hong *et al.*, 2012; Zhang *et al*., 2014).

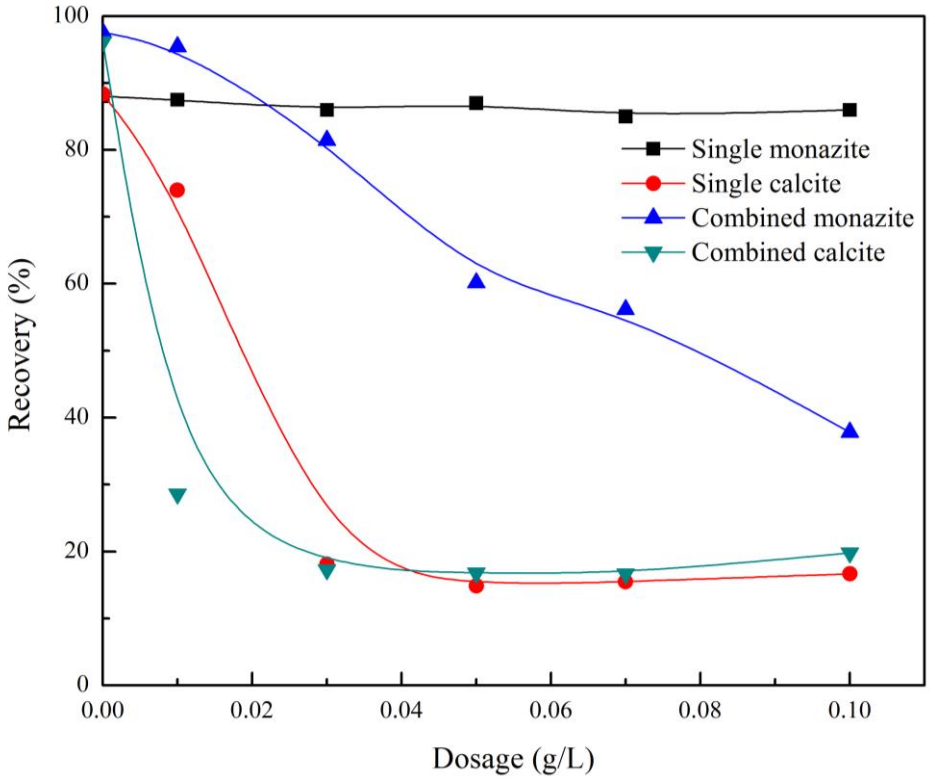

Figure 6. 11. Effects of sodium silicate on single mineral and mixed monazite and calcite flotation when using 2.5×10^{-4} M octanohydroxamic acid at pH 9.0.

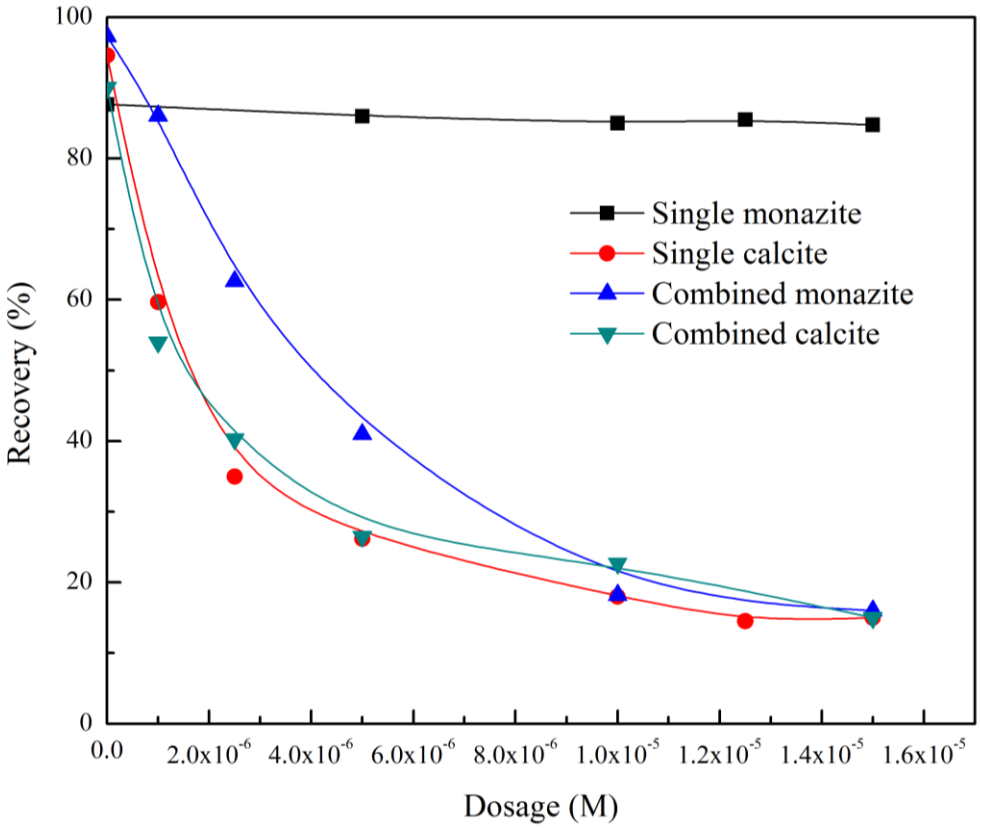

Figure 6. 12. Effects of sodium hexametaphosphate on single mineral and combined flotation of monazite and calcite when using 2.5×10^{-4} M octanohydroxamic acid at pH 9.0.

Calcite is a semi-soluble mineral and calcium ions will be dissolved from its surfaces. The dissolved calcium ions will re-adsorb onto monazite surfaces, which may explain the depression of monazite in the combined system. Figure 6.14 and 6.15 show the effects of sodium silicate and SHMP on monazite floatability when calcium ions were added into the single mineral system. The flotation recovery was sensitive to calcium concentration when calcium ions and sodium silicate or SHMP co-existed in the system. For example, with the addition of 0.05 g/L sodium silicate, the recovery values decreased from nearly 85% to less than 10% with the increases in calcium concentration from 1×10^{-4} to 2.5×10^{-4} M. The depression effect might be due to the co-adsorption of calcium and depressants on monazite surfaces.

Flotation results with addition of sodium silicate and SHMP prior to calcium ions were also shown in Figure 6.14 and 6.15, respectively. As shown in the figures, the adding sequence did not make a significant difference, indicating that instead of an ordered

structure with calcium immediately above monazite surfaces and depressant next to the calcium layers, the co-adsorbed species were more likely form a disordered compact layer around monazite surfaces. Both the single and combined mineral flotation tests indicated that sodium silicate perform better than SHMP due to the existence of calcium ions. As such, in the following study, sodium silicate was selected as the depressant for calcite.

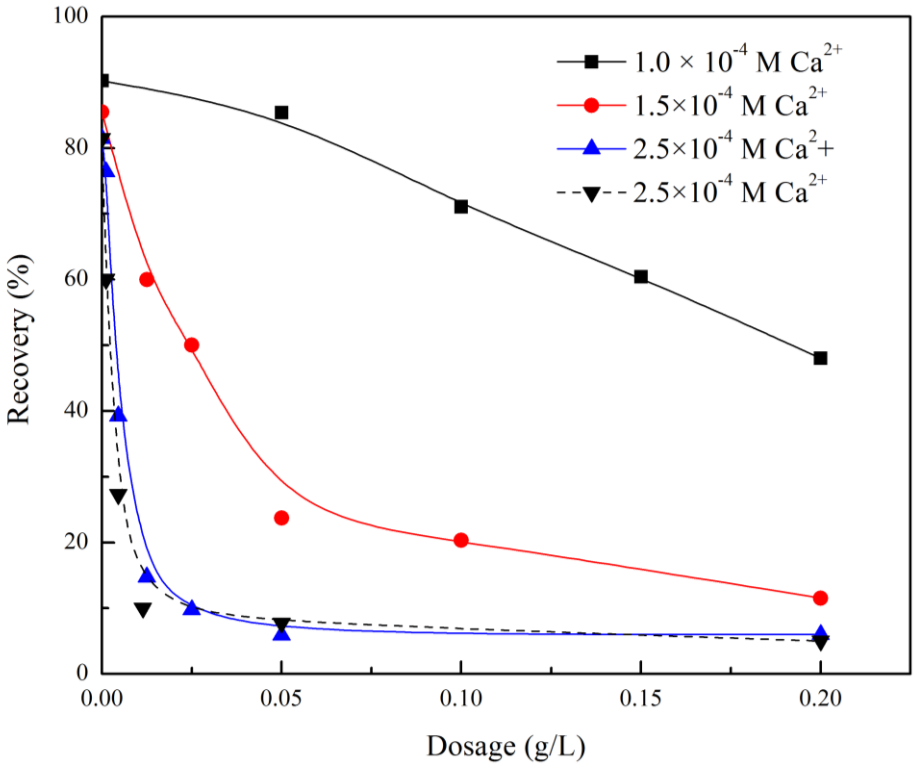

Figure 6. 13. Effects of calcium ions and sodium silicate on monazite single mineral flotation (the dash line means sodium silicate was added before calcium ions).

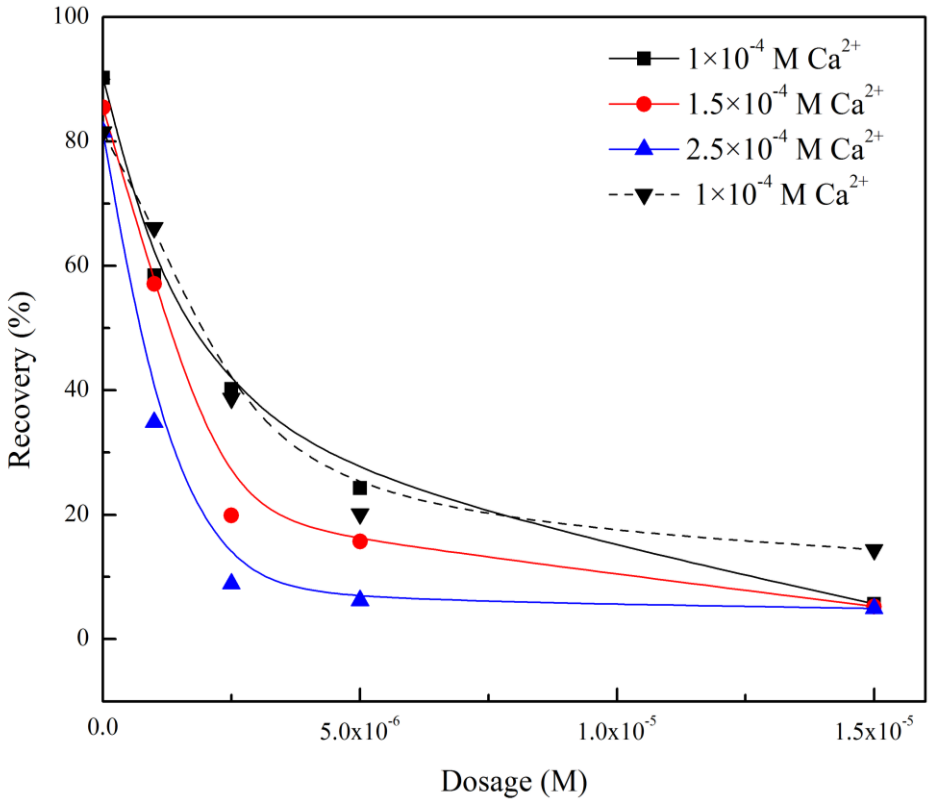

Figure 6. 14. Effects of calcium ions and SHMP on monazite single mineral flotation (the dash line means SHMP was added before calcium ions).

To achieve efficient separation of monazite from calcite, the negative effects of calcium ions need to be removed using appropriate regulators. In the current study, two chelating reagents, i.e., citric acid and EDTA, were used to clean monazite surfaces. Figure 6.16 shows the effects of the two regulators on pure monazite and calcite floatability. As shown in the figure, both monazite and calcite recoveries were decreased with the increases in regulator dosages. Citric acid had stronger depression effects compared with EDTA, thus, calcite was more likely to be depressed when using citric acid as the regulator. Depression was not expected based on the fact that the purpose is to remove calcium from monazite surfaces. However, when using less than 5×10^{-4} M regulators, the depression effect was negligible.

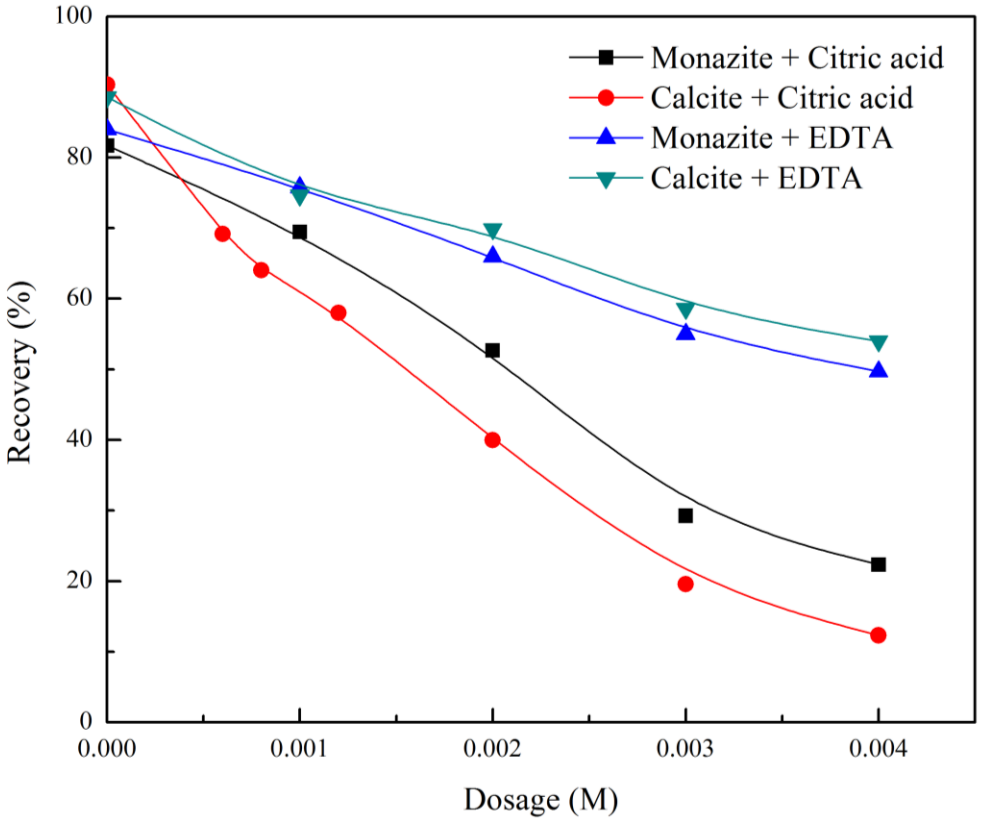

Figure 6. 15. Effects of citric acid and EDTA on single mineral flotation of monazite and calcite.

To evaluate the efficiency of citric acid and EDTA regarding calcium removal from monazite surfaces, flotation tests were conducted with sequential addition of calcium ions, regulators, and sodium silicate. As shown in Figure 6.17, flotation recovery of monazite increased from 10% to about 85% and 90% using citric acid and EDTA as regulators, respectively. As such, both of them can eliminate the negative effects of calcium ions by preventing the co-adsorption of sodium silicate and calcium ions on monazite surfaces. However, flotation recovery was decreased with higher dosages of regulators, which agreed with the pure mineral flotation results shown in Figure 6.17 and might be due to the adsorption of excessive citric acid and EDTA on monazite surfaces.

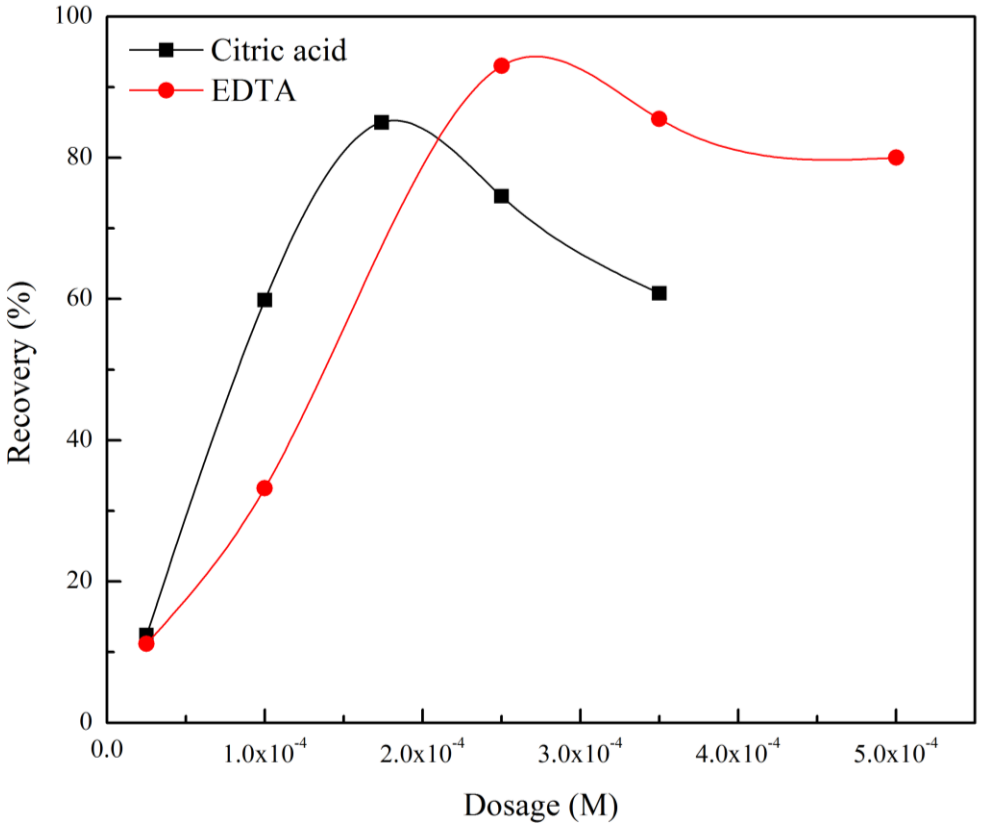

Figure 6. 16. Effects of citric acid and EDTA dosages on monazite flotation with the addition of 2.5×10^{-4} M Ca^{2+} and 0.05 g/L sodium silicate

Combined mineral flotation tests were conducted to evaluate the effects of citric acid and EDTA on the separation performance. As shown in Figure 6.18, both citric acid and EDTA could effectively improve monazite recovery from 60% to about 90%, while they had minor effects on calcite recovery. As such, the negative effects of calcium ions on monazite-calcite flotation separation can be eliminated using appropriate regulators such as citric acid and EDTA. Furthermore, EDTA performed better than citric acid, which agreed with previous tests and might be due to the stronger depression effects of citric acid.

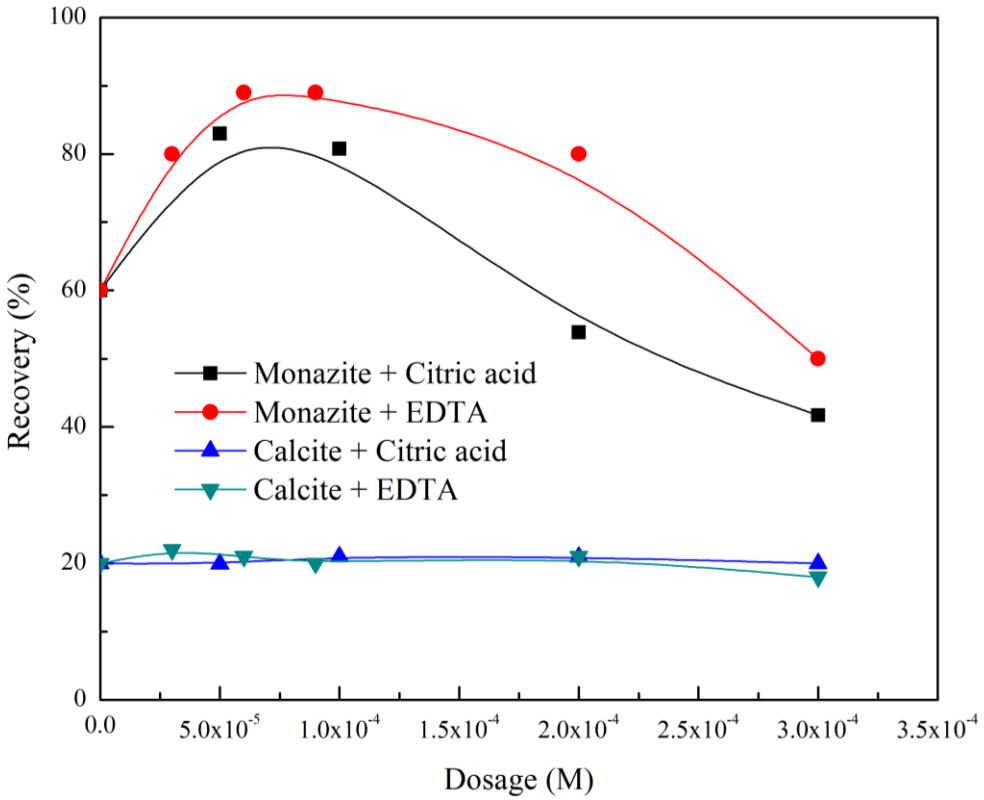

Figure 6. 17. Effects of citric acid and EDTA dosages on monazite and calcite combined mineral flotation separation using 0.05 g/L sodium silicate and 2.5×10^{-4} M octanohydroxamic acid.

6.6.2 Electrokinetic Tests

Adsorption of chemicals on mineral surfaces may change the electrokinetic properties such as isoelectric point (IEP) and potential distribution of mineral particles. As such, electrokinetic tests were conducted to evaluate the adsorption of calcium, sodium silicate, citric acid and EDTA on monazite surfaces. Figure 6.19 shows the effects of 1 mM Ca^{2+} and/or 0.05 g/L sodium silicate on monazite surface potential. As shown in the figure, the IEP of monazite occurred at pH 5.5, which agrees with the data reported by Cheng *et al*. (2000) and Zhang *et al*. (2017a). Larger zeta potential changes were observed in basic environments with the addition of 0.1 mM Ca^{2+}, which might be due to the specific adsorption of the hydrolyzed calcium species. Strong specific adsorption of sodium silicate on monazite surfaces occurred, as indicated by the left shift of IEP. Based on the fact that sodium silicate has no effects on monazite flotation when using octanohydroxamic acid as the collector (Figure 6.12), octanohydroxamic acid has

higher affinity for monazite than sodium silicate. For pH values less than 5.5, the addition of sodium silicate together with calcium is similar to the addition of solely sodium silicate regarding the zeta potential changes. However, for pH values above 5.5, zeta potential of monazite conditioned with both sodium silicate and calcium ions gradually increased with the increases in pH values. As such, co-adsorption of calcium and sodium silicate occurred on monazite surfaces when pH values exceeded 5.5.

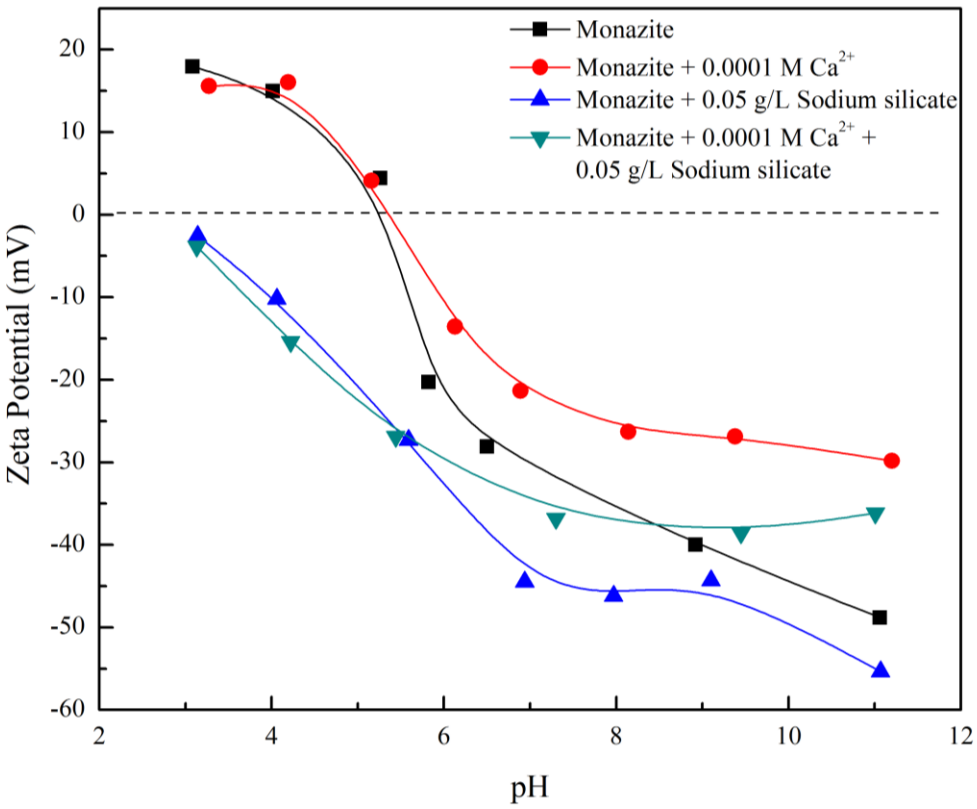

Figure 6. 18. Effects of calcium and/or sodium silicate on monazite zeta potential.

IEP of the calcite used in current study occurred at about pH 10.5 (Figure 6.21). Decreases in zeta potential and left shits of IEP were observed when adding sodium silicate, citric acid, or EDTA, which indicates the occurrence of specific adsorption. Furthermore, octanohydroxamic acid adsorption on calcite surfaces is pretty weak due to the lower stability of the hydroxamate-calcium complex. As such, the sodium silicate, citric acid, or EDTA competes with octanohydroxamic acid for calcite surfaces and results in depression.

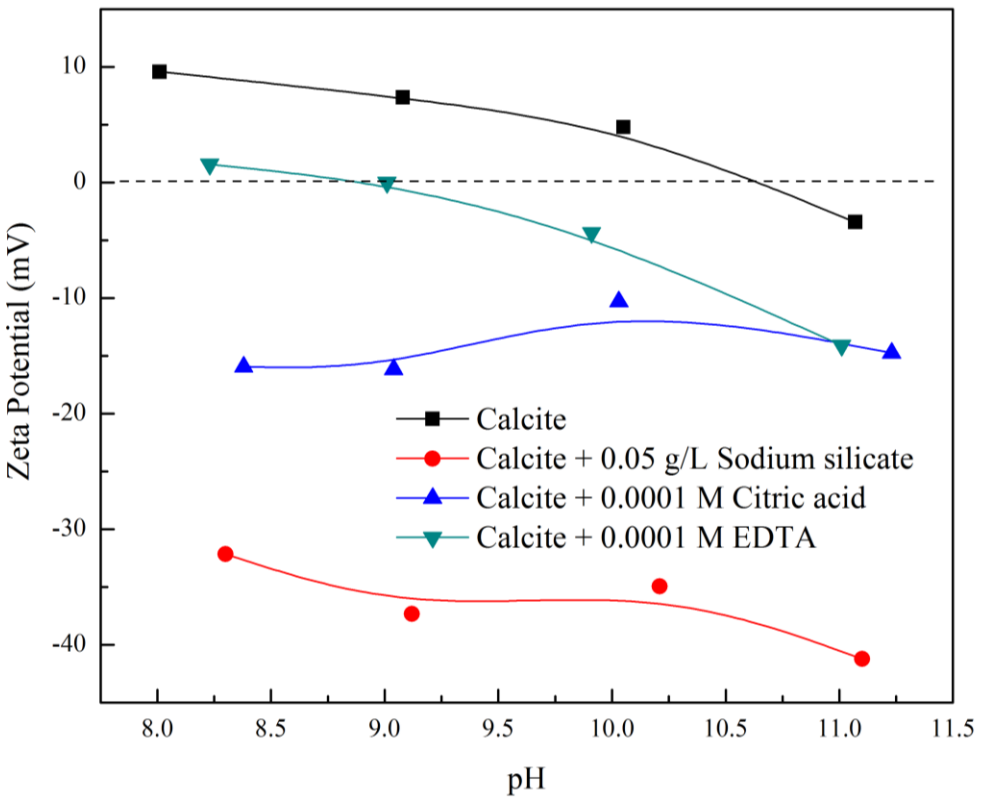

Figure 6. 19. Effects of sodium silicate, citric acid and EDTA on calcite zeta potential.

IEP of monazite decreased significantly when conditioned with 0.1 mM citric acid or EDTA, indicating the occurrence of specific adsorption (Figure 6.21). Both citric acid and EDTA of 0.1 mM had minor effects on monazite floatability when using 2.5×10^{-4} M octanohydroxamic acid as the collector, which indicated stronger interaction between the collector and monazite surfaces. Furthermore, as shown in Figure 6.21, citric acid made monazite surfaces carry more negative charges than EDTA when using the same dosage, which agreed with the fact that citric acid provides stronger depression effects on monazite floatability than EDTA.

When calcium ions were added together with regulators, the zeta potentials are between the values observed for monazite conditioned with regulators and unconditioned monazite. For low pH values, the zeta potentials are close to the former, which is due to the lack of hydrolyzed calcium species. For high pH values, hydrolyzed calcium species such as $Ca(OH)^{+}$ specifically adsorb onto monazite surfaces. In addition, both citric acid and EDTA can form soluble complexes and clean monazite surfaces. As such,

when calcium was added together with citric acid and/or EDTA, the zeta potential of monazite was expected to remain unchanged. Figure 6.21 shows that for high pH values, the zeta potential of monazite conditioned with both calcium and regulators especially EDTA was close to unconditioned monazite, proving the surface cleaning function.

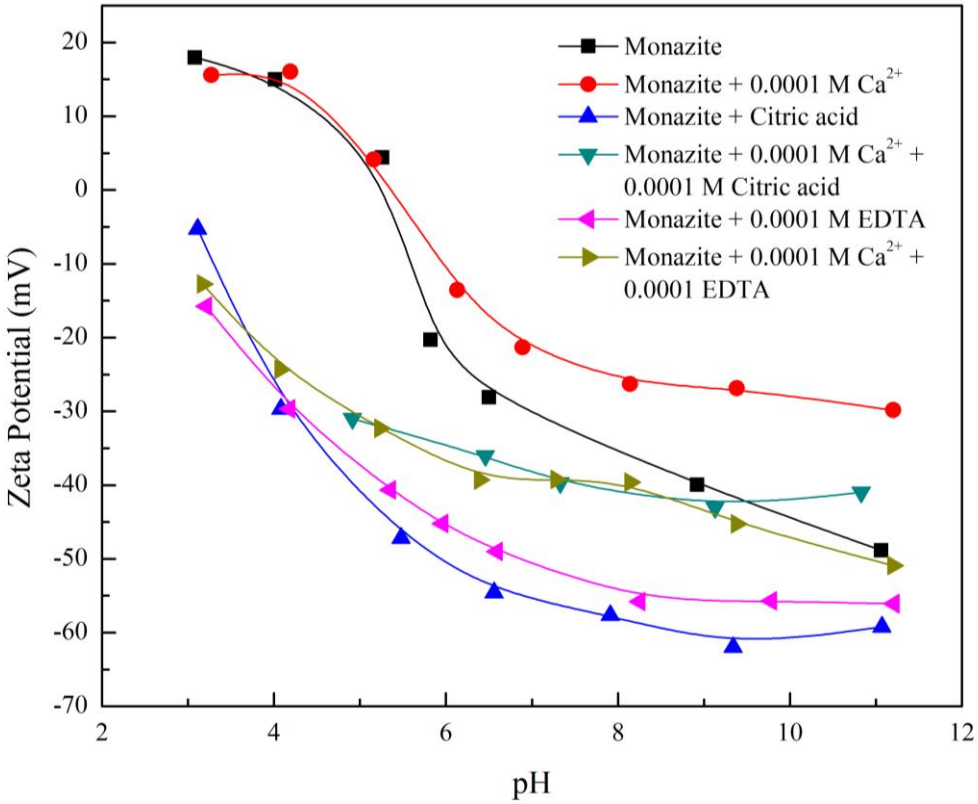

Figure 6. 20. Effects of calcium, citric acid and EDTA on monazite zeta potential.

6.6.3 Solution Chemistry Study

The electrokinetic study showed that the hydrolyzed calcium species (e.g. $Ca(OH)^{+}$) which have higher concentration in basic environment co-adsorbed with sodium silicate on monazite surfaces, and thus reducing collector adsorption as well as flotation recovery. Both citric acid and EDTA can be used as regulators to eliminate the negative effects caused by calcium ions. To better understand the role of different solution species involved in monazite-calcite flotation system, solution chemistry calculation was conducted. The reactions and reaction constants used for calculation were listed in Table 6.2.

Table 6. 2. Reactions and constants for solution chemistry calculation.

Reactions	Reaction Constants
$H_2O \leftrightarrows H^+ + OH^-$	10^{-14}
$Ca^{2+} + OH^- \leftrightarrows Ca(OH)^+$	$10^{1.4}$
$Ca^{2+} + 2OH^- \leftrightarrows Ca(OH)_{2(aq)}$	$10^{2.77}$
$Ca^{2+} + 2OH^- \leftrightarrows Ca(OH)_{2(s)}$	$10^{5.22}$
$SiO_{2(s)} + 2H_2O \leftrightarrows Si(OH)_{4(aq)}$	$10^{-2.64}$
$Si(OH)_4 + OH^- \leftrightarrows SiO(OH)_3^- + H_2O$	$10^{4.29}$
$SiO(OH)_3^- + OH^- \leftrightarrows SiO_2(OH)_2^{2-} + H_2O$	$10^{0.99}$
$4Si(OH)_4 + 2OH^- \leftrightarrows Si_4O_6(OH)_6^{2-} + 6H_2O$	$10^{15.03}$
$H^+ + Cit^{3-} \leftrightarrows CitH^{2-}$	$10^{6.33}$
$2H^+ + Cit^{3-} \leftrightarrows CitH_2^-$	$10^{11.05}$
$3H^+ + Cit^{3-} \leftrightarrows CitH_3$	$10^{14.18}$
$Ca^{2+} + Cit^{3-} \leftrightarrows CaCit^-$	$10^{11.35}$
$Ca^{2+} + Cit^{3-} + H^+ \leftrightarrows CaCitH$	$10^{18.48}$
$H^+ + Edta^{4-} \leftrightarrows EdtaH^{3-}$	$10^{9.96}$
$2H^+ + Edta^{4-} \leftrightarrows EdtaH_2^{2-}$	$10^{16.61}$
$3H^+ + Edta^{4-} \leftrightarrows EdtaH_3^-$	$10^{18.86}$
$4H^+ + Edta^{4-} \leftrightarrows EdtaH_4$	$10^{20.93}$
$5H^+ + Edta^{4-} \leftrightarrows EdtaH_5^+$	$10^{23.464}$
$Ca^{2+} + Edta^{4-} \leftrightarrows CaEdta^{2-}$	$10^{12.4}$
$Ca^{2+} + Edta^{4-} + H^+ \leftrightarrows CaEdtaH^-$	10^{16}

(Data sources: Marinakis and Shergold, 1985; Westin and Rasmuson, 2005; Zhang *et al.*, 2017b. Note: CitH and Edta represent citric acid and EDTA, respectively.)

Sodium silicate of 0.05 g/L which was used for the flotation and electrokinetic tests contains 8.33×10^{-4} M of silica assuming the SiO_2 content was 100%. As such, speciation diagram of 1×10^{-3} M silica was calculated (Figure 6.22). As shown in the figure, $Si(OH)_4$ and $SiO(OH)_3^-$ were dominant species for pH values below and above 9.8, respectively. Both of the two species have hydroxyl groups, which explains the specific adsorption of sodium silicate on monazite and calcite surfaces via hydrogen bonding. Hydrolyzed calcium species such as $Ca(OH)^+$ also carry hydroxyl groups. As

such, the co-adsorption of $Ca(OH)^+$ and $Si(OH)_4$ as well as $SiO(OH)_3^-$ around monazite surfaces is possible due to the existence of hydrogen bonding. The compact layer of calcium and silica around monazite surfaces is hydrophilic and may introduce steric hindrance for octanohydroxamic acid adsorption, thus, reducing the flotation recovery (Figure 6.12).

In addition to hydrogen bonding, surface reaction was also suggested to occur between calcium and silicate on calcite surfaces (Mishra, 1982; Marinakis and Shergold, 1985; Rao *et al.*, 1988, 1990; Rao, 1989; Feng *et al.*, 2015). The surface reaction were represented as follows:

$$Ca^{2+}_{(surf)} + SiO(OH)_3^- \rightleftarrows Ca^{2+} - SiO(OH)_{3(surf)} \quad \text{(Eq. 6.10)}$$

$$Ca^{2+} - OH_{(surf)} + SiO(OH)_4 \rightleftarrows Ca^{2+} - OSi(OH)_{3(surf)} + H_2O \quad \text{(Eq. 6.11)}$$

Based on the above discussion, the possible adsorption mechanisms were presented in Figure 6.23. The interactions presented in the figure include specific adsorption of $Ca(OH)^+$, $SiO(OH)_3^-$, and $Ca(OH)^+$ on monazite surfaces; hydrogen bonding among the above three species; and surface reaction between calcium and silicate species.

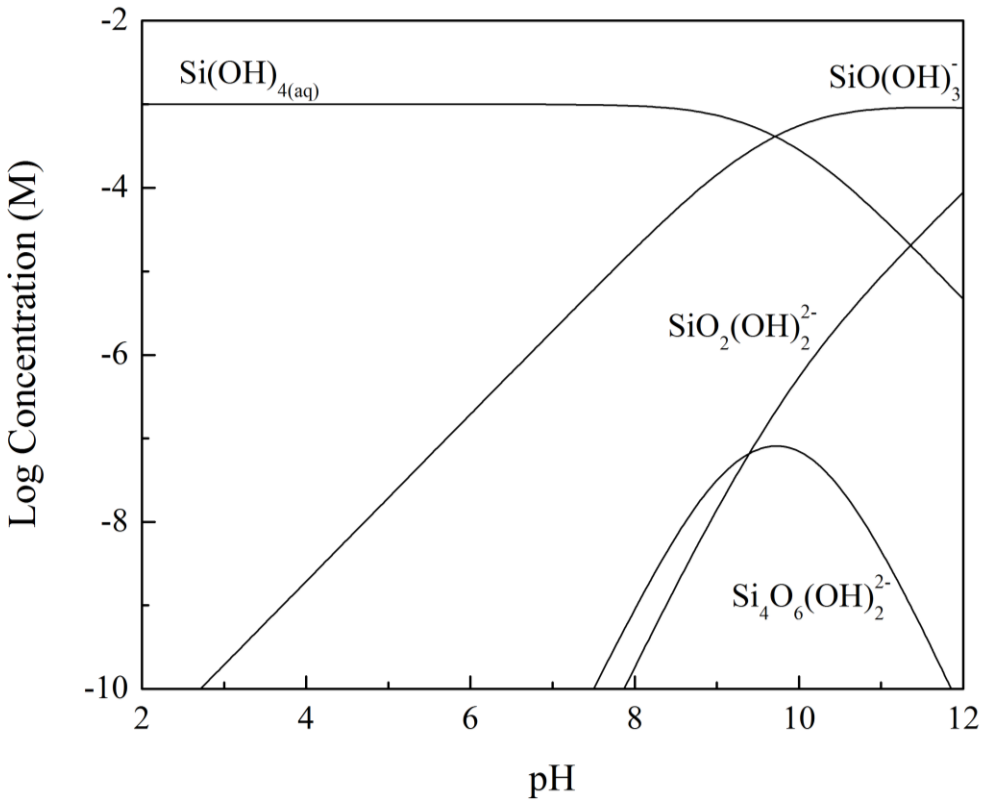

Figure 6. 21. Speciation diagram of silicate in water with a total concentration of 1×10^{-3} M.

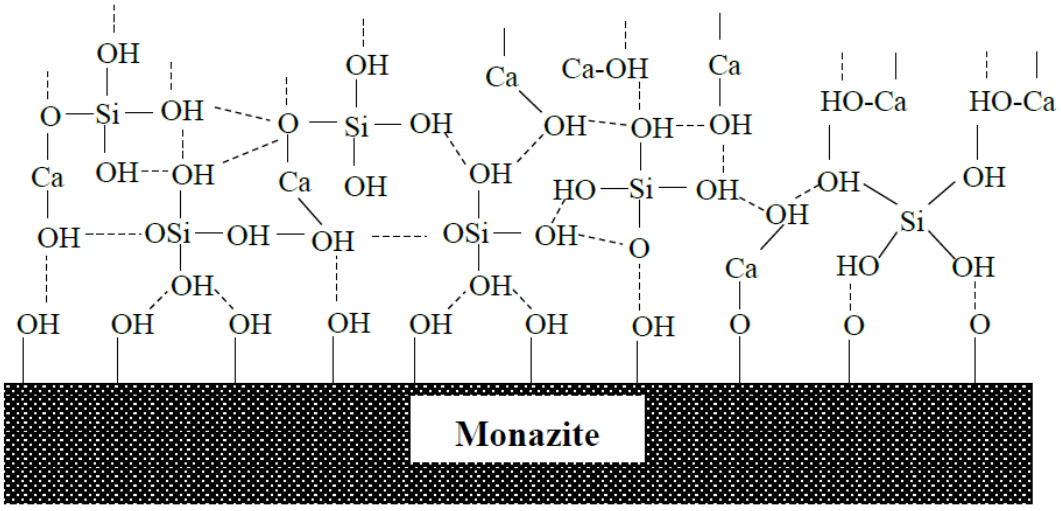

Figure 6. 22. Schematic diagram representing the co-adsorption of calcium and silicate on monazite surfaces.

The speciation diagrams of two different systems, i.e., calcium-citric acid-water and calcium-EDTA-water, were shown in Figure 6.24. As shown in the figure, instead of Ca^{2+} or $Ca(OH)^{+}$, $CaCit^{-}$ and $CaEdta^{2-}$ were the dominant species when calcium was

mixed with citric acid and EDTA, respectively. The $CaCit^-$ and $CaEdta^{2-}$ chelates were more soluble in water and more calcium will stay in solution instead of monazite surfaces. As such, the negative effects of calcium species were removed. Furthermore, compared with citric acid, EDTA was more efficient to reduce the $Ca(OH)^+$ concentration, which explained its better performance for the mixed mineral micro-flotation (Figure 6.18).

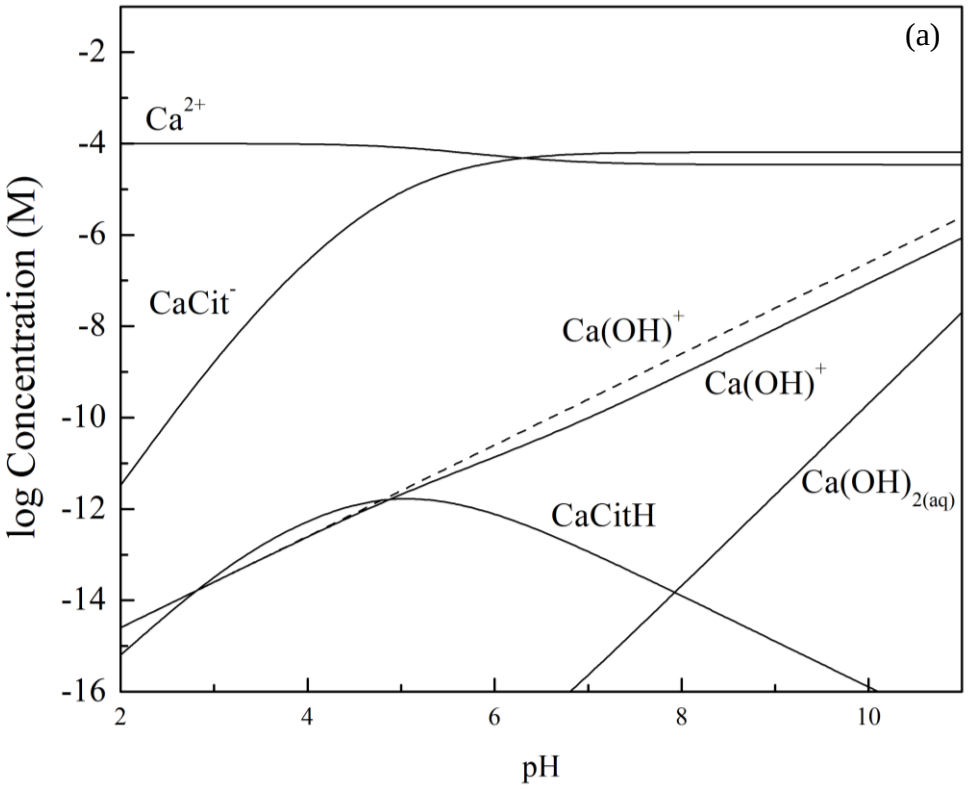

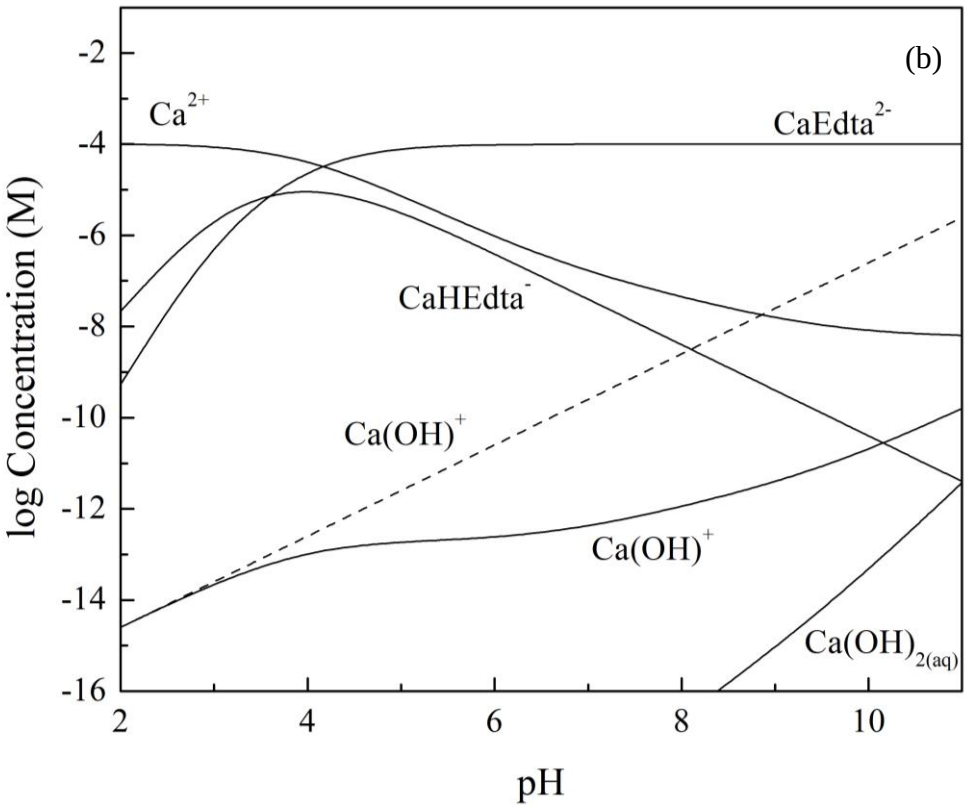

Figure 6. 23. Speciation diagrams: (a) 1×10^{-4} M Ca^{2+} and 1×10^{-4} M M citric acid in water; (b) 1×10^{-4} M Ca^{2+} and 1×10^{-4} M EDTA in water. (Dash line means the $Ca(OH)^{+}$ concentration of 1×10^{-4} M calcium-water system).

The speciation diagrams of two systems (0.1 mM Ca^{2+} plus 0.1 mM citric acid; 0.1 mM Ca^{2+} plus 0.1 mM EDTA) were shown in Figure 6.20. As shown in the figure, instead of Ca^{2+} or $Ca(OH)^{+}$, $CaCit^{-}$ and $CaEdta^{2-}$ are the dominant species when calcium was mixed with citric acid and EDTA, respectively.

6.7. CONCLUSIONS

Systematic studies of the problems involved in monazite-calcite flotation systems were reported in this chapter. Hydrolyzed species of calcium ions dissolved from calcite surfaces were adsorbed onto monazite surface, which depressed monazite floatability. In addition, the hydrolyzed calcium species could be co-adsorbed onto monazite surfaces with silicates by hydrogen bonding and/or surface reaction. The co-adsorbed species formed a compact hydrophilic layer on monazite surfaces, which reduced the collector adsorption due to steric hindrance and made the depressants nonselective. Using appropriate chelating reagents such as EDTA, the negative effects of calcium

species were eliminated. The detailed findings of this chapter included:

(1) Monazite recovery decreased from 90% to 40% using 1×10^{-4} M octanohydroxamic acid when floated together with calcite. With the increases in calcium concentration from 0 to 1×10^{-3} M, monazite recovery in single-mineral flotation tests decreased from 90% to less than 20%. As such, depression of monazite in the combined system was due to the calcium ions dissolved from calcite surfaces.

(2) Maximum adsorption density of octanohydroxamic acid on monazite and calcite surfaces occurred at pH 9.0 and 10.0, respectively. The adsorption density of octanohydroxamic acid decreased initially with an increase in calcium concentration before reaching a minimum at a concentration of 5×10^{-6} M. Further increases in calcium concentration increased the collector adsorption.

(3) Electrokinetic tests indicated that monazite zeta potential became less negative in weak acidic and basic environments, which was due to the specific adsorption of hydrolyzed calcium species on monazite surfaces. When calcium ions existed in the system, the FTIR bands corresponding to the metallic hydroxamate chelates changed from 1604 cm^{-1} to 1608 cm^{-1}, indicating that calcium ions served as new active sites for octanohydroxamic acid adsorption.

(4) It was conclude that with low calcium concentration, $Ca(OH)^+$ competed with the collector for P-OH surface sites, while with high calcium concentration, $Ca(OH)^+$ served as new active sites. However, monazite floatability was depressed due to the hydration of $Ca(OH)^+$ on monazite surfaces.

(5) Single-mineral flotation results indicated that calcite was intensively depressed using sodium silicate, while providing minimal effect on monazite recovery. However, in combined systems, monazite recovery was decreased from 90% to 40% with the increases in sodium silicate concentration from 0 to 0.1 g/L.

(6) In single-mineral flotation systems, monazite was depressed by sodium silicate when calcium ions were added, indicating that the depression observed in the

combined systems was due to the calcium ions dissolved from calcite surfaces. Electrokinetic tests proved the co-adsorption of $Ca(OH)^+$ and silicate species on monazite surfaces.

(7) In the combined system, monazite recovery increased from 60% to 90% and 80% using EDTA and citric acid, respectively. The relative inefficiency of citric acid was due to its weaker chelating ability with calcium ions.

CHAPTER 7. CONCENTRATION OF RARE EARTH MINERALS FROM COAL BY FROTH FLOTATION

7.1 RELEASE TESTS

Flotation release tests provided an estimate of the ultimate separation performance achievable under a given set of conditions for the Fire Clay thickener underflow material. As shown in Figure 7.1, the selectivity achieved by flotation of the sample was excellent which produced a clean coal concentrate containing 10% ash-forming minerals while recovering 85% of the combustible material. The results indicated the potential of significant economic gains from the recovery of coal prior to the concentration stages needed for REE recovery.

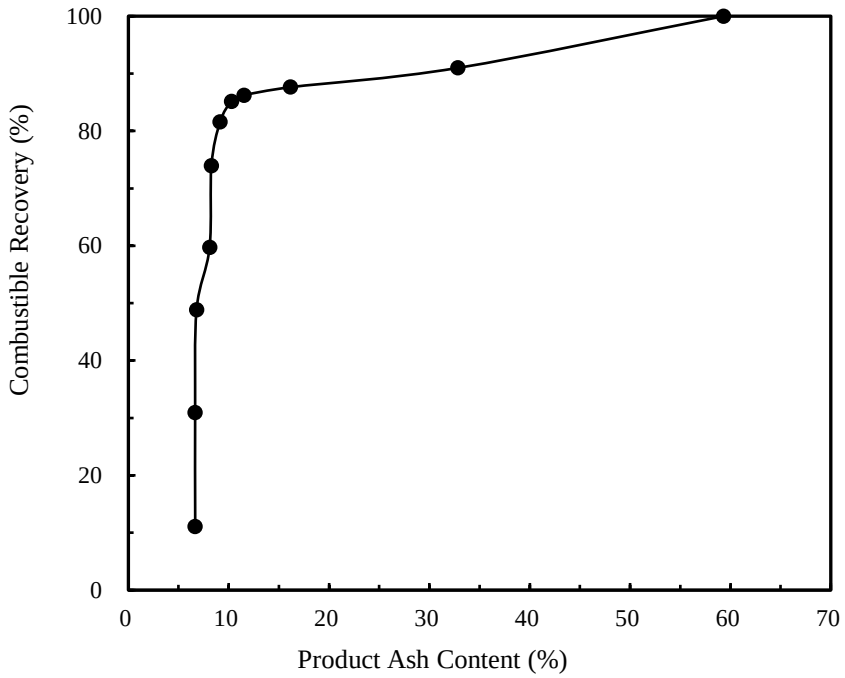

Figure 7. 1. Release test results of Fire Clay coal fine refuse.

The release analyses samples were analyzed for REE content and the results plotted in Figure 7.2 on a dry whole mass basis and dry ash basis. Products with low ash contents contained higher REE values on an ash basis but lower values on whole coal basis, a consequence of organic dilution. After the organic matter was burned, the REE associated with the organic matter reported to the residual ash. As such, a higher REE

content in the residual ash is expected as a result of organic matter through an organic affinity with humic acids or micro-dispersed as minerals or mineral associations. However, the amount of total REEs (TREEs) in the organic matrix is relatively small in total weight.

The maximum REE content on a whole sample basis occurred in flotation products containing 80% ash. Above this value, the TREE content was reduced to the dilution effect caused by the presence of low TREE content rock.

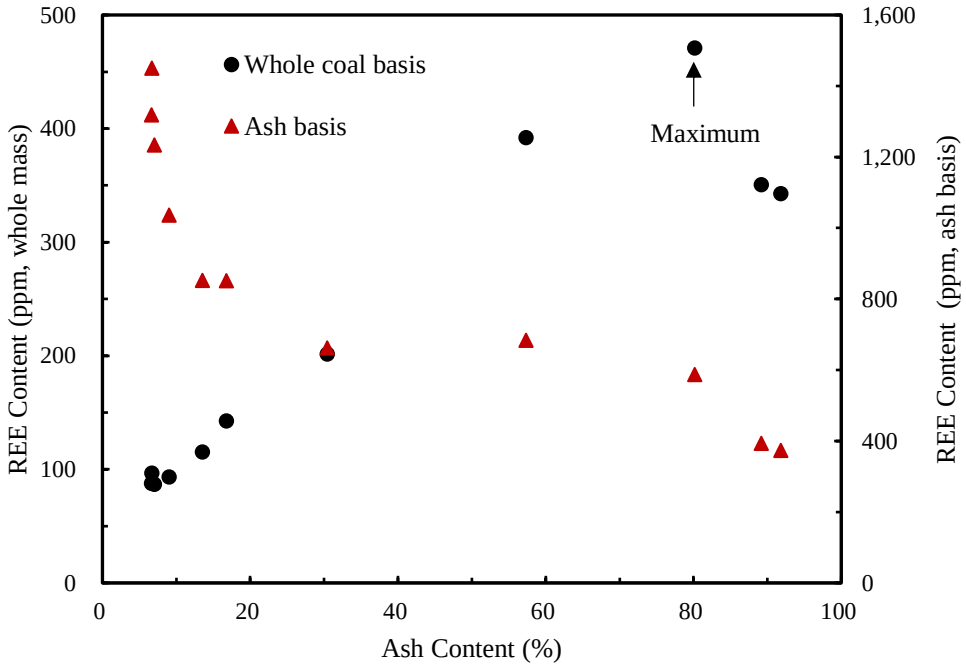

Figure 7. 2. REE content on both whole mass basis and ash basis as a function of the ash content.

The more valuable heavy REEs was found to be concentrated in the low ash content products as shown by the increase in the HREE/LREE ratio in Figure 7.3. The affinity of the HREEs may be associated with their 3^+ valence and high ionic charge density. After transfer of the REEs into the coal bed by geothermal fluids and/or exposure to volcanic ash, it is hypothesized that humic acid chelates with the HREEs and, as the humic acid content decreases, associates with the clays that fill the micro-cracks existing within the coal (Hower *et al.*, 1999; Dai *et al.*, 2016).

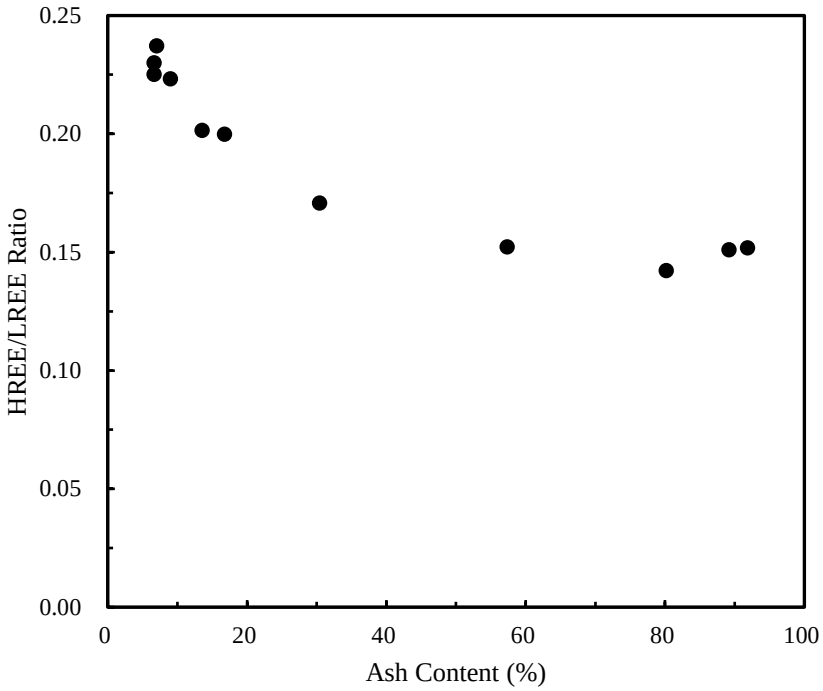

Figure 7. 3. HREE/LREE ratio as a function of the ash content.

7.2 MINERALOGICAL STUDIES

Ash materials liberated at different particle sizes might have different mineral compositions, which contributes to the understanding of the association characteristics of REEs. Figure 7.4 shows the XRD patterns of the tailings obtained from different stages of the REE release tests. Mineral compositions of the coarse tailings are more complicated than the fine tailings. Namely, in addition to the major minerals such as kaolinite, illite, and quartz, the coarse tailings also contain small amounts of calcite, dolomite, pyrite, and rutile. The changes in mineralogy of the tailings might represent the variances in the sources of ash materials from coal seams, i.e., ultra-fine ash materials completely came from the coal organic matrix while coarse materials were mainly from the partings, roofs, floors, and out of seam segments.

Kaolinite contents of the liberated ash materials gradually increased with the decreases in particle sizes and kaolinite became the dominate material in the final tailings (T7). Based on the fact that REEs are more concentrated in the ultra-fine tailings, it is possible that REEs are closely associated with the clay minerals that are dispersed in coal organic

matrix, which has also been reported by other researchers (Eskenazy, 1987; Seredin, 1996; Birk and White, 1999; Hower *et al.*, 1999)

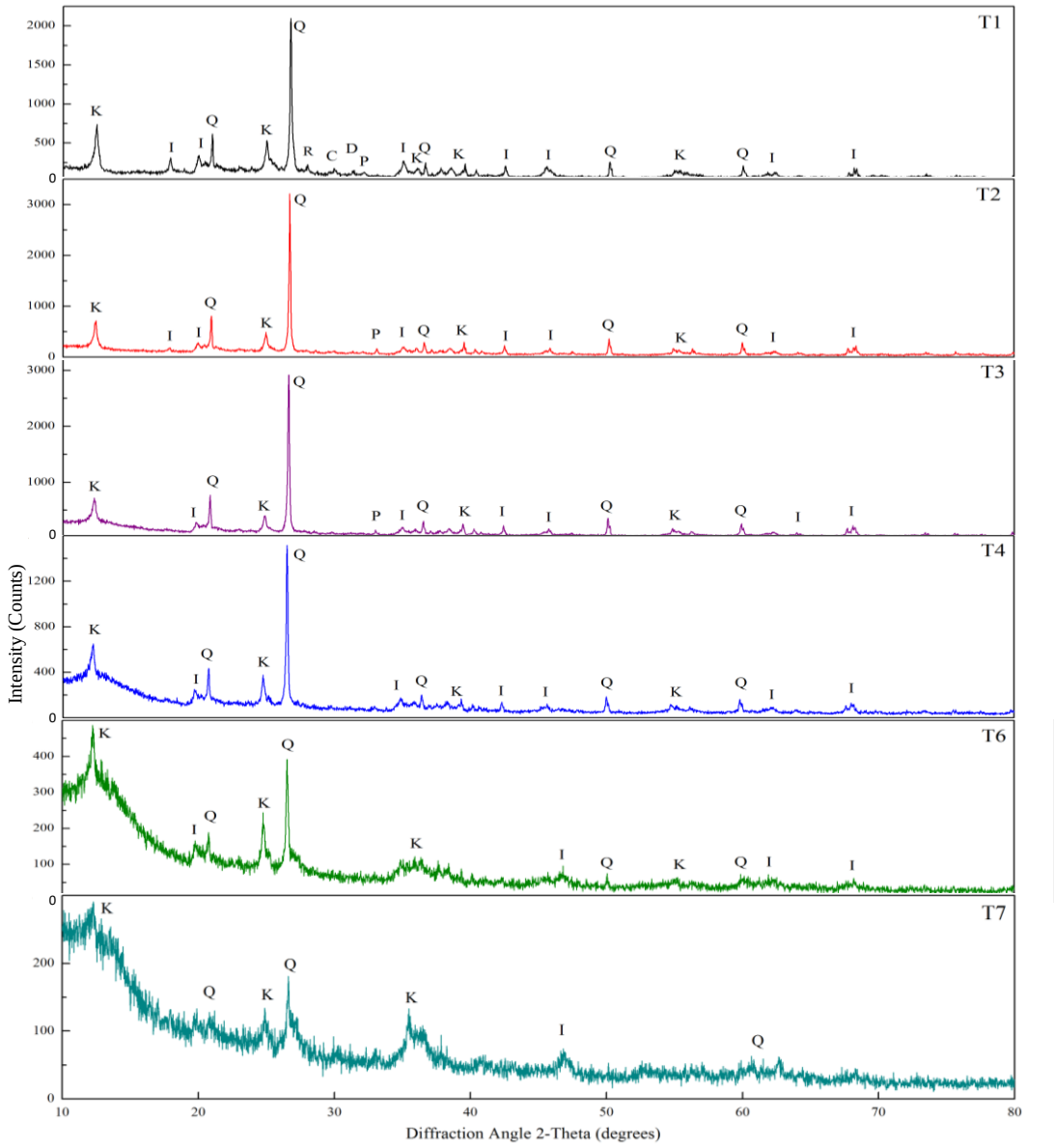

Figure 7. 4. XRD patterns of rare earth release test samples (C-calcite; D-dolomite; I-illite; K-kaolinite; P-pyrite; Q-quartz; R-rutile; T1-T7 means the liberated ash materials from the Fire Clay middlings).

To get more detailed information of REE mineralogy in the Fire Clay middlings, SEM-EDX characterization was conducted. Figure 7.5 shows the SEM pictures of the tailing materials produced from the rare earth release tests. Five particles labelled in the Figure 7.5 have more than 1% of total REEs and the particles are of irregular shapes with less than 1μm particle size. (Table 7.1 and Figure 7.5). Instead of existing as separate

particles, all of the six particles were associated with parent particles which are mainly aluminosilicates. This finding agrees with the rare earth mineral release test and XRD characterization results, i.e., REEs are more enriched in the ultra-fine kaolinite dispersed in the coal organic matrix. The association of rare earth phosphate minerals with clay minerals has also been found for coals from other deposits, such as the Russian Far East and the Sydney deposits (Seredin, 1996; Birk and White, 1991).

As shown in Table 7.2, REEs were strongly correlated with phosphorous contents with a correlation coefficient factor of 0.94, which suggested that REEs mainly existed as rare earth phosphates. Heavy REEs were not detected in the samples using SEM-EDX, which might due to a couple reasons: 1) the concentrations of heavy REEs in those particles were out of EDX detection limit; 2) heavy REEs were associated with nano-scale particles which require higher magnification equipment to characterize. Based on the fact that HREE/LREE ratios of rare earth release test tailings gradually increased with the decreases in particle sizes, HREE phosphate minerals are finer than the LREE phosphate minerals.

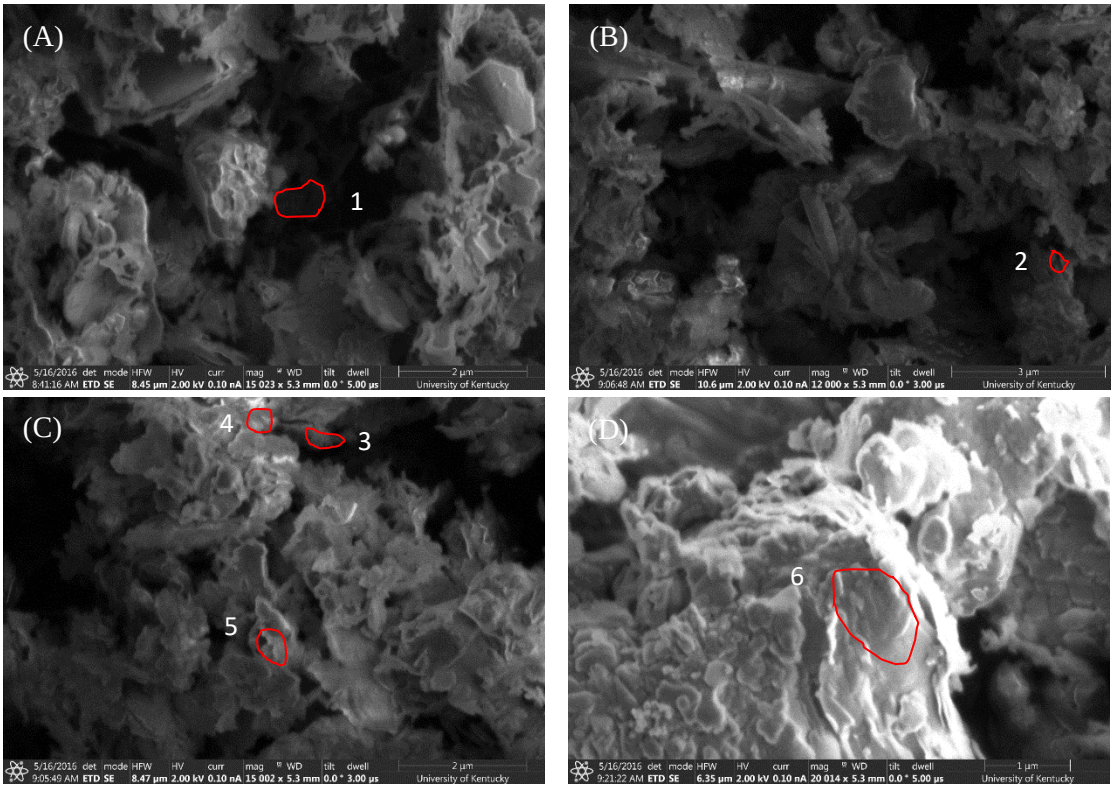

Figure 7. 5. SEM pictures of the Fire Clay middlings and locations of spectra with

high REE content.

Table 7. 1. EDX elemental composition of spectra marked in Figure 7.5.

Spectrum	O	Al	Si	Fe	Ca	Ti	P	S	Ce	La	Nd	Y	TREE
1	70.7	9.4	8.6	1.0	0.9	0.6	4.2	1.9	1.5	0.3	0.8	0.0	2.6
2	67.4	13.2	13.2	0.9	0.8	0.2	2.9	0.0	0.9	0.3	0.0	0.0	1.2
3	69.2	7.3	13.3	2.0	2.4	0.3	1.6	3.0	0.3	0.5	0.1	0.1	1.0
4	71.0	8.8	16.0	0.5	1.3	0.0	1.4	0.0	0.3	0.2	0.0	0.0	0.5
5	74.2	10.2	10.2	0.4	0.5	0.5	0.9	1.7	0.1	0.0	0.1	0.0	0.2
6	72.6	11.8	12.3	0.2	0.1	0.0	1.3	0.2	0.5	0.2	0.3	0.1	1.1

Table 7. 2. Pearson correlation coefficient for elements as % of locations shown in Figure 7.5 with high REE contents.

	O	Al	Si	Fe	Ca	Ti	P	S	TREE
O	1.00	-0.11	-0.34	-0.62	-0.50	0.13	-0.52	0.05	-0.58
Al	-0.11	1.00	-0.09	-0.56	-0.76	-0.23	0.14	-0.70	0.09
Si	-0.34	-0.09	1.00	0.03	0.36	-0.84	-0.47	-0.45	-0.38
Fe	-0.62	-0.56	0.03	1.00	0.89	0.30	0.27	0.73	0.38
Ca	-0.50	-0.76	0.36	0.89	1.00	0.07	0.01	0.60	0.09
Ti	0.13	-0.23	-0.84	0.30	0.07	1.00	0.48	0.69	0.31
P	-0.52	0.14	-0.47	0.27	0.01	0.48	1.00	0.08	0.94
S	0.05	-0.70	-0.45	0.73	0.60	0.69	0.08	1.00	0.12
TREE	-0.58	0.09	-0.38	0.38	0.09	0.31	0.94	0.12	1.00

SEM-EDX scanning was conducted to characterize the particles with high REE content. A particle with high REE content is shown in Figure 7.6 (a). A small portion of the particle was enriched in REEs, which means the REE mineral was not liberated, thereby indicating the need for grinding to liberate the mineral for an effective REE recovery process. A focused ion beam (FIB) unit was used to mill out the high REE content grain which measured to be around 2 μm. Figure 7.6 (b) shows the SEM image of one lamella together with the transmission electron microsocpy-Fourier transformation (TEM-FFT) image. The fraction with a high REE content had an irregular shape and was embedded into the parent particle. The TEM-FFT images shows that the fraction was well

crystallized and the compositon of the grain was pure rare earth phosphate ((La, Ce, Nd, Sm, Th)PO_4), thereby indicating that the REEs were present in the form of monazite.

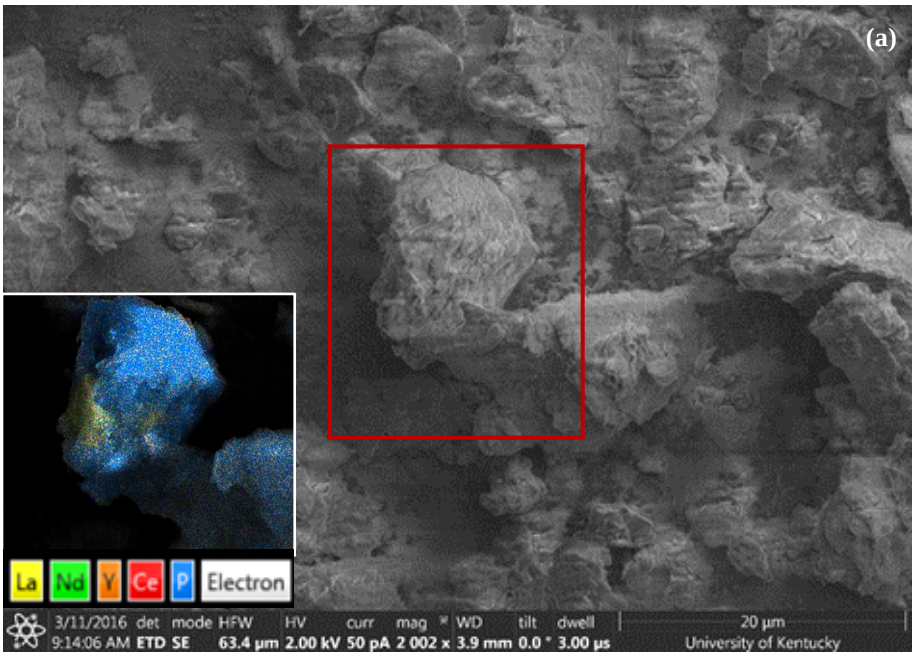

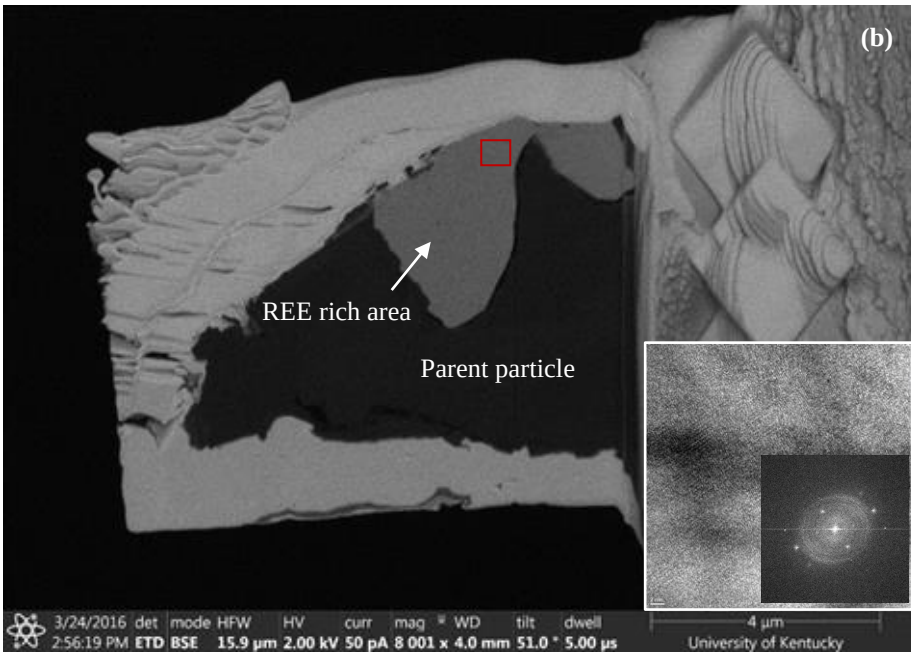

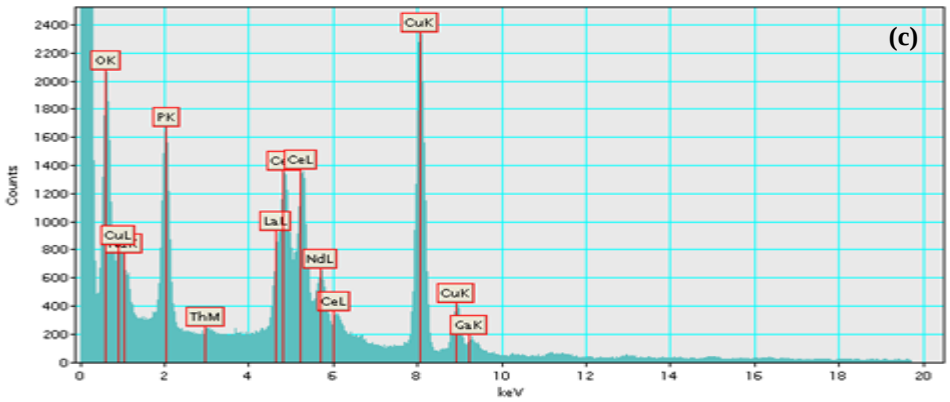

Figure 7. 6. SED, TEM, EDX Analyses of rare earth minerals in Fire Clay fine coal refuse: (a) SEM-EDX map; (b) lamella with high REE concentration milled using focused ion beam (FIB) and the TEM-FFT images of specific area with high REE concentration; (c) EDX images of the area selected from (b).

7.3 FLOTATION TESTS

Solution pH values and grinding time were the two critical parameters evaluated to improve the selectivity of the REE flotation tests. Figure 7.7 shows the effects of pH and particle size on the enrichment ratio, i.e., the REE concentration in the concentrate divided by the concentration in the feed. As shown in Figure 7.7 (a), maximum enrichment ratio occurred at pH 9, which agreed with previous findings reported in chapter five. Maximum surface active sites ($REE(OH)^{+}$ and $REE(OH)^{2+}$) exist on monazite surfaces at pH 9.0 and, as such, higher adsorption kinetic rates and maximum adsorption capacity occurs. Figure 7.7 (b) shows that a particle size of 2.76 μm (D50) produced by 60 minutes of grinding in an attrition mill provided the highest enrichment ratio.

Multiple stages of flotation were conducted using a batch-type conventional cell and continuous flotation column in separate test programs. Figure 7.8 (a) shows the cumulative REE content in the products as a function the cumulative REE recovery. For recovery values below 20%, column flotation was more efficient than the conventional flotation, i.e., the REE contents in the column flotation products were two times higher than the products obtained using conventional flotation. Column flotation produced a concentrate containing around 4700 ppm of TREEs from a feed containing 431 ppm of TREEs on an ash basis which equates to an enrichment ratio of over 10:1.

The improved selectivity provided by column flotation was due to the ability to minimize hydraulic entrainment and maximize recovery of the ultrafine REE containing particles as a result of the plug-flow environment. As shown in Figure 7.7 (b), LREEs were preferentially recovered using flotation methods based on a decrease in the HREE/LREE ratio with an increase in product REE content, which agrees with the fact that rare earth minerals such as monazite are more enriched in LREEs.

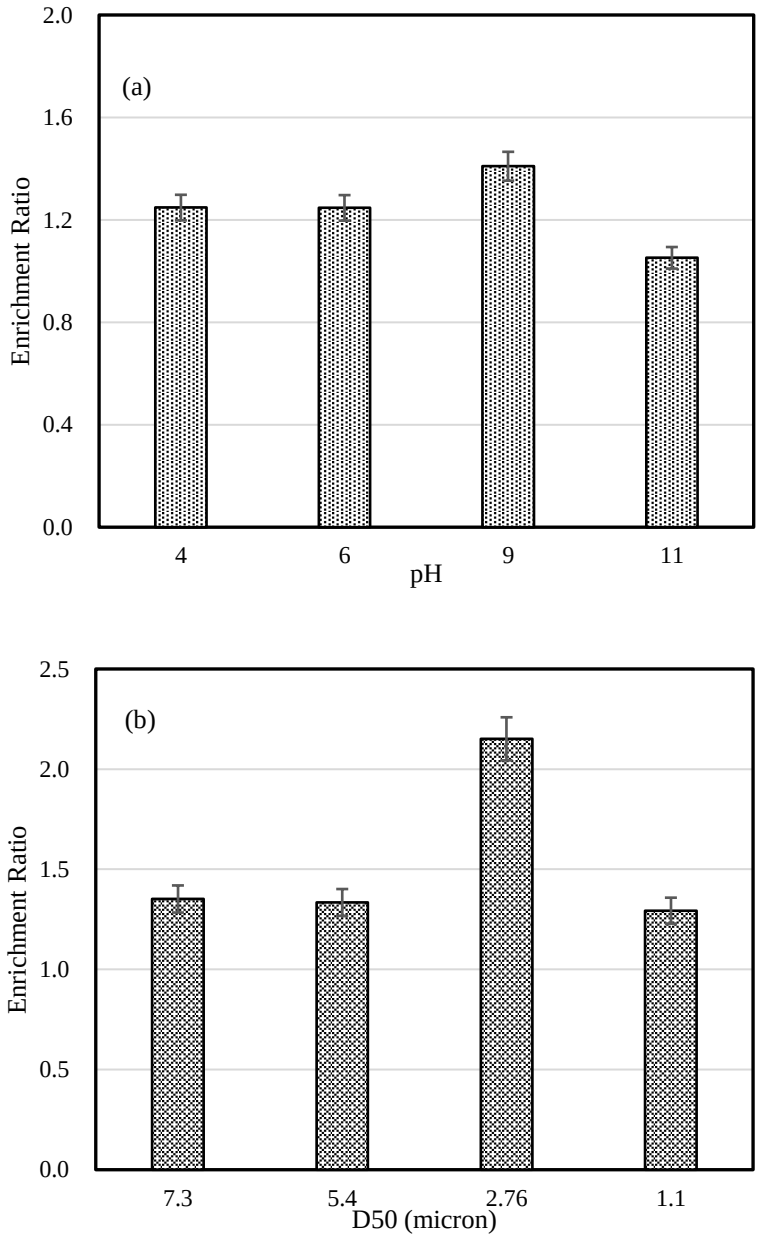

Figure 7. 7. Effects of pH and particle size on the rare earth flotation separation: (a) pH effects; (b) particle size effects.

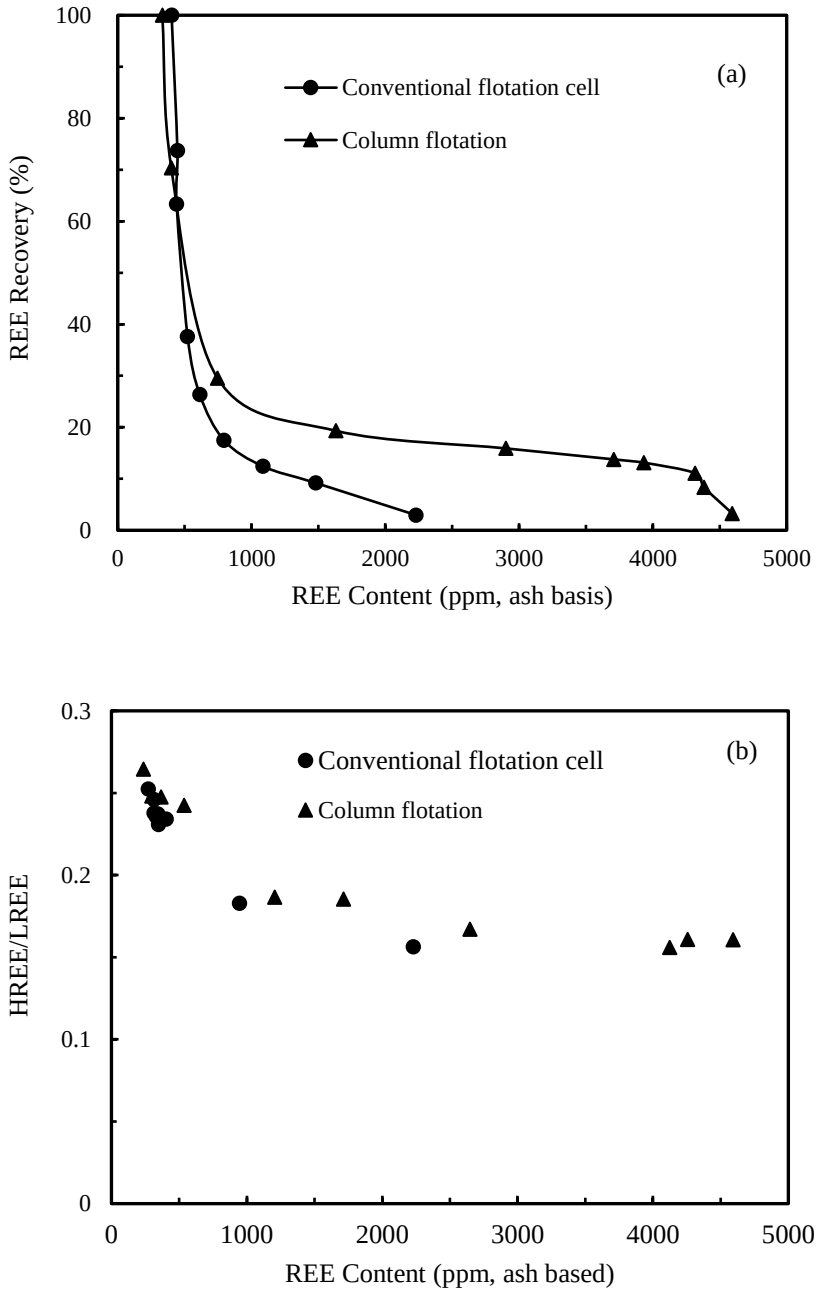

Figure 7. 8. A comparison of the REE recovery performances achieved through multiple cleaning stages using conventional and column flotation cells: (a) REE content on an ash basis as a function of cumulative recovery; (b) HREE/LREE ratio as a function of REE content on an ash basis.

7.4 CONCLUSIONS

The mineralogy of REEs in a Fire Clay fine coal refuse sample was studied using the SEM-EDX analysis. Unliberated monazite particles with an REE content of around 60% were discovered having a particle sizes less than two microns. Results from a flotation

release analysis found that heavy rare earth elements were likely associated with finely dispersed ash materials within the organic matrix. Furthermore, due to the organic and inorganic dilutions, maximum REE content occurred in particles with an ash content of around 80%. The TREE content decreased for particles containing greater amounts of ash due to the dilution effect caused by low TREE content rock particles.

Optimum flotation of rare earth minerals from the coal refuse material occurred using a pH value of 9.0 and grinding time of 60 min. Column flotation was found to be more effective than conventional flotation due to the effects of hydraulic entrainment and hydrodynamic conditions. A final concentrate containing around 4700 ppm of REEs was obtained using column flotation and multiple cleaning stages. Due to the concentration of monazite, the light REES were preferentially recovered in the flotation product.

CHAPTER 8. CONCLUSIONS

Systematic study of monazite flotation chemistry was conducted in the current research dissertation. Specifically, the charging mechanisms of monazite in aqueous systems were studied using electrokinetic tests, solution equilibrium calculation, crystal structure analysis, and electrostatic model prediction. Adsorption mechanisms of octanohydroxamic acid on monazite surfaces were investigated using adsorption tests, FTIR analysis, titration, and micro-flotation tests. Effects of calcium ions dissolved from calcite surfaces on monazite flotation were studied in detailed using micro-flotation and electrokinetic tests as well as FTIR analysis and solution chemistry calculation. Selective depression of calcite flotation in the monazite-calcite system was achieved using a combination of sodium silicate and chelating reagents such as EDTA. The chemistry aspects involved in the selective depression were systematically studied. Finally, concentration of rare earth minerals from coal fine refuse was performed using both conventional flotation cell and column flotation. The detailed findings of the present research dissertation were listed as follows:

(1) Monazite surface charges were developed through protonation/deprotonation reactions and the potential determining ions were hydrogen and hydroxyl ions. Lattice ions such as Ce3+ and PO_4^{3-} provided minor effects on monazite surface charges.

(2) Electrokinetic results indicated that the IEP of the natural monazite sample used in the current study occurred at about pH 6.0. Solution equilibrium calculation for cerium monazite ($CePO_4$) showed that equal amounts of positive and negative charges were achieved at pH 7.2 and 4.5 in open and closed systems, respectively. As such, an IEP value of pH 7.2 was obtained based on equilibrium calculation.

(3) Electrostatic prediction of the cleavage surface on (100) plane based on surface composition indicated that the PZC of the surface occurred at pH 7.2, which agreed with the solution equilibrium calculation. The discrepancy between the electrostatic predictions and the electrokinetic results was attributed to two factors: i) different

rare earth atoms might play distinct roles in surface charge development; ii) carbon dioxide dissolved in solution might decrease the IEP values.

(4) Multilayer adsorption of octanohydroxamic acid on monazite surfaces occurred at pH 3.0, 6.0, 9.0, and 11.0. For low pH values and/or low collector dosages, the adsorption was achieved via an exothermic chemisorption interaction, while for high pH values and/or high collector dosages, the adsorption was achieved via a surface reaction and/or surface precipitation reaction.

(5) The chemisorption was accomplished by the chemical reaction between surface active sites, i.e., hydrolyzed rare earth species (e.g., $REE(OH)^{2+}$), which had maximum concentrations at pH 9.0. As such, for below monolayer coverages, maximum adsorption rate and density occurred at pH 9.0.

(6) Hydroxyl ions contribute to the surface precipitation reaction, which might be due to the formation of basic rare earth hydroxamate salts on monazite surfaces. As such, for beyond monolayer coverages, maximum adsorption density occurred at pH 11.0.

(7) Depression of monazite occurred in the monazite-calcite combined system, which was due to the dissolved calcium ions from calcite surfaces. Hydrolyzed species of calcium, i.e., $Ca(OH)^{+}$, specifically adsorbed onto monazite surfaces, which was proven by electrostatic and micro-flotation tests.

(8) For low calcium concentrations, the adsorption of octanohydroxamic acid on monazite surfaces was decreased due to the competitive adsorption on P-OH sites. For high calcium concentration, the collector adsorption was increased due to the fact that $Ca(OH)^{+}$ served as new surface active sites. However, the floatability of monazite was decreased resulting from the hydration of the $Ca(OH)^{+}$ on monazite surfaces.

(9) In single mineral flotation systems, sodium silicate could efficiently depress calcite while providing minimal effects on monazite floatability. However, in the monazite-calcite combined system, depression of monazite flotation occurred when using

sodium silicate as a depressant. Micro-flotation and electrokinetic tests as well as solution chemistry study indicated that hydrolyzed calcium species, i.e., $Ca(OH)^+$, co-adsorbed onto monazite surfaces with silicates, which formed a hydrophilic layer by hydrogen bonding and/or surface reaction. The collector adsorption was decreased due to steric hindrance, and thus monazite floatability was impaired.

(10) Reagents such as citric acid and EDTA formed soluble chelates with calcium ion solution. As such, the negative effects of calcium species were eliminated. Using 6×10^{-5} M EDTA together with 2.5×10^{-4} M octanohydroxamic acid and 0.05 g/L sodium silicate, monazite recovery of more than 90% was achieved while only recovering 20% of calcite.

(11) EDTA performed better than citric acid due to two reasons: i) EDTA has a stronger chelating ability with calcium ions; ii) citric acid was more likely depress monazite due to a stronger affinity.

(12) Maximum rare earth concentration occurred at pH 9.0 for the Fire Clay fine coal refuse. Column flotation works better than the conventional flotation due to the low entrainment, smaller particle size limits, and better hydrodynamic condition. A product with 4700 ppm of total REEs was finally produced.

CHAPTER 9. SUGGESTIONS FOR FUTURE STUDY

The current research dissertation has accomplished a systematic study of monazite flotation chemistry in coal refuse systems. However, due to the complexity of the fundamental aspects and the mineralogy of coal refuse, efforts should be continuously devoted to get more in-depth understanding of the monazite surface chemistry and achieve more efficient concentration of rare earth minerals from coal refuses. Suggestions for future study were provided as follows:

(1) The present study investigated the nature monazite charging mechanisms. However, based on the fact that REE composition changes for monazite samples from different deposits, it is suggested to synthesize pure single REE monazite (e.g., lanthanum monazite $LaPO_4$) and pure artificially combined monazite (e.g., lanthanum lutetium monazite $La_{0.5}Lu_{0.5}PO_4$). Systematic study of the synthesized monazite samples will significantly contribute to the monazite surface and crystal chemistry.

(2) Previous electrostatic models for surface charge calculation could effectively predict the PZCs of pure ionic crystals such as Al_2O_3, MgO, La_2O_3, Fe_2O_3, etc. However, the models cannot correctly predict the PZCs when crystal filed effects (CFEs) exist. For example, in monazite crystal the REE-O is completely ionic bond, which means the CFEs can be neglected. However, the P-O bond has some covalent fraction, which means in addition to electrostatic interaction, the CFEs also need to be considered. The calculation for the hydrogen bonded to P-O based on electrostatic model is ineffective. The quantum chemistry calculation is becoming more and more important in recent years, which allows to perform first-principles quantum mechanics calculations. Using this kind of calculation, both the electrostatic and CFE effects can be considered for attachment of H to surface sites.

(3) Current research dissertation proposed that the chemisorption and surface precipitation or surface reaction of octanohydroxamic acid on mineral surfaces could be distinguished by the enthalpy changes. However, the effect of

displacement of surface active sites was not studied and elucidated. The surface site displacement is also a vague concept in flotation chemistry. Literature only reported its existence, while the quantitative study has not been achieved. It is suggested to use systematic solid and solution chemistry calculation and simulation to do this kind of research in future.

(4) The influence of calcium species in monazite flotation systems was systematically studied in the current research. However, the effect on other heavy sand minerals such as zircon and rutile has not been studied and reported yet. As such, it is suggested to do a systematic study of calcium effects on heavy sand mineral flotation. Furthermore, utilization of metallic cations to selectively depress some minerals might be an approach to improve flotation performance in some specific systems.

(5) More efforts need to be devoted to overcome the low particle size limit of flotation for rare earth mineral recovery from fine coal refuses. On the premise of economically feasible, it is suggested to perform selective agglomeration to increase rare earth mineral apparent particle size and nanobubble flotation which has been reported to be efficient for fine particle separation.

REFERENCES

Abeidu A. M., 1972. The separation of monazite from zircon by flotation. *J. Less Common Met.*, 29, 113-119.

Aktas Z., Woodburn E. T., 1994. The adsorption behaviour of nonionic reagents on two low rank British coals. *Miner. Eng*., 7, 1115-1126.

Ananthapadmanabhan, K. P., Somasundaran, P., 1985. Surface precipitation of inorganics and surfactants and its role in adsorption and flotation. *Colloid Surf.*, 13, 151-167.

Antti, B. M. and Forssberg, E., 1989. Pulp chemistry in industrial mineral flotation. studies of surface complex on calcite and apatite surfaces using FTIR spectroscopy. *Miner. Eng*., *2*(2), 217-227.

Assis, S. M., Montenegro, L. C. M., Peres, A. E. C., 1996. Utilisation of hydroxamates in minerals froth flotation. *Miner. Eng.*, 9(1), 103-114.

Arnold, B. J., Aplan, F. F. 1986. The effect of clay slimes on coal flotation, part II: the role of water quality. *Int. J. Miner. Process.*, *17*(3), 243-260.

Beattie D. A., Huynh L., Kaggwa G. B., Ralston J., 2006. Influence of adsorbed polysaccharides and polyacrylamides on talc flotation. *Int. J. Miner. Process.*, 78, 238-249.

Beck, M.T., 1954. Correlation between the Isoelectric Point and Stability of Complex Compounds. *Acta Chim. Acad. Sci. Hung*, *4*, 227.

Beall, G.W., Boatner, L.A., Mullica, D.F., Milligan, W.O., 1981. The structure of cerium orthophosphate, a synthetic analogue of monazite. *J. Inorg. Nucl. Chem.*, *43*, 101-105.

Binnemans, K., Jones, P. T., Blanpain, B., Van Gerven, T., Yang, Y., Walton, A., Buchert, M., 2013. Recycling of rare earths: a critical review. *J. Clean. Prod.*, 51, 1-22.

Bohmer, M. R., Koopal, L. K., 1990. Association and adsorption of nonionic flexible

chain surfactants. *Langmuir*, *6*(9), 1478-1484.

Bohmer, M. R., Koopal, L. K., 1992a. Adsorption of ionic surfactants on variable-charge surfaces. 1. Charge effects and structure of the adsorbed layer. *Langmuir*, *8*(11), 2649-2659.

Bohmer, M. R., Koopal, L. K., 1992b. Adsorption of ionic surfactants on variable-charge surfaces. 2. Molecular architecture and structure of the adsorbed layer. *Langmuir*, *8*(11), 2660-2665.

Bohmer, M. R., Koopal, L. K., 1992c. Adsorption of ionic surfactants on constant charge Surfaces. Analysis based on a self-consistent field lattice model. *Langmuir*, *8*(6), 1594-1602.

Bohmer, M. R., Koopal, L. K., Janssen, R., Lee, E. M., Thomas, R. K., Rennie, A. R., 1992. Adsorption of nonionic surfactants on hydrophilic surfaces. An experimental and theoretical study on association in the adsorbed layer. *Langmuir*, *8*(9), 2228-2239.

Bowden, J.W., Posner, A.M., Quirk, J.P., 1977. Ionic adsorption on variable charge mineral surfaces. Theoretical charge development and titration curves. *Soil Res.*, *15*, 121-136.

Buckley, A. N., Parker, G. K., 2013. Adsorption of n-octanohydroxamate collector on iron oxides. *Int. J. Miner. Process.*, *121*, 70-89.

Celik, M. S., Somasundaran, P., 1986. The effect of multivalent ions on the flotation of coal. *Sep. Sci. Technol.*, *21*(4), 393-402.

Cetiner, Z. S., Wood, S. A., Gammons, C. H., 2005. The aqueous geochemistry of the rare earth elements. Part XIV. The solubility of rare earth element phosphates from 23 to 150 ^{o}C. *Chem Geol*, 217(1), 147-169.

Chandar, P., Somasundaran, P., Turro, N. J., 1987. Fluorescence probe studies on the structure of the adsorbed layer of dodecyl sulfate at the alumina—water interface. *J. Colloid Interf. Sci.*, *117*(1), 31-46.

Chatterjee, B., 1978. Donor properties of hydroxamic acids. *Coord. Chem. Rev.*, 26(3), 281-303.

Chernyshova, I. V., Rao, K. H., Vidyadhar, A., Shchukarev, A. V., 2000. Mechanism of Adsorption of Long-Chain Alkylamines on Silicates. A Spectroscopic Study. 1. Quartz. *Langmuir*, *16*(21), 8071-8084.

Chelgani, S.C., Rudolph, M., Leistner, T., Gutzmer, J., Peuker, U.A., 2015. A review of rare earth minerals flotation: Monazite and xenotime. *Int. J. Mining Sci. Tech*., 25, 877-883.

Chennakesavulu, K., Raju, G. B., Prabhakar, S., Nair, C. M., Murthy, K. V. G. K., 2009. Adsorption of oleate on fluorite surface as revealed by atomic force microscopy. *Int. J. Miner. Process.*, *90*(1), 101-104.

Cheng, T.W., 2000. The point of zero charge of monazite and xenotime. *Miner. Eng.*, *13*, 105-10.

Cheng T. W., Holtham P. N., Tran T., 1993. Froth flotation of monazite and xenotime. *Miner. Eng.*, 6, 341-351.

Cheng, T.W., Holtham, P.N., Tran, T., 1993. Froth flotation of monazite and xenotime. *Miner. Eng.*, *6*, 341-351.

Cetiner, Z.S., Wood, S.A., Gammons, C.H., 2005. The aqueous geochemistry of the rare earth elements. Part XIV. The solubility of rare earth element phosphates from 23 to 150 ^{o}C. *Chem. Geol.*, *217*, 147-169.

Cui, J., Hope, G. A., Buckley, A. N., 2012. Spectroscopic investigation of the interaction of hydroxamate with bastnaesite (cerium) and rare earth oxides. *Miner. Eng.*, *36*, 91-99.

Degen, A., Kosec, M., 2000. Effect of pH and impurities on the surface charge of zinc oxide in aqueous solution. *J. Eu. Ceram. Soc.*, *20*, 667-673.

Dixit S. G., Biswas A. K., 1969. pH-Dependence of the flotation and adsorption

properties of some beach sand minerals. *T. I. Min. Metall.*, 244, 173-178.

Espiritu, E.R.L., Waters, K.E., 2017. Flotation studies of monazite and dolomite. Miner. Eng., (accepted). doi.org/10.1016/j.mineng.2017.02.010

Ekholm, P., Blomberg, E., Claesson, P., Auflem, I. H., Sjöblom, J., Kornfeldt, A., 2002. A quartz crystal microbalance study of the adsorption of asphaltenes and resins onto a hydrophilic surface. *J. Colloid Interf. Sci.*, *247*(2), 342-350.

Fan, A., Somasundaran, P., Turro, N. J., 1997. Adsorption of alkyltrimethylammonium bromides on negatively charged alumina. *Langmuir*, *13*(3), 506-510.

Fan, X., Rowson, N. A., 2000. The effect of $Pb(NO_3)_2$ on ilmenite flotation. *Miner. Eng.*, *13*(2), 205-215.

Fan, X., Waters, K. E., Rowson, N. A., Parker, D. J., 2009. Modification of ilmenite surface chemistry for enhancing surfactants adsorption and bubble attachment. *J. Colloid Interf. Sci.*, *329*(1), 167-172.

Feng B., Luo X., Wang J., Wang P., 2015. The flotation separation of scheelite from calcite using acidified sodium silicate as depressant. *Miner. Eng.*, 80, 45-49.

Franus, W., Wiatros-Motyka, M.M., Wdowin, M., 2015. Coal fly ash as a resource for rare earth elements. *Environ. Sci. Technol.*, 22(12), 9464-9474.

Fredriksson A., Holmgren A., 2008. An in situ ATR-FTIR investigation of adsorption and orientation of heptyl xanthate at the lead sulphide/aqueous solution interface. *Miner. Eng.*, 21, 1000-1004.

Fredriksson A., Holmgren A., 2007. An in situ ATR-FTIR study of the adsorption kinetics of xanthate on germanium. *Colloids Surf. A*, 302, 96-101.

Fredriksson A., Holmgren A., Forsling W., 2006. Kinetics of collector adsorption on mineral surfaces. *Miner. Eng.*, 19, 784-789.

Freundlich H., 1907. Ueber die adsorption in loesungen. *Z. Phys. Chem.*, 57, 385–470.

Fowler R.H., Guggenheim E.A., 1939. Statistical Thermodynamics, Cambridge University Press, London, 431–450.

Free, M. L., Miller, J. D., 1997. Kinetics of 18-carbon carboxylate adsorption at the fluorite surface. *Langmuir*, 13(16), 4377-4382.

Fuerstenau, M. C., Jameson, G. J., Yoon, R. H., 2007. *Froth flotation: a century of innovation*. SME. Colorado, USA.

Fuerstenau M. C., 2005. Chelating Agents as Flotation Collectors, In C. Young, J. J. Kellar, M. L. Free (Eds): Innovations in natural resource processing: proceedings of the Jan D. Miller symposium, Society for Mining, Metallurgy & Exploration.

Fuerstenau D. W., Herrera-Urbina R., McGlashan D. W, 2000. Studies on the applicability of chelating agents as universal collectors for copper minerals. *Int. J. Miner. Process.*, 58, 15-33.

Fuerstenau, M. C., Miller, J. D., Gutierrez, G., 1967. Selective flotation of iron oxide. *Trans. of AIME, 238,* 200-203.

Fuerstenau, M. C., Miller, J. D., 1967. The role of the hydrocarbon chain in anionic flotation of calcite. *Trans. of AIME, 238*(2), 153-160.

Fuerstenau, M.C., Miller, J.D., Pray, R.E., Perinne, B.F., 1965. Metal ion activation in xanthate flotation of quartz. *Trans. AIME, 232*, 359-365.

Fuerstenau, M. C., Harper, R. W., Miller, J. D., 1970. Hydroxamate vs fatty-acid flotation of iron oxide. *T. Soc. Min. Eng., AIME, 247*(1), 69-73.

Fulford, G. D., Lever, G., Sato, T., 1991. U.S. Patent No. 5,030,424. Washington, DC: U.S. Patent and Trademark Office.

Gaudin, A. M., Fuerstenau, D. W., 1955. Streaming Potential Studies. Quartz Flotation with Cationic Collectors. *Min. Eng., 7.*

Hamdaoui O., Naffrechoux E., 2007. Modeling of adsorption isotherms of phenol and chlorophenols onto granular activated carbon: Part I. Two-parameter models and

equations allowing determination of thermodynamic parameters. *J. Hazard. Mater.*, 147, 381-394.

Hanson, J. S., Fuerstenau, D. W., 1987. An electrochemical investigation of the adsorption of octyl hydroxamate on chalcocite. *Colloid Surf., 26,* 133-140.

Harwell, J. H., Hoskins, J. C., Schechter, R. S., Wade, W. H., 1985. Pseudophase separation model for surfactant adsorption: isomerically pure surfactants. *Langmuir, 1*(2), 251-262.

Ho Y. S., McKay G., 1999. Pseudo-second order model for sorption processes. *Process Biochem.*, 34, 451-465.

Honaker, R., Groppo J., Yoon R.H., Luttrell G.H., Noble A., Herbst J., 2017. Process evaluation and flowsheet development for the recovery of rare earth elements from coal and associated byproducts. *Miner. Metall. Proc.*, (Accepted).

Honaker, R.Q., Hower, J.C., Eble, C., Weisenfluh, G., Groppo, J., Rezaee, M., Bhagavatula, A., 2014. Laboratory and Bench-Scale Testing for Rare Earth Elements, Final Report. National Energy Technology Laboratory (NETL), Report ID 9bab59f6-4047-42cf-a851-cfee1791306e.

Hong, T., Qin, Z., Qian, Z., Fei, W., 2012. Study on the dispersion behavior of microfine hematite. *Nonferr. Metal (Miner. Process.)*, 6, 10.

Hope, G. A., Buckley, A. N., Parker, G. K., Numprasanthai, A., Woods, R., and McLean, J., 2012. The interaction of n-octanohydroxamate with chrysocolla and oxide copper surfaces. *Miner. Eng.*, *36*, 2-11.

Hower, J. C., Ruppert, L. F., Eble, C. F., 1999. Lanthanide, yttrium, and zirconium anomalies in the Fire Clay coal bed, Eastern Kentucky. *Int. J. Coal Geol.*, 39(1), 141-153.

Hunter, R.J., 2013. *Zeta potential in colloid science: principles and applications* (Vol. 2). Academic Press, New South Wales.

Idris S. A. M., 2015. Adsorption, kinetic and thermodynamic studies for manganese extraction from aqueous medium using mesoporous silica. *J. Colloid Interf. Sci.*, 440, 84-90.

Iwasaki, I., Cooke, S. R. B., Choi, H. S., 1960. Flotation characteristics of hematite, goethite, and activated quartz with 18-carbon aliphatic acids and related compounds. *American Institute of Mining, Metallurgical and Petroleum Engineers. Transactions, 217*, 237-244.

James, R.O., Healy, T.W., 1972a. Adsorption of hydrolyzable metal ions at the oxide—water interface. I. Co (II) adsorption on SiO_2 and TiO_2 as model systems. *J. Colloid Interf. Sci., 40*, 42-52.

James, R. O., Healy, T.W., 1972b. Adsorption of hydrolyzable metal ions at the oxide—water interface. II. Charge reversal of SiO_2 and TiO_2 colloids by adsorbed Co(II), La(III), and Th(IV) as model systems. *J. Colloid Interf. Sci., 40*, 53-64.

James, R. O., Healy, T.W., 1972c. Adsorption of hydrolyzable metal ions at the oxide—water interface. III. A thermodynamic model of adsorption. *J. Colloid Interf. Sci., 40*, 65-81.

Jazi M. B., Arshadi M., Amiri M. J., Gil A., 2014. Kinetic and thermodynamic investigations of Pb (II) and Cd (II) adsorption on nanoscale organo-functionalized SiO_2 Al_2O_3. *J. Colloid Interf. Sci.*, 422, 16-24.

Jie, Z., Weiqing, W., Jing, L., Yang, H., Qiming, F., Hong, Z., 2014. Fe (III) as an activator for the flotation of spodumene, albite, and quartz minerals. *Miner. Eng., 61*, 16-22.

Kellar, J. J., Young, C. A., Miller, J. D., 1992. In-situ FT-IR/IRS investigation of double-bond reactions of adsorbed oleate at a fluorite surface. *Int. J. Miner. Process.*, 35(3), 239-251.

Kellar, J. J., Young, C. A., Knutson, K., Miller, J. D., 1991. Thermotropic phase transition of adsorbed oleate species at a fluorite surface byin situ FT-IR/IRS

spectroscopy. *J. Colloid Interf. Sci.*, 144(2), 381-389.

Khelifa A., Benchehida L., Derriche Z., 2004. Adsorption of carbon dioxide by X zeolites exchanged with Ni^{2+} and Cr^{3+}: isotherms and isosteric heat. *J. Colloid Interf. Sci.*, 278, 9-17.

Kossiakoff, A., Harker, D., 1938. The calculation of the ionization constants of inorganic oxygen acids from their structures. *J. Am. Chem. Soc.*, *60*, 2047-2055.

Kragten, J., Decnop-Weever, L.G., 1987. Hydroxide complexes of lanthanides—VIII: Lanthanum (III) in perchlorate medium. *Talanta*, *34*, 861-864.

Kragten, J., Decnop-Weever, L.G., 1978. Hydroxide complexes of cerium (III). *Talanta*, *25*, 147-150.

Kurniawan, A. U., Ozdemir, O., Nguyen, A. V., Ofori, P., Firth, B., 2011. Flotation of coal particles in $MgCl_2$, NaCl, and $NaClO_3$ solutions in the absence and presence of Dowfroth 250. *Int. J. Miner. Process*,, *98*(3), 137-144.

Langmuir, I., 1918. The adsorption of gases on plane surfaces of glass, mica and platinum. *J. Am. Chem. Soc.*, 40(9), 1361-140

Lee K., Archibald D., McLean J., Reuter M. A., 2009. Flotation of mixed copper oxide and sulphide minerals with xanthate and hydroxamate collectors. *Miner. Eng.*, 22, 395-401.

Lee, J.H., Byrne, R.H., 1992. Examination of comparative rare earth element complexation behavior using linear free-energy relationships. *Geochim. Cosmochim. Acta*, *56*, 1127-1137.

Li, H., Zhang, S., Zhou, S., Cao, X., 2009. Bonding characteristics, thermal expansibility, and compressibility of RXO_4 (R=rare earths, X=P, as) within monazite and zircon structures. *Inorg. Chem.*, 48, 4542-4548.

Li, H., Zhou, S., Zhang, S., 2007. The relationship between the thermal expansions and structures of ABO_4 oxides. *J. Solid State Chem.*,180, 589-595.

Liu, W., Zhang, S., Wang, W., Zhang, J., Yan, W., Deng, J., Feng Q., Huang, Y., 2015. The effects of Ca (II) and Mg (II) ions on the flotation of spodumene using NaOl. *Miner. Eng.*, *79*, 40-46.

Marinakis, K.I., Shergold, H.L., 1985. Influence of sodium silicate addition on the adsorption of oleic acid by fluorite, calcite and barite. *Int. J. Miner. Process.*, 14(3), 177-193.

McEwen R., Hansen G. W., Lee G. F, 1976. Single-stage flotation of alkali feldspars, ilmenite, rutile, garnet, and monazite, with mixed cationic/anionic collectors. *T. I. Min. Metall.*, 260, 97-100.

Mehdilo, A., Irannajad, M., and Rezai, B., 2015. Effect of crystal chemistry and surface properties on ilmenite flotation behavior. *Int. J. Miner. Process.*, *137*, 71-81.

Memon S. Q., Bhanger M. I., Khuhawar M. Y., 2009. Use of modified sorbent for the separation and preconcentration of chromium species from industrial waste water. *J. Hazard. Mater.*, 163, 511-516.

Mielczarski, E., De Donato, P., Mielczarski, J. A., Cases, J. M., Barres, O., Bouquet, E., 2000. Solution chemistry in adsorption layer formation of oleate on fluorite. *J. Colloid Interf. Sci.*, *226*(2), 269-276.

Miller, J.D., Fa, K., Calara, J.V., Paruchuri, V.K., 2004. The surface charge of fluorite in the absence of surface carbonation. *Colloids Surf. A, 238*, 91-97.

Miller J.D., Wang X., Li M., 2001. A new collector chemistry for phosphate flotation. In *SME annual meeting*, Denver, Colorado, February, 26-28.

Miller, J. D., Wang, X., Li, M., 2001. Bench scale flotation of sedimentary phosphate rock with hydroxamic acid collectors. In *Proceedings of the Engineering Foundation Conference on Beneficiation of Phosphate III,* St. Pete Beach, Florida.

Miller, J. D., Wang, X., Li, M., 2001. Selective flotation of phosphate minerals with alcoholic solutions of alkyl hydroxamic acids. In *Proceedings of the Engineering*

Foundation Conference on Beneficiation of Phosphate III, St. Pete Beach, Florida.

Mishra, S. K., 1982. Electrokinetic properties and flotation behaviour of apatite and calcite in the presence of sodium oleate and sodium metasilicate. *Int. J. Miner. Process.*, 9(1), 59-73.

Mobasherpour I., Salahi E., Ebrahimi M., 2014. Thermodynamics and kinetics of adsorption of Cu (II) from aqueous solutions onto multi-walled carbon nanotubes. *J. Saudi Chem. Soc.*, 18, 792-801.

Monnin, C., Galinier, C., 1988. The solubility of celestite and barite in electrolyte solutions and natural waters at 25 C: a thermodynamic study. *Chem. Geol.,* 71(4), 283-296.

Moon, K. S. and Fuerstenau, D. W., 2003. Surface crystal chemistry in selective flotation of spodumene ($LiAl[SiO_3]_2$) from other aluminosilicates. *Int. J. Miner. Process.*, *72*(1), 11-24.

Mullica, D.F., Milligan, W.O., Grossie, D.A., Beall, G.W., Boatner, L.A., 1984. Ninefold coordination $LaPO_4$: Pentagonal interpenetrating tetrahedral polyhedron. *Inorg. Chim. Acta*, 95, 231-236

Nagaraj, D. R., 1988. The chemistry and application of chelating or complexing agents in minerals separations. Marcel Dekker, Inc., *Reagents in Mineral Technology*, 257-334.

Natarajan R., Fuerstenau D. W., 1983. Adsorption and flotation behavior of manganese dioxide in the presence of octyl hydroxamate. *Int. J. Miner. Process.,* 11, 139-153.

Nduwa-Mushidi, J., Anderson, C. G., 2017. Surface chemistry and flotation behaviors of monazite–apatite–ilmenite–quartz–rutile–zircon with octanohydroxamic acid. *J. Sust. Metall.*, 3(1), 62-72.

Neilands, J. B., 1966. Naturally occurring non-porphyrin iron compounds. In *Structure and bonding*. Springer, Berlin Heidelberg, 59-108.

Ni X., Liu Q., 2012. The adsorption and configuration of octyl hydroxamic acid on

pyrochlore and calcite. *Colloids Surf. A*, 411, 80-86.

Ng C., Losso J. N., Marshall W. E., Rao R. M, 2002. Freundlich adsorption isotherms of agricultural by-product-based powdered activated carbons in a geosmin–water system. *Bioresour. Technol.*, 85, 131-135.

Ni, Y., Hughes, J.M., Mariano, A.N., 1995. Crystal chemistry of the monazite and xenotime structures. *Am. Mineral.*, *80*, 21-26.

Oelkers, E.H., Poitrasson, F., 2002. An experimental study of the dissolution stoichiometry and rates of a natural monazite as a function of temperature from 50 to 230 ^{o}C and pH from 1.5 to 10. *Chem. Geol., 191*, 73-87.

Ofor O., Anusiem A. C. I., 1999. Kinetics of Oleate Adsorption at a Nigerian Hematite–Water Interface. *J. Colloid Interf. Sci*., 220, 219-223.

Ofor, O., Nwoko, C., 1997. Oleate flotation of a Nigerian baryte: The relation between flotation recovery and adsorption density at varying oleate concentrations, pH, and temperatures. *J. Colloid Interf. Sci*., *186*(2), 225-233.

Oguz E., 2005. Thermodynamic and kinetic investigations of PO_4^{3-}adsorption on blast furnace slag. *J. Colloid Interf. Sci.*, 281, 62-67.

Ordoñez-Regil, E., Drot, R., Simoni, E., 2003. Surface complexation modeling of uranium (VI) sorbed onto lanthanum monophosphate. *J. Colloid Interface Sci., 263*, 391-399.

Ozdemir, O., Taran, E., Hampton, M. A., Karakashev, S. I., Nguyen, A. V., 2009. Surface chemistry aspects of coal flotation in bore water. *Int. J. Miner. Process., 92*(3), 177-183.

Paiva, P. R. P., Monte, M. B. M., Simão, R. A., Gaspar, J. C., 2011. In situ AFM study of potassium oleate adsorption and calcium precipitate formation on an apatite surface. *Miner. Eng., 24*(5), 387-39.

Parks, G.A., 1965. The isoelectric points of solid oxides, solid hydroxides, and aqueous

hydroxo complex systems. *Chem. Rev.*, *65*, 177-198.

Parks, G.A., Bruyn, P.D., 1962. The zero point of charge of oxides. *J. Phys. Chem.*, *66*, 967-973.

Paria, S., Khilar, K. C., 2004. A review on experimental studies of surfactant adsorption at the hydrophilic solid–water interface. *Adv. Colloid Interface Sci.*, *110*(3), 75-95.

Paul, S., Paul, D., Basova, T., Ray, A. K., 2008. Studies of adsorption and viscoelastic properties of proteins onto liquid crystal phthalocyanine surface using quartz crystal microbalance with dissipation technique. *J. Phys. Chem. C*, *112*(31), 11822-11830.

Pavez, O., Peres, A.E.C., 1994. Technical note bench scale flotation of a Brazilian monazite ore. *Miner. Eng.*, *7*, 1561-1564.

Pavez O., Peres A. E. C., 1993. Effect of sodium metasilicate and sodium sulphide on the floatability of monazite-zircon-rutile with oleate and hydroxamates. *Miner. Eng.*, 6, 69-78.

Parker, R. L., 1937. A note on the morphology of monazite: Am. *Studies in Mineralogy: Dedicated to Charles Palache*, 572.

Peng X., Huang D., Odoom-Wubah T., Fu D., Huang J., Qin Q., 2014. Adsorption of anionic and cationic dyes on ferromagnetic ordered mesoporous carbon from aqueous solution: Equilibrium, thermodynamic and kinetics. *J. Colloid Interf. Sci.*, 430, 272-282.

Peterson, H. D., Fuerstenau, M. C., Rickard, R. S., Miller, J. D., 1965. Chrysocolla flotation by the formation of insoluble surface chelates. *Transactions of AIME*, *232*, 388-392.

Plazinski W., Rudzinski W., Plazinska A., 2009. Theoretical models of sorption kinetics including a surface reaction mechanism: a review. *Adv. Colloid Interf.*, 152, 2-13.

Plummer, L. N., Busenberg, E., 1982. The solubilities of calcite, aragonite and vaterite in CO_2-H_2O solutions between 0 and 90 C, and an evaluation of the aqueous model for

the system $CaCO_3$-CO_2-H_2O. *Geochim. Cosmochim. Acta*, 46(6), 1011-1040.

Pradip, Fuerstenau D. W., 2013. Design and development of novel flotation reagents for the beneficiation of Mountain Pass rare-earth ore. *Miner. Metall. Proc.*, 30, 1-9.

Pradip, Fuerstenau, D. W., 1991. The role of inorganic and organic reagents in the flotation separation of rare-earth ores. *Int. J. Miner. Process.*, *32*(1), 1-22.

Pradip, Fuerstenau D. W., 1985. The adsorption of hydroxamate collectors on semi-soluble minerals. Part II: Effect of temperature on adsorption. *Colloids Surf*, 15, 137-146.

Pradip, Fuerstenau, D. W., 1983. The adsorption of hydroxamate on semi-soluble minerals. Part I: Adsorption on barite, Calcite and Bastnaesite. *Colloids Surf.*, 8(2), 103-119.

Qi G. W., 1993. Use of the QEM∗ SEM analyses in flotation testwork on a phosphate ore containing monazite. *Int. J. Miner. Process.*, 37, 89-108.

Qu X., Xiao J., Liu G., Liu S., Zhang Z., 2016. Investigation on the flotation behavior and adsorption mechanism of 3-hexyl-4-amino-1, 2, 4-triazole-5-thione to chalcopyrite. *Miner. Eng.*, 89, 10-17.

Quast, K.B., Readett, D.J., 1987. The surface chemistry of low-rank coals. *Adv. Colloid Interface Sci.*, *27*, 169-187.

Raghavan S., Fuerstenau D. W., 1975. The adsorption of aqueous octylhydroxamate on ferric oxide. *J. Colloid Interf. Sci.*, 50, 319-330.

Rai, D., Yui, M., Schaef, H. T., Kitamura, A., 2011. Thermodynamic model for SnO2 (cr) and SnO2 (am) solubility in the aqueous Na^+–H^+–OH^-–Cl^-–H2O system. *J. Solution Chem*., 40(7), 1155-1172.

Rao, K. H., Forssberg, K. S. E., 1991. Mechanism of fatty acid adsorption in salt-type mineral flotation. *Miner. Eng.*, *4*(7), 879-890.

Rao, K.H., Antti, B.M., Forssberg, E., 1990. Mechanism of oleate interaction on salt-

type minerals, Part II. Adsorption and electrokinetic studies of apatite in the presence of sodium oleate and sodium metasilicate. *Int. J. Miner. Process.*, 28(1-2), 59-79.

Rao K. H., Antti B. M., Forssberg E., 1989. Mechanism of oleate interaction on salt-type minerals part I. Adsorption and electrokinetic studies of calcite in the presence of sodium oleate and sodium metasilicate. *Colloids Surf.*, 34, 227-239.

Rao, K.H., Antti, B.M., Forssberg, E., 1988. Mechanism of oleate interaction on salt-type minerals part I. Adsorption and electrokinetic studies of calcite in the presence of sodium oleate and sodium metasilicate. *Colloids Surf.*, 34(3), 227-239.

Rath R. K., Subramanian S., 1997. Studies on adsorption of guar gum onto biotite mica. *Miner. Eng.*, 10, 1405-1420.

Ren J., Song S., Lopez-Valdivieso A., Lu S., 2000. Selective flotation of bastnaesite from monazite in rare earth concentrates using potassium alum as depressant. *Int. J. Miner. Process.*, 59, 237-245.

Ren J., Lu S., Song S., Niu J., 1997. A new collector for rare earth mineral flotation. *Miner. Eng.*, 10, 1395-1404.

Sampat Kumar, V. Y., N. Mohan, A. K. Biswas, 1971. Fundamental studies on the role of carbon dioxide in a calcite flotation system. *Trans. AIME,* 250, 182.

Scamehorn, J. F., Schechter, R. S., Wade, W. H., 1982. Adsorption of surfactants on mineral oxide surfaces from aqueous solutions: I: Isomerically pure anionic surfactants. *J. Colloid Interf. Sci.*, *85*(2), 463-478.

Scheutjens, J. M. H. M., Fleer, G. J., 1979. Statistical theory of the adsorption of interacting chain molecules. 1. Partition function, segment density distribution, and adsorption isotherms. *J. Phys. Chem.*, *83*(12), 1619-1635.

Scheutjens, J. M. H. M., Fleer, G. J., 1980. Statistical theory of the adsorption of interacting chain molecules. 2. Train, loop, and tail size distribution. *J. Phys. Chem.*, *84*(2), 178-190.

Seredin, V. V., Dai, S. 2012. Coal deposits as potential alternative sources for lanthanides and yttrium. *J. Colloid Interf. Sci.*, 94, 67-93.

Seredin, V. V., 1996. Rare earth element-bearing coals from the Russian Far East deposits. *J. Colloid Interf. Sci.*, 30(1), 101-129.

Siegbahn, K., 1982. Electron spectroscopy for atoms, molecules, and condensed matter. *Rev. Mod. Phys.*, 54(3), 709.

Somasundaran, P., 1969. Adsorption of starch and oleate and interaction between them on calcite in aqueous solutions. *J. Colloid Interf. Sci.e*, *31*(4), 557-565.

Somasundaran P., Fuerstenau D. W., 1966. Mechanisms of alkyl sulfonate adsorption at the alumina-water interface. *J. Phys. Chem.*, 70, 90-96.

Somasundaran, P., Amankonah, J.O., Ananthapadmabhan, K.P., 1985. Mineral-solution equilibria in sparingly soluble mineral systems. *Colloids Surf.*, *15*, 309-333.

Somasundaran, P., Agar, G.E., 1967. The zero point of charge of calcite. *J. Colloid Interface Sci.*, *24*, 433-440.

Sreenivas T., Padmanabhan N. P. H., 2002. Surface chemistry and flotation of cassiterite with alkyl hydroxamates. *Colloids Surf. A*, 205, 47-59.

Sverjensky, D.A., 1994. Zero-point-of-charge prediction from crystal chemistry and solvation theory. *Geochim. Cosmochim. Acta*, *58*, 3123-3129.

Tekin N., Ateş Y., 2012. Adsorption of poly (vinylimidazole) from aqueous solutions onto Na-bentonite. *Int. J. Miner. Process.*, 112, 49-54.

U.S. Geological Survey, Mineral Commodity Summaries, January, 2017

Veeramasuneni, S., Hu, Y., Miller, J.D., 1997. The surface charge of alkali halides: consideration of the partial hydration of surface lattice ions. *Surf. Sci.*, *382*, 127-136.

Vidyadhar, A., Rao, K. H., Chernyshova, I. V., Forssberg, K. S. E., 2002. Mechanisms of amine–quartz interaction in the absence and presence of alcohols studied by

spectroscopic methods. *J. Colloid Interface Sci.*, *256*(1), 59-72.

Wang, Y. H., Yu, F. S., 2007. Effects of metallic ions on the flotation of spodumene and beryl. *J. China Univ. Min. Tech.*, *17*(1), 35-39.

Westin, K. J., Rasmuson, Å. C., 2005. Nucleation of calcium carbonate in presence of citric acid, DTPA, EDTA and pyromellitic acid. *J. Colloid Interface Sci.*, *282*(2), 370-379.

Yalamanchili, M.R., Kellar, J.J., Miller, J.D., 1993. Adsorption of collector colloids in the flotation of alkali halide particles. *Int. J. Miner. Process.*, *39*, 137-153.

Yan L. G., Yang K., Shan R. R., Yan T., Wei J., Yu S. J., Yu H., Du B., 2015. Kinetic, isotherm and thermodynamic investigations of phosphate adsorption onto core–shell Fe_3O_4@LDHs composites with easy magnetic separation assistance. *J. Colloid Interf. Sci.*, 448, 508-516.

Yehia A., Miller J. D., Ateya B. G., 1993. Analyses of the adsorption behaviour of oleate on some synthetic apatites. *Miner. Eng.*, 6, 79-86.

Yoon R. H., Nagaraj D. R., Wang S. S., Hildebrand T. M., 1992. Beneficiation of kaolin clay by froth flotation using hydroxamate collectors. *Miner. Eng*., 5, 457-467.

Yoon, R.H., Salman, T., Donnay, G., 1979. Predicting points of zero charge of oxides and hydroxides. *J. Colloid Interface Sci.*, *70*, 483-493

Young, C. A., Miller, J. D., 2000. Effect of temperature on oleate adsorption at a calcite surface: an FT-NIR/IRS study and review. *Int. J. Miner. Process.*, *58*(1), 331-350.

Yopps, J.A., Fuerstenau, D.W., 1964. The zero point of charge of alpha-alumina. *J. Colloid Sci.*, *19*, 61-71.

Yu, F., Wang, Y., Zhang, L., Zhu, G., 2015. Role of oleic acid ionic− molecular complexes in the flotation of spodumene. *Miner. Eng.*, *71*, 7-12.

Zhang W., Honaker R.Q., Groppo J., 2017a. Concentration of rare earth minerals from coal by froth flotation. *Miner. Metall. Proc.*, (Accepted).

Zhang W., Honaker R.Q., Groppo J., 2017b. Flotation of monazite in the presence of calcite part I: Calcium ion effects on the adsorption of hydroxamic acid. *Miner. Eng.*, 100, 40-48.

Zhang W., Honaker R.Q., Groppo J., 2016. Fundamental study of the effects of sodium hexametaphosphate in monazite-calcite flotation system, *XXVIII International Mineral Processing Congress*, Québec, Canada, Sep 11-15.

Zhang, W., Rezaee, M., Bhagavatula, A., Li, Y., Groppo, J., Honaker, R., 2015. A review of the occurrence and promising recovery methods of rare earth elements from coal and coal by-products.*Int. J. Coal Prep. Util.*, *35*(6), 295-330.

VITAE

EDUCATION

- M.S., Mineral Processing Engineering

  Thesis Title: “Studies on Bauxite Flotation and Froth Zone Stability”

  June 2013

  Central South University, Changsha, China

- B.S., Mineral Processing Engineering

  Thesis Title: “Processing Plant Design for Bei Ming He Iron Mine”

  June 2011

  Shandong University of Science and Technology, Qingdao, China

AREA OF EXPERTISE

- Flotation, Coal Preparation, Surface Chemistry, Adsorption, Solid Waste Material Processing, Hydrometallurgy, Environmental Remediation

RESEARCH EXPERIENCE

- 09/2013-Present Research Assistant, Department of Mining Engineering, University of Kentucky, Lexington, KY, USA
- 01/2017-05/2017 Teaching Assistant, Department of Mining Engineering, University of Kentucky, Lexington, KY, USA
- 01/2016-05/2016 Teaching Assistant, Department of Mining Engineering, University of Kentucky, Lexington, KY, USA
- 09/2011-06/2013 Research Assistant, Department of Mineral Processing and Bioengineering, Central South University, Changsha, Hunan, China
- 09/2007-06/2011 Shandong University of Science and Technology, Department of Environmental and Chemical Engineering, Qingdao, Shandong, China

INDUSTRIAL EXPERIENCE

- Intern at FGX Sep Tech, Lexington, KY, 2015

- Pilot scale process modifications of a multi-metal processing plant, Yunnan Zinc Corporation, Chenzhou, Hunan China, 2012
- Intern at an iron ore processing plant of Luzong Mineral Corporation, Laiwu, Shandong, China, 2010
- Intern at a coal processing plant of Xinwen Mineral Corporation, Taian, Shandong, China, 2009

SELECTED PROJECTS

- "Pilot-Scale Testing of An Integrated Circuit for the Extraction of Rare Earth Minerals and Elements from Coal and Coal Byproducts Using Advanced Separation Technologies" funded by the U.S. Department of Energy (DOE), March 2016-present.
- "Evaluation of Kentucky Coal Waste Slurries for Rare Earth Element and Valuable Mineral Recovery" funded by the Department for Energy Development and Independence (DEDI) of Kentucky, July 2015-Feburary 2016.
- "Laboratory and Bench-Scale Testing for Rare Earth Elements from Coal and Coal Byproducts" funded by the U.S. Department of Energy (DOE), July 2014-December 2014.
- "Magnetite Reverse Flotation Using Appropriate Reagents", funded by SNF FloMin Corporation, 2013-2014.
- "Efficient Recovery of the Multi-Metallic Minerals from Wu Chang Ping Plant refuse" funded by Yunan Tin Industry, 2012-2013.
- "Preparation of Hydrogen Storage Composite Nano Materials and Performance Evaluations", funded by Shandong University of Science and Technology, 2009.

AWARDS & HONORS

- G. William Kalb Scholarship award, Coal Preparation Society of America (CPSA), 2015
- WAAIME Scholarship, Society for Mining, Metallurgy & Exploration (SME), 2014-2015 & 2015-2016

- Outstanding Graduate Award, Central South University, 2012
- National Encouragement Scholarship, Ministry of Education of the People's Republic of China, 2009

PUBLICATIONS

Peer-reviewed Journals – Accepted and Published

1. Zhang W., Honaker R.Q., Groppo J. (2017), Flotation of Monazite in the Presence of Calcite Part I: Calcium Ion Effects on the Adsorption of Hydroxamic Acid, *Minerals Engineering*, 100, 40-48.
2. Zhang W., Honaker R.Q., Groppo J. (2017), Concentration of Rare Earth Minerals from Coal by Froth Flotation, *Minerals & Metallurgical Processing*.
3. Zhang W., Honaker R. (2015), Studies on Carbon Flotation from Fly Ash, *Fuel Processing Technology*, 139, 236-241.
4. Zhang W., Rezaee M., Bhagavatula A., Li Y., Groppo J., Honaker R. (2015), A Review of the Occurrence and Promising Recovery Methods of Rare Earth Elements from Coal and Coal Byproducts, *International Journal of Coal Preparation and Utilization*, 35(6), 295-330.
5. Hower J., Groppo J., Henke K. R., Hood M. M., Eble C. F., Honaker R. Q., Zhang W., Qian D. (2015), Notes on the Potential for the Concentration of Rare Earth Elements and Yttrium in Coal Combustion Fly Ash, *Minerals*, 5(2), 356-366.
6. Zhang W., Honaker R., Li Y., Chen J. (2014), The Importance of Mechanical Scrubbing in Magnetite Concentrate Reverse Flotation, *Minerals Engineering*, 69, 133-136.
7. Ou L., Zhang W., Feng Q., Wang L., Li H. (2014), Study of Gas Hold-up in a Horizontal Packing Flotation Column, *Nonferrous Metals (Mineral Processing Section)*, 2, 65-69.

Peer-reviewed Journals – Submitted and Under Review

1. Zhang W., Honaker R.Q., Groppo J. (2017), Association Characteristic Study and Preliminary Recovery Investigation of Rare Earth Elements (REEs) from a Fire Clay Coal, *Fuel*.

2. Zhang W., Honaker R.Q., Groppo J. (2017), Flotation of Monazite in the Presence of Calcite Part II: Efficient Separation Using Appropriate Depressants and Regulators, *Minerals Engineering*.
3. Zhang W., Honaker R.Q. (2017), Surface Charges of Monazite in Aqueous Systems, *Powder Technology*.
4. Zhang W., Honaker R.Q. (2016), A Fundamental Study of the Adsorption of Octanohydroxamic Acid on Monazite, *International Journal of Mineral Processing*.

Conferences

1. Zhang W., Honaker R.Q., Groppo J. (2017), Concentration of Rare Earth Minerals from Coal by Froth Flotation, *SME Annual Conference & Expo*, Denver, Colorado, USA, Feb 19-22.
2. Honaker R.Q., Yoon R.H., Luttrell J., Zhang W., Eble C., Hower J. (2017), Rare Earth Elements from Coal and Coal Byproducts, *SME Annual Conference & Expo*, Denver, Colorado, USA, Feb 19-22.
3. Zhang W., Honaker R., Groppo J. (2016), Fundamental Study of the Effects of Sodium Hexametaphosphate in Monazite-Calcite Flotation System, *XXVIII International Mineral Processing Congress*, Québec, Canada, Sep 11-15.
4. Honaker R., Groppo J., Bhagavatula A., Rezaee M., Zhang W. (2016), Recovery of Rare Earth Minerals and Elements from Coal and Coal Byproducts, *International Coal Preparation Conference*, Louisville, USA, April 25-27.
5. Zhang W., Groppo J., Honaker R. (2015), Ash Beneficiation for REE Recovery, *World of Coal Ash Conference*, Nasvhille, TN, May 5-7.
6. Zhou S., Zhang T., Zhang M., Zhang C., Lu S., Zhao P., Zhang W. (2010), Effects of Atmospheres on the Reaction Between Magnesium-Based Hydrogen-Storage Material and Thiophene, *the 7th National Conference on Functional Materials and Applications*, Changsha, China.

PATENTS

- China Patent Office, Patent No. CN101912776A, Co-authored (2010), Hydrogenation Material for Olefins in Coke Oven Gas and Preparation Method Thereof.
- China Patent Office, Patent No. CN102277206B, Co-authored (2013), Coke Oven Gas Desulfurization via Adding Hydrogen.

PRESENTATIONS

- "Fundamental Study on the Adsorption of Hydroxamic Acid on Monazite Surfaces", Denver, Colorado, February 22, 2017.
- "Concentration of Rare Earth from Coal Using Flotation", Denver, Colorado, February 22, 2017.
- "Recovery of Rare Earth Minerals and Elements from Coal and Coal Byproducts", Phoenix, Arizona, February 22, 2016.